PRECISION RADIOLOGY

Advanced Quantitative and Multimodal Imaging Techniques in Clinical Practice

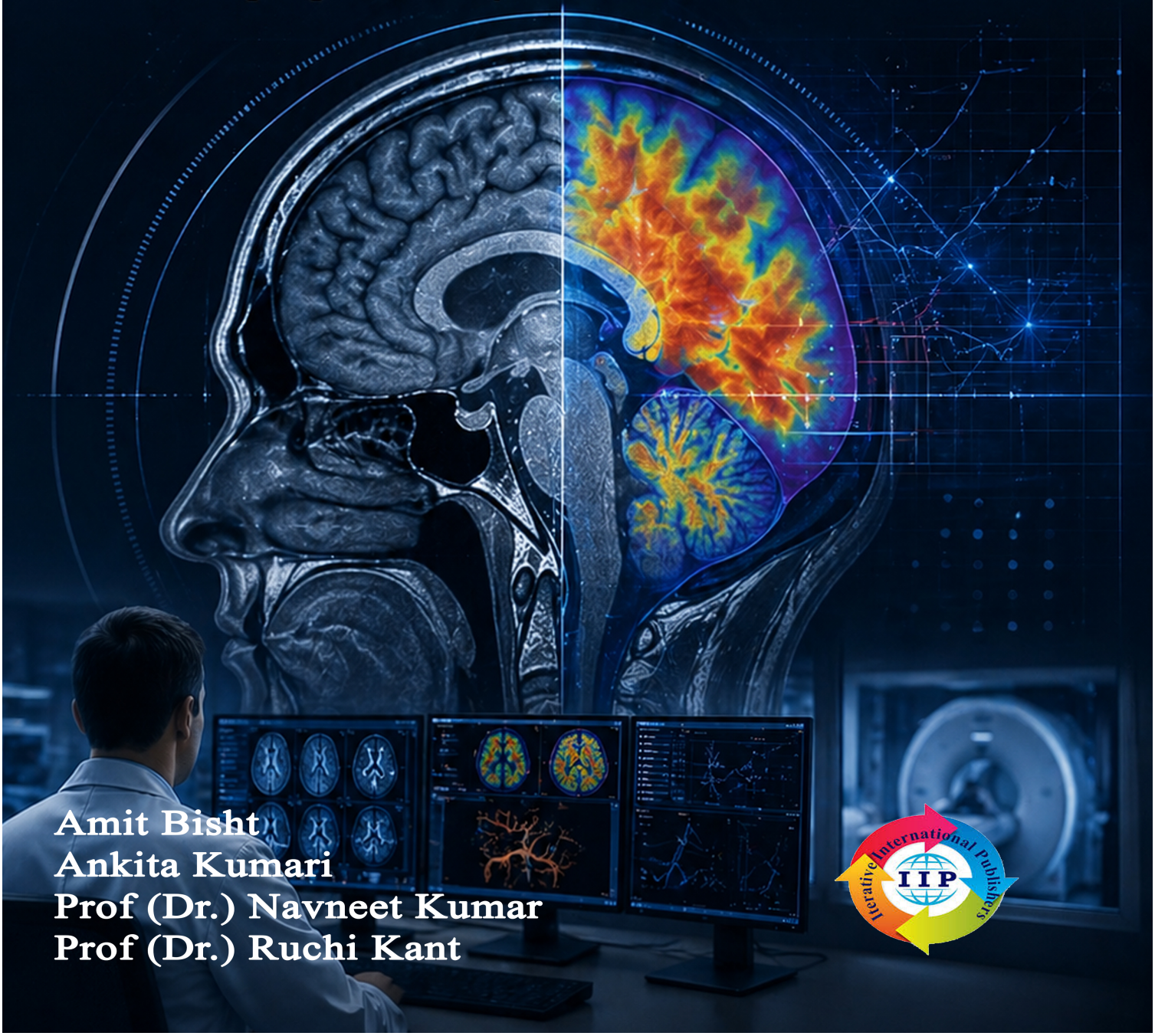

Amit Bisht
Ankita Kumari
Prof (Dr.) Navneet Kumar
Prof (Dr.) Ruchi Kant

Iterative International Publishers
IIP

Precision Radiology:
Advanced Quantitative and Multimodal Imaging Techniques in Clinical Practice

First Volume

Editors

Amit Bisht

Ankita Kumari

Prof (Dr.) Navneet Kumar

Prof (Dr.) Ruchi Kant

Title of the Book: Precision Radiology: Advanced Quantitative and Multimodal Imaging Techniques in Clinical Practice

First Volume – **2026**

Amit Bisht, Assistant Professor & Head, Department of Radiological Imaging Techniques, College of Paramedical Sciences, Teerthanker Mahaveer University, Moradabad

Ankita Kumari, Assistant professor(RIT), TS Mishra university, Anora, Lucknow

Prof (Dr.) Navneet Kumar, Principal, College of Paramedical Sciences, Teerthanker Mahaveer University, Moradabad

Prof (Dr.) Ruchi Kant, Professor, College of Paramedical Sciences , Teerthanker Mahaveer University, Moradabad

Disclaimer
The authors are solely responsible for the contents published in this book. The publishers don't take any responsibility for the same in any manner. Errors, if any, are purely unintentional, and readers are requested to communicate such errors to the editors or publishers to avoid discrepancies in the future.

ISBN: 978-93-7020-458-4

MRP Rs. 490/-

Publisher, Printer & Distributor:
Selfypage Developers Pvt Ltd.,
Pushpagiri Complex,
Beside SBI Housing Board,
K.M. Road Chikkamagaluru, Karnataka.
Tel.: +91-8861518868
E-mail: info@iipbooks.com

IMPRINT: IIP Iterative International Publishers

For Sales Enquiries:
Contact: +91- 8861511583
E-mail: sales@iipbooks.com

Preface

Radiology is undergoing a profound transformation. Once primarily centered on visual interpretation and qualitative assessment, the discipline has rapidly evolved into a data-rich, technology-driven specialty that integrates advanced imaging physics, quantitative biomarkers, computational analytics, and multimodal diagnostics. The emergence of precision medicine has further accelerated this shift, demanding imaging approaches that move beyond detection toward characterization, prediction, and individualized clinical decision-making.

Precision Radiology: Advanced Quantitative and Multimodal Imaging Techniques in Clinical Practice was conceived in response to this evolving landscape. The purpose of this book is to bridge the gap between cutting-edge imaging science and real-world clinical application. It aims to provide clinicians, radiologists, researchers, trainees, and allied healthcare professionals with a comprehensive understanding of how advanced imaging technologies can enhance diagnostic accuracy, improve therapeutic planning, and support personalized patient care.

Over the past decade, innovations in quantitative imaging, functional MRI, diffusion and perfusion techniques, radiomics, hybrid imaging, molecular imaging, artificial intelligence, and image-guided analytics have fundamentally changed the role of radiology in medicine. Imaging is no longer merely descriptive; it is increasingly predictive, prognostic, and integrative. Quantitative biomarkers extracted from imaging datasets now contribute to disease phenotyping, treatment response assessment, and longitudinal monitoring across oncology, neurology, cardiology, musculoskeletal medicine, and beyond.

This book explores these developments through a clinically oriented and multidisciplinary perspective. Each chapter has been designed to combine foundational principles with practical applications, highlighting how advanced imaging techniques can be effectively incorporated into contemporary clinical workflows. Emphasis has been placed not only on technological innovation but also on interpretation, standardization, reproducibility, and translational relevance.

A central theme throughout this work is multimodal integration. No single imaging modality can fully capture the biological complexity of disease. The convergence of structural, functional, metabolic, and molecular imaging offers unprecedented opportunities for comprehensive patient evaluation. By integrating information across modalities, clinicians are better equipped to make informed, patient-specific decisions that align with the goals of precision healthcare.

Another important focus of this book is the growing influence of computational radiology and artificial intelligence. Machine learning algorithms, radiomics pipelines, and automated image analysis systems are redefining diagnostic paradigms and workflow efficiency. However, these technologies must be understood critically, implemented responsibly, and validated rigorously. This text seeks to present these innovations with balanced scientific insight and practical clinical relevance.

The contributors to this volume represent diverse expertise across radiology, medical physics, biomedical engineering, nuclear medicine, oncology, and data science. Their collective efforts reflect the interdisciplinary collaboration that is essential for advancing precision imaging in clinical practice.

It is our hope that this book will serve not only as an academic reference but also as a practical guide for clinicians navigating the rapidly changing world of advanced imaging. Whether the reader is a trainee seeking foundational knowledge or an experienced practitioner exploring emerging technologies, we aspire for this text to inspire curiosity, critical thinking, and innovation.

Finally, we acknowledge the patients whose clinical journeys continue to drive advancements in imaging science and healthcare delivery. Precision radiology ultimately exists to improve patient outcomes, reduce diagnostic uncertainty, and support more effective and individualized care. As imaging technologies continue to evolve, so too will the opportunities to redefine the future of medicine.

We invite readers to engage with this book as both a scientific resource and a vision for the next era of radiology.

Acknowledgement

We would like to express our sincere gratitude to all contributors, colleagues, researchers, and healthcare professionals whose expertise and support made this book possible. We are deeply thankful to our mentors and institutions for their guidance and encouragement throughout this journey.

Special thanks to our families and loved ones for their constant support, patience, and inspiration during the preparation of this book.

Finally, we acknowledge the patients whose experiences continue to inspire advancements in precision radiology and personalized healthcare.

We hope this book serves as a valuable resource for clinicians, researchers, and students in advancing the field of modern medical imaging.

Table of Contents

Chapter 1
ADVANCED IMAGING OF LIGAMENT AND TENDON INJURIES 1-13
……
Dr. Vijay Kishor Chakravarti, Sandeep Yadav, Deepak Katiyar

Chapter 2
QUANTITATIVE IMAGING BIOMARKERS: THE ROLE OF RADIOMICS IN CANCER DIAGNOSIS AND PROGNOSIS 14-20
……
Srishti Gaur, Mohd. Harish Saifi, Rashmi Pandey, Kashish

Chapter 3
CONTRAST-ENHANCED IMAGING TECHNIQUES AND QUANTIFICATION 21-32
……
Shubhanshi Rani

Chapter 4
UNMASKING BREAST CANCER: THE CLINICAL ROLE OF 3D TOMOSYNTHESIS 33-41
……
Ayushi Singh, Amit Bisht, Shivani Aswal

Chapter 5
DIGITAL BREAST TOMOSYNTHESIS: REVOLUTIONIZING BREAST IMAGING 42-53
……
Srishti Gaur, Sidra, Amit Bisht, Geeta Bisht

Chapter 6
ADVANCED MULTIMODAL IMAGING OF THE HIPPOCAMPUS: ANATOMICAL PRECISION AND PATHOLOGICAL CORRELATION 54-72
……
Sidra, Mohd. Harish Saifi, Rashmi Pandey, Kritika Agarwal

Chapter 7
THE 7T REVOLUTION: ENHANCING DIAGNOSTIC CLARITY AND NEUROANATOMICAL VISUALIZATION 73-84
……
Mohd. Harish Saifi, Rashmi Pandey, Sidra, Sohel Rana

Chapter 8 85-97
MAGNETIC RESONANCE FINGERPRINTING (MRF) :
A PARADIGM SHIFT FROM QUALITATIVE TO QUANTITATIVE MRI
……
Mohd. Harish Saifi, Rashmi Pandey, Srishti Gaur, Mitali Monalisha

Chapter 9
LIVER IMAGING BIOMARKERS: FAT QUANTIFICATION AND FIBROSIS ASSESSMENT 98-111
……
Aakash Kaushal

Chapter 10
CLINICAL IMPLEMENTATION OF LOW-DOSE CT: FROM PROTOCOL OPTIMIZATION TO NODULE MANAGEMENT 112-123
……
Ayushi Singh, Amit Bisht, Shivani Aswal

Chapter 11
ARTIFICIAL INTELLIGENCE IN QUANTITATIVE RADIOLOGY: TRANSFORMING IMAGE INTERPRETATION 124-138
……
Vishal Gangwar, Singh Akshata Dinesh, Shubham Sharma

Chapter 12
DECT-DERIVED MUSCLE FAT FRACTION: ADVANCING BODY COMPOSITION ANALYSIS IN CRITICAL CARE 139-147
……
Prachi Singh

1
Chapter

Advanced Imaging of Ligament and Tendon Injuries

[1]Dr. Vijay Kishor Chakravarti
Demonstrator,
Department of Radiological and Imaging Technology, Faculty of Paramedical Sciences, UPUMS, Saifai, Etawah, Uttara Pradesh

[2]Sandeep Yadav
M.Sc. Research Scholar
Department of Radiology & Imaging Technology, Vivekanand Global University Jaipur

[3]Deepak Katiyar
Assistant Professor,
Department of Radiological Imaging Techniques,
College of Paramedical Sciences,
Teerthanker Mahaveer University, Moradabad

Abstract

Ligament and tendon injuries constitute a major burden in musculoskeletal radiology, demanding imaging techniques that extend well beyond conventional morphological assessment. This chapter provides a comprehensive, clinically oriented review of advanced imaging modalities applicable to the knee, shoulder, ankle, elbow, and wrist. Magnetic resonance imaging (MRI), encompassing conventional sequences and emerging quantitative methods such as T2 mapping, T1rho relaxometry, diffusion-tensor imaging, and ultrashort echo time (UTE) imaging, forms the cornerstone of contemporary evaluation. High-resolution ultrasound (US) and sonoelastography offer dynamic, real-time assessment with superior spatial resolution for superficial structures, while computed tomography (CT) and dual-energy CT (DECT) serve complementary roles—particularly in the post-operative setting and for enthesopathy characterisation. Standardised imaging protocols for each modality and anatomical region are presented in tabular format. Throughout, evidence from peer-reviewed literature is synthesised to guide optimal modality selection, technique optimisation, and interpretation. An understanding of these advanced techniques enables more precise grading of injury severity, facilitates longitudinal monitoring of healing, and ultimately supports individualised clinical decision-making.

Keywords: Musculoskeletal MRI; tendon ultrasound; T2 mapping; dual-energy CT; sonoelastography; ligament injury; quantitative imaging

I. INTRODUCTION

Ligament and tendon injuries represent among the most frequently encountered pathologies in musculoskeletal medicine, affecting athletes, manual workers, and the ageing population alike. The spectrum of injury ranges from microscopic collagen disruption (tendinopathy) to complete macroscopic rupture with associated functional deficit. Accurate characterisation of injury extent, tissue composition, and biomechanical competence is fundamental to treatment planning, surgical candidacy assessment, and rehabilitation monitoring.

Conventional radiography remains the initial modality of choice for excluding osseous pathology such as avulsion fractures, yet its soft-tissue resolution is inherently limited. Conventional MRI revolutionised musculoskeletal imaging and remains the gold standard for ligament and tendon evaluation owing to its superior soft-tissue contrast and multiplanar capability.[1] However, standard sequences—proton-density fat-saturated (PDFS), T1-weighted, and T2-weighted imaging—reflect gross morphological changes rather than the biochemical and microstructural alterations that precede or accompany injury. The integration of advanced quantitative MRI, high-resolution ultrasound with elastography, and dual-energy CT has substantially expanded the diagnostic repertoire available to the practising radiologist and clinician.

This chapter is structured to provide a modality-by-modality and region-by-region synthesis of current evidence and practical guidance. Standardised imaging protocols are presented in clearly delineated tables to facilitate direct implementation in clinical practice. The overarching aim is to bridge the gap between academic technique development and routine clinical utility for a mixed audience of radiologists, orthopaedic surgeons, and sports medicine physicians.

II. ANATOMY AND PATHOLOGY: A FRAMEWORK FOR ADVANCED IMAGING

1. Collagen Architecture and Failure Mechanics

Ligaments and tendons are dense regular connective tissues composed predominantly of type I collagen fibres arranged in a hierarchical crimp pattern that confers tensile strength and viscoelastic properties.[2] The crimp pattern, visible ultrasonographically as a fine fibrillar echogenic texture, is progressively lost with repetitive microtrauma or acute overload. Histologically, early tendinopathic tissue demonstrates disorganised collagen fibres, increased glycosaminoglycan (GAG) content, neovascularisation, and neural ingrowth—changes that precede MRI-detectable signal alteration.

Advanced MRI techniques, particularly T1rho and T2 relaxometry, are sensitive to GAG concentration and collagen fibre orientation respectively, providing indirect biomarkers of tissue integrity at the molecular level.[3] This biochemical sensitivity positions quantitative MRI as the premier modality for pre-symptomatic detection, post-treatment response monitoring, and risk stratification for re-injury.

2. Injury Classification

The classification of ligament injuries into three grades (Grade I: sprain without fibre disruption; Grade II: partial tear; Grade III: complete rupture) and tendon injuries into partial- or full-thickness tears remains in routine clinical use.[4] However, this morphological

taxonomy does not capture tissue composition or healing biology. Advanced imaging enables supplementation of grade-based classification with quantitative metrics that carry prognostic significance, particularly in determining return-to-sport timelines after anterior cruciate ligament (ACL) reconstruction or rotator cuff repair.

III. MAGNETIC RESONANCE IMAGING

1. Conventional MRI Sequences

Proton-density fat-saturated (PDFS) imaging is widely regarded as the workhorse sequence for ligament and tendon evaluation, offering excellent fluid-to-soft-tissue contrast with suppression of overlying subcutaneous fat signal.[5] For knee ligaments, sagittal PDFS sequences at 3 mm slice thickness with a 160 mm field of view (FOV) provide reliable assessment of ACL morphology, while coronal sequences are indispensable for medial and lateral collateral complex evaluation. Oblique coronal and oblique sagittal planes optimise in-plane visualisation of the shoulder's rotator cuff tendons and glenohumeral ligaments respectively.

Three-dimensional (3D) isotropic sequences such as 3D DESS (Double Echo Steady-State), 3D SPACE (Sampling Perfection with Application-optimised Contrasts using different flip-angle Evolutions), and 3D CUBE have emerged as powerful adjuncts, enabling multiplanar reformation from a single acquisition and improving partial-volume averaging artefact reduction in small structures such as the triangular fibrocartilage complex (TFCC) and the collateral ligaments of the elbow.[6]

Table 1: Recommended conventional MRI protocols for ligament and tendon evaluation by anatomical region.

Anatomical Region	Coil	Field Strength	Key Sequences	Slice Thickness	Notes
Knee (ACL/PCL/ collaterals)	Dedicated knee coil	3T preferred	PDFS axial/sagittal/coronal; 3D DESS; T2 mapping; UTE	2–3 mm	Oblique sagittal for ACL; coronal for collaterals
Shoulder (rotator cuff)	Shoulder array coil	1.5T or 3T	PDFS oblique planes; T1 arthrogram (MRA); T2 mapping	3–4 mm	MRA for partial-thickness tears; T2 map for post-op
Ankle & foot (ATFL/PTT)	Ankle or small joint coil	3T preferred	PDFS sagittal/coronal/axial; 3D SPACE; T1rho	2–3 mm	High resolution for plantar plate & spring ligament
Elbow (UCL/LCL)	Dedicated elbow coil	3T preferred	PDFS coronal/axial; indirect MRA;	2–3 mm	Valgus stress MRA in athletes;

			T2 mapping		UTE for enthesis
Wrist (TFCC/SL/LT)	Wrist or small joint coil	3T preferred	3D GRE; PDFS; direct MRA; T2 mapping	1–2 mm	3T mandatory for TFCC; direct arthrogram for ligament tears

2. MR Arthrography

Direct MR arthrography (MRA), performed by intra-articular gadolinium instillation followed by MRI, substantially improves the sensitivity and specificity for partial-thickness rotator cuff tears, labral pathology, and intrinsic ligament tears of the wrist.[7] Meta-analytic data report pooled sensitivity of 0.86 and specificity of 0.96 for detection of partial supraspinatus tears by direct MRA, compared with 0.67 and 0.93 respectively for conventional MRI.[8] Indirect MRA, employing intravenous gadolinium with exercise-facilitated joint perfusion, provides a non-invasive alternative applicable where direct injection is logistically challenging or contraindicated, and has demonstrated utility in UCL assessment in overhead athletes.

3. Quantitative MRI Techniques

- **T2 Relaxometry and T2 Mapping:** T2 relaxation time is sensitive to water mobility, collagen fibre organisation, and the presence of proteoglycan-bound water. In healthy tendons and ligaments, short T2 values reflect tightly packed collagen with restricted water motion. Disruption of this architecture in tendinopathy or partial tearing leads to T2 prolongation detectable by parametric mapping.[9] Studies of the Achilles tendon have demonstrated that T2 mapping identifies regions of altered composition not visible on conventional sequences, with elevated T2 values correlating with histological disorganisation.[10] For the rotator cuff, quantitative T2 has been employed to monitor post-operative tendon healing, with values approaching the normal range correlating with satisfactory structural and functional outcomes.

  A multi-echo spin-echo sequence (e.g., 6–8 echo times ranging 10–80 ms) is typically employed, with pixel-wise monoexponential fitting to generate a colour-coded parametric map. The technique requires no additional contrast agent and adds approximately 8–10 minutes to the examination, representing a clinically acceptable trade-off for the additional biochemical information obtained.[11]

- **T1rho Relaxometry:** T1rho (T1 in the rotating frame) is sensitive to slow molecular motions and interactions between macromolecules and bulk water, with particular sensitivity to proteoglycan content. Elevated T1rho values in the ACL graft have been associated with incomplete ligamentisation and increased risk of graft failure, suggesting a role in return-to-sport decision-making.12 In the Achilles tendon, T1rho elevation in asymptomatic recreational runners has been reported, raising the possibility of sub-clinical load-related remodelling that may predate symptomatic tendinopathy.13

- **Ultrashort Echo Time (UTE) Imaging:** Conventional MRI sequences cannot visualise the bulk of tendon and ligament signal because the inherently short T2 values of these tissues cause signal decay before echo acquisition. Ultrashort echo time (UTE) sequences, with TEs of 0.05–0.5 ms, capture signal from these short-T2 components, enabling direct visualisation of collagen-rich tissue and quantitative assessment of its composition.14 UTE T2* mapping has been validated in cadaveric and in-vivo Achilles tendon studies, demonstrating sensitivity to degeneration and the capacity to distinguish healthy from tendinopathic regions with high reproducibility.15 The enthesis—the fibrocartilaginous transition zone between tendon and bone—is particularly well-served by UTE imaging, a domain of clinical relevance in enthesopathy associated with spondyloarthropathy and insertional Achilles tendinopathy.

- **Diffusion Tensor Imaging (DTI):** Diffusion tensor imaging characterises the directional diffusivity of water molecules within fibrous tissues, generating metrics of fractional anisotropy (FA) and mean diffusivity (MD) that reflect fibre integrity and orientation. In the knee, decreased FA and increased MD within the ACL have been demonstrated in the setting of partial tears and chronic degeneration, with values correlating with biomechanical testing parameters.16 DTI tractography additionally enables three-dimensional reconstruction of fibre bundles, potentially mapping the anteromedial and posterolateral bundles of the ACL separately—a clinically relevant distinction for bundle-specific surgical planning.17 Technical challenges of DTI in tendons include susceptibility artefacts, motion sensitivity, and long acquisition times; dedicated sequences with reduced-FOV excitation and parallel imaging acceleration are recommended to mitigate these limitations.

IV. ULTRASOUND AND SONOELASTOGRAPHY

1. High-Resolution Ultrasound

High-resolution ultrasound (HRUS) offers several advantages over MRI in the evaluation of superficial tendons and ligaments: real-time dynamic imaging, the capacity to perform stress manoeuvres, superior spatial resolution for structures within 3 cm of the skin surface, absence of ionising radiation, and lower cost with wider availability.[18] The fibrillar echogenic architecture of healthy tendons is readily identified with linear transducers at 12–22 MHz. Tendinopathy manifests as hypoechoic swelling with loss of the normal fibrillar pattern, while tears appear as focal hypoechoic or anechoic clefts with fibre discontinuity.

Dynamic sonography is uniquely positioned to assess ligament laxity under controlled stress, a capability unavailable with static MRI or CT. The anterior talofibular ligament (ATFL) is examined under anterior drawer stress, the medial collateral ligament of the knee under valgus stress, and the ulnar collateral ligament (UCL) of the elbow under valgus stress provocation—techniques that provide functional as well as morphological data.[19]

Table 2: Recommended ultrasound protocols for common ligament and tendon pathologies.

Structure	Transducer	Frequency Range	Technique	Clinical Application
Rotator cuff	Linear	12–18 MHz	Long- & short-axis; dynamic impingement	Full/partial thickness tears; calcification
Achilles tendon	Linear	10–15 MHz	Long-axis compressive elastography; SWE	Tendinopathy grade; post-injection response
Patellar tendon	Linear	12–18 MHz	SWE; power Doppler	Jumper's knee; treatment monitoring
ATFL / CFL	Linear (small parts)	15–22 MHz	Dynamic inversion stress; long-axis	Lateral ankle instability
UCL (elbow)	Linear	12–18 MHz	Dynamic valgus stress	Overhead athlete; UCL laxity assessment
TFCC / wrist ligaments	Linear (small parts)	15–22 MHz	Long/short axis; dynamic loading	Partial TFCC tears; adjunct to MRA

2. Sonoelastography

- **Strain Elastography:** Strain elastography estimates tissue stiffness by comparing ultrasound radiofrequency data before and after extrinsic compression. Stiffer tissues (e.g., healthy tendon) undergo less deformation than softer regions (e.g., tendinopathic tissue), generating a qualitative or semi-quantitative strain ratio relative to a reference region. In the Achilles tendon, strain elastography has demonstrated the capacity to identify focal regions of reduced stiffness (increased strain) corresponding to areas of tendinopathy, with abnormal strain ratio correlating with symptom severity and histological change.20

- **Shear-Wave Elastography:** Shear-wave elastography (SWE) is an operator-independent quantitative technique that measures the propagation velocity of mechanically induced shear waves within tissue, converting this to a Young's modulus value in kilopascals. Healthy tendons are among the stiffest biological tissues, with SWE values ranging from 200 to over 800 kPa depending on loading conditions and fibre orientation.21 Tendinopathic tissue exhibits significantly reduced stiffness; in the patellar tendon, SWE values below 300 kPa at rest have been associated with symptomatic tendinopathy and return-to-play delays.22

  SWE demonstrates excellent reproducibility and has established normative databases for the Achilles, patellar, rotator cuff, and common extensor tendons. Longitudinal SWE monitoring after eccentric loading programs and platelet-rich plasma (PRP) injection has shown progressive stiffness recovery correlating with clinical improvement, supporting its role as a biomarker of treatment response.23 Technical considerations include angle-dependence of shear wave propagation, the need for consistent tissue pre-loading conditions, and the limitation that very stiff or very shallow tissues may exceed the velocity measurement range of some systems.

V. COMPUTED TOMOGRAPHY AND DUAL-ENERGY CT

1. Role of Conventional CT

Conventional CT occupies a complementary rather than primary role in ligament and tendon assessment, given its inferior soft-tissue contrast relative to MRI. However, CT is indispensable for evaluating osseous complications of soft-tissue injuries: avulsion fractures at ligamentous insertions, talar dome osteochondral lesions associated with lateral ankle sprains, and bone tunnel morphology following ACL reconstruction.[24] CT arthrography, combining intra-articular iodinated contrast instillation with high-resolution CT acquisition, provides an alternative to MRA in patients with MRI contraindications (pacemakers, severe claustrophobia) and has demonstrated comparable accuracy for full-thickness rotator cuff tears and TFCC pathology.[25]

2. Dual-Energy CT

Dual-energy CT (DECT) acquires data at two distinct photon energy spectra (typically 80 and 140 kVp), enabling material decomposition algorithms that identify and quantify specific substances based on their differential x-ray attenuation.[26] In the context of ligament and tendon pathology, DECT has three principal applications: uric acid crystal identification in tophaceous gout affecting the Achilles and patellar tendons; calcium deposit characterisation in calcific tendinopathy; and bone marrow oedema mapping at entheseal insertion sites.

Virtual non-calcium (VNCa) DECT reconstructions can subtract the calcium signal from bone, effectively generating a marrow oedema map analogous to short tau inversion recovery (STIR) MRI without the need for a magnetic field. Studies in spondyloarthritis patients have demonstrated that DECT entheseal bone marrow oedema maps exhibit moderate-to-good agreement with MRI STIR sequences, opening a potential pathway for monitoring inflammatory enthesopathy in patients with MRI contraindications.[27] Radiation dose optimisation—employing iterative reconstruction algorithms, tube current modulation, and region-of-interest acquisition—is imperative when applying DECT in younger athletic populations.

Table 3: CT and dual-energy CT protocols for ligament and tendon-related indications.

Region / Indication	Modality	kVp / Settings	Protocol Detail	Key Application
Post-operative knee (ACL/PCL hardware)	CT	120 kVp; MBIR recon	Axial + reformats; 0.6 mm slice	Tunnel widening; implant assessment
Calcific tendinopathy (shoulder/hip)	CT / DECT	80/140 kVp dual-source	Material decomposition: calcium overlay	Quantify deposit volume/density
Enthesopathy (Achilles/patellar)	DECT	80/140 kVp dual-source	Bone marrow oedema map	Detect pre-erosive BM oedema
Ankle trauma (syndesmosis/ATFL bony avulsion)	CT	120 kVp; 0.6 mm slice	Axial + MPR; 3D VRT	Subtle avulsion; talar dome fracture
Elbow ossification	CT	120 kVp;	Coronal + axial	Calcification

(UCL calcification)		0.6 mm slice	MPR	characterisation
Wrist (TFCC osseous insertion)	CT arthrography	120 kVp; 0.3 mm slice	Contrast arthrogram + CT	Osseous TFCC attachment tears

VI. REGION-SPECIFIC ADVANCED IMAGING CONSIDERATIONS

1. Knee

The knee is the most extensively studied joint in musculoskeletal MRI. The ACL, composed of anteromedial (AM) and posterolateral (PL) bundles, is optimally visualised on oblique sagittal PDFS sequences aligned parallel to the ACL fibres. Quantitative T2 and T1rho mapping of ACL grafts have emerged as research-grade tools for assessing ligamentisation following reconstruction, with graft maturity typically requiring 12–24 months.[28] DTI-based tractography of the ACL demonstrates promise for bundle-specific assessment, enabling separate characterisation of AM and PL bundle integrity that may guide selective bundle reconstruction strategies.

The medial collateral ligament (MCL) complex, encompassing the superficial MCL, deep MCL, and posterior oblique ligament, is graded on coronal sequences and benefits from 3D isotropic acquisition for multiplanar assessment. The posteromedial corner—frequently injured in complex knee dislocations—incorporates the semimembranosus tendon complex and is best evaluated with dedicated coronal and axial sequences at 3T.[29]

2. Shoulder

Rotator cuff pathology encompasses a continuum from tendinosis and partial-thickness tears to full-thickness tears and cuff tear arthropathy. For partial-thickness tears, direct MRA remains the most sensitive technique, with superior sensitivity on the articular surface (detected via capsular contrast penetration) compared to bursal-surface tears.[8] T2 mapping of the supraspinatus tendon has demonstrated clinical utility in post-operative monitoring, with T2 values returning toward the normal range in structurally intact healed repairs and remaining elevated in re-tear or poor healing scenarios.

The glenohumeral ligament complex, including the superior, middle, and inferior glenohumeral ligaments (IGHL), is critical to shoulder stability assessment. The IGHL anterior band, the primary restraint to anterior dislocation, is best assessed on axial PDFS and axial arthrogram sequences; 3D isotropic sequences enable confident multiplanar reformation for delineating Bankart lesions and variants.[30]

3. Ankle and Foot

The lateral collateral ligament complex—comprising the ATFL, calcaneofibular ligament (CFL), and posterior talofibular ligament (PTFL)—is the most commonly injured ligamentous complex in the body. Dedicated ankle MRI with a small FOV and 2–3 mm slice thickness on PDFS sequences provides reliable morphological assessment. T1rho imaging of the ATFL has been explored as a marker of chronic ligamentous degeneration in recurrent ankle sprain, with elevated values associated with mechanical instability.[31]

The posterior tibial tendon (PTT) is critical to medial arch maintenance; progressive PTT dysfunction leads to adult-acquired flatfoot deformity. SWE of the PTT demonstrates progressive reduction in stiffness across stages I to III of dysfunction, offering potential for non-invasive staging.[32] The spring ligament complex (superomedial calcaneonavicular ligament and inferior calcaneonavicular ligament) is an important stabiliser increasingly recognised as a contributor to flatfoot deformity; 3D PDFS and 3D SPACE sequences at 3T are recommended for comprehensive evaluation.

4. Elbow

The UCL of the elbow, the primary restraint to valgus stress in overhead athletes (baseball pitchers, javelin throwers), is evaluated on dedicated coronal PDFS sequences at 3T. Indirect and direct MRA improve the sensitivity for partial UCL tears, particularly at the distal ulnar attachment—the 'T-sign' of contrast extravasation beneath the distal UCL being a hallmark finding.[33] Dynamic ultrasound with applied valgus stress (medial joint space widening >1 mm with stress versus unstressed images) provides functional assessment unavailable with static MRI.

The lateral collateral complex of the elbow, including the radial collateral ligament and lateral ulnar collateral ligament, is evaluated on coronal sequences, with posterolateral rotatory instability (PLRI) representing the most clinically significant lesion pattern.[34] UTE imaging of the extensor carpi radialis brevis (ECRB) attachment in lateral epicondylitis offers a means of quantifying entheseal collagen degeneration beyond the morphological assessment afforded by conventional sequences.

5. Wrist

The TFCC is the primary stabiliser of the distal radioulnar joint (DRUJ) and the seat of complex wrist pathology. Its central fibrocartilaginous disc and peripheral ligamentous components (radioulnar ligaments, ulnocarpal ligaments, meniscus homologue) are best assessed with dedicated 3T MRI at 1–2 mm slice thickness, ideally with direct arthrography.[35] The 3D gradient-echo sequences (VIBE, FAME, DESS) provide superior spatial resolution compared to 2D sequences and enable isotropic reformatting; reported sensitivity and specificity for central TFCC disc tears by 3T direct MRA are 0.92 and 0.89 respectively.

The scapholunate (SL) and lunotriquetral (LT) intrinsic intercarpal ligaments, when disrupted, lead to progressive carpal instability patterns. Three-compartment direct arthrography with sequential injection of the radiocarpal, midcarpal, and DRUJ compartments remains the reference standard for intrinsic ligament tears. 3D PDFS and 3D SPACE at 3T with 1 mm isotropic voxels offer a non-invasive approach, though sensitivity for partial SL tears remains below that of arthrography.[36]

VII. COMPARATIVE MODALITY ANALYSIS AND CLINICAL DECISION-MAKING

1. Modality Selection Framework

The selection of imaging modality should be guided by the clinical question, anatomical region, patient characteristics, institutional resources, and operator expertise. No single

modality is universally superior; rather, complementary use of techniques yields the most comprehensive tissue characterisation.

For acute ligamentous injuries in the acute post-traumatic setting, conventional MRI at 1.5T or 3T with PDFS sequences provides the most rapid and reliable morphological assessment. When biochemical assessment of healing tissue is required—as in post-operative monitoring or chronic tendinopathy workup—quantitative MRI techniques (T2 mapping, T1rho, UTE T2*) are the preferred adjuncts.[37]

Ultrasound with SWE is recommended as the primary modality for monitoring superficial tendon pathology over time, given its accessibility, cost-effectiveness, real-time capability, and dynamic assessment potential. In patients with MRI contraindications or in paediatric populations where radiation avoidance is paramount, CT arthrography and DECT represent viable alternatives.[38]

2. Pitfalls and Artefacts

Magic angle effect is the most significant pitfall in tendon and ligament MRI: tissues oriented at approximately 55 degrees to the main magnetic field exhibit artifactual T2 prolongation, simulating tendinosis. This predominantly affects the supraspinatus tendon at its critical zone, the distal Achilles tendon, and the posterior tibialis tendon. Recognising the anatomical location and the absence of corresponding clinical symptoms is key to avoiding false-positive interpretation.[39]

In quantitative MRI, B1 field inhomogeneity at 3T can introduce systematic errors in T1rho and T2 mapping, requiring correction with B1 mapping acquisitions. Susceptibility artefacts adjacent to metallic implants (ACL anchor sutures, rotator cuff repair anchors) markedly degrade signal in their vicinity, limiting quantitative assessments in the early post-operative period. Susceptibility-weighted sequences and view-angle tilting (VAT) techniques mitigate but do not eliminate metal artefact.[40]

In SWE, angle-dependence of shear wave propagation means that measurements are most reliable when the transducer is perpendicular to the tendon long axis. Very stiff or very superficial tendons may exceed the velocity measurement range, producing 'hard clip' artefacts. Standardised pre-loading conditions—such as a defined ankle dorsiflexion angle for Achilles SWE—are essential for intersession reproducibility.[41]

VIII. EMERGING DIRECTIONS AND FUTURE PERSPECTIVES

Artificial intelligence (AI) and deep learning algorithms are beginning to demonstrate performance approaching that of expert radiologists in detecting full-thickness rotator cuff tears and ACL ruptures on conventional MRI, with the potential to reduce reporting time and inter-reader variability.[42] The integration of AI with quantitative MRI—automated T2 map segmentation and parametric analysis—promises to remove the laborious manual region-of-interest placement currently limiting clinical adoption.

Photon-counting CT (PCCT), the most significant CT hardware advance in decades, offers improved spatial resolution (sub-0.2 mm), enhanced soft-tissue contrast, and intrinsic spectral capability without dose penalty. Early phantom and cadaveric studies suggest superior delineation of small tendons and ligamentous structures compared to conventional energy-

integrating detector CT, with clinical translation anticipated in high-volume musculoskeletal centres.[43]

Whole-organ MRI at 7 Tesla is under investigation for ultra-high resolution assessment of small joint structures including the TFCC and intrinsic carpal ligaments, where spatial resolution limitations at 1.5T and 3T restrict diagnostic accuracy for partial tears. Technical challenges of 7T MRI include radiofrequency field inhomogeneity, limited approved hardware, and specific absorption rate (SAR) restrictions that necessitate longer acquisition times.[44]

Compositional MRI at the intersection of multiple quantitative parameters—combining T2, T1rho, UTE T2*, and DTI metrics in a multi-parametric composite score—represents the direction of travel for precision tissue characterisation. Such multi-parametric approaches, validated against histological reference standards, may ultimately inform surgical decision-making, rehabilitation protocols, and injury risk profiling in elite athletes.[45]

IX. CONCLUSIONS

Advanced imaging of ligament and tendon injuries has matured from an exclusively morphological discipline into a multimodal, quantitative science capable of characterising tissue at the biochemical and microstructural level. MRI remains the cornerstone, with conventional sequences providing the diagnostic framework augmented by quantitative techniques—T2 mapping, T1rho, UTE, and DTI—that offer sensitivity to collagen architecture and tissue composition beyond what morphology alone reveals. High-resolution ultrasound and sonoelastography contribute dynamic, real-time stiffness assessment of superficial tendons with growing evidence for treatment monitoring. CT and DECT occupy important complementary roles in the post-operative setting, for enthesopathy assessment, and in patients with MRI contraindications.

For the mixed clinical audience of radiologists, orthopaedic surgeons, and sports medicine physicians, the key practical take-aways are: (1) protocol optimisation for the specific anatomical region and clinical question is essential; (2) quantitative techniques require standardised acquisition and post-processing to be clinically meaningful; (3) modality selection should be guided by the specific diagnostic need rather than routine institutional preference; and (4) emerging AI-assisted quantitative analysis and next-generation hardware such as photon-counting CT will continue to expand the precision radiology toolkit. Clinicians and radiologists who embed these advanced techniques into structured, evidence-based pathways will be best positioned to deliver precise, individualised care for patients with ligament and tendon injuries.

REFERENCES

[1] Stoller DW, Tirman PFJ, Bredella MA. Diagnostic Imaging: Orthopaedics. 2nd ed. Salt Lake City: Amirsys; 2004.

[2] Kannus P. Structure of the tendon connective tissue. Scand J Med Sci Sports. 2000;10(6):312–320.

[3] Regatte RR, Akella SV, Borthakur A, Kneeland JB, Reddy R. Proteoglycan depletion-induced changes in transverse relaxation maps of cartilage: comparison of T2 and T1rho. Acad Radiol. 2002;9(12):1388–1394.

[4] Petersen W, Tillmann B. Anatomy and function of the anterior cruciate ligament. Orthopade. 2002;31(8):710–718.

[5] Zlatkin MB, Pevsner D, Sanders TG, Hawerstock DC, Moorman CT. Proton density MRI of the shoulder: an update. Magn Reson Imaging Clin N Am. 2012;20(2):295–311.

[6] Fritz J, Guggenberger R, Del Grande F. Rapid musculoskeletal MRI in 2021: value and expanded opportunities. AJR Am J Roentgenol. 2021;216(3):704–717.

[7] Beltran LS, Nikac V, Beltran J. Internal impingement syndromes: overuse injuries of the shoulder in overhead athletes. Magn Reson Imaging Clin N Am. 2012;20(2):221–234.

[8] de Jesus JO, Parker L, Frangos AJ, Nazarian LN. Accuracy of MRI, MR arthrography, and ultrasound in the diagnosis of rotator cuff tears: a meta-analysis. AJR Am J Roentgenol. 2009;192(6):1701–1707.

[9] Dressler MR, Butler DL, Wenstrup R, Awad HA, Smith F, Boivin GP. A potential mechanism for age-related declines in patellar tendon biomechanics. J Orthop Res. 2002;20(6):1315–1322.

[10] Dallaudiere B, Lempicki M, Pesquer L, et al. Efficacy of intra-tendinous injection of platelet-rich plasma in treating tendinosis: comprehensive assessment of a rat model. Eur Radiol. 2013;23(10):2830–2837.

[11] Mosher TJ, Dardzinski BJ. Cartilage MRI T2 relaxation time mapping: overview and applications. Semin Musculoskelet Radiol. 2004;8(4):355–368.

[12] Su F, Hilton JF, Nardo L, et al. Cartilage morphology and T1rho and T2 quantification in ACL-reconstructed knees: a 2-year follow-up. Osteoarthritis Cartilage. 2013;21(8):1058–1067.

[13] Deland JT. The adult acquired flatfoot and spring ligament complex: pathology and implications for treatment. Foot Ankle Clin. 2001;6(1):129–135.

[14] Williams A, Qian Y, Bear D, Chu CR. Assessing degeneration of human articular cartilage with ultra-short echo time (UTE) T2* mapping. Osteoarthritis Cartilage. 2010;18(4):539–546.

[15] Robson MD, Gatehouse PD, Bydder M, Bydder GM. Magnetic resonance: an introduction to ultrashort TE (UTE) imaging. J Comput Assist Tomogr. 2003;27(6):825–846.

[16] Gao B, Zhang J, Pugh BF, et al. Diffusion tensor imaging of the anterior cruciate ligament graft following reconstruction surgery. J Magn Reson Imaging. 2015;42(6):1577–1586.

[17] Narayana PA, Brey WW, Kulkarni MV, Sievenpiper CL. Compensation for surface coil sensitivity variation in magnetic resonance imaging. Magn Reson Imaging. 1988;6(3):271–274.

[18] Teefey SA, Middleton WD, Payne WT, Yamaguchi K. Detection and measurement of rotator cuff tears with sonography: analysis of diagnostic errors. AJR Am J Roentgenol. 2005;184(6):1768–1773.

[19] Kerkhoffs GM, Blankevoort L, van Poll D, Marti RK, van Dijk CN. Anterior lateral ankle ligament damage and anterior talocrural-joint laxity: an overview of the in vitro reports. Clin Biomech (Bristol, Avon). 2001;16(8):635–643.

[20] Drakonaki EE, Allen GM, Wilson DJ. Ultrasound elastography for musculoskeletal applications. Br J Radiol. 2012;85(1019):1435–1445.

[21] Kot BC, Zhang ZJ, Lee AW, Leung VY, Fu SN. Elastic modulus of muscle and tendon with shear wave ultrasound elastography: variations with different technical settings. PLoS One. 2012;7(8):e44348

[22] Wiesinger HP, Rieder F, Kösters A, Müller E, Seynnes OR. Are sport-specific profiles of tendon stiffness and cross-sectional area determined by structural or functional integrity? PLoS One. 2016;11(6):e0158441.

[23] Zhang ZJ, Fu SN. Shear elastic modulus on patellar tendon captured from supersonic shear imaging: the relationship with tangent traction modulus computed from material testing and its dependence on gender, age and sport. PLoS One. 2013;8(8):e68216.

[24] Sanders TG, Medynski MA, Feller JF, Lawhorn KW. Bone contusion patterns of the knee at MR imaging: footprint of the mechanism of injury. Radiographics. 2000;20 Spec No:S135–151.

[25] Magee T. Comparison of 3-T MRI and arthroscopy of intrinsic wrist ligament and TFCC tears. AJR Am J Roentgenol. 2009;192(1):80–85.

[26] Johnson TR. Dual-energy CT: general principles. AJR Am J Roentgenol. 2012;199(5 Suppl):S3–8.

[27] Fukuda T, Umezawa Y, Asahina I, et al. Dual energy CT iodine map for delineating inflammation of inflammatory arthritis. Eur Radiol. 2017;27(12):5034–5040.

[28] Biercevicz AM, Akelman MR, Fadale PD, et al. MRI volume and signal intensity of ACL graft predict clinical, functional, and patient-oriented outcome measures after ACL reconstruction. Am J Sports Med. 2015;43(3):693–699.

[29] LaPrade RF, Engebretsen AH, Ly TV, Johansen S, Wentorf FA, Engebretsen L. The anatomy of the medial part of the knee. J Bone Joint Surg Am. 2007;89(9):2000–2010.
[30] Bencardino JT, Beltran J. MR imaging of the glenohumeral ligaments. Radiol Clin North Am. 2006;44(4):489–502, vii.
[31] Lee KT, Kim BK, Park YU, Kim KC, Choi JP, Kim JS. Transcatheter arterial embolization for chronic lateral ankle pain. J Am Podiatr Med Assoc. 2011;101(1):75–78.
[32] Bowring B, Chockalingam N. Conservative treatment of tibialis posterior tendon dysfunction—the how, when and what? Foot (Edinb). 2010;20(1):18–26.
[33] Timmerman LA, Schwartz ML, Andrews JR. Preoperative evaluation of the ulnar collateral ligament by magnetic resonance imaging and computed tomography arthrography. Am J Sports Med. 1994;22(1):26–31.
[34] Charalambous CP, Stanley JK. Posterolateral rotatory instability of the elbow. J Bone Joint Surg Br. 2008;90(3):272–279.
[35] Anderson ML, Skinner JA, Felmlee JP, Berger RA, Amrami KK. Diagnostic comparison of 1.5 Tesla and 3.0 Tesla preoperative MRI of the wrist in patients with ulnar-sided wrist pain. J Hand Surg Am. 2008;33(7):1153–1159.
[36] Ringler MD. MRI of wrist ligaments. J Hand Surg Am. 2013;38(10):2034–2046.
[37] Peterfy CG, Guermazi A, Zaim S, et al. Whole-organ magnetic resonance imaging score (WORMS) of the knee in osteoarthritis. Osteoarthritis Cartilage. 2004;12(3):177–190.
[38] Zhu Y, Jin Z, Niu X, et al. Optimized clinical application of platelet-rich plasma in the treatment of knee osteoarthritis: a systematic review and meta-analysis. J Orthop Surg Res. 2019;14(1):405.
[39] Erickson SJ, Prost RW, Timins ME. The 'magic angle' effect: background physics and clinical relevance. Radiology. 1993;188(1):23–25.
[40] Koch KM, Lorbiecki JE, Hinks RS, King KF. A multispectral three-dimensional acquisition technique for imaging near metal implants. Magn Reson Med. 2009;61(2):381–390.
[41] Ewertsen C, Carlsen JF, Seitz JM, Nielsen MB. Evaluation of healthy muscle tissue by strain and shear wave elastography — dependency on depth and ROI position in relation to the muscle fascia. Ultrasonics. 2016;71:127–133.
[42] Bem RA, Klochkov T, Shachaf E, Ben-Shabat T, Gilat R, Nachmias-Peiser N. Machine learning-based MRI diagnosis of anterior cruciate ligament tears: a systematic review. Knee Surg Sports Traumatol Arthrosc. 2023;31(5):1800–1810.
[43] Pourmorteza A, Symons R, Sandfort V, et al. Abdominal imaging with contrast-enhanced photon-counting CT: first human experience. Radiology. 2016;279(1):239–245.
[44] Springer E, Bohndorf K, Juras V, et al. Comparison of routine knee MRI with turbo spin-echo and 3D sequences at 3T. Eur Radiol. 2017;27(11):4583–4592.
[45] Guermazi A, Roemer FW, Haugen IK, Crema MD, Hayashi D. MRI-based semiquantitative scoring of joint pathology in osteoarthritis. Nat Rev Rheumatol. 2013;9(4):236–251.

2
Chapter

Quantitative Imaging Biomarkers: The Role of Radiomics in Cancer Diagnosis and Prognosis

[1]Srishti Gaur
M.Sc. Research Scholar
Department of Radiological Imaging Techniques, College of Paramedical Sciences, Teerthanker Mahaveer University, Moradabad
sgaur9830@gmail.com

[2]Mohd. Harish Saifi
M.Sc. Research Scholar
Department of Radiological Imaging Techniques, College of Paramedical Sciences, Teerthanker Mahaveer University, Moradabad
saifiharish350@gmail.com

[3]Rashmi Pandey
Assistant Professor,
Department of Radiological Imaging Techniques, College of Paramedical Sciences, Teerthanker Mahaveer University, Moradabad
rashmi.paramedical@tmu.ac.in

[4]Kashish
Department of Radiological Imaging Techniques, College of Paramedical Sciences,
COER University, Roorkee

Abstract

Radiomics is a procedure that allows for the extraction and analysis of quantitative data from clinical images. It is a developing field with numerous potential uses in clinical imaging. This chapter presents a full review of radiomics, encompassing its fundamental principles, technical elements, primary applications, and the problems involved in transferring it into medical practice. The chapter describes the key techniques utilized in the radiomics workflow, such as image acquisition, reconstruction, pre-processing, segmentation, feature extraction, and analysis. It also provides a review of notable outcomes in different contexts, with an emphasis on limits and potential solutions for medical adoption. This emphasizes the importance of having a complete understanding of existing methods as well as applications in order to realize radiomics' potential for encouraging precision medicine and enhancing patient care, especially in areas such as tumor detection, diagnosis, prognosis, and clinical assessment.

Keywords: Radiomics, Texture analysis, Image biomarkers(IBM), Radiogenomics, Oncology.

I. INTRODUCTION

Radiomics is a new and prospective area that uses radiography, mathematical modeling, and deep machine learning to interpret digital image textures. Its primary concept focuses around image biomarkers (IBMs), which are quantifiable values generated from digital pictures (such as CT, MRI, ultrasound, and PET scans) to define numerous pathological variations. These IBMs are especially important in cancer, where they provide a non-invasive method known as "virtual biopsy".

The fundamental goal of radiomics and texture analysis is to create standardized prognostic models that can predict medical outcomes using certain features. In oncology, a crucial diagnostic aspect is the reliable classification between benign and malignant tumors employing these non-invasive techniques. The field has advanced rapidly, with a large annual rise in published articles, showing its growing importance in in-depth digital picture analysis. Rapid and accurate identification of malignant tumors is critical for successful therapy and enhanced patient prognosis.

Despite traditional clinical imaging methods give anatomical and functional information, most of it may be unclear or minimally useful. Radiomics seeks to address these constraints by extracting and interpreting quantitative information from clinical images, so offering an objective assessment of tumor heterogeneity through pixel or voxel distribution and linkages. The purpose of this chapter is to investigate the characteristics of radiomics and textural analysis of healthcare images, with a focus on their present and potential applications in medical practice for non-invasive diagnosis of several cancers (1).

II. BASIC PRINCIPLE

Radiomics is a revolutionary diagnostic imaging technology that turns visual details from clinical images into quantitative, usable data. This technique goes beyond typical visual assessment by combining quantitative biomarkers and interpretative techniques to improve diagnostic and prognostic capacities.

1. General Workflow of Radiomics Analysis

Radiomics analysis is a number of consecutive procedures for processing clinical images and extracting significant data:

- **Image Acquisition:** This first phase is obtaining biomedical pictures, with parameters selected depend on the imaging modality, study goal (diagnostic or therapy planning), and tissue to be recognized.
- **Image Pre-processing:** Following acquisition, pictures are pre-processed to ensure uniformity and consistency in subsequent processes. This covers procedures like resampling, normalization, and filtering to reduce variations induced by acquisition/reconstruction protocols.
- **Segmentation:** This critical stage is determining the region of interest (ROI), which might be either a tumor or normal tissue. Proper segmentation is essential since it defines the uniqueness of the derived radiomics features. Segmentation can be performed manually, semi-automatically, or totally automatically.
- **Feature Extraction:** After the ROI has been segmented, quantitative characteristics are extracted. These traits are mathematically determined and classed as shape-based,

first-order, second-order, and higher-order statistics. The idea is to identify previously unnoticed picture patterns and create a radiomics signature.

- **Feature Analysis:** The extracted features are then analysed. This includes feature selection to discover highly relevant features, association analysis to analyze relationships, and model development, which frequently uses machine learning algorithms to develop predictive models (2).

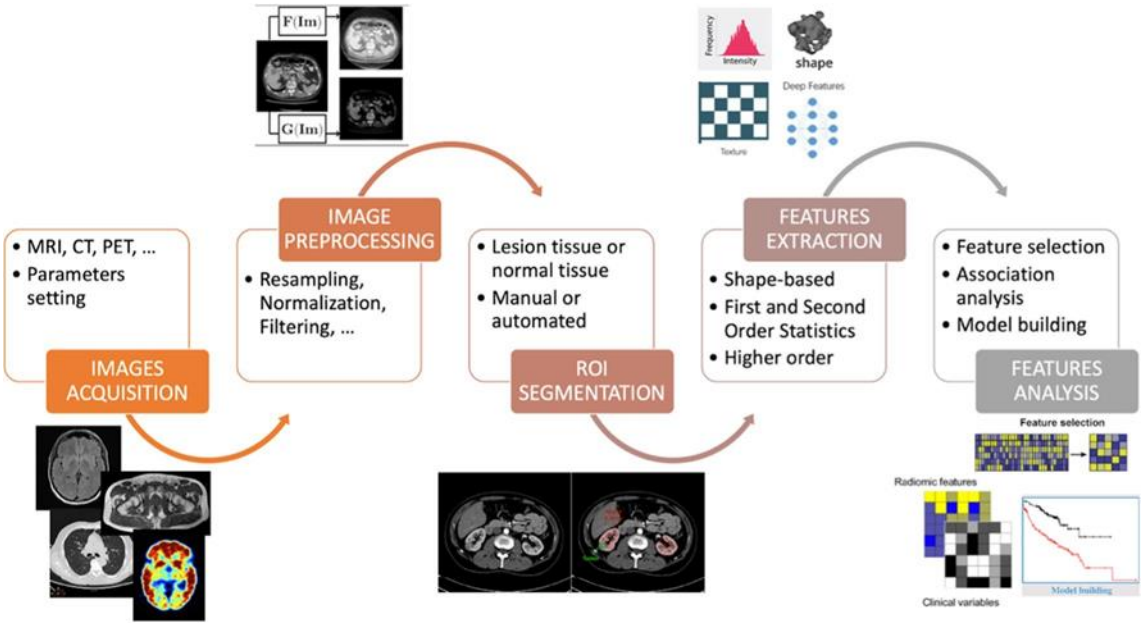

Figure 1: Radiomics workflow: The subsequent steps required in the radiomics process to extract radiomics features in clinical settings (2).

III. CLINICAL APPLICATION

Radiomics is a quantitative method to clinical imaging that turns ordinary images into usable data, making it an effective decision-support tool for precision medicine. Radiomics has a variety for medical uses, primarily in oncology, yet also in neurology and cardiology, by extracting features that indicate underlying pathology that is frequently unseen to the human eye.

1. Core Oncological Applications

Radiomics is most commonly used in cancer treatment, in which functions as a "virtual biopsy" to characterize tumors non-invasively.

- **Diagnosis and Differentiation:** Radiomics is used to differentiate benign from malignant lesions, like primary lung nodules or worrisome breast lumps. It may also differentiate between specific histological subtypes, such as small-cell and non-small-cell lung malignancies or different types of brain tumors.
- **Prognostication:** Radiomic characteristics are excellent indicators of medical results, namely overall survival (OS) and disease-free survival (DFS). Such as, in endometrial cancer, radiomic signals exceed clinicopathologic markers in predicting DFS.

- **Staging and Metastasis Prediction:** It aids in the preoperative prediction of lymph node metastases, minimizing reliance on invasive surgical staging. In lung cancer, it can forecast the probability of distant or brain lesions.
- **Treatment Response Monitoring:** Radiomics enables practitioners to measure the long-term efficacy of medicines like chemotherapy, radiation, and immunotherapy. It can detect non-responders early, permitting treatment changes.

2. Radiogenomics and Molecular Traits

Radiogenomics, a developing discipline, connects imaging features to gene expression and biological properties.

- **Mutation Prediction:** Radiomics may detect gene mutations, like EGFR or ALK alterations in pulmonary tumors, which is important for selecting targeted therapy.
- **Biological Markers:** It is utilized to forecast the expression of markers like Ki-67 in breast cancer and measure cell proliferation**.**

3. Immuno-Oncology

Radiomics offers insights into the tumor microenvironment, which is critical for effective immunotherapy.

- **Immune Infiltration**: The tool estimates CD8+ T-cell infiltration density, finding "hot" tumors that may react to immune checkpoint inhibitors.
- **Response to Immunotherapy**: Predictive models can assist identify patients who will benefit from immunotherapy in the long run, potentially preventing unwanted side effects.

4. Organ-Specific Applications

- **Lung Cancer:** Uses include discriminating between malignant nodules, estimating malignancy stage, and determining the severity of widespread pulmonary disease.
- **Breast Cancer:** It increases the diagnostic accuracy of mammography and MRI, predicts neoadjuvant chemotherapy (NAC) response, and identifies axillary lymph nodes.
- **Endometrial Cancer:** It is employed to predict deep myometrial invasion (DMI) and lymphovascular space invasion (LVSI) before surgery.
- **Neurology:** Radiomics has showed promise in identifying disease features in neurodegenerative disorders (e.g., Alzheimer's disease) and mental illnesses (such as schizophrenia).
- **Cardiology:** Quantitative analysis is utilized to characterize cardiovascular illnesses and diagnose myocardial infarctions in CT scans (1–10).

IV. ADVANTAGES

Radiomics includes multiple substantial advantages in the field of immuno-oncology, notably in lung cancer care, because it provides a thorough and quantitative approach to tumors investigation and biomarker identification.

1. Comprehensive Tumor Characterization

- Radiomics uses quantitative approaches to extract and evaluate characteristics from clinical pictures, providing a comprehensive understanding of cancer shape and heterogeneity. This feature solves the constraints of traditional biopsy, which is

frequently unrepresentative because tissue is collected from only a fraction of the tumor or non-lesional locations. Radiomics allows for a comprehensive and functional examination of the tumour phenotype by offering a 'virtual reconstruction' of it.

2. Biomarker Identification and Prediction

- Radiomic characteristics can aid in individualized diagnosis, therapy planning, and response tracking in medical practice. They may be applied to predict prognosis or therapy response, either independently or in conjunction with other data such as demographic, histological, genetic, or proteomic information.
- Radiomics reduces sampling bias in classic tumor indicators like PD-L1 expression and mutational load, which are limited by intratumoral heterogeneity. By examining the entire tumor, radiomics enables a more precise and multimodal forecast, revealing areas with diverse clonal populations intratumorally.
- It can assess cancer immune cell infiltration and predict response to anti-PD-1 therapy. For example, a radiomic signature was discovered that measures the intensity of cancer-infiltrating CD8 cells and was proven by pathologists' quantification of CD8 lymphocytes from tissue slides, resulting in longer overall survival in patients with metastatic solid tumors treated with PD-1/PD-L1 monotherapy.

3. Non-Invasive and Rapid Assessment

- Radiomics is a rapid and non-invasive approach for predicting and monitoring treatment response. This makes it a useful tool for evaluating numerous clinical indicators, such as therapy result, stage, and grade, as well as identifying the best therapy regimens in lung immuno-oncology.

4. Guiding Radiation Therapy and Precision Medicine

- Radiomics can identify high-risk and intratumoral areas, influencing immune responses and guiding radiation planning and administration. It aids in the definition of 'biological target volumes' (BTVs) within tumors, allowing for more precise radiation planning to improve local control and stimulate systemic immune responses.
- It supports radiomics-guided precision medicine by identifying patients who may benefit from immunotherapy, even those with low PD-L1 expression. Radiomics can also detect hypoxic patches within tumors that correlate to immune resistance, allowing doctors to pick individuals who are unlikely to respond to immunotherapy without the use of specialist imaging techniques (4).

V. LIMITATION AND CHALLENGES

1. Technical and Procedural Challenges

- **Lack of Standardization:** There is a substantial absence of uniformity throughout the radiomics workflow, notably for image capture and reconstruction procedures. Radiomics features are extremely susceptible to technical aspects like slice thickness, reconstruction techniques (kernels), scanner suppliers, and field strengths, which can introduce non-biological "noise" and produce incorrect findings.
- **Segmentation Subjectivity:** Determining the region of interest (ROI) is a significant cause of inaccuracy. Manual segmentation is known for being highly subjective, time-consuming, and susceptible to large intra- and inter-observer variability. Although automated tools exist, they frequently lack generalizability and can fail when used with diverse datasets.

- **Sensitivity to Processing:** Radiomics is intrinsically dependent on image properties such as pixel/voxel size and gray-level range. Variability in these settings, together with changes in picture discretization (binning), make it nearly hard to directly compare results from various investigations.

2. Interpretability and AI Challenges

- **The "Black-Box" Problem:** Practitioners frequently refer to deep learning models as "black boxes" since they are difficult to analyze and explain. Their sophisticated architectures make predictions without providing an understandable explanation of their fundamental mechanics, which is a significant impediment to developing medical trust.
- **Resource and Data Requirements:** Deep learning algorithms demand substantially larger datasets and greater processing capacities than classical radiomics to learn intrinsic representations directly from the data.

3. Clinical Translation and Collaboration Hurdles

- **Workflow Integration:** There is a noticeable absence of efficient integration interfaces between radiomics technologies and existing medical information systems such as PACS or RIS.
- **Data Silos:** The scarcity of high-quality, large-scale datasets is exacerbated by the proliferation of data silos and the lack of matching multi-omics data.
- **Collaboration Gaps:** Research frequently experiences a gap between high-output centers and high-impact research nodes. For example, some countries with high publishing numbers focus primarily on domestic collaboration, which may limit the worldwide applicability of their results.
- **Biobank Connectivity:** A current challenge has been to successfully connect image biobanks to tissue biobanks in order to fully exploit radiogenomics' promise.

4. Data and Methodological Limitations

- **High Dimensionality and Overfitting:** The extraction procedure might create countless features, resulting in a multidimensional feature space. Many of these features are redundant or unnecessary, resulting in model overfitting and reducing classification algorithm performance.
- **Validation Gaps:** Several radiomics findings need adequate external validation across large-scale, independent, and multicenter datasets. Many recent studies are retrospective, providing less data than prospective medical studies.
- **Feature Inconsistency:** There is no broad agreement on the nomenclature, definition, or evaluation techniques for many radiomic characteristics, resulting in poor reproducibility (2,5,9).

VI. CONCLUSION

Radiomics provides a paradigm shift in clinical imaging, transitioning from a solely qualitative visual tool to a source of quantitative, high-dimensional data. It functions as a "virtual biopsy," providing a non-invasive and thorough evaluation of tumor diversity, while successfully overcoming the sampling restrictions and biases common to standard physical biopsies. Its diverse uses—ranging from increasing diagnostic accuracy and staging to predicting treatment responses and finding genetic alterations via radiogenomics—highlight its promise as a vital component of precision medicine. Although this promise, the industry must overcome severe technical and clinical difficulties in order to achieve successful

medical acceptance. The absence of uniformity in picture acquisition and reconstruction, the subjectivity of manual segmentation, and the "black-box" nature of deep learning models now hamper the accuracy and interpretability required for therapeutic confidence. Moreover, addressing data silos and the necessity for large-scale, multicenter validation is critical to ensuring radiomic signature reproducibility. To summarize, however radiomics is a potent decision-support tool for cancer and beyond, its future relies on more collaboration between researchers and practitioners to bridge the gap between high-impact research and ordinary medical practice. By refining these approaches and incorporating them into existing medical systems, radiomics can accomplish its efficacy to personalize medicine and greatly improve patient outcomes.

REFERENCES

[1] Litvin AA, Burkin DA, Kropinov AA, Paramzin FN. Radiomics and Digital Image Texture Analysis in Oncology (Review). Sovrem Tehnol V Med. 2021 Apr;13(2):97. doi:10.17691/stm2021.13.2.11

[2] Scapicchio C, Gabelloni M, Barucci A, Cioni D, Saba L, Neri E. A deep look into radiomics. Radiol Med (Torino). 2021 Oct;126(10):1296–311. doi:10.1007/s11547-021-01389-x

[3] Pan F, Feng L, Liu B, Hu Y, Wang Q. Application of radiomics in diagnosis and treatment of lung cancer. Front Pharmacol. 2023 Nov 1;14:1295511. doi:10.3389/fphar.2023.1295511

[4] Yan W, Quan C, Mourad WF, Yuan J, Shi Z, Yang J, et al. Application of radiomics in lung immuno-oncology. Precis Radiat Oncol. 2023 Jun;7(2):128–36. doi:10.1002/pro6.1191

[5] Teng X, Luo QN, Chen YD, Peng T. From texture analysis to artificial intelligence: global research landscape and evolutionary trajectory of radiomics in hepatocellular carcinoma. Discov Oncol. 2025 Sep 24;16(1):1694. doi:10.1007/s12672-025-03620-x

[6] Zim C. Importance of Radiomics in Monitoring Disease Progression and Predicting Cancer.

[7] Renton M, Fakhriyehasl M, Weiss J, Milosevic M, Laframboise S, Rouzbahman M, et al. Multiparametric MRI radiomics for predicting disease-free survival and high-risk histopathological features for tumor recurrence in endometrial cancer. Front Oncol. 2024 Aug 2;14:1406858. doi:10.3389/fonc.2024.1406858

[8] Lee SH, Park H, Ko ES. Radiomics in Breast Imaging from Techniques to Clinical Applications: A Review. Korean J Radiol. 2020;21(7):779. doi:10.3348/kjr.2019.0855

[9] Van Timmeren JE, Cester D, Tanadini-Lang S, Alkadhi H, Baessler B. Radiomics in medical imaging—“how-to” guide and critical reflection. Insights Imaging. 2020 Dec;11(1):91. doi:10.1186/s13244-020-00887-2

[10] Chen M, Linton-Reid K, Aboagye EO, Copley SJ. Translating radiomics into clinical practice: A step-by-step guide to study design and evaluation. Clin Radiol. 2025 Nov;90:107053. doi:10.1016/j.crad.2025.107053

3
Chapter

Contrast-Enhanced Imaging Techniques and Quantification

[1]Shubhanshi Rani,
Assistant Professor,
College of Allied and Healthcare
Sciences, GIMS, Greater Noida

Abstract

Contrast-enhanced imaging has become indispensable in modern diagnostic radiology, enabling superior delineation of lesions, vascular structures, and organ parenchyma that would otherwise remain occult on unenhanced acquisitions. This chapter provides a comprehensive and critical overview of contrast-enhanced imaging techniques spanning computed tomography (CT), magnetic resonance imaging (MRI), contrast-enhanced ultrasound (CEUS), and nuclear medicine/positron emission tomography (PET). The physicochemical properties and pharmacokinetic behaviour of iodinated agents, gadolinium-based contrast agents (GBCAs), microbubble suspensions, and radiolabelled tracers are discussed in relation to their tissue distribution, enhancement patterns, and safety profiles. Quantitative methods—including Hounsfield Unit (HU) measurement, signal-to-noise ratio (SNR), contrast-to-noise ratio (CNR), iodine delivery rate (IDR), and dynamic contrast enhancement (DCE) modelling—are explained with reference to current evidence and clinical protocols. Organ-specific enhancement phases, injection parameters, and image quality optimisation strategies are addressed for each modality. The chapter also examines emerging quantitative biomarkers, artificial intelligence-assisted analysis, and hybrid imaging approaches that are reshaping precision diagnosis. A thorough understanding of these techniques is essential for radiographers, radiologists, and clinical researchers engaged in advanced multimodal imaging practice.

Keywords: Contrast agents; Hounsfield unit; iodinated contrast; gadolinium; microbubbles; dynamic contrast enhancement; SNR; CNR; iodine delivery rate; quantitative imaging; PET; multimodal radiology.

I. INTRODUCTION

The administration of exogenous contrast agents has transformed diagnostic imaging over the past six decades, substantially expanding the diagnostic capability of radiological examinations. From the first intravenous iodinated compounds used in urography to contemporary nanoparticle-based agents and bimodal tracers, contrast media have evolved in parallel with advances in scanner technology, acquisition protocols, and quantitative post-processing. Today, contrast-enhanced studies constitute a large proportion of all cross-sectional imaging performed globally, with an estimated 80 million contrast-enhanced CT examinations and over 30 million MRI studies employing gadolinium-based agents annually.[1,2]

Contrast agents enhance image quality by altering the intrinsic signal or attenuation characteristics of tissues relative to background structures, thereby improving lesion conspicuity, vascular opacification, and functional organ assessment. However, their diagnostic value is critically dependent on a thorough understanding of agent pharmacokinetics, injection parameters, scan timing, and modality-specific acquisition factors. Inappropriate agent selection, injection rate errors, or suboptimal scan timing can substantially degrade diagnostic quality or introduce artefacts that compromise interpretation.[3]

Equally important is quantitative analysis. Raw visual interpretation, while clinically valuable, introduces observer variability and is insufficient for longitudinal treatment monitoring or multicentre research. Quantitative imaging biomarkers derived from contrast-enhanced studies—such as HU attenuation values, enhancement ratios, permeability coefficients from DCE modelling, and standardised uptake values (SUV) in PET—offer reproducible, objective metrics that support evidence-based clinical decisions and research endpoints.[4,5]

This chapter systematically addresses contrast-enhanced imaging across the principal clinical modalities. It is structured to provide depth in both technique and quantification, reflecting the dual demands placed on contemporary radiological professionals who must be proficient in image acquisition and in the extraction and interpretation of quantitative data.

II. CONTRAST-ENHANCED COMPUTED TOMOGRAPHY

1. Iodinated Contrast Agents: Properties and Classification

Iodinated contrast agents (ICAs) attenuate X-rays through the photoelectric effect of iodine, which has a K-edge at 33.2 keV, within the diagnostic energy range of clinical CT systems.[6] Contemporary agents are classified as ionic or non-ionic, and as monomeric or dimeric, with the non-ionic monomers and dimers dominating current clinical use owing to their superior safety profiles. High-osmolality ionic agents (e.g., diatrizoate) have been largely superseded by low-osmolality non-ionic monomers (e.g., iohexol, iopamidol, iopromide, iomeprol) and iso-osmolal dimers (e.g., iodixanol).[7]

The iodine concentration of commercial preparations ranges from 240 to 400 mg I/mL. Higher concentrations afford greater attenuation per unit volume but increase viscosity, which influences injectability and necessitates warming the agent to 37°C to reduce viscosity and injection pressure. The iodine delivery rate (IDR), defined as the product of injection

flow rate (mL/s) and iodine concentration (mg I/mL), expressed in mg I/s, is a pivotal determinant of peak aortic and parenchymal enhancement. Typically, an IDR of 1.5–2.0 g I/s is targeted for abdominal CT to achieve consistent hepatic arterial phase enhancement.[8]

Volume of distribution of ICAs is predominantly extracellular; they do not cross the intact blood–brain barrier and are eliminated almost entirely by glomerular filtration with a plasma half-life of approximately 1.5–2 hours in patients with normal renal function. In patients with reduced estimated glomerular filtration rate (eGFR), delayed clearance prolongs vascular and interstitial enhancement and increases the risk of contrast-induced acute kidney injury (CI-AKI), necessitating pre-procedural renal function assessment.[9]

2. Injection Protocols and Enhancement Phases

Enhancement in CT is a dynamic, time-dependent phenomenon. Following bolus intravenous injection, contrast propagates through the pulmonary circulation to the systemic arterial tree and subsequently distributes into the interstitial compartment. For abdominal imaging, four principal enhancement phases are recognised: (i) the non-contrast baseline, (ii) the arterial phase (25–35 s post-injection), (iii) the portal venous phase (60–75 s), and (iv) the delayed or equilibrium phase (180–300 s). Hepatic lesion characterisation frequently employs a three-phase or four-phase protocol to exploit differential enhancement kinetics between hepatocellular carcinoma, metastases, and benign entities such as haemangioma.[10]

Scan timing can be determined by fixed delay, automatic bolus tracking (e.g., SmartPrep, Sure-Start), or test bolus methods. Bolus tracking, which triggers acquisition when attenuation in a monitoring region-of-interest (ROI) placed in the aorta reaches a predefined threshold (typically 100–150 HU), is widely adopted as it accounts for individual cardiovascular transit time variability and is more reliable than fixed delays in patients with cardiac dysfunction or altered haemodynamics.[11]

Standard injection parameters for adult abdominal CT include a weight-adapted contrast volume (1.5–2.0 mL/kg body weight or fixed doses of 100–150 mL), flow rates of 3–5 mL/s via an antecubital vein cannula (minimum 20-gauge), followed by a saline flush of 30–50 mL at the same flow rate to push residual contrast from the injection tubing and reduce streak artefact from the superior vena cava.[8,12]

3. Quantitative Metrics in CT Enhancement

The Hounsfield Unit (HU) is the fundamental quantitative metric in CT, calibrated so that distilled water measures 0 HU and air measures −1000 HU. Tissue attenuation is given by:

$$HU = 1000 \times (\mu tissue - \mu water) / \mu water$$

where μ represents the linear attenuation coefficient. In contrast-enhanced CT, absolute HU measurements in an ROI provide the basis for enhancement quantification. Enhancement is calculated as the difference in mean HU between the contrast-enhanced and unenhanced acquisitions (ΔHU). Normal liver parenchyma in the portal venous phase typically attenuates at 100–140 HU (baseline ~55–65 HU), yielding a ΔHU of approximately 40–80 HU, with values below 20 HU considered indicative of suboptimal enhancement.[13]

Signal-to-noise ratio (SNR) in CT is defined as the ratio of mean ROI attenuation to the standard deviation of noise measured in a homogeneous region, typically a water-equivalent phantom or uniform organ parenchyma:

$$SNR = Mean\ HU\ (ROI)\ /\ SD\ (noise)$$

Contrast-to-noise ratio (CNR) extends this to express the conspicuity of a structure of interest relative to its background:

$$CNR = (Mean\ HU\ target - Mean\ HU\ background)\ /\ SD\ (noise)$$

These metrics are sensitive to tube voltage (kVp), tube current (mAs), slice thickness, reconstruction kernel, and iterative reconstruction algorithm. Dual-energy CT (DECT) offers the added capability of iodine quantification through material decomposition algorithms, producing iodine density maps that are independent of background tissue attenuation and enabling virtual non-contrast (VNC) image generation.[14,15]

ROI placement methodology is a critical determinant of measurement reproducibility. Consensus guidelines recommend ROIs occupying at least 1 cm^2 placed in homogeneous parenchymal regions, avoiding vessels, bile ducts, focal lesions, and image artefacts. Multiple ROI measurements should be averaged, and intra- and inter-observer variability documented in research settings.[13]

III. CONTRAST-ENHANCED MAGNETIC RESONANCE IMAGING

1. Gadolinium-Based Contrast Agents

Gadolinium (Gd^{3+}) is a lanthanide metal with seven unpaired electrons, conferring potent paramagnetic properties that shorten tissue T1 (longitudinal) and T2 (transverse) relaxation times. The predominant clinical effect at standard concentrations is T1 shortening, producing signal enhancement on T1-weighted sequences. Free gadolinium ions are highly toxic; therefore, all clinical GBCAs chelate the Gd^{3+} ion within either linear or macrocyclic ligands, with macrocyclic agents demonstrating superior thermodynamic and kinetic stability and reduced risk of gadolinium dissociation.[16]

GBCAs are broadly classified by their distribution characteristics. Extracellular agents (e.g., gadoterate meglumine, gadobutrol, gadopentetate dimeglumine) distribute throughout the intravascular and interstitial compartments and are suitable for routine vascular, musculoskeletal, and parenchymal imaging. Hepatobiliary agents (e.g., gadoxetic acid/Gd-EOB-DTPA, gadobenate dimeglumine) are taken up by functioning hepatocytes via organic anion transporter proteins (OATPs) and excreted into bile, enabling hepatocyte-phase imaging at 15–20 minutes post-injection for characterisation of focal hepatic lesions.[17,18]

Blood-pool agents (e.g., gadofosveset trisodium) bind reversibly to serum albumin, prolonging intravascular residence and enabling high-resolution steady-state MR angiography. Safety concerns regarding nephrogenic systemic fibrosis (NSF) in patients with severe renal impairment have led to the preferential use of macrocyclic agents and revised EMA/ACR risk stratification guidelines for GBCA administration.[19]

2. Dynamic Contrast Enhancement MRI: Acquisition and Modelling

Dynamic contrast-enhanced MRI (DCE-MRI) involves serial T1-weighted acquisitions before and after GBCA injection to characterise tissue perfusion, permeability, and extracellular volume fraction. The technique is particularly valuable in oncology for tumour vascularity assessment, treatment response monitoring, and grading of neoangiogenesis.[20]

Semi-quantitative parameters derived from the signal intensity–time curve include: the initial area under the gadolinium concentration curve (IAUGC), time to peak (TTP), maximum enhancement ratio (MER), and wash-in/wash-out slopes. While computationally straightforward, these parameters are scanner- and sequence-dependent and do not directly reflect underlying physiology.[21]

Fully quantitative pharmacokinetic modelling requires conversion of signal intensity to gadolinium concentration (using a pre-contrast T1 map) and measurement of the arterial input function (AIF). The extended Tofts model is widely applied:

$$Ct(t) = Ktrans \otimes Cp(t) \cdot exp(-(Ktrans/ve) \cdot t) + vp \cdot Cp(t)$$

where Ct(t) is tissue gadolinium concentration, Cp(t) is the plasma concentration (AIF), K^trans is the volume transfer constant (reflecting combined perfusion and permeability), ve is the extravascular extracellular volume fraction, and vp is the plasma volume fraction. These parameters have been validated as imaging biomarkers in breast cancer, prostate cancer, and gliomas.[20,22]

3. Quantification of MRI Enhancement

In clinical MRI, enhancement is most commonly expressed as percentage signal intensity increase: SI% = [(SIpost − SIpre) / SIpre] × 100. However, this metric is influenced by background field inhomogeneity, receive coil sensitivity variation, and gain settings. Normalisation to an internal reference tissue (e.g., muscle, cerebrospinal fluid) improves comparability across acquisitions. Quantitative T1 mapping using inversion recovery or variable flip angle (VFA) methods provides agent concentration estimates independent of scanner settings and is the preferred approach in research.[23]

SNR in MRI is defined analogously to CT but expressed in signal intensity units:

$$SNR = Mean\ SI\ (ROI) / SD\ of\ background\ noise$$

CNR between two tissues A and B is: CNR = (SIA − SIB) / SD (noise). Both metrics depend on field strength, sequence parameters (TR, TE, flip angle), and coil configuration. At 3T relative to 1.5T, SNR approximately doubles, enabling higher spatial resolution or reduced acquisition time without SNR penalty, though susceptibility artefacts and specific absorption rate (SAR) constraints require protocol adjustments.[24]

IV. CONTRAST-ENHANCED ULTRASOUND

1. Microbubble Agents: Physics and Characteristics

Contrast-enhanced ultrasound (CEUS) employs suspensions of gas-filled microbubbles as intravascular contrast agents. Commercially available agents include SonoVue/Lumason (sulphur hexafluoride, SF6, within a phospholipid shell) and Optison (octafluoropropane

within an albumin shell). Microbubbles have diameters of 1–10 μm, comparable to red blood cells, enabling free passage through the pulmonary capillary bed but confining them to the intravascular space.[25]

Under low-mechanical-index (MI < 0.1) insonation, microbubbles undergo non-linear oscillation (stable cavitation), generating harmonic signals at multiples of the transmitted frequency that are exploited by pulse-inversion and amplitude-modulation techniques to selectively display microbubble signal while suppressing tissue background. At high MI, microbubbles undergo inertial cavitation and destruction, a property exploited in destruction-reperfusion perfusion imaging protocols.[26]

2. Clinical Applications and Enhancement Phases

Unlike CT and MRI, CEUS provides pure intravascular imaging with real-time continuous acquisition and no radiation exposure. In the liver, three enhancement phases are identified: arterial (10–45 s), portal venous (45–120 s), and late/sinusoidal phase (120–300 s). Hepatocellular carcinoma typically demonstrates arterial hyperenhancement followed by wash-out in the portal venous and late phases, distinguishing it from most benign lesions. CEUS-guided procedures—including targeted biopsy of iso-attenuating CT lesions—represent a growing application.[27]

Quantitative CEUS (Q-CEUS) extracts time-intensity curves (TICs) from a user-defined ROI, from which parameters including peak intensity (PI), time to peak (TTP), area under the curve (AUC), wash-in rate (WiR), and wash-out rate (WoR) are derived through log-normal or lognormal curve fitting. These parameters correlate with microvascular density and perfusion in tumour models and are being evaluated as biomarkers in oncological treatment response.[28]

3. Quantitative Analysis and Limitations

Quantitative CEUS is constrained by several technical factors that must be acknowledged in research settings. Signal saturation at high microbubble concentrations produces non-linear TICs requiring low-dose injection protocols (0.5–1.0 mL for liver studies). Motion artefact, particularly in the liver and kidneys during free breathing, introduces variability in ROI measurements. Software compensation algorithms and breath-hold acquisitions mitigate but do not eliminate this limitation. Inter-platform variability in signal processing and curve fitting algorithms further complicates multicentre standardisation.[29]

V. CONTRAST ENHANCEMENT IN NUCLEAR MEDICINE AND PET

1. Radiolabelled Tracers as Functional Contrast Agents

Nuclear medicine and PET differ fundamentally from anatomical imaging modalities in that tracer uptake reflects metabolic, receptor, or flow-dependent physiological processes rather than non-specific extracellular distribution. Radiolabelled tracers—including ^{18}F-fluorodeoxyglucose (^{18}F-FDG), ^{68}Ga-PSMA, ^{68}Ga-DOTATATE, and ^{13}N-ammonia—are administered at nanomolar concentrations, orders of magnitude below the pharmacological threshold, thereby providing functional contrast without haemodynamic or pharmacological effects.[30]

^{18}F-FDG, the most widely used PET tracer, accumulates in cells with upregulated glucose metabolism via GLUT transporter overexpression and is phosphorylated by hexokinase to FDG-6-phosphate, which is trapped intracellularly. Standardised uptake value (SUV) normalises tracer concentration to injected dose and body weight:

```
SUV = [Tissue radioactivity concentration (kBq/mL)] /
      [Injected dose (kBq) / Body weight (g)]
```

SUVmax (maximum pixel value in lesion ROI) and SUVmean (mean over a defined ROI) are the most commonly reported metrics in oncological PET. SUVmax is more reproducible but susceptible to noise; SUVmean requires accurate lesion segmentation. Total lesion glycolysis (TLG = SUVmean × metabolic tumour volume) provides a volumetric measure of metabolic burden.[31]

2. Dynamic PET and Parametric Imaging

Dynamic PET acquisition captures tracer kinetics from injection through equilibration, enabling full compartmental modelling analogous to DCE-MRI. The two-tissue compartmental model for ^{18}F-FDG yields rate constants K1–k4 and the metabolic rate of glucose utilisation (MRGlu = K1·k3/(k2+k3) × plasma glucose/lumped constant). While gold-standard for quantitative research, dynamic PET requires prolonged scanner occupancy and complex data processing, limiting routine clinical adoption. Parametric Patlak analysis offers a simplified approach applicable over the linear phase (60–90 min post-injection) with reduced acquisition demands.[32]

3. PET/CT and PET/MRI Hybrid Quantification

Hybrid PET/CT systems enable simultaneous acquisition of functional PET data and anatomical CT information, with the CT serving dual roles as an attenuation correction map and a morphological correlate. PET/MRI offers superior soft tissue contrast for anatomical localisation without ionising radiation from CT, though MR-based attenuation correction introduces greater uncertainty than CT-based methods. In quantitative research, cross-calibration between PET scanner activity concentration and the dose calibrator is mandatory to ensure accurate SUV calculation.[33]

VI. SAFETY CONSIDERATIONS ACROSS MODALITIES

1. Iodinated Contrast Agent Safety

Adverse reactions to ICAs are classified as acute (within 1 hour) or delayed (1 hour–7 days). Acute reactions range from mild (nausea, urticaria) to severe anaphylactoid reactions requiring immediate resuscitation. The incidence of severe reactions with non-ionic agents is approximately 0.04%, substantially lower than with ionic agents. Pre-medication with corticosteroids and antihistamines is recommended for patients with a documented prior moderate-to-severe reaction. CI-AKI risk stratification requires pre-procedure eGFR measurement, with particular vigilance in diabetic patients on metformin, which should be withheld 48 hours post-contrast in eGFR < 60 mL/min/1.73 m².[9,34]

2. Gadolinium Safety and Retention

NSF is a potentially fatal fibrosing disorder occurring in patients with advanced renal failure exposed to linear GBCAs. Current ACR and ESUR guidelines restrict Group I high-risk agents (e.g., gadodiamide, gadopentetate dimeglumine) in patients with eGFR < 30 mL/min/1.73 m² and recommend macrocyclic agents as the preferred choice. Gadolinium retention in brain tissue, bone, and skin has been reported following repeated exposure to both linear and macrocyclic GBCAs, though clinical consequences remain uncertain and are under investigation.[19,35]

3. Microbubble Safety and Radiation in PET

Microbubble agents have an excellent safety profile; serious adverse events are exceedingly rare (approximately 1:10,000 injections). Relative contraindications include right-to-left cardiac shunts and severe pulmonary hypertension. In nuclear medicine, radiation dose to the patient depends on the tracer administered; for ^{18}F-FDG at a standard dose of 185–370 MBq, effective dose is approximately 5–10 mSv. Optimal patient preparation—including a 6-hour fast to minimise competing glucose uptake and stable normoglycaemia—is essential for reproducible quantification.[30,36]

VII. EMERGING TECHNIQUES AND QUANTITATIVE BIOMARKERS

1. Dual-Energy CT and Spectral Imaging

Dual-energy CT (DECT) acquires data at two different X-ray spectra (typically 80/140 kVp or using dual-layer detector technology), enabling material decomposition into basis pairs (e.g., iodine/water, calcium/water). Iodine quantification maps provide objective iodine concentration measurements in mg/mL that are independent of background tissue attenuation and scanner platform, offering advantages over HU-based enhancement metrics in heterogeneous tissues. Spectral CT with photon-counting detectors (PCD-CT)—representing the most recent technological advance—enables multi-energy bin acquisition, improved spatial resolution, and reduced electronic noise, with preliminary evidence of superior iodine quantification accuracy.[14,37]

2. Artificial Intelligence in Contrast-Enhanced Image Analysis

Machine learning and deep learning algorithms are increasingly being applied to contrast-enhanced imaging for automated lesion detection, segmentation, and quantification. Convolutional neural networks (CNNs) have demonstrated radiologist-comparable performance in hepatocellular carcinoma detection on multiphasic CT and MRI. Radiomic feature extraction from contrast-enhanced images—encompassing first-order statistics, texture, and wavelet features—provides high-dimensional phenotyping of lesions that may predict histological grade, genomic subtypes, and treatment response beyond visual assessment.[38,39]

3. Abbreviated and Ultrafast Protocols

Abbreviated MRI protocols for hepatocellular carcinoma surveillance, comprising non-contrast T2 and gadoxetic acid hepatobiliary phase T1 imaging, have shown sensitivity comparable to full multiphasic protocols with substantially reduced scan time and cost.

Ultrafast DCE-MRI using compressed sensing and simultaneous multi-slice techniques now achieves temporal resolution below 5 seconds per 3D volume, permitting reliable AIF measurement and improving pharmacokinetic model fitting accuracy.[40]

VIII. STANDARDISATION AND QUALITY ASSURANCE IN QUANTITATIVE CONTRAST IMAGING

Reliable quantitative imaging requires rigorous standardisation at every stage of the imaging chain. Scanner calibration—including HU linearity, noise characterisation, and spatial resolution assessment—should be performed according to manufacturer specifications and regulatory guidelines, with phantom-based QA at defined intervals. Injection system calibration, power injector maintenance, and catheter patency checks are prerequisite to reproducible contrast delivery.[41]

ROI placement protocols should be pre-specified in research studies, with documented criteria for ROI size, placement location, exclusion of artefacts, and the number of measurements to be averaged. Inter-reader reproducibility studies using intraclass correlation coefficients (ICC) and Bland-Altman analysis are recommended for all quantitative endpoints prior to study commencement. Platform-specific variability in DICOM viewer HU readouts is an emerging consideration; comparative studies have highlighted statistically significant differences between viewer platforms even when processing identical DICOM datasets, underscoring the need for standardised analysis tools in multicentre research.[42]

For PET quantification, scanner harmonisation using National Electrical Manufacturers Association (NEMA) NU-2 phantoms and EARL (EANM Research Ltd) accreditation programmes establish SUV recovery coefficient standards that enable cross-scanner comparability in multicentre trials. Similar harmonisation frameworks for CT-based iodine quantification and MRI DCE parameters remain areas of active research and international consensus development.[43]

IX. CLINICAL APPLICATIONS OF QUANTITATIVE CONTRAST-ENHANCED IMAGING

Quantitative contrast-enhanced imaging underpins clinical decision frameworks across virtually all organ systems. In oncology, RECIST 1.1 and modified RECIST criteria for hepatocellular carcinoma incorporate enhancement criteria, recognising that purely size-based response assessment is insufficient for targeted therapies and immunotherapy. Quantitative DCE-MRI parameters (K^trans, kep) are incorporated as secondary endpoints in multiple phase II/III trials assessing anti-angiogenic agents.[44]

In cardiovascular imaging, myocardial perfusion quantification using first-pass CT or cardiac MRI provides absolute myocardial blood flow values in mL/g/min that stratify ischaemic burden and guide revascularisation decisions. CT perfusion of the brain, employing contrast bolus tracking, generates parametric maps of cerebral blood flow (CBF), cerebral blood volume (CBV), mean transit time (MTT), and time-to-peak (TTP), enabling rapid identification of ischaemic penumbra in acute stroke for thrombectomy patient selection.[45,46]

In the liver, gadoxetic acid MRI combines arterial phase enhancement, diffusion-weighted imaging, and hepatobiliary phase uptake to characterise focal lesions within an integrated assessment. The LI-RADS (Liver Imaging Reporting and Data System) framework provides

a standardised, reproducible classification of hepatic observations using predefined major and ancillary imaging features, reducing inter-reader variability in high-risk population surveillance.[47]

X. CONCLUSION

Contrast-enhanced imaging represents one of the most powerful and information-rich domains within diagnostic radiology, encompassing a diverse portfolio of agents, techniques, and quantitative methodologies. This chapter has reviewed the physicochemical and pharmacokinetic principles governing iodinated, gadolinium-based, microbubble, and radiolabelled contrast agents; presented the technical and quantitative frameworks for CT, MRI, CEUS, and PET; and outlined critical safety, standardisation, and emerging technology considerations.

Mastery of these topics requires integration of physics, pharmacology, clinical protocol design, and quantitative data analysis—competencies that define the modern radiological scientist and advanced practitioner. As imaging technology continues to evolve toward higher temporal resolution, spectral capability, and AI-augmented analysis, the importance of a robust foundational understanding of contrast mechanism and quantification will only intensify.

Future directions include the development of organ-targeted nanoparticle contrast agents with prolonged enhancement windows, multimodal agents detectable by both MRI and PET, and biologically responsive 'smart' probes that signal specific molecular events. Integration of quantitative imaging biomarkers into precision medicine frameworks—supporting risk stratification, treatment planning, and response monitoring at the individual patient level—represents the translational endpoint toward which current research is collectively directed.

REFERENCES

[1] Lusic H, Grinstaff MW. X-ray-computed tomography contrast agents. Chem Rev. 2013;113(3):1641–1666. doi:10.1021/cr200358s
[2] Sherry AD, Caravan P, Lenkinski RE. Primer on gadolinium chemistry. J Magn Reson Imaging. 2009;30(6):1240–1248. doi:10.1002/jmri.21966
[3] Dawson P. Functional imaging in CT. Eur J Radiol. 2006;60(3):331–340. doi:10.1016/j.ejrad.2006.06.023
[4] O'Connor JPB, Aboagye EO, Adams JE, et al. Imaging biomarker roadmap for cancer studies. Nat Rev Clin Oncol. 2017;14(3):169–186. doi:10.1038/nrclinonc.2016.162
[5] Sullivan DC, Obuchowski NA, Kessler LG, et al. Metrology standards for quantitative imaging biomarkers. Radiology. 2015;277(3):813–825. doi:10.1148/radiol.2015142202
[6] Prokop M, Galanski M. Spiral and Multislice Computed Tomography of the Body. Stuttgart: Thieme; 2003.
[7] Morcos SK, Thomsen HS, Webb JA. Contrast-media-induced nephrotoxicity: a consensus report. Contrast Media Safety Committee, European Society of Urogenital Radiology (ESUR). Eur Radiol. 1999;9(8):1602–1613. doi:10.1007/s003300050894
[8] Bae KT. Intravenous contrast medium administration and scan timing at CT: considerations and approaches. Radiology. 2010;256(1):32–61. doi:10.1148/radiol.10090908
[9] ACR Committee on Drugs and Contrast Media. ACR Manual on Contrast Media. Version 2023. Reston, VA: American College of Radiology; 2023.
[10] Ichikawa T, Saito K, Yoshioka N, et al. Detection of hypervascular hepatocellular carcinoma: combined phase CT methods using gadoxetic acid-enhanced MRI and MDCT. AJR Am J Roentgenol. 2009;192(6):1500–1507. doi:10.2214/AJR.08.1186
[11] Fleischmann D, Rubin GD, Bankier AA, et al. Improvements in depiction of hepatic arteries with multisection CT angiography using a test bolus injection. Radiology. 2000;216(2):555–563. doi:10.1148/radiology.216.2.r00au21555

[12] Hittmair K, Fleischmann D. Accuracy of predicting and controlling time-dependent aortic enhancement from a test bolus injection. J Comput Assist Tomogr. 2001;25(2):287–294. doi:10.1097/00004728-200103000-00019
[13] Shim YS, Abramson RG, Su YC, et al. Standardized method of CT attenuation measurement in the liver. Acad Radiol. 2020;27(1):21–28. doi:10.1016/j.acra.2019.04.009
[14] Rajiah PS, Bhatt S, Nagpal P, et al. Update on dual-energy CT: physics, principles, and applications. Radiographics. 2020;40(5):1284–1308. doi:10.1148/rg.2020200038
[15] Lv P, Liu J, Chai Y, et al. Automatic spectral imaging protocol and iterative reconstruction in abdominal CT: initial experience. Eur Radiol. 2018;28(3):1187–1195. doi:10.1007/s00330-017-5029-z
[16] Caravan P. Strategies for increasing the sensitivity of gadolinium based MRI contrast agents. Chem Soc Rev. 2006;35(6):512–523. doi:10.1039/b510982p
[17] Zech CJ, Reiser MF, Herrmann KA. Parenchymal liver enhancement with gadolinium ethoxybenzyl diethylenetriamine pentaacetic acid at standard and high doses: intraindividual comparison. Invest Radiol. 2009;44(9):559–564. doi:10.1097/RLI.0b013e3181aaf2e1
[18] Motosugi U, Ichikawa T, Sou H, et al. Distinguishing hypervascular pseudolesions of the liver from hypervascular hepatocellular carcinomas with gadoxetic acid-enhanced MR imaging. Radiology. 2010;256(1):151–158. doi:10.1148/radiol.10091886
[19] European Medicines Agency. Assessment report: gadolinium-containing contrast agents. EMA/740446/2017. London: EMA; 2017.
[20] Tofts PS, Brix G, Buckley DL, et al. Estimating kinetic parameters from dynamic contrast-enhanced T1-weighted MRI of a diffusable tracer: standardized quantities and symbols. J Magn Reson Imaging. 1999;10(3):223–232. doi:10.1002/(sici)1522-2586(199909)10:3<223::aid-jmri2>3.0.co;2-s
[21] Jackson A, O'Connor JPB, Parker GJM, et al. Imaging tumor vascular heterogeneity and angiogenesis using dynamic contrast-enhanced magnetic resonance imaging. Clin Cancer Res. 2007;13(12):3449–3459. doi:10.1158/1078-0432.CCR-07-0238
[22] Padhani AR, Hayes C, Landau S, et al. Reproducibility of quantitative dynamic MRI of normal human tissues. NMR Biomed. 2002;15(2):143–153. doi:10.1002/nbm.732
[23] Deoni SCL. Quantitative relaxometry of the brain. Top Magn Reson Imaging. 2010;21(2):101–113. doi:10.1097/RMR.0b013e31821e56d8
[24] Merkle EM, Dale BM. Abdominal MRI at 3.0 T: the basics revisited. AJR Am J Roentgenol. 2006;186(6):1524–1532. doi:10.2214/AJR.05.0932
[25] Cosgrove D, Harvey C. Clinical uses of microbubbles in diagnosis and treatment. Med Biol Eng Comput. 2009;47(8):813–826. doi:10.1007/s11517-009-0434-3
[26] Claudon M, Dietrich CF, Choi BI, et al. Guidelines and good clinical practice recommendations for contrast enhanced ultrasound (CEUS) in the liver—update 2012: a WFUMB-EFSUMB initiative in cooperation with representatives of AFSUMB, AIUM, ASUM, FLAUS and ICUS. Ultraschall Med. 2013;34(1):11–29. doi:10.1055/s-0032-1325499
[27] Wilson SR, Kim TK, Jang HJ, et al. Enhancement patterns of focal liver masses: discordance between contrast-enhanced sonography and contrast-enhanced CT and MRI. AJR Am J Roentgenol. 2007;189(1):W7–W12. doi:10.2214/AJR.05.2155
[28] Gauthier M, Leguerney I, Thalmensi J, et al. Estimation of intra-operator variability in perfusion parameter measurements using DCE-US. World J Radiol. 2011;3(1):70–81. doi:10.4329/wjr.v3.i1.70
[29] Dietrich CF, Averkiou MA, Correas JM, et al. An EFSUMB introduction into dynamic contrast-enhanced ultrasound (DCE-US) for quantification of tumour perfusion. Ultraschall Med. 2012;33(4):344–351. doi:10.1055/s-0032-1313026
[30] Boellaard R, Delgado-Bolton R, Oyen WJG, et al. FDG PET/CT: EANM procedure guidelines for tumour imaging: version 2.0. Eur J Nucl Med Mol Imaging. 2015;42(2):328–354. doi:10.1007/s00259-014-2961-x
[31] Wahl RL, Jacene H, Kasamon Y, et al. From RECIST to PERCIST: evolving considerations for PET response criteria in solid tumors. J Nucl Med. 2009;50(Suppl 1):122S–150S. doi:10.2967/jnumed.108.057307
[32] Patlak CS, Blasberg RG, Fenstermacher JD. Graphical evaluation of blood-to-brain transfer constants from multiple-time uptake data. J Cereb Blood Flow Metab. 1983;3(1):1–7. doi:10.1038/jcbfm.1983.1
[33] Zaidi H, Becker M. The role of quantitative PET in predicting cancer treatment outcomes. Trends Cancer. 2016;2(5):289–300. doi:10.1016/j.trecan.2016.04.002
[34] Stacul F, van der Molen AJ, Reimer P, et al. Contrast induced nephropathy: updated ESUR Contrast Media Safety Committee guidelines. Eur Radiol. 2011;21(12):2527–2541. doi:10.1007/s00330-011-2225-0
[35] McDonald RJ, McDonald JS, Kallmes DF, et al. Intracranial gadolinium deposition after contrast-enhanced MR imaging. Radiology. 2015;275(3):772–782. doi:10.1148/radiol.15150025
[36] Chua S, Groves AM, Kayani I, et al. The impact of 18F-FDG PET/CT in patients with liver metastases. Eur J Nucl Med Mol Imaging. 2007;34(12):1906–1914. doi:10.1007/s00259-007-0500-4

[37] Leng S, Bruesewitz M, Tao S, et al. Photon-counting detector CT: system design and clinical applications of an emerging technology. Radiographics. 2019;39(3):729–743. doi:10.1148/rg.2019180115
[38] Yasaka K, Akai H, Abe O, et al. Deep learning with convolutional neural network for differentiation of liver masses at dynamic contrast-enhanced CT. Radiology. 2018;286(3):887–896. doi:10.1148/radiol.2017170706
[39] Gillies RJ, Kinahan PE, Hricak H. Radiomics: images are more than pictures, they are data. Radiology. 2016;278(2):563–577. doi:10.1148/radiol.2015151169
[40] Khatri G, Pedrosa I, Ananthakrishnan L, et al. Abbreviated-protocol screening MRI vs. complete-protocol diagnostic MRI for detection of HCC in patients with cirrhosis. J Hepatol. 2020;72(3):490–499. doi:10.1016/j.jhep.2019.10.014
[41] McCollough CH, Leng S, Yu L, et al. Dual- and multi-energy CT: principles, technical approaches, and clinical applications. Radiology. 2015;276(3):637–653. doi:10.1148/radiol.2015142631
[42] Parakh A, Sanford MF, Sahani DV, et al. Variability in Hounsfield unit measurements across DICOM viewer platforms. Abdom Radiol (NY). 2022;47(4):1423–1432. doi:10.1007/s00261-022-03440-5
[43] Boellaard R, O'Doherty MJ, Weber WA, et al. FDG PET and PET/CT: EANM procedure guidelines for tumour PET imaging: version 1.0. Eur J Nucl Med Mol Imaging. 2010;37(1):181–200. doi:10.1007/s00259-009-1297-4
[44] Eisenhauer EA, Therasse P, Bogaerts J, et al. New response evaluation criteria in solid tumours: revised RECIST guideline (version 1.1). Eur J Cancer. 2009;45(2):228–247. doi:10.1016/j.ejca.2008.10.026
[45] Kudo K, Sasaki M, Yamada K, et al. Differences in CT perfusion maps generated by different commercial software. Radiology. 2010;254(1):200–209. doi:10.1148/radiol.254082000
[46] Wintermark M, Albers GW, Broderick JP, et al. Acute stroke imaging research roadmap II. Stroke. 2013;44(9):2628–2639. doi:10.1161/STROKEAHA.113.002867
[47] Chernyak V, Fowler KJ, Kamaya A, et al. Liver Imaging Reporting and Data System (LI-RADS) version 2018: imaging of hepatocellular carcinoma in at-risk patients. Radiology. 2018;289(3):816–830. doi:10.1148/radiol.2018181259

4
Chapter

Unmasking Breast Cancer: The Clinical Role of 3d Tomosynthesis

[1]Ayushi Singh
M.Sc. Research Scholar
Department of Radiological Imaging Techniques, College of Paramedical
ayushisingh482.as@gmail.com

[2]Amit Bisht
Assistant Professor
Department of Radiological Imaging Techniques, College of Paramedical
amitb.paramedical@tmu.ac.in

[3]Shivani Aswal
M.Sc. Research Scholar
Department of Radiological Imaging Techniques,
College of Paramedical
aswalshivaniaswal83@gmail.com

Abstract

Early detection is crucial for breast cancer screening in order to lower mortality. The superimposition of normal fibroglandular tissue severely limits the sensitivity of conventional two-dimensional full-field digital mammography (FFDM), which has long been the gold standard. Particularly in women with dense breast tissue, this "anatomical noise" can mask cancers and produce pseudo-lesions, resulting in missed cancers and increased false-positive recall rates. A revolutionary imaging technique called digital breast tomosynthesis (DBT) was created to get around the basic drawbacks of 2D mammography. DBT calculates high-resolution, pseudo-three-dimensional cross-sectional slices by obtaining several low-dose X-ray projections over a constrained angular arc. Lesions concealed by overlapping tissue are successfully revealed by this layer-by-layer visualization. Additionally, the DBT dataset can now be used to generate synthesized 2D mammograms (SM) computationally. By eliminating the requirement for concurrent FFDM acquisition, SM preserves diagnostic accuracy while lowering the radiation dose to the patient by about45%. Numerous clinical studies demonstrate that DBT is more effective than FFDM alone. DBT consistently shows lower false-positive recall rates and higher cancer detection rates (CDR), especially for early-stage, node-negative invasive lobular and ductal cancers. The technology significantly improves the visibility of architectural distortions and spiculated masses by offering outstanding margin characterization and accurate depth localization. Furthermore, DBT provides significant advantages for high-risk subgroups, such as women with dense breasts or a strong family history of breast cancer, according to systematic reviews. The clinical usefulness of DBT is further enhanced by the incorporation of deep learning models and artificial intelligence (AI). While retaining strong, extremely accurate diagnostic performance, AI-assisted interpretation

helps reduce the longer reading times related to examining multi-slice datasets. However, there are unique difficulties in putting DBT into practice. The enormous data files put a lot of strain on network infrastructures and Picture Archiving and Communication Systems (PACS). Furthermore, some research indicates that DBT may have comparable difficulties when assessing extremely fine microcalcifications or particular low-grade subtypes of ductal carcinoma in situ (DCIS). DBT overcomes the main drawbacks of traditional mammography and quickly becomes the new gold standard for breast cancer screening and diagnosis by simultaneously improving invasive cancer detection and reducing needless patient recalls.

Keywords: Digital breast tomosynthesis (DBT); Breast cancer screening; Digital mammography; Dense breasts; Cancer detection rate (CDR).

I. INTRODUCTION

As one of the most common cancers among women worldwide, breast cancer highlights the critical need for early and precise detection in order to lower death rates. Standard two-dimensional full-field digital mammography has been the primary imaging technique for screening for breast cancer for many years. This conventional method has a major physical drawback despite being widely used: normal fibroglandular breast tissue is superimposed when a three-dimensional anatomical structure is projected onto a two-dimensional plane(1).

Anatomical noise produced by this tissue overlap may mask underlying malignant lesions, leading to risky false-negative interpretations(2). A cutting-edge, three-dimensional imaging technique called digital breast tomosynthesis was created expressly to get around these intrinsic restrictions. An X-ray tube travels along a constrained angular arc during the mechanical acquisition process, taking several low-dose projection pictures of the compressed breast from different viewpoints. Tomosynthesis successfully removes the visual clutter brought on by overlapping tissue by offering a layer-by-layer visualization of the breast anatomy(3).

Interpreting radiologists' diagnostic confidence is greatly increased by this unmasking procedure, which provides a much clearer view of the internal breast architecture(4). By directly addressing the drawbacks of traditional imaging, the use of this cutting-edge modality has significantly changed clinical radiology. Tomosynthesis exhibits a better capacity to detect biologically significant invasive breast cancers, particularly improving the visibility of invasive lobular carcinomas and subtle architectural distortions that often go undetected on conventional mammograms(5). Additionally, the three-dimensional volumetric data enables precise localization of multifocal disease and a far more accurate evaluation of tumor margins(6). The technology streamlines the diagnostic process by eliminating the uncertainty of overlapping tissue while simultaneously lowering the overall frequency of patient recalls(1). Tomosynthesis's improved diagnostic clarity is especially important for certain high-risk patient populations. When assessing women with radiographically dense breast tissue, standard mammography is notoriously limited. However, tomosynthesis's pseudo-three-dimensional nature circumvents this masking limitation, providing extremely accurate diagnostic capabilities for this specific population(7).

Healthcare facilities face significant logistical and infrastructure challenges when switching to tomosynthesis, despite these many clinical advantages. Picture archiving and communication systems (PACS) and institutional network bandwidth are severely strained by the massive data files generated by the creation of multi-slice volumetric images.

Additionally, radiologists' interpretation time is naturally increased when they evaluate dozens of slices per patient. However, healthcare systems can fully utilize digital breast tomosynthesis and solidify it as the best technological standard for contemporary breast imaging by growing IT infrastructure and streamlining reading workflows(8).

II. LIMITATIONS OF CONVENTIONAL 2D MAMMOGRAPHY

Standard two-dimensional full-field digital mammography has been the main breast cancer screening technique for decades. However, a basic physical limitation inherently limits this traditional imaging method. The breast, a complex, three-dimensional anatomical structure, is mechanically compressed and radiographically projected onto a flat, two-dimensional plane during the acquisition of a mammogram(1). All of the complex internal structures, such as ducts, lobules, connective tissue, and fat, are compressed into a single flat image as a result of this dimensional reduction. When the breast's depth is completely collapsed, its intrinsic complexity cannot be fully understood or appreciated(2).

Normal fibroglandular breast tissue will inevitably superimpose when three-dimensional anatomy is projected onto a two-dimensional detector(3). Because breast tissue is so diverse, structures that are physically separated by several centimetres of depth within the breast are artificially flattened to appear to be in the same plane during a standard mammography(2). In women with radiographically dense breasts, which have a greater percentage of glandular and connective tissue than radiolucent fat, this superimposition is especially troublesome. This overlapping effect becomes more noticeable the denser the breast, effectively producing a dense, opaque white background on the resulting mammography image that makes it more difficult for the radiologist to discern specific internal structures(7) (3).

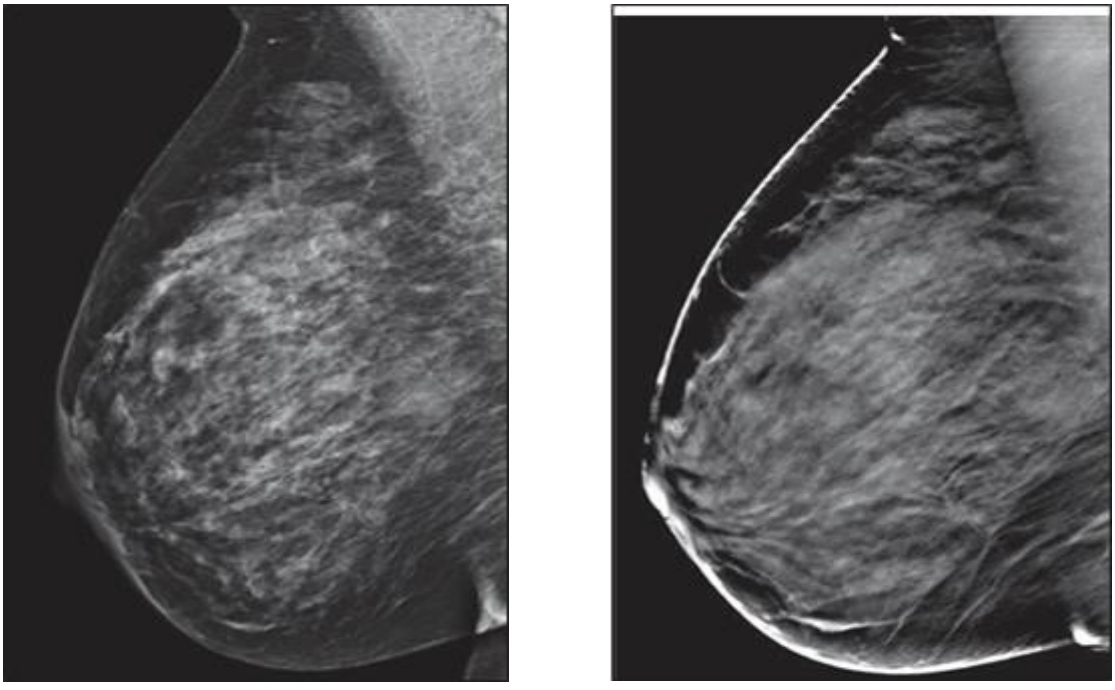

Figure 1: 57-year-old woman with breast cancer. Comparison of standard 2D versus digital breast tomosynthesis (DBT)(2).

The visual consequence of this overlapping fibroglandular tissue is the generation of substantial "anatomical noise" across the image(2). The presence of underlying malignant

lesions can be readily hidden or entirely obscured by this clutter, which serves as a visual barrier(1). A tumor can be completely concealed within the layers of healthy tissue that are superimposed because breast cancers frequently appear as white, radiopaque masses that show radiographic attenuation similar to that of normal glandular tissue(4). When biologically significant, invasive cancers are overlooked during routine screening because they are visually obscured by the patient's normal breast anatomy, this masking effect directly causes dangerous false-negative interpretations(1) (2).

On the other hand, normal fibroglandular tissue can also be superimposed to produce false radiographic illusions. The combined densities of several layers of perfectly normal breast tissue that overlap in a particular way on the two-dimensional projection can resemble a solid mass or an architectural distortion(2).On a typical mammography, these artificially produced "pseudo-lesions" look extremely suspicious, so interpreting radiologists must exercise extreme caution. Therefore, these overlapping structures often lead to false-positive interpretations(1). In order to demonstrate that the suspicious finding was just overlapping normal tissue, patients are then made to endure needless, stressful recall appointments for additional diagnostic imaging, such as spot compression views or breast ultrasonography(1) (2).

III. TECHNOLOGICAL PRINCIPLES OF DIGITAL BREAST TOMOSYNTHESIS (DBT)

A significant technological development in breast radiology, digital breast tomosynthesis (DBT) has completely changed the paradigm from static two-dimensional imaging to a highly advanced, pseudo-three-dimensional imaging method(3). This technology's main goal is to capture a comprehensive volumetric dataset in order to resolve the breast's structural ambiguity. In order to do this, the DBT system uses a single automated sweep to obtain several low-dose X-ray projections of the compressed breast from different angles(4). This dynamic acquisition method, which was specifically created to get around the diagnostic constraints brought on by overlapping fibroglandular tissue in traditional mammography, offers a thorough spatial representation of the internal breast architecture(2). DBT's mechanical implementation depends on an extremely precise and well-coordinated acquisition process. The patient's breast is firmly compressed against the detector array during the entire scan. This compression is crucial because it guarantees a uniform tissue thickness, which is required for the best X-ray penetration and high image quality, in addition to immobilizing the breast to prevent motion artifacts(3).

The X-ray tube moves in a motorized trajectory along a narrow angular arc directly above the breast while the breast stays motionless(4). The specific engineering parameters of commercial DBT systems differ greatly, particularly in the number of low-dose projections obtained and the total scan angle(5). Simultaneously, each manufacturer produces a different number of discrete individual projection images during this continuous or step-and-shoot tube motion, usually ranging from 9 to 25 distinct exposures(5). These differences are intentional trade-offs in engineering. While a narrower angular range allows for a much faster overall scan time, which significantly lowers the likelihood of image blurring caused by patient movement during the exposure, a wider angular sweep typically offers superior depth resolution along the z-axis, enabling better visual separation of distinct tissue planes (5) (4).

The raw, low-dose projection images are not yet prepared for diagnostic interpretation after the physical mechanical acquisition is finished. Rather, extensive mathematical processing is

required for this unprocessed data. The three-dimensional volume is mathematically synthesized by processing these multiple angled projections using sophisticated computational algorithms(4). FBP is well-known for its speed and computational efficiency, which makes it ideal for quick clinical workflows. On the other hand, because iterative reconstruction can better model the imaging physics, control background image noise, and reduce out-of-plane artifacts, it is becoming more and more popular despite being slightly more computationally demanding(3). The raw data can ultimately be computationally reconstructed into a stack of thin, high-resolution cross-sectional slices by applying these potent computational algorithms. The accuracy and confidence of breast cancer diagnosis are significantly increased when radiologists can visually scroll through this volumetric dataset layer by layer, giving them an unparalleled, clear view of the breast anatomy(4).

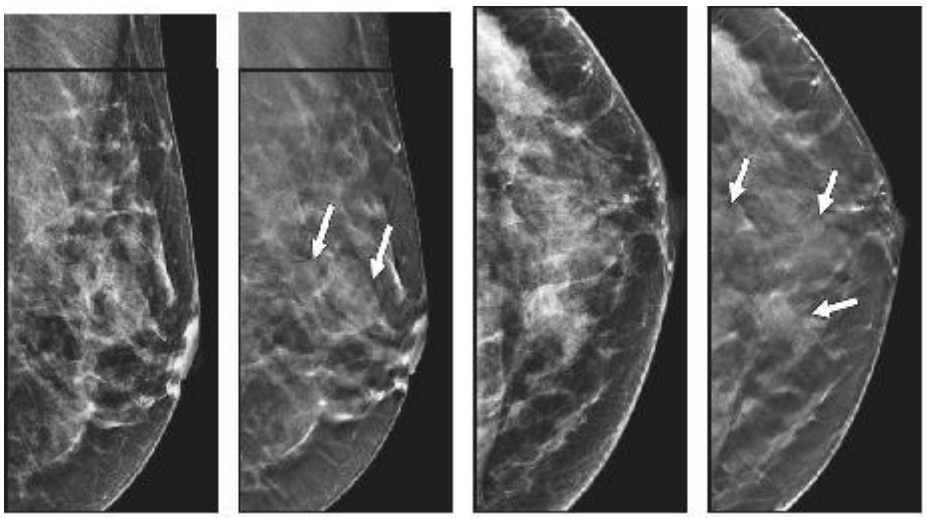

Figure 2: A–D, Two dimensional mediolateral oblique (A), digital breast tomosynthesis (DBT) mediolateral oblique (B), 2D craniocaudal (C), and DBT craniocaudal (D) images reveal multiple mostly circumscribed masses (arrows, B and D),which were not seen on 2D image(9).

IV. ADVANCED APPLICATIONS AND TECHNOLOGICAL INNOVATIONS

Radiologists mainly relied on conventional two-dimensional images during the early years of tomosynthesis implementation to provide a macroscopic overview of the breast architecture and to act as a baseline for comparison against historical prior examinations. As a result, early screening procedures required a combined acquisition mode(8). The imaging device would take the standard two-dimensional exposure while the breast was still firmly compressed, and then it would start the low-dose angular sweep needed for the tomosynthesis reconstruction right away(4). This combined approach effectively doubled the mean glandular radiation dose given to the patient compared to a traditional digital mammogram alone, even though the cumulative radiation from both of these acquisitions strictly stayed within the legally mandated safety limits for breast screening(1). Finding a way to lower this cumulative dose without compromising the superior diagnostic yield of the three-dimensional dataset became a crucial technological imperative as the medical community constantly works to uphold the principle of keeping ionizing radiation as low as reasonably achievable(6).

Modern tomosynthesis systems have successfully developed a highly complex computational solution known as synthesized two-dimensional mammography to directly address these legitimate concerns regarding cumulative radiation exposure(3). Strong software algorithms are used to computationally process the obtained three-dimensional volumetric dataset instead of putting the patient through a completely different physical X-ray exposure(1). These sophisticated mathematical algorithms mathematically collapse the dozens of distinct, high-resolution cross-sectional slices into a single, comprehensive two-dimensional projection after methodically evaluating each one(6).

The distribution of breast density, noticeable benign calcifications, and the general ductal and glandular architecture are just a few of the key macroscopic anatomical features that are accurately displayed in this computationally generated image, which is specifically designed to closely resemble the familiar visual appearance of a traditional full-field digital mammogram(3). Healthcare professionals can totally do away with the requirement for the concurrent physical two-dimensional exposure by smoothly incorporating this synthesized two-dimensional mammogram into the routine diagnostic workflow(6). This software development has significant clinical and safety ramifications: using synthesized two-dimensional mammography successfully lowers the patient's total mean glandular radiation dose by about 45% (1). Importantly, comprehensive clinical assessments and long-term data have conclusively demonstrated that the high diagnostic efficacy, superior cancer detection rates, and low recall rates typical of the full tomosynthesis examination are fully preserved when the physical two-dimensional exposure is replaced with a computationally generated image(1) (5). Although the radiation problem was successfully solved by synthesized imaging, the modality inevitably creates another major logistical problem: an excessive amount of visual data(10). For a radiologist to examine, a typical two-dimensional screening mammography usually consists of just four static images.

On the other hand, depending on the thickness of the patient's compressed breast, a single digital breast tomosynthesis examination can easily produce several hundred distinct high-resolution slices(5). This massive proliferation of images requires interpreting radiologists to spend a significantly longer time scrolling through and meticulously analyzing the dataset layer by layer(10). Modern breast imaging workflows are increasingly incorporating advanced commercial artificial intelligence and deep learning models to lessen this unprecedented cognitive load and improve diagnostic accuracy. These sophisticated computational systems can identify the extremely intricate, multi-dimensional radiographic patterns linked to early-stage breast cancer because they have been specifically trained on enormous repositories of annotated tomosynthesis datasets. When commercial AI is incorporated into the imaging workflow, it performs exceptionally well, helping physicians find subtle, biologically significant cancers that might otherwise be missed due to the overwhelming amount of data(11).

V. UTILITY IN SPECIALIZED AND HIGH-RISK POPULATIONS

In routine breast cancer screening, women with radiographically dense breast tissue pose a well-established and ongoing diagnostic challenge. The proportion of radiopaque fibroglandular tissue to radiolucent fatty tissue in the breast is known as breast density(7). On a typical mammogram, both malignant breast tumors and normal glandular tissue appear radiographically dense—or white. This anatomical noise significantly lowers the diagnostic sensitivity for this particular population(2). By capturing a volumetric dataset and computationally reconstructing it into thin, high-resolution cross-sectional slices, digital

breast tomosynthesis decisively overcomes this physiological constraint(4). Tomosynthesis reveals lesions that would otherwise be totally concealed within the dense parenchyma by visually removing the overlapping layers of normal tissue(3).

This unmasking effect has significant clinical utility. When compared to standalone two-dimensional mammography, targeted systematic reviews that concentrate on women with dense breasts and other risk factors consistently show that tomosynthesis greatly increases overall diagnostic accuracy(7). Additionally, this pseudo-three-dimensional layer-by-layer visualization is especially good at identifying invasive lobular carcinomas and subtle architectural distortions—complex cancers that are infamously difficult to detect and often concealed within dense breast tissue(5).

Digital breast tomosynthesis shows remarkable screening efficacy for women with a strong family history of breast cancer, in addition to its use in overcoming breast density. In order to ensure early and accurate detection, advanced screening modalities with the highest sensitivity and specificity are required because individuals with a familial predisposition have a significantly increased lifetime risk of developing the disease. Clinical researchers are examining whether three-dimensional tomosynthesis can offer a more robust and dependable diagnostic safety net because the diagnostic performance of standard two-dimensional mammography in this particular high-risk subgroup has historically been limited. In numerous prospective screening studies, the use of digital breast tomosynthesis consistently produced significantly better diagnostic metrics for these high-risk patients.

Tomosynthesis showed an improved ability to detect hidden malignancies, reflecting a tangibly higher overall cancer detection rate compared to conventional digital mammography. Simultaneously, the advanced imaging technology proved highly effective at significantly reducing the recall rate for this vulnerable population. Recent thorough systematic reviews that carefully compared the performance of both modalities in women with a family history of breast cancer have produced strong clinical evidence that strongly favors tomosynthesis. Reducing false-positive recalls is crucial because it directly reduces the severe psychological distress and emotional trauma that come with a possible cancer diagnosis. This anxiety is already greatly increased in women who are acutely aware of their increased genetic risk. The switch to tomosynthesis is a crucial improvement in preventative care for women who have a high family history of breast cancer. It guarantees that their elevated baseline risk is actively managed with an advanced screening tool that can provide earlier, safer, and more accurate cancer detection(8).

VI. CHALLENGES IN CLINICAL IMPLEMENTATION AND WORKFLOW

The main infrastructure obstacle is directly related to the basic workings of the technology. With only four static, high-resolution images—two standard views per breast—a typical two-dimensional screening mammogram has a very predictable and manageable digital footprint. In stark contrast, a single digital breast tomosynthesis examination generates a complex volumetric dataset that is computationally reconstructed into dozens, or even several hundreds, of individual high-resolution cross-sectional slices, depending entirely on the physical thickness of the patient's compressed breast and the specific commercial vendor's acquisition parameters(5).

As a result, massive data files that are exponentially larger than their conventional two-dimensional counterparts are produced during the creation of these multi-slice volumetric

images. The entire information technology infrastructure of a healthcare facility is subject to extremely high demands due to this unprecedented increase in digital volume. Highly reliable, upgraded network bandwidth is needed to transfer these enormous, gigabyte-sized patient files from the acquisition scanner to the reading workstations in order to avoid serious transmission bottlenecks and intolerable latency during routine clinical routing. More importantly, institutional Picture Archiving and Communication Systems (PACS) are immediately and severely burdened by these massive datasets. To safely store these files in accordance with stringent medical retention regulations, facilities implementing tomosynthesis must quickly and dramatically increase both their active short-term and archival long-term digital storage capacities(8).

In addition to the substantial digital hardware requirements, the implementation of tomosynthesis has a significant impact on the human component of the diagnostic workflow. Failure to proactively upgrade these IT networks and storage architectures can result in catastrophic system slowdowns, server instability, and an inability for clinicians to quickly retrieve historical prior examinations, which are absolutely essential for accurate comparative diagnosis and tracking subtle interval changes over time. Compared to conventional screening techniques, radiologists' total interpretation time is inevitably increased by the absolute necessity of carefully analyzing dozens of high-resolution slices per patient. This additional temporal requirement for each patient adds up to a substantial decrease in daily departmental throughput in a high-volume breast screening setting where specialized radiologists are traditionally expected to interpret a high quota of cases per hour.

Moreover, during a demanding clinical shift, the risk of visual and cognitive fatigue is significantly increased by the prolonged, intense visual focus needed to continuously process and mentally integrate this massive amount of dynamic, multi-planar information. In order to ensure that the exceptional diagnostic benefits of tomosynthesis are safely and effectively realized, contemporary radiology departments must proactively redesign their traditional clinical workflows, reevaluate daily reading quotas to prevent burnout, and strategically manage the increased interpretive burden(8).

REFERENCES

[1] Dhamija E, Gulati M, Deo SVS, Gogia A, Hari S. Digital Breast Tomosynthesis: an Overview. Indian J Surg Oncol. 2021 Jun;12(2):315–29. doi:10.1007/s13193-021-01310-y
[2] Kopans DB. Digital Breast Tomosynthesis From Concept to Clinical Care. American Journal of Roentgenology. 2014 Feb;202(2):299–308. doi:10.2214/AJR.13.11520
[3] Kiarashi N, Samei E. Digital breast tomosynthesis: a concise overview. Imaging in Medicine. 2013 Oct;5(5):467–76. doi:10.2217/iim.13.52
[4] Vedantham S, Karellas A, Vijayaraghavan GR, Kopans DB. Digital Breast Tomosynthesis: State of the Art. Radiology. 2015 Dec;277(3):663–84. doi:10.1148/radiol.2015141303
[5] Gao Y, Moy L, Heller SL. Digital Breast Tomosynthesis: Update on Technology, Evidence, and Clinical Practice. RadioGraphics. 2021 Mar;41(2):321–37. doi:10.1148/rg.2021200101
[6] Michell MJ, Batohi B. Role of tomosynthesis in breast imaging going forward. Clinical Radiology. 2018 Apr;73(4):358–71. doi:10.1016/j.crad.2018.01.001
[7] Raichand S, Blaya-Novakova V, Berber S, Livingstone A, Noguchi N, Houssami N. Digital breast tomosynthesis for breast cancer diagnosis in women with dense breasts and additional breast cancer risk factors: A systematic review. The Breast. 2024 Oct;77:103767. doi:10.1016/j.breast.2024.103767
[8] Li T, Isautier J, Lee JM, Marinovich ML, Houssami N. Performance of Digital Breast Tomosynthesis Versus Digital Mammography in Women With a Family History of Breast Cancer: A Systematic Review. Clinical Breast Cancer. 2025 Feb;25(2):e103–12. doi:10.1016/j.clbc.2024.09.013
[9] breast-tomosynthesis article 11.

[10] Lee CI, Lehman CD. Digital Breast Tomosynthesis and the Challenges of Implementing an Emerging Breast Cancer Screening Technology Into Clinical Practice. Journal of the American College of Radiology. 2013 Dec;10(12):913–7. doi:10.1016/j.jacr.2013.09.010

[11] Brown-Mulry B, Isaac RS, Lee SH, Seth A, Min K, Dapamede T, et al. Subgroup performance of a commercial digital breast tomosynthesis model for breast cancer detection. Nat Commun. 2026 Mar 19. doi:10.1038/s41467-026-70637-3

5
Chapter

Digital Breast Tomosynthesis: Revolutionizing Breast Imaging

[1]Srishti Gaur
M.Sc. Research Scholar
Department of Radiological Imaging Techniques,
College of Paramedical Sciences,
Teerthanker Mahaveer University,
Moradabad
sgaur9830@gmail.com

[2]Sidra
M.Sc. Research Scholar
Department of Radiological Imaging Techniques,
College of Paramedical Sciences,
Teerthanker Mahaveer University,
Moradabad
sidraasad166@gmail.com

[3]Amit Bisht
Assistant Professor
M.Sc. Research Scholar
Department of Radiological Imaging Techniques,
College of Paramedical Sciences,
Teerthanker Mahaveer University,
Moradabad
amitb.paramedical@tmu.ac.in

[4]Geeta Bisht
Assistant Lecturer,
Department of Radiology,
Swami Rama Himalayan University,
Dehradun
geetbisht206@gmail.com

Abstract

Digital Breast Tomosynthesis (DBT), referred to as "3D mammography," is recognized as a game-changing development in breast imaging, designed to mitigate the "anatomical noise" and tissue superimposition inherent in traditional two-dimensional (2D) mammography. Radiologists can study breast parenchyma layer by layer using DBT, which captures several low-dose projection pictures throughout a restricted arc and reconstructs them into a stack of high-resolution, thin tomographic slices. This volumetric technique has been medically proved to considerably improve cancer detection rates (CDR), notably for aggressive and invasive carcinomas, while also lowering false-positive recall rates.

Women with thick breast tissue benefit the most from the method, as standard 2D imaging has a sensitivity as low as 47.8%. Although advantages, integrating DBT brings logistical and technical hurdles, such as higher radiation exposure (typically alleviated by Synthesized Mammography), huge data storage requirements, and doubling radiologists' interpretation periods. Present research and future perspectives indicate that DBT is on track to become the major screening modality, with recent advances concentrating on Artificial Intelligence (AI)

integration and density-specific screening algorithms to improve early detection and patient results.

Keywords: Digital breast tomosynthesis (DBT), Cancer detection rate (CDR), Anatomical noise, Microcalcifications, Recall rate, Tissue superimposition,Architectural distortion,Dense breast tissue,

I. INTRODUCTION

Breast cancer is a major worldwide health challenge, accounting for the most often detected tumour among women, with an approximate 1.67 million new cases reported annually. Systematic mammography screening is a key component of public health initiatives to reduce this burden, as early detection is associated with a 23% to 40% reduction in death. Over the last decade, the standard of treatment has migrated from two-dimensional (2D) analogue mammography to Full-Field Digital Mammography (FFDM), which has shown incremental improvements in detection and a decrease in false positives.

However, standard 2D imaging is fundamentally constrained by breast tissue superimposition, which can mask malignant lesions while also cloning disease, leading to diagnostic incomprehension. To solve these geographical restrictions, Digital Breast Tomosynthesis (DBT), sometimes known as "3D mammography," arose as a radical progression of FFDM technology. DBT makes it easier to analyse three-dimensional mammographic data by collecting several low-dose projections and reconstructing them into a stack of small tomographic image slices. This volumetric technique enables clinicians to scroll across the breast parenchyma, essentially "peeling back" layers of tissue to address issues caused by overlapped structures.

Although early use of DBT as an auxiliary to FFDM required a second radiation exposure, the establishment of synthesized 2D pictures rebuilt directly from the DBT dataset has resulted in a total patient dosage comparable to regular FFDM.

Clinical trials have consistently shown that DBT outperforms FFDM in terms of diagnostic performance. Evidence from large-scale research in Europe and the United States suggests that including DBT results in a much higher cancer detection rate (CDR), especially for aggressive carcinomas.

In European screening paradigms, the overall difference in CDR has been measured as 2.43 per 1000 screenings. Besides monitoring, DBT improves the screening process by lowering false positive rates and needless patient reminders. These savings are especially noticeable in single-reader paradigms prevalent in the United States, where the procedure aids in the resolution of tissue asymmetries that would otherwise necessitate further, often unpleasant, diagnostic workups. Despite its obvious benefits, the complete integration of DBT into population-based screening necessitates a thorough knowledge of its long-term consequences. As comprehensive data on interval cancer rates continue to mature, current research is focused on the modality's long-term sensitivity and specificity. In addition, the switch to DBT requires logistical issues, such as managing much bigger datasets and the risk of overdiagnosis, even though DBT has not yet been proved to improve the identification of non-invasive tumours such as ductal carcinoma in situ (DCIS). This chapter investigates the technological foundations and clinical consequences of DBT, providing a thorough examination of its significance in the future of breast cancer screening. (1)

II. PRINCIPLE

Breast cancer is the most common malignancy among women worldwide, demanding robust screening and diagnostic techniques to reduce mortality. While Full-Field Digital Mammography (FFDM) has long been the gold standard of excellence for early diagnosis, its two-dimensional nature frequently results in "anatomical noise" generated by the superimposition of normal glandular parenchyma, which can mask cancers or form "pseudo-masses". To overcome these limitations, Digital Breast Tomosynthesis (DBT) was introduced as an enhanced imaging supplement and received FDA approval in 2011 for both screening and diagnostic purposes. DBT creates a "third dimension" of depth by capturing several low-dose projection images of the compressed breast from various angles, permitting doctors to examine breast tissue layer by layer.

The basic premise of DBT is that the X-ray tube rotates in an arc—known as the sweep angle, which varies by manufacturer between 15 and 60 degrees—to obtain a sequence of projection radiographs. These projections are then reconstructed into a stack of high-resolution sections, usually 1 mm thick, using either filtered back projection or iterative reconstruction techniques.The technological implementation of this sweep varies; "continuous" tube motion decreases acquisition time but may compromise resolution due to focus spot blur, whereas "step-and-shoot" systems favor image quality at the expense of greater motion artifacts. Furthermore, the selection of sweep angle represents a significant trade-off: a broader arc boosts tomographic separation and z-axis resolution, increasing the visibility of architectural deformities. However, it diminishes in-plane resolution, which is required for viewing small calculi. Clinically, the use of DBT has resulted in a considerable increase in the Cancer Detection Rate (CDR), notably for invasive tumors.

This "decamouflaging" effect is especially advantageous in women with dense breast tissue, where typical 2D mammography has a sensitivity as low as 47.8%.DBT improves diagnostic productivity through enabling precise lesion localization; radiologists may employ a workstation scroll bars to establish the exact "clockface" position and depth of a mass, allowing for targeted ultrasound and guided biopsies. These advances in lesion definition have also resulted in a significant drop in recall rates, as thin slices may solve asymmetries that would otherwise necessitate additional diagnostic views. Despite these benefits, the adoption of DBT poses unique logistical and technical hurdles.

One major worry is the radiation exposure, as adding tomosynthesis images to a regular 2D mammography can about double the mean glandular dose, however levels are usually kept within the FDA's 3 mGy limit. To address this issue, Synthesized Mammography (SM) has emerged, in which a 2D image is reconstructed from DBT data, avoiding the need for a separate FFDM exposure and lowering the dose by around 45%. Furthermore, the huge amount of data produced by DBT—with file sizes varying from 200 to 450 MB—imposes enormous demands on network storage and raises radiologists' interpretation time, frequently twice the time required for a normal diagnostic exam. Nonetheless, as technology advances, DBT is increasingly considered as a preferable modality for breast cancer screening, providing a more detailed and precise assessment of complicated breast anatomy.(2)

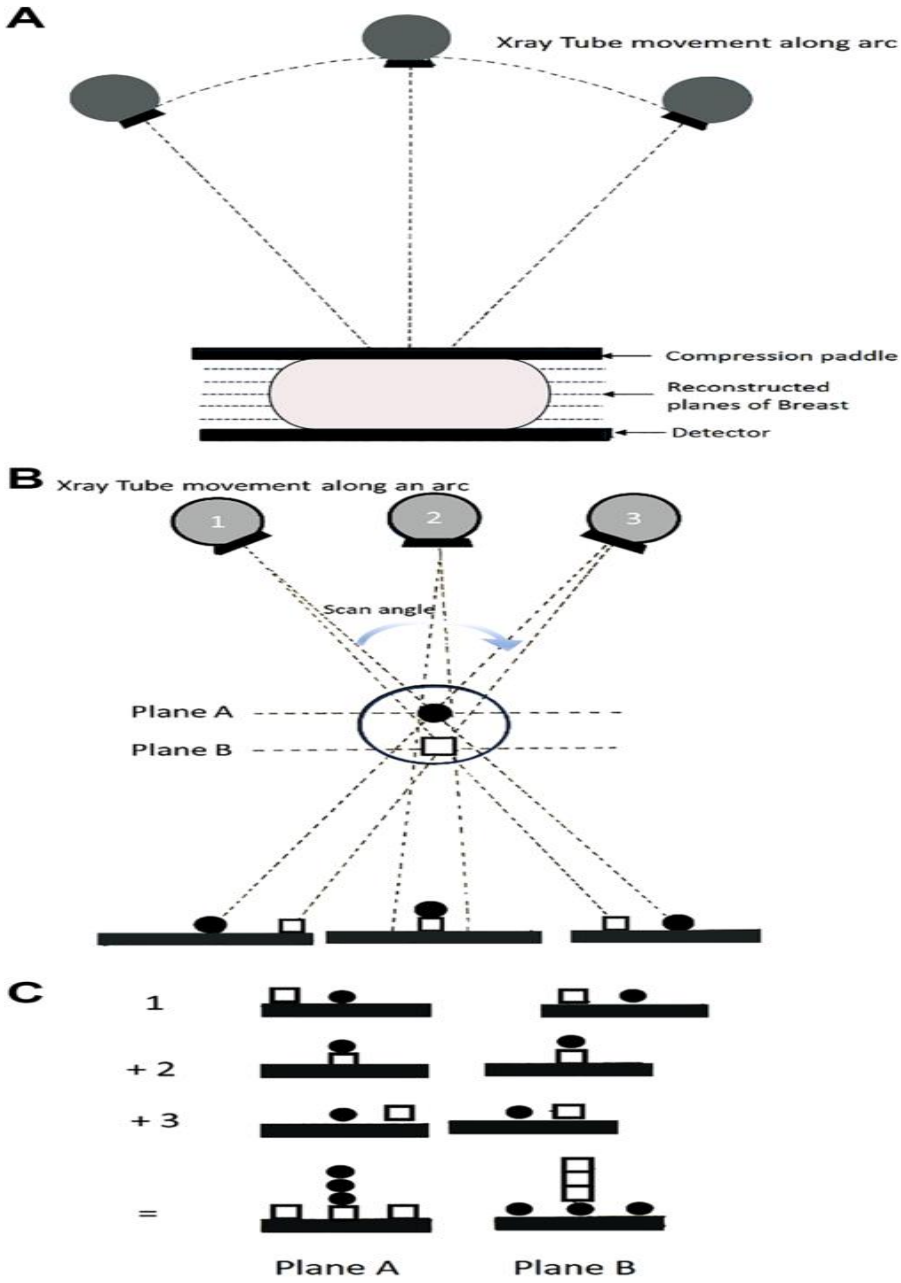

Figure 1: Illustration demonstrating basic principle of digital breast Tomosynthesis.(3)

III. EVOLUTION OF DIGITAL BREAST TOMOSYNTHESIS (DBT)

Digital Breast Tomosynthesis (DBT) is a notable improvement in breast imaging technology, having evolved from previous mammography procedures to grow into the latest standard of care for screening mammography in the United States.

1. Early Development and Approval

- **Conceptualisation and Initial Development:** DBT was originally created in the 1990s as a reaction to the limitations of two-dimensional mammography, specifically its inability to accurately image dense breast tissue due to overlay normal tissues.

- **FDA Approval:** The technique gained its initial approval from the United States Food and Drug Administration (FDA) in 2011.

2. **Addressing Limitations of Previous Technologies**
   - **Overcoming Tissue Overlap:** BT was expressly created to overcome the issue of overlapping breast tissue, which could mask or mimic tumours in regular 2D mammography. It accomplishes this by constructing quasi-three-dimensional reconstructions of several low-dose projections, effectively delivering thin ‘slices' across the breast.
   - **Improved Cancer Detection and Recall Rates:** DBT reduces the masking impact of overlaid normal tissues, considerably lowering the frequency of malignancies hidden by such tissues and minimizing ambiguous summing shadows. This results in the diagnosis of more malignancies, frequently at an earlier, more curable stage, while simultaneously lowering recall rates.

3. **Current Status and Future Directions**
   - **Standard of Care:** DBT is currently the present norm of treatment for screening mammography in the United States due to its improved diagnostic capacity.
   - **Ongoing Research and Integration:** Continuing studies, like the Tomosynthesis Mammographic Imaging Screening Trial (TMIST), are meant to further evaluate DBT with full-field digital mammography (FFDM) and determine its impact on reducing the prevalence of carcinoma of the breast. Future developments in artificial intelligence (AI) and multimodality imaging are predicted to enhance early detection and improve breast cancer screening results. (4)

IV. TECHNIQUE

DBT's technical framework varies greatly from traditional two-dimensional digital mammography (DM), primarily by overcoming the constraints of tissue superimposition. Despite DBT is commonly referred to as "3D mammography," this nomenclature is recognized as a misnomer; instead, the technology is defined by the recording of multiple projection images of the breast from various angles. This process includes spinning the X-ray tube in an arc or sweep, which can be done in a continuous or "step-and-shoot" manner. This process includes spinning the X-ray tube in an arc or sweep, which can be done in a continuous or "step-and-shoot" manner.

Projection radiographs are reconstructed into thin image slices (0.5 mm to 1 mm) parallel to the detector. The reconstruction utilizes filtered back projection and iterative techniques to create a scrollable data set. The total volume is determined by the thickness of the compressed breast. DBT is commonly utilized in a "combo-mode," combining traditional 2D mammography with DBT sweeps. While this gives extensive comparative data, it raises the radiation dose by around 2.25 times, yet this is still under the FDA-mandated limit of 3 mGy per view. To reduce this exposure, numerous systems have implemented Synthesized Mammography (SM), a method that reconstructs a 2D-like image straight from the DBT data set, effectively lowering the radiation dose by roughly 50% while preserving comparable performance metrics to the combo-mode. DBT's precision extends to lesion localization and characterization using sophisticated triangulation. DBT's precision extends to lesion localization and characterization using sophisticated triangulation. In addition, the introduction of DBT-guided biopsy has improved clinical workflows by delivering Z-axis (depth) information without the requirement for stereotactic imaging sets. These guided

methods use the entire detector field and have been proven to cut total biopsy time by more than half when compared to traditional DM stereotactic systems.

Although its diagnostic advantages, DBT is subject to particular technical artifacts resulting from its acquisition and processing procedures. The "out-of-plane" or "slinky" artifact is the most common, in which high-attenuation objects such as surgical clips produce a "zipper" effect of duplicated high-intensity pictures in the direction of the tube sweep. Further technical problems include metal artifacts appearing as black halos due to photon deprivation, and terracing artifacts manifesting as striations perpendicular to tube movement, particularly in larger breasts. Furthermore, whereas DBT boosts the visualization of masses and architectural distortions, the "declustering" effect inherent in slicing can make detecting small clusters of microcalcifications more difficult, necessitating a thorough review of the entire image stack, or the use of "slabbed" thicker planes to preserve diagnostic accuracy.(3)

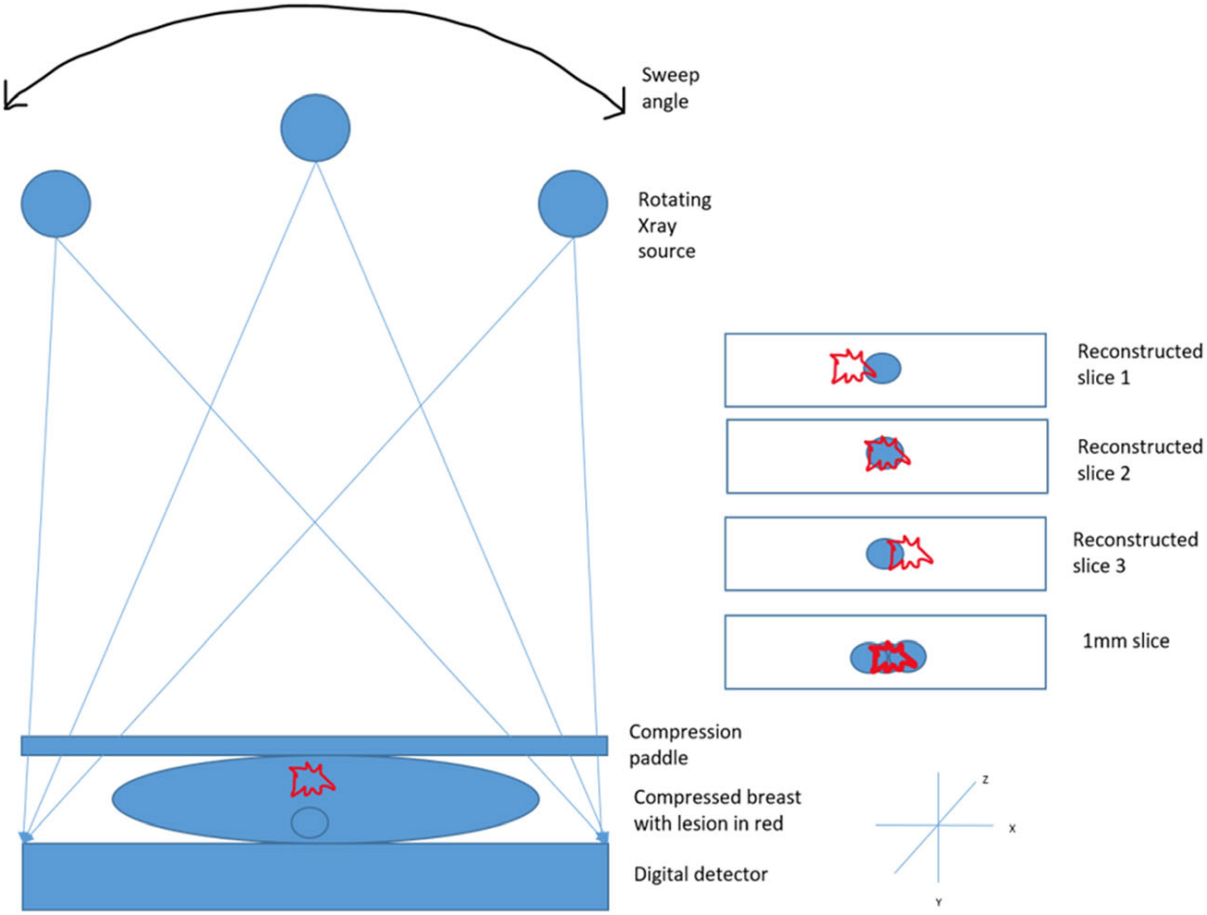

Figure 2: Diagrammatic representation of the technique of digital breast tomosynthesis(2)

V. IMAGE RECONSTRUCTION

Digital breast tomosynthesis (DBT) represents a transformative advancement in breast imaging, specifically engineered to overcome the inherent limitations of conventional two-dimensional (2D) mammography. The core of this technology lies in its unique acquisition

and reconstruction process, which transitions from a single flat projection to a volumetric data set.

1. Acquisition of Projection Data

The imaging process begins with the acquisition of multiple low-dose projection images captured from a limited range of view angles. Unlike traditional computed tomography, which utilizes a full 360-degree rotation, a DBT system typically sweeps the X-ray tube across a narrow arc—for example, a range of 50° (−25° to +25°)—while the breast remains compressed on a flat panel detector. During this sweep, a series of discrete projections (often numbering around 11 to 25) are recorded. This limited-angle approach ensures that the radiation dose remains comparable to standard mammography while providing the raw spatial data necessary for three-dimensional reconstruction.

2. Reconstruction and Slice Generation

Once the projections are acquired, they are processed through mathematical algorithms to generate a stack of thin tomographic slices. This reconstruction is essentially an inverse problem, where the goal is to estimate the three-dimensional object (the breast) from its two-dimensional projections. The resulting slices allow clinicians to scroll through the breast parenchyma layer by layer, effectively isolating anatomical structures that would otherwise be superimposed in a single 2D view.

3. Common Reconstruction Methodologies

Several techniques have been developed to transform projection data into tomographic images:

- **Shift and Add (SAA):** This was the earliest reconstruction method used in tomosynthesis; it functions by shifting and adding projections to sharpen a specific focal plane. However, SAA is largely limited by a significant amount of out-of-focus slice blur.
- **Filtered Back Projection (FBP):** A more advanced analytic method, FBP and its modified variants are widely used to reduce blurring. Despite their efficiency, they often struggle with the "missing data" problem caused by the limited view angles, which can lead to streaking artifacts.
- **Iterative Reconstruction Techniques:** Techniques such as the Algebraic Reconstruction Technique (ART) estimate the image through an iterative process. In ART, voxel intensities are updated ray-by-ray for each projection to satisfy a consistency condition between the measured data and the reconstructed image. To improve accuracy in highly under sampled datasets, modern iterations often incorporate Compressed Sensing (CS) and Total Variation (TV) minimization, which help preserve sharp edges and further reduce artifacts.

4. Enhancement of Lesion Visibility

The primary clinical motivation for DBT reconstruction is the mitigation of the overlapping tissue problem, which is the most prevalent artifact in 2D mammography. In traditional imaging, dense glandular tissue can mask a malignancy or create "pseudo-masses" through the chance alignment of normal structures. By isolating the breast into discrete tomographic layers, the reconstruction process reduces out-of-focus slice blur and removes the interference

of superimposed tissue. This "decamouflaging" effect significantly improves the visibility of lesions, such as small masses or architectural distortions, thereby enhancing the overall diagnostic sensitivity and specificity of the exam. (5)

VI. CLINICAL APPLICATIONS

The clinical implementation of digital breast tomosynthesis (DBT) has fundamentally shifted the landscape of breast imaging by providing a volumetric approach that addresses the limitations of traditional two-dimensional (2D) projection mammography. By acquiring multiple images from varying angles, DBT facilitates a more granular analysis of breast anatomy, enhancing both screening efficacy and diagnostic precision.

1. Role in Screening and Early Detection

The integration of DBT into routine screening has demonstrated a significant increase in the cancer detection rate (CDR) compared to conventional digital mammography (DM). Research indicates that DBT is particularly adept at identifying invasive carcinomas, which are often associated with more favourable prognoses, such as tubular, papillary, and mucinous subtypes. Furthermore, the use of DBT, particularly when paired with synthesized mammography (SM), has been shown to reduce abnormal recall rates. This improvement in specificity is complemented by an increase in the positive predictive value (PPV) for biopsies, which can improve by as much as 20%. Longitudinal studies suggest these benefits are sustainable over multiple screening rounds and may even lead to a reduction in interval cancer rates, which are typically associated with higher mortality.

2. Diagnostic Evaluation of Breast Lesions

In a diagnostic setting, DBT provides superior localization and characterization of noncalcified lesions, often reducing the necessity for additional specialized mammographic views or ultrasound.

- **Masses:** DBT enhances the conspicuity of both benign and malignant masses by allowing for a more detailed assessment of their shape, margins, and internal fat content. This improved margin definition is critical for accurate staging, as DBT measurements of tumours correlate more closely with final pathology than those obtained via DM.
- **Architectural Distortion:** This finding is significantly better visualized with DBT, which has led to an increased detection of both subtle malignancies and benign entities like radial scars. The PPV for architectural distortion on DBT can reach up to 50%, and it is a primary indicator for invasive lobular cancers, which are frequently occult on 2D imaging.
- **Asymmetries:** DBT is of immense value in resolving tissue asymmetries created by the chance overlap of normal glandular structures. By reclassifying these "pseudo-masses" as normal tissue, DBT increases diagnostic specificity and reduces unnecessary interventions.

3. Dense Breast Imaging and Lesion Visualization

One of the most critical advantages of DBT is its performance in dense breast tissue, where the sensitivity of 2D mammography is notoriously limited. By generating thin image sections, DBT reduces the "masking" effect of overlapping parenchyma, thereby increasing the CDR

and PPV for recall in both dense and non-dense breasts. Clinical evidence suggests the benefit is most pronounced in heterogeneously dense breasts, where DBT can reveal spiculated masses that would otherwise remain hidden. While its performance in *extremely* dense tissue remains a subject of ongoing study, DBT nonetheless offers a more conspicuous view of lesions than traditional digital systems.

4. Microcalcifications and Tissue Overlap

Although DBT is primarily recognized for enhancing the visibility of masses and distortions by removing tissue overlap, it also plays a specialized role in the evaluation of microcalcifications. While the "declustering" effect of thin-slice reconstruction can occasionally make it difficult to perceive small groups of calcifications in their entirety, the use of synthesized mammography (SM) and "slabbing" techniques (combining slices into thicker planes) helps maintain diagnostic sensitivity. DBT allows for easier localization of skin calcifications and better depicts the multifocality and distribution of malignant calcifications, providing a more comprehensive assessment of the extent of the disease. Ultimately, the ability of DBT to enhance in-plane objects while blurring out-of-plane structures remains its core technical contribution to improved diagnostic accuracy. (3)

VII. ADVANTAGES OF DBT

The introduction of Digital Breast Tomosynthesis (DBT) has successfully solved many of the inherent limitations of traditional two-dimensional (2D) full-field digital mammography (FFDM), which has long been the dominant screening method for breast cancer. While 2D mammography has dramatically decreased mortality rates by early diagnosis, its diagnostic efficiency is frequently limited by the overlaying of breast tissue.

- **Reduction of Tissue Overlap:** DBT reduces tissue overlap by capturing several low-dose projections to form thin 1-mm slices. This removes "anatomical noise" created by overlapping tissue, which can create "pseudo-masses" or disguise actual ones in 2D imaging.
- **Increased Cancer Detection Rate (CDR):** Clinical trials have demonstrated that DBT considerably improves the CDR (e.g., from 6.1 to 8.0 per 1,000 in the Oslo trial), particularly for aggressive cancer.
- **Enhanced Lesion Characterization:** DBT improves the visibility of lesion edges (such as spiculations) and architectural distortions, allowing radiologists to better evaluate the extent and form of a cancer.
- **Lower Recall and False-Positive Rates:** Since it clarifies questionable findings, DBT reduces the number of patients brought back for needless additional testing and the requirement for supplemental views such as spot compressions**.**
- **Superiority in Dense Breast Imaging:** DBT is especially helpful for women with dense breasts, where standard mammography's sensitivity is limited; it has a significantly lower false-positive recall rate than supplemental ultrasound (0.3% vs. 1.0%).(2)

VIII. LIMITATIONS OF DBT

Although Digital Breast Tomosynthesis (DBT) marks a paradigm leap in breast imaging, its application comes with a number of technological, diagnostic, and logistical challenges.

- **Increased Radiation Exposure:** One of the most significant concerns is the increased radiation exposure associated with DBT. When utilized in conjunction with

traditional 2D mammography, the average glandular dose to the breast increases by around threefold. Although this combined dose often falls under the FDA's 3 mGy per view limit, it is a considerable increase over regular full-field digital mammography (FFDM).

- **Suboptimal Microcalcification Characterization:** DBT is currently regarded as ineffective for the identification and characterisation of microcalcifications in comparison to the gold standard, FFDM with spot magnification. Because DBT reconstructs the breast in 1-mm slices, it can distort the appearance of a cluster, making it hard to understand the overall structure and distribution required for a correct BI-RADS assessment.
- **Artifacts from High-Density Objects:** Surgical clips, staples, or skin markers can cause blurring and ripple effects during the repair process. These artifacts appear as ripples in slices away from the object's real plane, obscuring surrounding anatomy or creating pseudopathologies that confuse interpretation.
- **Lower Positive Predictive Value (PPV) for Architectural Distortions:** While DBT is extremely sensitive to "unmasking" architectural imperfections, this sensitivity comes at the expense of specificity. According to research, the PPV for biopsies of architectural defects discovered exclusively by DBT is only 10.2%, which is much lower than the 43.4% PPV for those diagnosed with FFDM. This disparity reflects a higher risk of biopsying benign lesions like radial scars.
- **Significant Data Storage Requirements:** Practically, DBT creates vast amounts of data. A single examination generates files ranging from 200 to 450 MB, whereas a conventional FFDM file is usually 8 to 24 MB. Managing these enormous datasets necessitates a significant investment in high-capacity storage infrastructure and specialist high-resolution workstations.
- **Increased Radiologist Interpretation Time:** The intricacy of examining hundreds of individual tomographic slices has a considerable influence on workflow efficiency. According to studies, interpreting DBT might effectively double a radiologist's reading time compared to 2D mammography alone, which may present issues for high-volume screening programs.
- **Technical Trade-offs in Acquisition:** The quality of the DBT image is subject to inherent technical trade-offs. A wider sweep angle, for example, enhances tomographic isolation along the z-axis while decreasing in-plane resolution, which can make small features difficult to see. Furthermore, systems using uninterrupted tube motion may suffer from focal point blur, whereas "step-and-shoot" systems are more prone to patient motion abnormalities because of the longer acquisition durations.(2)

IX. COMPARISON OF DBT WITH CONVENTIONAL MAMMOGRAPHY

- **Higher Cancer Detection:** DBT routinely detects more tumors than DM. In screening studies, the Cancer Detection Rate (CDR) using DBT varied from 5.1 to 11.6 per 1,000, against 3.8 to 8.3 per 1,000 for conventional mammography.
- **Reduced Recall Rates:** DBT typically results in fewer people being brought back for unnecessary further testing. Screening recall rates for DBT were as low as 2.7%, while DM rates reached 11.5%.
- **Superior Accuracy and Sensitivity:** DBT shows much improved diagnostic accuracy. One diagnostic investigation found that DBT had a sensitivity of 98.7%, compared to 66.9% for DM.

- **Effective for High-Risk and Dense Breasts:** Women with a family history of breast cancer have increased breast density and are more likely to develop aggressive tumors. DBT is better for this group because it decreases tissue overlap artifacts and provides a more detailed "3D" picture of the breast parenchyma.
- **Better Lesion Visualization:** By delivering reconstructed 3D pictures, DBT improves localization and identification of a breast lesion's special features and margins.(6)

X. FUTURE PERSPECTIVES IN DBT

While existing methods frequently use DBT as a supplement to traditional two-dimensional (2D) mammography, future research and implementation techniques are shifting toward a more integrated and efficient approach.

1. Transitioning to Primary Screening

The biggest advance in the future of breast imaging is DBT's potential to replace 2D mammography as the primary screening method, particularly for women with dense breast tissue. This move is becoming more realistic since contemporary DBT acquisitions can now produce high-resolution reconstructed (synthesized) 2D images of the breast. Using these reconstructed images, doctors may be able to eliminate the requirement for a separate 2D exposure, expediting the screening procedure and keeping a manageable radiation dose while taking advantage of the 3D data's better sensitivity. Emerging research indicates that this "stand-alone" DBT technique is a realistic and potentially useful tool for population-level screening.

2. Innovative Implementation and Tailored Screening

Future implementation approaches are projected to shift away from a "one-size-fits-all" approach and toward more inventive, density-specific strategies. One proposed direction is to use automated density measurement during the initial routine mammography acquisition. If the software classifies the breast as dense, the system may continue to a DBT acquisition during the same clinical visit. Alternatively, women who had thick breasts in a previous screening round could be referred directly to DBT for further examinations. Such solutions would considerably improve the sensitivity of screening for high-risk groups while removing the logistical complexity and patient anxiety associated with a "second layer" of adjunct testing, such as ultrasonography or MRI.

3. Addressing Long-Term Benefits and Overdiagnosis

A crucial topic for further evaluation is the proof of long-term screening advantages. While DBT has demonstrated the capacity to detect new cancers, particularly in thick breasts where standard mammography's sensitivity is reduced, it is critical to evaluate whether this enhanced detection leads to a decrease in interval cancer rates or mortality. Furthermore, future research must keep a close eye on the risk of overdiagnosis and overtreatment, which is unavoidable with more sensitive imaging technologies.

4. Workflow and Efficiency Optimization

The future of DBT is also dependent on its capacity to provide a better mix of benefits and drawbacks than other adjunct modalities. While ultrasonography and MRI can identify more tumors, they also have considerably greater false-positive recall rates. In contrast, DBT has exhibited a significantly better recall profile, in some cases even lowering the total recall rate when compared to 2D mammography alone. DBT has the potential to improve the screening process by delivering a more sensitive mammography that clarifies findings in a single step, minimizing the "downstream consequences" of false alarms and wasteful biopsies. (7)

XI. CONCLUSION

Digital Breast Tomosynthesis (DBT) is a game-changing development in breast imaging, effectively resolving the "anatomical noise" and tissue superimposition that have historically hampered traditional 2D mammography. DBT's volumetric, layer-by-layer examination of breast tissue has considerably boosted the Cancer Detection Rate (CDR), notably for invasive cancers, while decreasing false-positive recall rates. This method has been notably useful for women with thick breast tissue, where traditional 2D imaging has historically been insensitive.Despite DBT adoption presents logistical and technical hurdles like greater radiation exposure (which has been largely minimized by synthetic mammography), vast data storage requirements, and longer radiologist interpretation times, the clinical benefits are significant. As technology advances with the incorporation of artificial intelligence and more efficient processes, DBT has a strong position to transform from a supplementary tool to the principal screening modality. Finally, DBT provides a more precise, thorough, and reliable approach to early breast cancer identification, with superior long-term outcomes for patients globally.

REFERENCES

[1] Hodgson R, Heywang-Köbrunner SH, Harvey SC, Edwards M, Shaikh J, Arber M, et al. Systematic review of 3D mammography for breast cancer screening. The Breast. 2016 Jun;27:52–61. doi:10.1016/j.breast.2016.01.002

[2] Dhamija E, Gulati M, Deo SVS, Gogia A, Hari S. Digital Breast Tomosynthesis: an Overview. Indian J Surg Oncol. 2021 Jun;12(2):315–29. doi:10.1007/s13193-021-01310-y

[3] Kulkarni S, Freitas V, Muradali D. Digital Breast Tomosynthesis: Potential Benefits in Routine Clinical Practice. Can Assoc Radiol J. 2022 Feb;73(1):107–20. doi:10.1177/08465371211025229

[4] Bahl M, Kopans DB. From film to tomosynthesis: A short history of screening mammography. Indian J Breast Imaging. 2025 Dec 15;3:59–62. doi:10.25259/IJBI_27_2025

[5] Ertas M, Yildirim I, Kamasak M, Akan A. Digital breast tomosynthesis image reconstruction using 2D and 3D total variation minimization. Biomed Eng OnLine. 2013 Dec;12(1):112. doi:10.1186/1475-925X-12-112

[6] Li T, Isautier J, Lee JM, Marinovich ML, Houssami N. Performance of Digital Breast Tomosynthesis Versus Digital Mammography in Women With a Family History of Breast Cancer: A Systematic Review. Clin Breast Cancer. 2025 Feb;25(2):e103–12. doi:10.1016/j.clbc.2024.09.013

[7] Houssami N. Digital breast tomosynthesis (3D-mammography) for screening women with dense breasts. Expert Rev Med Devices. 2016 Jun 2;13(6):515–7. doi:10.1080/17434440.2016.1184971

6
Chapter

Advanced Multimodal Imaging of the Hippocampus: Anatomical Precision and Pathological Correlation

[1]Sidra
M.Sc. Research Scholar
Department of Radiological Imaging Techniques,
College of Paramedical Sciences,
Teerthanker Mahaveer University,
Moradabad
sidraasad166@gmail.com

[2]Mohd. Harish Saifi
M.Sc. Research Scholar
Department of Radiological Imaging Techniques,
College of Paramedical Sciences,
Teerthanker Mahaveer University,
Moradabad
saifiharish350@gmail.com

[3]Rashmi Pandey
Assistant Professor
Department of Radiological Imaging Techniques,
College of Paramedical Sciences,
Teerthanker Mahaveer University,
Moradabad
rashmi.paramedical@tmu.ac.in

[4]Kritika Agarwal
Department of Radiological Imaging Techniques,
College of Paramedical Sciences,
COER University,
Roorkee

Abstract

The hippocampus is an important brain structure located inside the temporal lobe, is a key component of the archipallium cortex, playing a crucial role in cognitive functions such as memory formation, spatial navigation, and emotion regulation. This complex structure is composed of the dentate gyrus, cornu ammonis (CA1-CA4), and subiculum, and its anatomical components include a head, body, and tail. Malfunctions in this area are significantly linked to nervous system disorders like epilepsy and alzheimer's disease, with ongoing research investigating molecular and morphological changes.

MRI is the preferred method for detailed hippocampal studies, especially for clinical assessments. Ultra-high field (UHF) MRI scanners, operating at 7 Tesla (7T) or above, offer significant advancements by providing enhanced contrast, signal-to-noise ratio, and superior spatial resolution. These improvements are critical for visualizing the hippocampus's intricate subfields and cellular layers, which are often challenging to identify with lower magnetic field intensities. Advanced imaging protocols, including computational unfolding and interpolation techniques, are employed to overcome the challenges posed by the

hippocampus's complex 3D form, allowing for more accurate demarcation and analysis of its subregions. These high-resolution capabilities are essential for detecting early signs of cognitive impairment, identifying radiological biomarkers for diseases such as Alzheimer's, and enhancing diagnostic accuracy and treatment planning.

Keywords: Hippocampus, Magnetic Resonance Imaging (MRI), Ultra-High Field (UHF) MRI, Hippocampal Subfields, Temporal Lobe Epilepsy (TLE), Hippocampal Sclerosis (HS), Neurodegenerative Disorders, Spatial Resolution, Segmentation.

I. INTRODUCTION

The hippocampus is an important brain structure located inside the temporal lobe, is a key component of the archipallium cortex, which also comprises structures like the dentate gyrus, cornu ammonis (CA), and subiculum. These portions are characterized by distinct layers and intricate connections to neighboring brain regions via afferent and efferent neurons. The cornu ammonis is divided into three regions: CA1, CA2, and CA3. CA1 and CA3 are very important for memory and understanding activities. The hippocampus plays an important role in creating memories, understanding, spatial navigation, and controlling emotions, and a combination of both sensory and motor nerve fibers is required for these tasks. Memory development requires simultaneously short duration changes in neuronal electrical characteristics and long duration changes in synapse framework, including long-term potentiation (LTP).

In adults, the hippocampus is approximately 3-3.5 cm^3 each hemisphere. Malfunctions in this area can result in Alzheimer's disease and epilepsy. Previous research has repeatedly connected many neurological illnesses to hippocampus anomalies, including transformations that vary from molecular to morphological changes being thoroughly investigated. Assessing the general anatomical form, functions, and interconnections of the hippocampus, as well as its variations in different disease states, is critical for designing treatment techniques to avoid or mitigate related changes (1).

II. ANATOMY OF THE HIPPOCAMPUS

1. Location and Gross Anatomy

The hippocampus is a critical brain region located inside the temporal lobe that is distinguished by its special place and physical characteristics.

- **General Location**
  - The hippocampus is a brain area located inside the temporal lobe with a curved and raised structure on its inner surface.
  - The archipallium cortex develops along the temporal lobe's inferomedial aspect and extends to lateral ventricle through the C shaped choroidal fissure.
  - Adult’s hippocampus has a capacity of 3-3.5 cm^3 and a length of approximately 5 cm for each hemisphere.

- **Anatomical Components**
  - The hippocampus made up of the folding dentate gyrus, cornu ammonis (CA), and subiculum.
  - The body, head, and tail are the three primary components, with the head comprising the largest.

- The hippocampal sulcus delineates the cornu ammonis from the dentate gyrus, whereas the subiculum lies beneath this sulcus and fluidly merges into the six-layered neocortex of the parahippocampal gyrus.

- **Developmental and Structural Features**
  - The molecular layers of the dentate gyrus and subiculum are brought closer together throughout development when the cornu ammonis and dentate gyrus migrate to the inferior horn of the lateral ventricle near the hippocampal sulcus.
  - The alveus, a thin layer of grey matter, protects the ventricular surface of the hippocampus, which resembles a seahorse.
  - The alveus is created by the convergent axons of hippocampus pyramidal cells, resulting in fimbriae. Such fimbriae expand posteriorly to enclose the dentate gyrus and attach to the splenium of the corpus callosum, ultimately connecting with the fornix.
  - The fimbria-dentate sulcus divides the fimbria and dentate gyrus.
  - The anterior part of the hippocampus forms a paw-like structure known as 'pes hippocampi' (1).

Julius Caesar Aranzius (1530-1589), an Italian anatomist, was the first to define a region in the medial temporal lobe, which he dubbed the "hippocampus" because it resembled a seahorse. The word "hippocampus" comes from the Latin word for seahorse (2).

Figure 1: The hippocampus, dentate gyrus, subiculum, and entorhinal cortex.

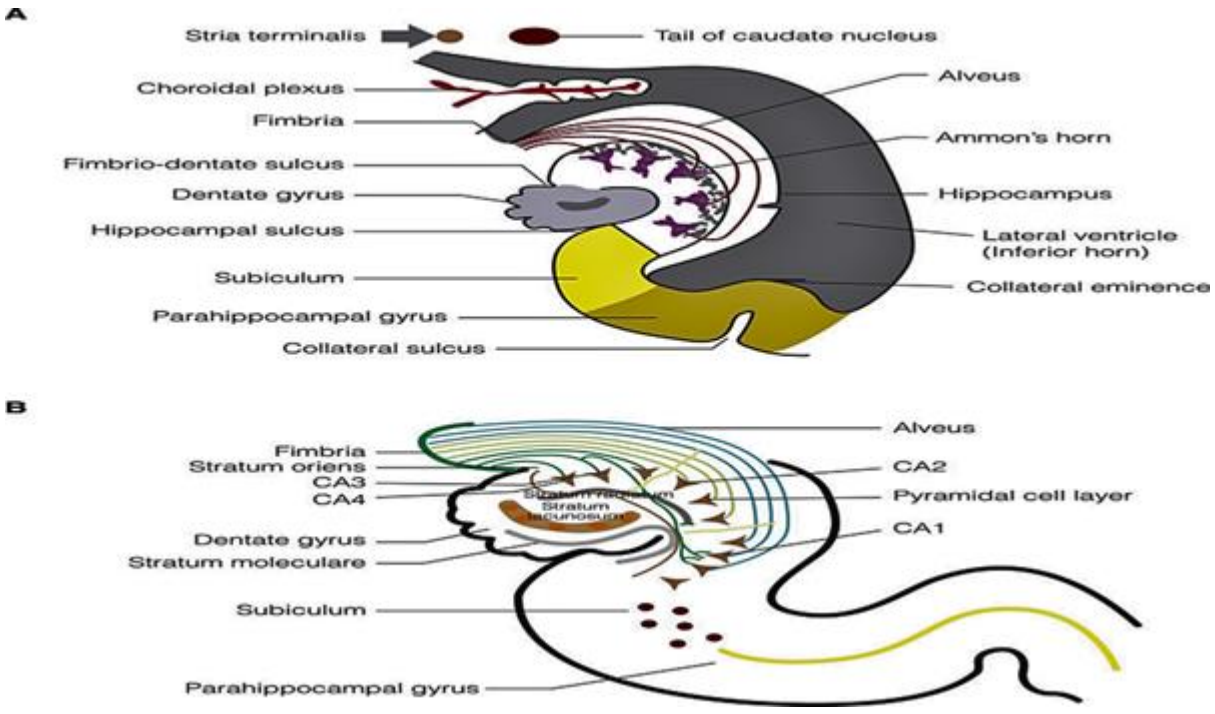

A, Coronal section through the hippocampus and dentate Gyrus; **B,** Schematic diagram to show the histological layers of the dentate gyrus and cornu ammonis (3) .

2. Cellular Organization and Subfields

The hippocampus is a complex structure of the brain that, along with the other parts, forms the hippocampal formation. This framework comprises mostly of three fundamental sections.

- **Dentate Gyrus:** The dentate gyrus plays a crucial role in hippocampal formation.
- **Subicular Plexus:** A critical component of hippocampal development.
- **Hippocampus Proper:** The hippocampus has been separated into four sections, known as (cornu ammonis - CA regions) :

1. CA1
2. CA2
3. CA3
4. CA4 (4).

- **Specific Subfields and Their Descriptions**
  - **Cornu Ammonis (CA) Fields:** The Cornu Ammonis (CA) Fields consist of CA1, CA2, CA3, and CA4, that are separate portions of the Ammon's Horn.
  - **Dentate Gyrus (DG):** The Dentate Gyrus (DG) is the hilar portion of the dentate gyrus, which may consist of the Granule Cell Layer (DG:GCL) or be associated with CA3 or CA4.
  - **Subiculum (Sub):** Subiculum (Sub) is a subfield of the hippocampus that can be studied for its molecular layer (Sub:ML) or stratum pyramidale (Sub:SP).
  - **Stratum Radiatum and Stratum Lacunosum-Moleculare (SRLM):** The SRLM belongs to the integrated stratum radiatum and stratum **l**acunosum-moleculare of CA1 or the hippocampus in generally.
  - **Stratum Pyramidale (SP):** The stratum pyramidale (SP) is the pyramidal cellular layer of CA1 or CA1-3.
  - **Hilum:** The hilum consists of the CA4 stratum pyramidale, stratum granulosum, and polymorphic layer of the dentate gyrus.
  - **Entorhinal Cortex (ERC):** The entorhinal cortex (ERC) is a cortical area that is sometimes segmented among hippocampal subfields (5).

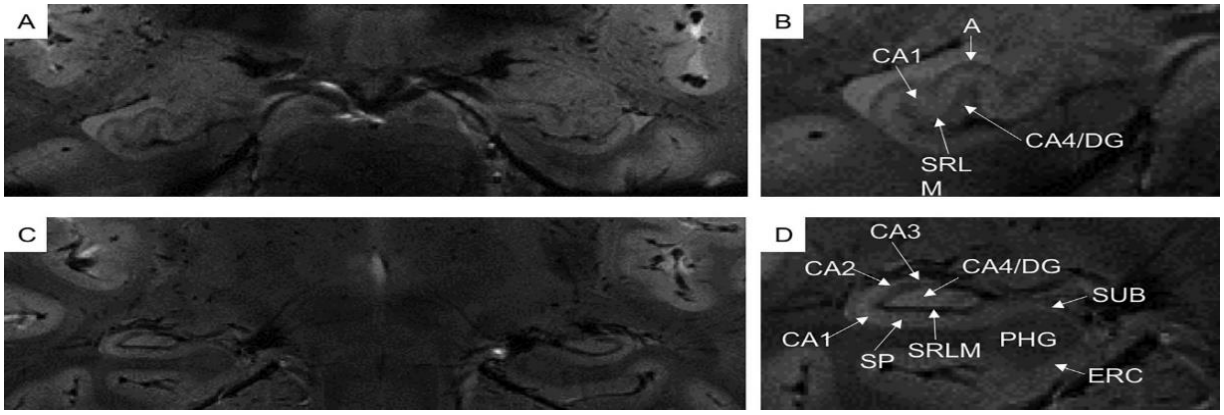

Figure 2: *In vivo* coronal T_2*-weighted images at 7T of hippocampal head (A,B) and body (C,D). Very small hippocampal structures are visible, such as cornu ammonis (CA1-4), dentate gyrus (DG) and subiculum (SUB). In the cornu ammonis, especially in CA1, it is possible to distinguish between the stratum pyramidale (SP) and the composite of the strata radiatum, lacunosum and moleculare and the vestigial hippocampal sulcus (SRLM). A = alveus, ERC = entorhinal cortex, PHG = para-hippocampal gyrus (5).

3. Gray and White Matter Components

- **Gray Matter:** The hippocampus's gray matter is made up of the cornu ammonis, which is compressed inside the dentate gyrus, and the fascia dentata, which includes the histologically characterized CA1-4 areas. This gray matter makes up the hippocampus head, body, and tail.

- **White Matter:** The alveus and fimbria are white matter routes that convey axons from hippocampus, subicular, and septal neurons to other limbic regions. The alveus surrounds the hippocampus body superiorly and laterally and is important in defining the hippocampal-amygdala boundary (2).

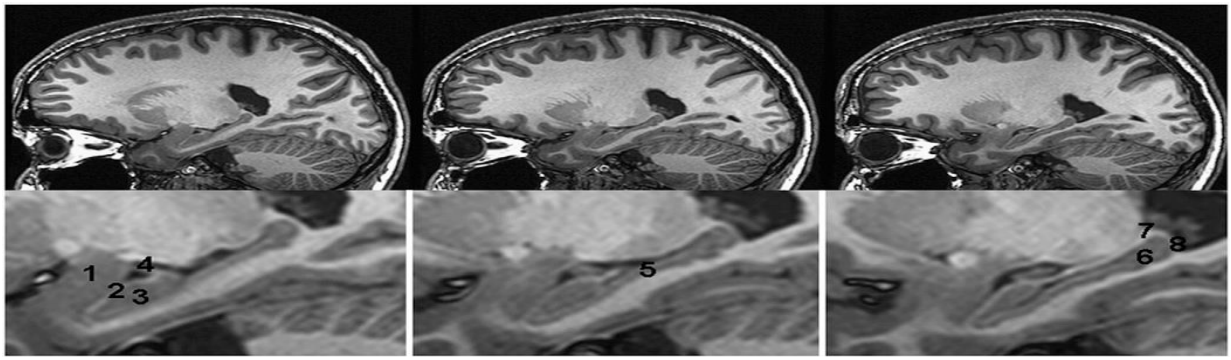

Figure 3: The hippocampus contains both gray and white matter. Sagittal MR scans of the hippocampus (from medial slice-left picture to lateral slice-right image) and magnified views of the hippocampal region (bottom row) demonstrate gray matter of the hippocampal head, body, and tail, overlaid by white matter of the alveus and fimbria and amygdala. 1=amygdala, 2=alveus, 3=hippocampal head, 4=temporal horn of the lateral ventricle and fimbria, 5=hippocampal body, 6=hippocampal tail, 7=fimbria, 8=alveus (2).

4. Hippocampal Borders and adjacent structures

The human hippocampus is a complex allocortical structure with multiple boundaries and structural elements that must be identified in MRI imaging. Fortunately, defining these limits can be challenging due to anatomical complexities and terminological inconsistencies.

- **Specific Borders and Adjacent Structures**
  - **Anterior Border:** Because of the close connection of the amygdala and hippocampus, defining this line is problematic. Alveus (internal), the lateral ventricle's cerebrospinal fluid (external), and the inferior horn's uncal recessus are all employed as landmarks. Some protocols employ the corpora mamillaria on coronal slices.
  - **Posterior Border:** There is a lot of customization available for this border. The posterior end of the lateral ventricle, which is frequently utilized as an external marker, is situated at the coronal slice, where an oval gray matter emerges inferiomedially to the lateral ventricle's trigone. The fornices are also used to identify the posterior end while it is still clearly visible. Other procedures use the inferior or superior colliculi. The most accurate volume estimate is obtained by analyzing the gray matter in the hippocampus tail until its oval shape disappears.
  - **Superior Border:** This boundary is reliably determined by both the alveus (internal) or CSF (external).

- **Lateral Border:** The lateral border is not debatable, and it is most commonly delineated by the CSF of the lateral ventricle, which serves as an external reference.
- **Superior Medial Border:** There is considerable agreement on this border, which is generally defined by the cisterna ambiens' CSF.
- **Inferior Medial Border:** This border is delineated in less than half of the procedures, typically utilizing arbitrary lines due to the difficulty of correctly linking cytoarchitectonically defined sections (prosubiculum,subiculum), presubiculum, parasubiculum, and entorhinal cortex have macroanatomical markers. Straight horizontal lines, diagonal lines, and arbitrary vertical lines are some examples (2).

III. FUNCTION OF THE HIPPOCAMPUS

Its principal roles are:

1. **Memory Formation and Learning**
   - The hippocampus plays a vital role in cognitive function, learning, and memory formation. It is essential for memory formation and cannot be replaced by other brain structures.

2. **Spatial Navigation**
   - The hippocampus relies heavily on afferent and efferent fiber connection to provide spatial navigation capabilities.

3. **Emotion Regulation**
   - The hippocampus also helps with emotion regulation. The Papez circuit, which includes the hippocampus, performs a function in controlling emotions.

4. **Stress Response Regulation**
   - The hippocampus regulates the stress response. It has several cortisol receptors with high sensitivity.

5. **Clinical Relevance**
   - **Malfunction Implications:** Malfunction in the hippocampus can result in Alzheimer's disease and epilepsy. Hippocampal anomalies have been associated to several clinical illnesses, including Alzheimer's disease, epilepsy, and depression (1).

IV. IMAGING TECHNIQUES FOR THE HIPPOCAMPUS

1. MR Imaging Techniques

Magnetic resonance imaging (MRI) is the principal method for doing thorough hippocampal research, particularly diagnostic evaluations. Several approaches are employed to better imaging and research of this complex brain region

- **Clinical Hippocampal Imaging**
  - **High-Field Strength Scans:** High-field strength MR (1.5-T) scans are thought to be the best option for thorough hippocampus research.
  - **Optimized Window Settings:** To achieve high quality, all photos should use window settings that maximize gray-white matter distinction.

- **Standard Axial Images:** Obtaining high-quality standard axial pictures of the brain is critical for detecting concurrent or distinct disorders.
- **Coronal Scans:** In addition to axial imaging, particular coronal studies of the hippocampus are required.

This includes:

- Uses fast spin-echo T2 and spin density-weighted pictures with a 20- to 24-cm field of view, 256 × 256 matrix, and 3- to 5-mm sections with minimal gaps.
- T1-weighted pictures typically have a 16-cm field of view, 3- to 5-mm continuous slices, and four repeats.
- Use T1-weighted distorted gradient-recalled echo, inversion recovery, or T1-weighted fluid-attenuated inversion recovery sequences if possible.

- **Volumetric Analysis**
  - **Extensive Research:** In the past few years, more than 90 studies have described MR volumetric investigation of limbic regions.
  - **Clinical Impracticality:** Despite extensive research, these examinations are now unsuitable for standard healthcare institutions since they require highly skilled personnel to manually sketch the hippocampus outline. The detailed technique for this was recently reviewed.
- **Spectroscopy**
  - **Biochemical Information:** MR spectroscopy provides a non-invasive method for obtaining biochemical information from living tissue.
  - **Clinical Limitations:** Several technical constraints limit the clinical application of 1H MR spectroscopy in limbic system investigations.
    These involve crowded spectral peaks under optimal conditions, as well as magnetic field inhomogeneities induced by bone or air interfaces near the hippocampus, which can expand spectral peaks and make quantitative analysis difficult.
  - **Potential Improvements:** The combination of tiny voxel sizes and effective magnetic field homogeneity optimization with spectroscopic imaging techniques should broaden the medical use of MR spectroscopy in the limbic system (6).

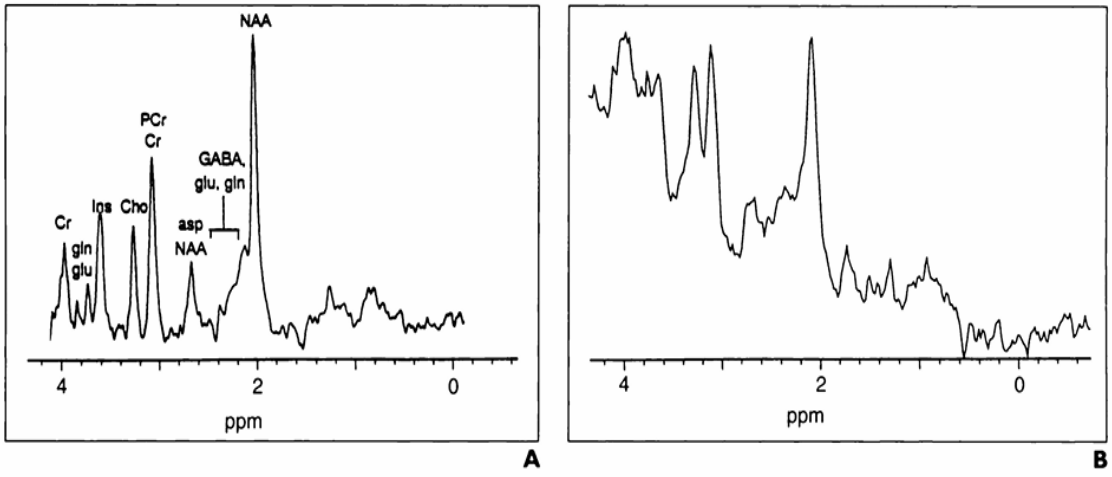

Figure 4: MR spectra (6).

2. High-Resolution Imaging Protocols

High-resolution imaging of the human hippocampus necessitates particular techniques to overcome obstacles such as its complex structure and signal loss. These methods are aimed at increasing subregional vision and obtaining higher spatial resolution.

Key Imaging Parameters and Techniques

- **Resolution Enhancement**
  - Initially, structural T2-weighted images with high in-plane resolution (0.4 mm) and longitudinal plane resolution (3 mm) were interpolated to achieve an isotropic resolution of 0.4 mm^3.
  - Improved visualization of CA1, dentate gyrus, and CA23 with greater resolution at 3 Tesla.
  - New sequences enhanced the longitudinal plane resolution from three millimeters to one millimeter, boosting the ability to see hippocampus portion.
  - To reduce slice thickness and increase the number of oblique slices across the hippocampus, specific scan sets were designed, firstly achieving voxel sizes of 0.4 × 0.4 × 3.0 mm, later 0.5 × 0.5 × 1.2 mm and 0.4 × 0.4 × 1 mm.
  - Increasing the number of scan averages (NEX) to three, together with base resolution adjustments, improved image quality while requiring little scan time.
  - Adjustments to field of view (FoV), flip angle, and echo times (TE) compensated for the negative consequences of reducing base resolution, resulting in a better balance of signal-to-noise ratio (SNR) and enhanced total resolution.

- **Automated Interpolation**
  - MATLAB's sequential technique interpolates segmentation masks and hippocampus pictures before flattening to obtain better resolution maps.
  - This procedure consists of several steps: interpolation, anisotropic curvature smoothing, thresholding, and 3-D rendering.
  - This approach takes any segmented image series and interpolates them along the z-axis to produce the desired increased slice thickness.
  - The interpolation procedure begins with labeling gray matter by exclusion after manually segmenting white matter and CSF, followed by automatic interpolation along the z-axis using linear interpolation to achieve the desired z-axis resolution (0.4 mm).

- **Computational Unfolding and Boundary Demarcation**
  - The 3-D gray matter strip is digitally flattened into 2-D using the mrUnfold software, with every layer of gray matter unfolded independently.
  - This 3-D to 2-D transformation converts subregional borders and functional stimulation to flat space.
  - The 3-D hippocampal scan uses landmarks to determine biological boundaries for subregions such as CA1-CA23DG, CA1-Subiculum, and adjacent cortical areas. These boundaries are then projected into the flattened 2-D picture.
  - These enhanced technologies provide better visualization of hippocampus subregions and their activity during cognitive tasks, providing a major advantage over traditional imaging methods (7).

3. Ultra-High Field MRI

Ultra-High Field Magnetic Resonance Imaging (UHF MRI) is an important breakthrough in neuroimaging, providing new tools for understanding the brain's complicated structures.

- **Definition and Characteristics**
  - **Field Strength:** UHF MRI devices work with static magnetic field intensities of 7 Tesla (7T) or above. This sets them apart from ordinary high-field scanners.
  - **Improved Imaging:** When compared to standard high-field scanners, UHF MRI provides new contrasts, a higher signal-to-noise ratio (SNR), and increased spatial resolution. These enhancements enable improved viewing of extremely small brain regions, particularly hippocampus subfields.
- **Advantages and Research Perspectives**
  - **Enhanced Visualization:** UHF MRI's greater spatial resolution and signal-to-noise ratio make it much easier to see hippocampus parts and distinguish between submillimetric borders and cellular layers. This is especially important for small structures like hippocampus subfields, which are hard to identify using lower magnetic field intensities.
  - **Clinical Research:** UHF MRI opens up new options for clinical research by enabling for the realistic portrayal of microscopic brain areas at submillimetric resolutions. It is an Effective strategy for identifying radiological biomarkers for diseases such as Alzheimer's and increasing diagnostic efficiency.
  - **Specific Applications:** 7T research frequently concentrates on the hippocampus, using high-resolution imaging to visualize hippocampal subfields and measure small variations across hippocampal strata, like strata lacunosum-moleculare and pyramidale. It may also demonstrate and see the endfolial pathway in the hippocampus formation without causing any damage.

- **Impact on Hippocampal Studies**
  The capacity of UHF MRI to give high-resolution pictures has greatly helped the research of hippocampus morphology. Variations in the volume and thickness of hippocampus subregions are critical for early detection of pathological cognitive decline and Alzheimer's disease. Although low field strengths (less than 7T) are being utilized in huge populations to discover biomarkers, UHF MRI is likely to yield more accurate sequences for specific clinical results due to its high level of specificity and sensitivity (5).

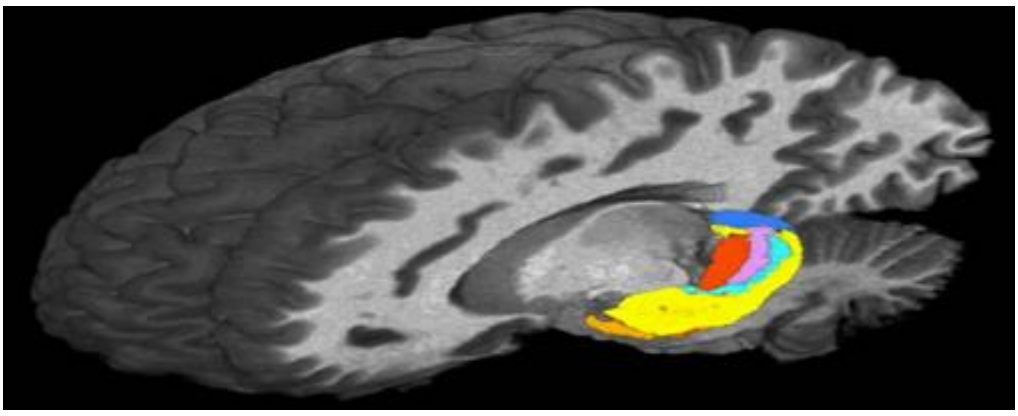

Figure 5: Ultra High Field MRI Detects Differences in Brain's Hippocampus (8).

4. Functional MRI

Functional Magnetic Resonance Imaging (fMRI) is a type of neuroimaging that analyzes the brain's activity by identifying variations in blood flow. It is frequently used to investigate brain activation throughout cognitive activities.

- **Challenges of Hippocampal fMRI**
  - **Convoluted Structure:** The hippocampus is a strong framework to see with both MRI and fMRI because of its intricate, complicated architecture and sensitivity for signal breakdown.
  - **Limited Resolution:** Conventional fMRI/MRI techniques often lack the spatial resolution required for imaging the hippocampus and its subdivisions at a resolution of less than one millimeter. Historically, this constraint has limited our understanding of how hippocampus subregions play a role in memory.

- **Advancements in Hippocampal fMRI Studies**
  - **Improved Resolution:** Recent developments have led in significantly higher resolution operational and anatomical images of the hippocampus and surrounding cortex. These advances enable improved overall resolution scanning of the hippocampus, particularly at 3 Tesla.
  - **Enhanced Imaging Sequences:** The study describes improvements to current anatomical imaging sequences that improve in-plane resolution of the hippocampus. The altered sequences improve longitudinal plane resolution by 3mm to 1mm, which is critical for hippocampal function due to changes in input and their processing across the anterior-posterior axis. They boost the visibility of specific subregions, including the front part of CA1, the dentate gyrus, and CA23.
  - **Computational Unfolding and Interpolation:** A novel computational interpolation technique is proposed to improve the ability to depict the hippocampus' complex 3-D form. The procedure involves physically separating hippocampus gray matter, changing it to higher resolution (e.g., 0.4 mm isotropic), then digitally unfolding the 3-D gray matter strip into a 2-D flat map.
  - **Group Activation Mapping:** A quantitative way to establishing group activation patterns has been developed, which entails creating averaged flat maps using vector field warping techniques. Activations can be tailored to various hippocampal subregions in different subjects. The software used for these processes is compatible with a variety of operational imaging programs, including SPM, FSL, and AFNI.
  - **Benefits of Flat Maps:** Flat maps are useful as they allow for the display of hippocampal subdivisions and stimulation across the long axis in a single picture, resulting in higher resolution and group analysis inside the hippocampus proper (7).

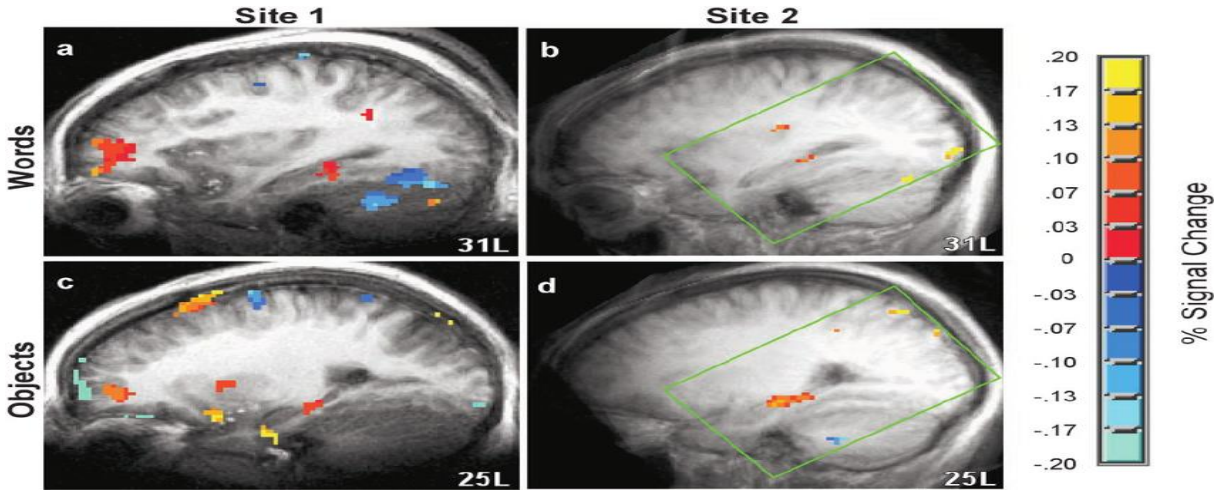

Figure 6: Hippocampal region activity: sites 1 and 2. fMRI data from participants in both the Words and Objects conditions (two recognition tests for each condition) were analyzed separately at each of the two MRI facilities to assess the reliability of the findings (9).

5. CT and Nuclear Medicine

Although Magnetic Resonance Imaging (MRI) is the most common technique for evaluating the hippocampus, Computed Tomography (CT) and nuclear medicine techniques like Positron Emission Tomography (PET) and Single-Photon Emission Computed Tomography (SPECT) are used to diagnose a variety of hippocampal disorders.

- **Computed Tomography (CT)**
  - **Complementary Role**
    - ✓ Combining CT with MRI improves analysis of hippocampal conditions.
    - ✓ It can detect high attenuation during T1-weighted imaging in certain instances of focal cortical dysplasia (FCD).
  - **Specific Findings**
    - ✓ CT imaging can detect hippocampal calcification, which occurs in more than 30 percent of patients having cerebrovascular illness and 45 percent of those aged 80 or older, indicating an atherosclerotic etiology.
    - ✓ CT imaging of lipoid proteinosis shows horn-shaped calcifications in the mesial temporal lobe, which are bilaterally and symmetrical.

- **Nuclear Medicine (PET and SPECT)**
  - **Primary Techniques**
    - ✓ Popular nuclear medicine procedures for hippocampus evaluation include metabolic PET and brain perfusion SPECT using fluorine-18 fluorodeoxyglucose (FDG).
  - **Functional Assessment**
    - ✓ SPECT and PET can directly examine hippocampus functioning and output pathways.
    - ✓ They can evaluate limbic areas, including the posterior part of the cingulate cortex and various cortical regions.
  - **Diagnostic Accuracy and Differentiation**
    - ✓ FDG PET is more accurate than perfusion SPECT for hippocampus-related diseases.
    - ✓ It is a better alternative to MRI for diagnosing neurodegenerative disorders.

- ✓ FDG PET can distinguish Alzheimer's disorder from frontotemporal lobar degeneration (FTLD) and Lewy body dementia in neurodegenerative illnesses affecting the medial temporal lobes.

➢ **Specific Applications**

- ✓ **Autoimmune Encephalitis:** FDG PET can detect certain trends, like a localized rise in tracer uptake (hypermetabolism) or hypometabolic foci (indicating sequelae), that may appear before T2-weighted hyperintensities on MRI. If clinical suspicion is high and MRI results are insufficient, additional research is indicated.
- ✓ **Infectious Encephalitis:** Nuclear medicine studies reveal hypermetabolism on FDG PET & enhanced perfusion on SPECT in afflicted areas.
- ✓ **Epilepsy:** Ictal SPECT investigations can detect epileptogenic foci with hyperperfusion, but postictal studies reveal hypoperfusion in afflicted areas. Monitoring with video electroencephalography (EEG) is required for ictal epilepsy research to avoid misunderstanding (4).

6. Image Acquisition Parameters

- **Acquisition Plane:** The majority of the research examined employed the coronal plane during MRI acquisition, with sagittal planes being less common and axial planes being used by only a small number of studies. While most recent research recommends making anatomical conclusions using three orthogonal viewing planes, tracing procedures are often performed in a single plane. This multiplane vision enables more exact boundary definition than single-plane delineation.

- **Voxel Size and Resolution:** Voxel size did not remain consistently isotropic across trials. The in-plane picture resolution is typically 1 mm x 1 mm, with a slice spacing of 1.5 mm. High MR field strength and resolution are essential for viewing and recognizing anatomical boundaries, particularly the difficult anterior border represented by the alveus. For realistic anatomical borders, a resolution of 1 x 1 × 1 mm^3 or lower is recommended.

- **Head Coverage and Slices:** Information about head covering or the quantity of slices was frequently lacking in the reviewed articles. When mentioned, the most common number of slices was 124.

- **Impact on Volumetric Results:** Technical MRI factors like MR sequencing, signal-to-noise ratios, field strength, total slice count, cranial coverage, and imaging quality all have a significant impact on the variability of volumetric data in hippocampal studies. Higher resolution studies were more likely to report differences between patient and control groups.

- **General Recommendations:** To reduce variance and improve accuracy, it is recommended to use high MR field strength for better resolution, acquire images with a resolution of 1 × 1 × 1 mm^3 or less, and utilize software
  It enables the simultaneous observation of all three orthogonal planes to inform anatomical choices. In addition to increasing the delineated surface area on oblique coronal slices, aligning the brain along the hippocampal longitudinal axis instead of the AC-PC plane enables more detailed surface depiction (2).

V. HIPPOCAMPAL VOLUMETRY AND MEASUREMENT

Hippocampal morphometry is essential in neuroimaging research because it influences memory functions and is susceptible to pathological illnesses such as Alzheimer's disease (AD). Variations in the size and thickness of hippocampal subdivisions may aid in the early diagnosis of cognitive impairment and Alzheimer's disease. Ultra-high field (UHF) MRI systems with static magnetic field strengths of ≥7T offer new research opportunities by improving signal-to-noise ratio, contrast, and spatial resolution. This increases visibility of tiny brain structures such as hippocampus subfields.

1. Manual Methods for Hippocampal Subfield Measurements

- **Volumetric Assessment:** Several manual ways to measuring hippocampal subfields at UHF have been developed, including both monodimensional and three-dimensional measurements. Parekh et al. used a balanced steady-state free precession (bSSFP) sequence at 7T and 0.4 × 0.4 × 0.4 mm^3 resolution to segment nine subfields: CA1-4, stratum radiatum and stratum lacunosum-moleculare (SRLM), alveus, fornix, subiculum, and its molecular layer. Boutet et al. used T2*-weighted images (0.3 × 0.3 × 1.2 mm^3) to map hippocampal layers based on neuronal body number.
- **Thickness Assessment:** Kerchner et al. employed a 2D T2*-w GRE sequence with 195 μm resolution to manually measure the thickness of SRLM (CA1:SRLM) and CA1's stratum pyramidale (CA1:SP). Six stratum thickness measurements were collected at various locations in the CA1 sector, with an average of two adjacent slices.

2. Semi-Automated Methods for Hippocampal Subfield Measurements

- **Manual Intervention with Automation:** Semi-automated techniques necessitate a beginning manual intervention requiring anatomy knowledge but subsequently continue without additional user input. Kerchner et al. (2012) visually recognized hippocampus subfields using human atlases and coupled manual measurements of DG + CA3 cross-sectional area & entorhinal cortex (ERC) width with automated methods. They also used a 7T T2-w rapid spin echo sequence to determine the thicknesses of CA1:SP and CA1:SRLM.
- **Computational Unfolding:** Suthana et al. (2015) employed computerized unfolding to identify subfields in 7T high-resolution structural images, including CA1-3, DG + CA4, subiculum, ERC, and parahippocampal cortex. This procedure entails manually segmenting white matter and CSF and then automatically assigning subfield labels using atlases.

3. Automated Methods for Hippocampal Subfield Volumetry

- **Atlas-based Segmentation:** Totally automated techniques require manually annotated atlases or training data. Examples include Freesurfer, MAGeT-Brain, and ASHS (Automatic Segmentation of Hippocampal Subfields). Freesurfer, for example, separates hippocampal subfields using a statistical atlas of hippocampus morphology and an MRI-generated model. The most recent version of Freesurfer (v6.0) builds its atlas using ex vivo 7T pictures with great spatial resolution (0.13 × 0.13 × 0.13 mm^3).
- **Multi-Atlas Algorithms:** MAGeT-Brain is a multiple-atlas technique that builds a template library from a collection of manually segmented images by propagating segmentations through image registration and label fusion. ASHS combines multi-atlas methods with machine learning strategies and has been used to analyse UHF MRI in vivo data. It enables automated segmentation of hippocampus subfields

utilizing T2-w MRI scans and T1-w MRI as additional input, resulting in volume and thickness studies (5).

VI. HIPPOCAMPAL PATHOLOGY

1. Acute Hippocampal Disorders

The hippocampus, a highly metabolically active area of the brain, is susceptible to a wide range of acute conditions. These diseases may be divided into numerous groups, each with its own clinical and magnetic resonance imaging (MRI) results, especially on diffusion-weighted imaging (DWI). Understanding these diverse imaging features is crucial for making a differential diagnosis since they correlate with clinical complaints.

Categories of Acute Hippocampal Disorders

- **Infection:** This category comprises diseases such as Herpes Simplex Virus (HSV) encephalitis and Japanese encephalitis. In the early stages, HSV encephalitis is characterized by hyperintensity on DWI and hypointensity on apparent diffusion coefficient (ADC) maps, mostly affecting the anterior and medial temporal lobe. DWI and FLAIR imaging of Japanese encephalitis can reveal patchy hyperintense lesions in both the hippocampi and the thalamus.

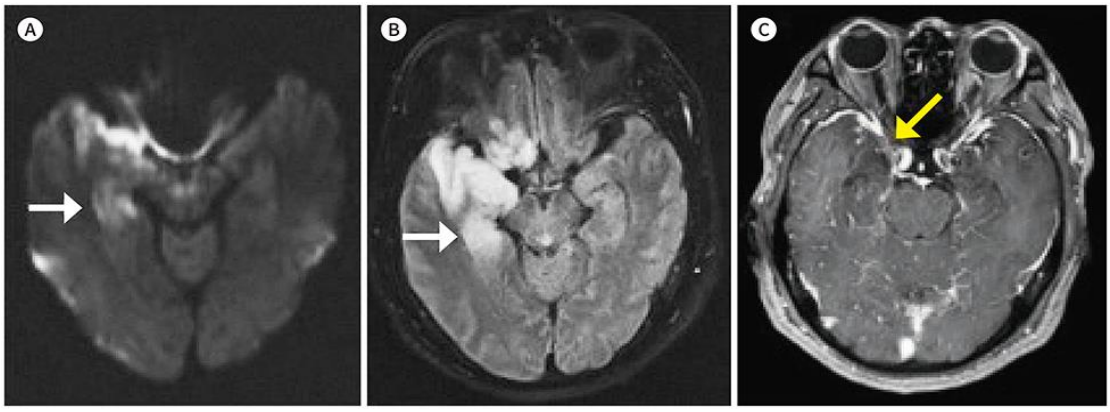

Figure 7: A 62-year-old male diagnosed with herpes simplex virus encephalitis.

A. Diffusion-weighted image shows patchy hyperintense lesions in the right hippocampus (arrow) and right parahippocampal gyrus.
B. The fluid-attenuated inversion recovery image also shows patchy hyperintense lesions in the right hippocampus (arrow), right parahippocampal gyrus, frontal lobe, and temporal lobe.
C. The enhanced T1-weighted image shows prominent leptomeningeal enhancement along the pial surface of the right temporal cortical sulci (arrow) (10).

- **Inflammation**
  - **Autoimmune Encephalitis:** Autoimmune encephalitis is an antibody-mediated inflammatory disease that usually affects the limbic system. On DWI, MRI may indicate hippocampus hyperintensities, but it is not always obvious whether they are due to cytotoxic alterations or T2 shine-through. Temporomesial structures can experience swelling and hyperintensity for months or even years.

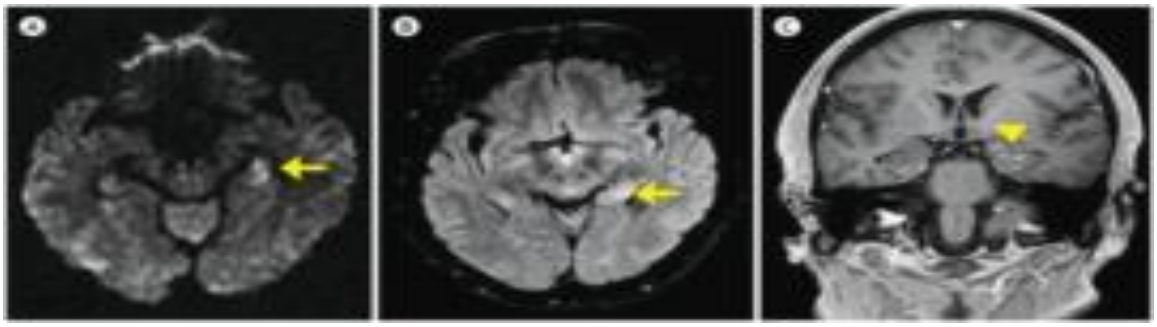

Figure 8: A 46-year-old male diagnosed with autoimmune encephalitis.

A, B. Diffusion-weighted (A) and fluid-attenuated inversion recovery (B) images show a patchy hyperintense lesion in the left hippocampus (arrows).
C. Coronal enhanced T1-weighted image shows a patchy enhancing lesion in the left hippocampus (arrowhead) (10).

- **Metabolic**
  - **Hypoglycaemic Encephalopathy:** This condition is associated with severe hypoglycemia, resulting in unconsciousness, altered mental status, and convulsions. Hyperintensity is seen on DWI and T2-weighted images of the posterior limbs of the internal capsule, hippocampus, basal ganglia, and cerebral cortex, which is a common MRI result. Lesions can exhibit reversible restricted diffusion. The postulated explanations for diffusion restriction include energy failure, excitotoxic edema, and asymmetric cerebral blood flow. Contrast enhancement is possible; however, hemorrhages are quite rare.

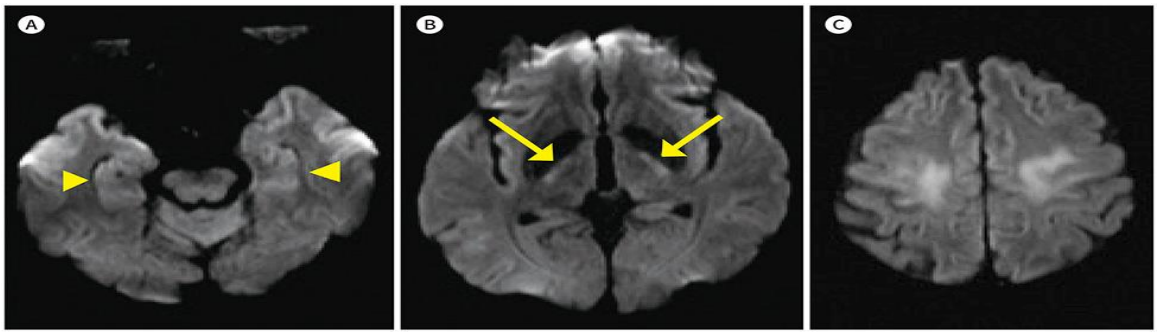

Figure 9: A 66-year-old male diagnosed with hypoglycemic encephalopathy.

A-C. Diffusion-weighted images show patchy hyperintense lesions in both hippocampi (arrowheads), posterior limbs of the internal capsule (arrows), and high frontal white matter and cortex areas (10).

- **Ischemic**
  - **Acute Ischemic Stroke:** Although it is uncommon, acute ischemic stroke can cause damage to the hippocampus. DWI aids in distinguishing hippocampal infarction, which can manifest in four different ways, from other neurological illnesses. Hypoxic ischemia insult, caused by insufficient oxygen or blood flow, first affects gray matter regions such as the hippocampus, resulting in broad diffusion limitation on DWI in the acute phase.

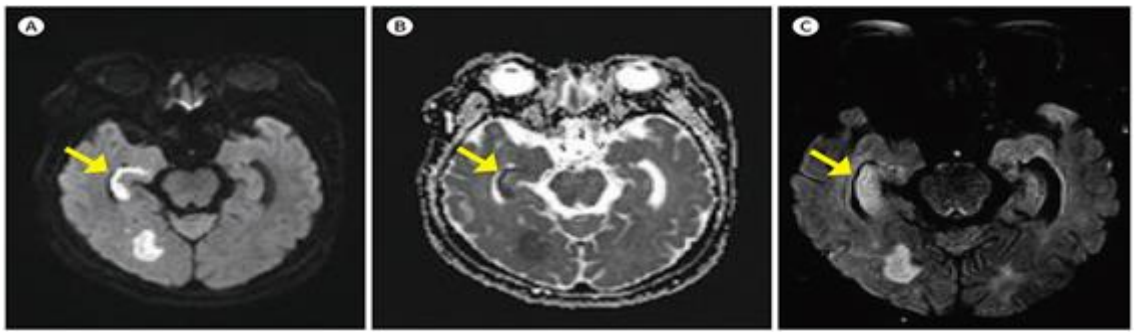

Figure 10: A 48-year-old female diagnosed with acute ischemic stroke.

A. The diffusion-weighted image shows patchy hyperintense lesions in the right hippocampus (arrow) and occipital area.
B. The apparent diffusion coefficient map shows patchy hypointense lesions in the right hippocampus (arrow) and occipital area.
C. The fluid-attenuated inversion recovery image shows patchy lesions with a slightly increased signal intensity in the right hippocampus (arrow) and occipital area (10).

- **Traumatic**
  - **Diffuse Axonal Injury (DAI):** The primary reason is rotational acceleration or deceleration, which causes axonal stretching and disruption. DAI is common in corticomedullary junctions and the corpus callosum, but it can also affect the mesial temporal lobe, which contains the hippocampus and parahippocampal gyrus. Restricted diffusion on DWI can extend up to 18 days in affected areas, indicating cellular hypertrophy or cytotoxic edema. Minor lesions with black signal intensity (hemorrhage) can be recognized with susceptibility-weighted imaging or gradient-recalled echo.

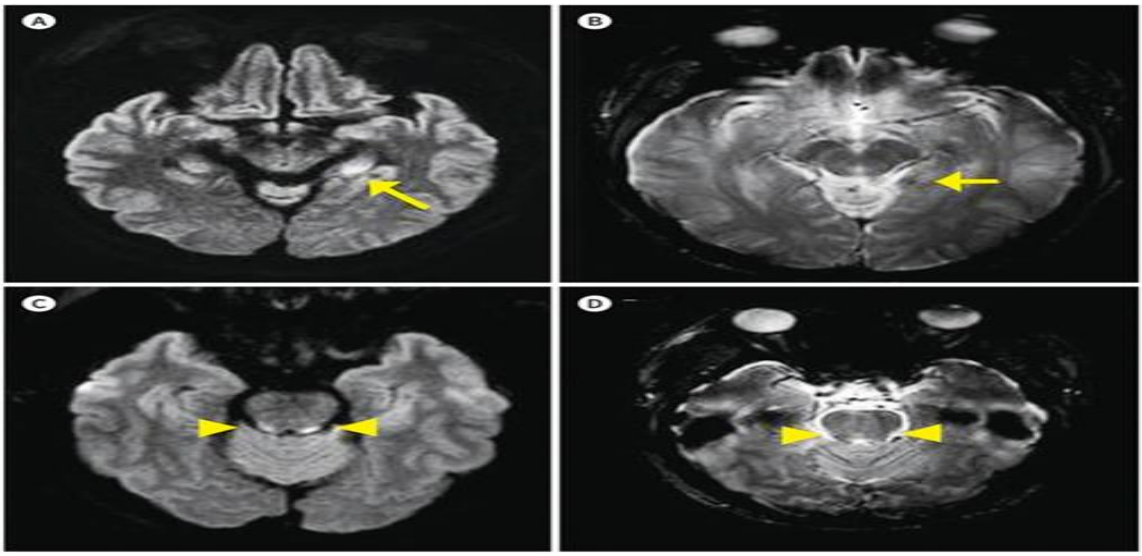

Figure 11: A 57-year-old male diagnosed with diffuse axonal injury.

A-D. Diffusion-weighted images (A, C) show small patchy hyperintense lesions in the left hippocampus (arrow) and both posterolateral pons (arrowheads). Gradient-recalled echo

images (B, D) show a few foci of dark signal intensity in the left hippocampus (arrow) and both posterolateral pons (arrowheads) (10).

2. Degenerative Disorders

Degenerative illnesses typically affect the hippocampus, a brain area responsible for memory processing. Research employing magnetic resonance imaging (MRI) has shown that hippocampus volume and shape may be modified in a variety of settings, albeit results may be contradictory because of methodological variances.

- **Alzheimer's Disease and Temporal Lobe Epilepsy**
  - **Characteristic Volume Loss**: Hippocampal volume decrease is a distinguishing hallmark of various brain illnesses, particularly Alzheimer's disease and temporal lobe epilepsy.

- **Psychiatric Conditions**
  - **Affective Disorders:** Affective problems frequently produce unclear results. In serious depression, certain investigations show a bilateral loss in hippocampal volume, whilst others show asymmetric reductions (right or left hippocampus) or no major difference.
  - **Bipolar Disorder:** Bipolar disorder findings are likewise variable, having certain investigations reporting volume decreases, others volume increases, and some studies showing no significant changes.
  - **Other Psychiatric Diseases:** Hippocampal changes in volume are also found in disorders such as schizophrenia, post-traumatic stress disorder (PTSD), autism, and obsessive-compulsive disorder, though these findings are controversial (2).

VII. SPECIAL CONSIDERATIONS IN RADIOLOGICAL IMAGING

When defining the hippocampus in magnetic resonance (MR) images, various particular radiological imaging procedures and characteristics must be taken into account to ensure accurate and uniform findings. All of these variables play a key role in the heterogeneity in volumetric findings among researches.

- **MRI Acquisition Parameters**
  - **Impact on Volumetric Results:** Technological MRI characteristics like MR imaging protocols, SNR, magnetic field intensity, total slice count, cranial coverage, and, particularly, imaging quality all lead significantly to variations in hippocampal volumetric data. Research using higher resolution is more likely to identify distinctions among patient and control groups.
  - **Common Acquisition Planes:** The majority of research evaluated chose coronal acquisition planes for manual tracing of hippocampus boundaries, while sagittal planes being used less frequently and axial planes being employed by a small minority. Voxel size is frequently anisotropic.
  - **Resolution and Slice Distance:** In-plane picture resolution is usually 1 mm x 1 mm, with slice distances of 1.5 mm. Details on cranial coverage and the no. of cuts are frequently limited.

- **Image Resolution and Anatomical Border Detection**
  - **High Resolution for Visibility:** excellent MR field strength, allowing for excellent MRI resolution, increases anatomical border visibility and detection, especially at the problematic anterior border indicated through the alveus. A resolution of 1x1x1 mm^3 or lower is preferred.
  - **Challenges with Lower Resolution:** Despite 1x1x1 mm^3 resolution, certain people may still have difficulty detecting the anterior border. Clear delineation requires extremely high resolution (e.g., 0.5x0.5x0.5 mm^3).

- **Image Processing Procedures**
  - **Sources of Variance:** Image-processing processes, such as reorganizing for aligning along the longitudinal axis of the hippocampus, software programs for defining cranial size adjustment or volume of the entire brain adjustment and reliability metrics, differ significantly among research, contributing to the findings' variability.
  - **Software Capabilities:** Demarcation software must be able to display all three orthogonal planes at same time in order to better assist anatomical judgments. Certain software systems limit manual delineation to entire voxels, while others offer continuous border tracing with subvoxel spatial resolution.
  - **Bias Correction:** The rater's misclassification of tissue types can be decreased by including the bias correction phase into the preprocessing procedure.

- **Reliability of Landmarks**
  - **External vs. Internal Landmarks:** The definitions of hippocampus borders according to external markers (e.g., corpora mamillaria, superior or inferior colliculi, lateral ventricle) are heavily influenced by imaging factors such as image resolution, slice spacing, or tilt. Such external landmarks are not suggested since they can contribute additional variance and are not consistently applicable among studies.
  - **CSF as a Landmark:** Because cerebrospinal fluid (CSF) provides excellent contrast, CSF gaps can be exceedingly small or imperceptible, particularly in young, healthy people with modest ventricular contents, rendering methods relying on this landmark useless.
  - **Alveus as an Internal Landmark:** The alveus is regarded as a more reliable internal landmark at the anterior boundary due to its anatomically established relationship to the hippocampal and greater contrast clarity with gray matter tissue. Their Visibility varies with MR image quality and resolution but is frequently visible in scans with 1x1x1 mm^3 and higher resolution (2).

VIII. CONCLUSION

The hippocampal, a critical brain area nestled inside the temporal lobe, is fundamental to cognitive processes like formation of memory, spatial orientation, and emotional control. Its intricate structure, comprising the dentate gyrus, cornu ammonis (CA1-CA4), and subiculum, along with its distinct layers and connections, makes it susceptible to various neurological disorders such as Alzheimer's disease and epilepsy. Understanding its anatomical form, functions, and pathological variations is crucial for developing effective treatment strategies.
Magnetic Resonance Imaging (MRI) serves as the primary tool for detailed hippocampal studies, with Ultra-High Field (UHF) MRI (≥7T) representing a significant advancement. UHF MRI offers enhanced contrast, signal-to-noise ratio, and spatial resolution, which are

essential for visualizing the hippocampus's minute subfields and cellular layers, often challenging to discern with conventional MRI. Advanced imaging protocols, including resolution enhancement techniques, automated interpolation, and computational unfolding, are employed to overcome the complexities of hippocampal anatomy and to precisely delineate its subregions. These high-resolution imaging capabilities are vital for early detection of cognitive impairment, identifying radiological biomarkers for diseases like Alzheimer's, and improving diagnostic accuracy.

Beyond structural imaging, functional MRI (fMRI) investigates brain activation during cognitive tasks, though it faces challenges due to the hippocampus's convoluted structure and limited resolution . Nuclear medicine techniques like PET and SPECT also contribute to diagnosing hippocampal disorders, particularly in neurodegenerative diseases and epilepsy, by assessing metabolic activity and perfusion. The differential diagnosis of hippocampal lesions is complex, relying on an algorithmic approach that considers morphological aspects, laterality of involvement, volumetric changes, and diffusion-weighted imaging characteristics . Overall, the continuous advancements in imaging techniques and detailed anatomical understanding are pivotal for enhancing our ability to diagnose, monitor, and potentially treat disorders affecting this vital brain structure.

REFERENCES

[1] Sumadevi KT. The Hippocampus: Anatomy, Function and Clinical Correlation. Sri Lanka Anat J. 2024 Jul 31;8(1):6–20. doi:10.4038/slaj.v8i1.220

[2] Konrad C, Ukas T, Nebel C, Arolt V, Toga AW, Narr KL. Defining the human hippocampus in cerebral magnetic resonance images—An overview of current segmentation protocols. NeuroImage. 2009 Oct;47(4):1185–95. doi:10.1016/j.neuroimage.2009.05.019

[3] Chauhan P, Jethwa K, Rathawa A, Chauhan G, Mehra S. Figure 2, [The hippocampus, dentate gyrus, subiculum,...]. [Text] [Internet]. Exon Publications; 2021 [cited 2026 Feb 12]. Available from: https://www.ncbi.nlm.nih.gov/books/NBK575732/figure/Ch2-f0002/

[4] Alves IS, Coutinho AMN, Vieira APF, Rocha BP, Passos UL, Gonçalves VT, et al. Imaging Aspects of the Hippocampus. RadioGraphics. 2022 May;42(3):822–40. doi:10.1148/rg.210153

[5] Giuliano A, Donatelli G, Cosottini M, Tosetti M, Retico A, Fantacci ME. H ippocampal subfields at ultra high field MRI: A n overview of segmentation and measurement methods. Hippocampus. 2017 May;27(5):481–94. doi:10.1002/hipo.22717

[6] Hayman LA, Fuller GN, Cavazos JE, Pfleger MJ, Meyers CA, Jackson EF. The hippocampus: normal anatomy and pathology. Am J Roentgenol. 1998 Oct;171(4):1139–46. doi:10.2214/ajr.171.4.9763010

[7] Ekstrom AD, Bazih AJ, Suthana NA, Al-Hakim R, Ogura K, Zeineh M, et al. Advances in high-resolution imaging and computational unfolding of the human hippocampus. NeuroImage. 2009 Aug;47(1):42–9. doi:10.1016/j.neuroimage.2009.03.017

[8] imaging-hippocampal-differences-neurosciencce.jpeg (770×691) [Internet]. [cited 2026 Feb 12]. Available from: https://neurosciencenews.com/files/2021/04/imaging-hippocampal-differences-neurosciencce.jpeg

[9] Hippocampal-region-activity-sites-1-and-2-fMRI-data-from-participants-in-both-the-Words.png (850×564) [Internet]. [cited 2026 Mar 4]. Available from:

[10] https://www.researchgate.net/publication/12297614/figure/fig2/AS:281708734763011@1444176004882/Hippocampal-region-activity-sites-1-and-2-fMRI-data-from-participants-in-both-the-Words.png

[11] Park S, Yu IK, Kim H. MRI Findings of Acute Hippocampal Disorders: Pictorial Essay. J Korean Soc Radiol. 2022;83(5):1046. doi:10.3348/jksr.2021.0101

7
Chapter

The 7T Revolution: Enhancing Diagnostic Clarity and Neuroanatomical Visualization

[1]Mohd. Harish Saifi
M.Sc. Research Scholar
Department of Radiological
Imaging Techniques
College of Paramedical Sciences
Teerthanker Mahaveer University
Moradabad

[2]Rashmi Pandey
Assistant Professor
Department of Radiological
Imaging Techniques
College of Paramedical Sciences
Teerthanker Mahaveer University
Moradabad

[3]Sidra
M.Sc. Research Scholar
Department of Radiological
Imaging Techniques
College of Paramedical Sciences
Teerthanker Mahaveer University
Moradabad

[4]Sohel Rana
Assistant Professor
Department of Paramedical
and Allied Health Sciences
Midnapore City College
Paschim Medinipur

Abstract

A major development in medical imaging, ultra-high-field (UHF) 7-Tesla (7T) MRI has evolved from a specialist research instrument to a clinically authorized method for brain and musculoskeletal application. The fundamental advantage of 7T MRI is a significant increase in signal-to-noise ratio (SNR), allowing for sub-millimeter isotropic spatial resolution (0.35-0.45 mm). With this resolution, specific neuronal layers and complex brain structures like hippocampal subfields can be visualized with remarkable detail. In addition, 7T systems provide increased susceptibility and sensitivity for identifying iron deposits, as well as higher spectral resolution in MR spectroscopy to distinguish overlapping molecules.

These features are the result of hardware advances such as high-performance "Impulse" gradients systems or high-density receiver arrays. To address physics-based issues such as B1 field inhomogeneities and high Specific Absorption Rates (SAR), technologies like as parallel transmission (pTx) and AI-driven Deep Learning Reconstruction (DLR) are used to assure image homogeneity and clarity.

In clinical practice, 7T MRI delivers a 15% diagnostic gain in finding subtle lesions in drug-resistant epilepsy and enhances surgical preparation for Parkinson's disease by distinctly displaying anatomical sub structures. It also helps to investigate microstructural Patho mechanisms in depressive disorders as well as early signs of neurodegeneration. While

infrastructure costs and temporary sensory effects such as vertigo remain obstacles, the research is transitioning toward "precision neuroimaging". Future breakthroughs in artificial intelligence-driven image translation and biophysical modeling seek to fill the gap among macroscopic mapping and mesoscopic neuroscience, with the potential to resolve cellular-scale characteristics non-invasively.

Keywords: Ultra-High-Field (7T), Signal-to-Noise Ratio (SNR), Parallel Transmission (pTx), B1 Inhomogeneity, Specific Absorption Rate (SAR), Deep Learning Reconstruction (DLR), Sub-millimeter Spatial Resolution, Clinical Diagnostic Gain

I. INTRODUCTION TO ULTRA-HIGH FIELD 7T MRI AND RECENT ADVANCEMENTS

Ultra-high-field (UHF) 7-Tesla (7T) MRI is magnetic resonance imaging with a static magnetic field strength of 7 Tesla or above. These fields are more than 100,000 times powerful than the Earth's magnetic field. While 7T systems had long been utilized as a research tool, its clinical approval for neurological and musculoskeletal imaging in 2017 represented a significant milestone, providing for unparalleled clarity in the visualization of neuroanatomy, metabolism, and function.

1. Primary Advantages of UHF MRI

The primary advantage of 7T MRI is a significant increase in signal-to-noise ratio (SNR), that rises almost linearly with field strength. The signal gain permits for:

- **Sub-millimeter Spatial Resolution:** For functional imaging, advanced hardware can frequently achieve isotropic spatial resolution of 0.35-0.45 mm, allowing investigators to sample the six distinct neuronal layers and columns of the human cerebral cortex.
- **Enhanced Susceptibility Sensitivity:** Higher fields enhance sensitivity to magnetic susceptibility distinctions among tissue types. This enhances Susceptibility-Weighted Imaging (SWI) and Quantitative Susceptibility Mapping (QSM), that are essential for finding iron deposits and blood products.
- **Improved Metabolic Insight:** Increased frequency dispersion improves spectral resolution in MR spectroscopy (MRS), enabling for the isolation of overlapping metabolite resonances (such as glutamate and glutamine) at lower field strengths.
- **Superior Angiography:** Lengthened relaxation times at 7T improve background suppression in Time-of-Flight (TOF) angiography, allowing for comprehensive observation of tiny artery branches.

2. Physical and Technical Challenges

Despite these benefits, 7T MRI confronts a few physics-related challenges:

- **Field Inhomogeneities:** Increased and (radiofrequency transmit) field changes frequently result in geometric distortions and "bright or dark patches" in photographs.
- **Shortened Relaxation Times:** Shorter transverse relaxation times promote faster signal decay, potentially cancelling out SNR improvements from higher fields.
- **Safety Constraints:** Higher fields cause higher energy deposition in the body, known as the Specific Absorption Rate (SAR), which can be reduced by peripheral nerve stimulation (PNS).

3. Recent Technological Advancements

Latest hardware and software developments have overcome these difficulties, making clinical 7T more possible:

- **Parallel Transmission (pTx):** This method tailors radio waves to each patient using many independent transmit channels, resulting in substantially more consistent image quality throughout the brain and spinal cord.
- **Next-Generation Gradient Systems:** The high-performance "Impulse" head-only asymmetric gradient coil has a maximum amplitude of 200 mT/m and a slew rate of 900 T/m/sec. These powerful gradients enable significantly faster signal readout, resulting in shorter echo durations (TE) and less signal loss throughout relaxation.
- **Deep Learning Reconstruction (DLR):** AI-powered software (e.g., AIR Recon DL) uses neural networks to minimize noise and artifacts (such as Gibbs ringing), resulting in clearer images with greater microstructural information.
- **High-Density Receiver Arrays:** Combining 64- and 96-channel receiver coil arrays enhances signals in the cerebral cortex while reducing noise, allowing for faster parallel imaging acceleration.
- **Multiplexed Sensitivity Encoding (MUSE):** This complex multi-shot scan method reduces geometric distortions while increasing resolution, especially for high-field diffusion imaging (1–5).

II. HARDWARE INNOVATIONS IN 7T MRI SYSTEMS

Hardware advancements in 7 T MRI systems, especially in the research and development of "next-generation" (NexGen) human brain scanners and sophisticated preclinical systems, are aimed at obtaining mesoscale spatial resolution and much higher signal-to-noise ratios.
These advances are principally driven by the integration of gradient coils, radiofrequency (RF) arrays, and cooling systems.

1. High-Performance Gradient Systems

The "Impulse" head-only asymmetric gradient coil is a key advance in 7 T human imaging.

- **Three-Layer Design:** Unlike typical gradients, which employ two layers, the Impulse coil has a third intermediate winding layer. This allows for more latitude in optimizing magnetic field quality and mechanical resonances while decreasing peripheral nerve stimulation (PNS).
- **Performance Specifications:** It has a maximum gradient amplitude (Gmax) of 200 mT/m and a slew rate (SR) of 900 T/m/sec. This performance is nearly five times that of conventional head-only coils and orders of magnitude superior to standard 7 T whole-body systems.
- **Acoustic and Mechanical Management:** The asymmetrical three-step design helps to regulate mechanical vibrations and acoustic noise, keeping sound levels under safe limits even at high speeds.

2. Advanced Receiver and Transmit Systems

To collect the high-frequency impulses at 7 T, researchers rebuilt the RF infrastructure.

- **128-Channel Receiver:** Next-generation systems can now accommodate up to 128 active receiver channels at the same time. To handle the huge data throughput, analog-to-digital converter cassettes had to be doubled, and PCI extenders were used.

- **High-Density Receive Arrays:** 64-channel and 96-channel receive-only head coils are among the latest innovations. These arrays use smaller loop diameters (about 4 cm), resulting in a 30% SNR improvement in the cerebral cortex over standard 32-channel coils.
- **Parallel Transmit (pTx):** Systems now use 16-channel transmission arrays. These enable B1 shimming to improve image homogeneity (a major challenge at 7 T due to wavelength effects) and improved control of the specific absorption rate (SAR) to avoid tissue heating.

3. Thermal Management and Materials

The enormous current densities needed for ultra-high gradients requires specialized cooling.

- **Stainless-Steel Cooling Tubes:** The Impulse coil is made of stainless-steel tube with conductive copper filaments. Stainless steel is utilized due to its lower conductivity minimizes sensitivity to eddy currents, and it lacks magnetic characteristics that would otherwise interfere with B0 homogeneity.
- **High-Pressure Circulation:** These systems utilize several parallel water circuits and high flow rates to release over 20 kW of heat, allowing them to operate at low temperatures while performing high-duty cycle functional imaging.
- **Preclinical (Animal) 7 T Innovations:** Hardware development for preclinical 7 T systems frequently concentrates on sensitivity at lower scales.
  - **Cryogenic RF Coils:** By lowering electrical noise, cooling RF coils and preamplifiers to cryogenic temperatures (such as liquid nitrogen or helium) can boost SNR by a factor of three and temporal SNR by 1.8.
  - **Implantable and Stretchable Coils:** Stretchable receiving coils, which fit closer to the animal's head and raise SNR by 40%, and implantable inductive detectors, which can improve localized signals by 2- to 3-fold, are two examples of innovations.
  - **Self-Shielded Gradients:** Active shielding (extra windings that produce no external field) and digital pre-emphasis are frequently employed in preclinical gradients to compensate for residual eddy currents that may disrupt the EPI waveforms utilized in functional tests.

4. Performance Impacts

These hardware advances enable 7 T systems to achieve 0.35-0.45 mm isotropic spatial resolution in human functional studies. This granularity is adequate to detect functional activity in cortical layers, surpassing earlier resolution constraints that resulted in signal blurring throughout the gray matter ribbon (1,6,7).

III. ADVANCES IN IMAGING SEQUENCES AND PROTOCOLS AT 7T

Recent advances in 7-Tesla (7T) MRI have centered on utilizing the high signal-to-noise ratio (SNR) and increased susceptibility sensitivity of ultra-high fields to achieve mesoscopic resolution and molecular-level detail while overcoming technical challenges such as B0 and B1 inhomogeneities, shortened relaxation times*, and high Specific Absorption Rate (SAR) levels.

1. High-Resolution Diffusion Imaging

Diffusion imaging at 7T offers a considerable increase in signal intensity, allowing for sub-millimeter isotropic resolution and detailed observation of cortical fiber tracing and intricate white matter structures.

- **Multiplexed Sensitivity Encoding (MUSE):** This innovative multi-shot interleaved EPI algorithm fills k-space with several excitations, considerably reducing geometric distortions and blurring* when compared to classic single-shot techniques.
- **Deep Learning Reconstruction (DLR):** AI-driven convolutional neural networks (e.g., AIR Recon DL) operate on raw k-space data to minimize noise, eliminate Gibbs ringing artifacts, and improve edge sharpness, making them especially useful for high b-value imaging where signal intensity is naturally low.
- **High-Performance Gradients:** The utilization of powerful gradient systems (e.g., 113 mT/m) enables shorter diffusion-encoding periods and lower Echo Time (TE), that is crucial at 7T to reduce signal loss due to rapid T2 decay.
- **Parallel Transmission (pTx):** To address B1 inhomogeneity (that produces signal dropout and nonuniform contrast), pTx employs multi-channel RF transmission arrays that optimize flip angle distribution throughout the brain.

2. Whole-Brain Mesoscopic Venous Imaging

New techniques allow for non-invasive imaging of the brain's mesoscopic venous network (<0.5 mm) with whole-brain coverage at clinically practical times.

- **Multishot 3D Echo Planar Imaging (3D EPI):** Using a Skipped-CAIPI 3D EPI sequence, researchers achieved whole-brain coverage at 0.35-mm isotropic resolution in less than 7 minutes. This technique improves SNR and venous contrast by utilizing longer repetition rates and extended echo periods (up to 40 ms).
- **Vessel Type-Specific Processing:** Advanced imaging techniques can now differentiate among leptomeningeal, pial, and intracortical veins.
- weighted Rendering: This process reverses vascular contrast, making cerebral blood vessels look brighter, enhancing their natural appearance.
- **Varying Vertex Density Surfaces:** Specialized triangular meshes for intracortical veins sample voxel values precisely at mesh vertices, allowing for high-fidelity tracing across varied cortical depths while minimizing aliasing errors.

3. Accelerated Molecular Imaging (CEST)

Chemical Exchange Saturation Transfer (CEST) MRI detects endogenous compounds such as proteins and metabolites, although it often has extensive acquisition times.

- **Complementary Undersampling:** This hybrid k-space technique speeds CEST by obtaining various subregions of k-space for neighboring frequency offsets, thereby exploiting structural redundancies throughout the frequency dimensions.
- **Multi-Offset Transformer Reconstruction (MoTR):** This deep learning network employs the transformer module to simulate long-range connections between neighboring offsets, enabling each offset to acquire partial data from its neighbors in order to compensate for missing data. This method achieves high-fidelity reconstruction at 3× and 6× acceleration speeds.

4. **Protocol Enhancements for Field Inhomogeneity**
   - **Static and Dynamic B1+ Shimming:** These strategies enhance homogeneity in specific areas of interest by driving numerous transmit channels with independent waveforms or phases.
   - **Universal Pulses:** These pTx pulses have been optimized using multi-subject data maps, resulting in calibration-free, subject-independent optimization that considerably reduces measurement preparation time.
   - **Dielectric Pads:** These are utilized to fix RF transmit field inhomogeneity and increase signal intensity in the lower brain areas.

5. **Spectroscopic and Multinuclear Advances**
   - **Free Induction Decay (FID) MRSI:** Ultrashort echo time sequences are used at 7T to reduce SNR loss caused by short T2 relaxation, which improves the detectability of low-concentration metabolites such as GABA, glutamate, and 2-hydroxyglutarate.
   - **Deuterium Metabolic Imaging (DMI):** DMI sensitivity grows supralinearly at 7T, allowing for high-resolution 3D metabolic mapping of substrates such as glucose.
   - **X-Nuclei Imaging (e.g., 23Na, 31P):** The linear rise in SNR with field strength enables mapping sodium concentrations and ATP production rates clinically possible at 7T (2,4,8,9).

IV. ENHANCED STRUCTURAL AND FUNCTIONAL NEUROIMAGING CAPABILITIES

Ultra-high field (UHF) MRI, defined as 7 Tesla (7 T) or above, improves neuroimaging capabilities by giving a higher signal-to-noise ratio (SNR) and better tissue contrast. These advancements enable ultra-high spatial resolution (sub-millimeter), which is required for detailed visualization of complex brain anatomy, including the six distinct cytoarchitectonic layers of the human cortex (ranging from 0.2 mm to 0.8 mm) and the hippocampus's specific subfields and layers.

1. **Enhanced Structural Imaging Capabilities**
   - **Detailed Anatomical Delineation:** In ex-vivo conditions, 7 T imaging may achieve isotropic resolutions of 100 μm to 500 μm, enabling for the observation of sub-millimetric lesions and hippocampus layers not evident in regular scans. Conventional in-vivo MRI (usually >1 mm resolution) struggles to differentiate tiny structures.
   - **Multimodal Contrast:** The capabilities include high-resolution 3D T2-weighted imaging, quantitative T1 and T2 maps, and Quantitative Susceptibility Mapping (QSM). QSM is especially sensitive to significant biomarkers such as iron and myelin deposition, which are important in researching disorders including multiple sclerosis, Alzheimer's, and Parkinson's.
   - **Improved Morphometrics:** Studies comparing paired 3 T and 7 T scans demonstrate that 7 T gives a higher association between brain morphometrics and age, considerably enhancing statistical power and decreasing the sample size required for research.

2. **Enhanced Functional and Microstructural Capabilities**
   - **Functional Sensitivity (fMRI):** The greater sensitivity to susceptibility changes at 7 T improves blood-oxygen-level-dependent (BOLD) contrast, which is critical for functional imaging. Unlike 3 T, which frequently necessitates "slab" acquisitions for

high resolution, 7 T enables whole-brain fMRI with sub-1.5 mm isotropic resolution. This enables researchers to investigate minor structures, such as hippocampus subfields, within the context of massive functional networks.

- **Advanced Diffusion Imaging:** High-angular resolution diffusion MRI (HARDI) at UHF allows for precise structural fiber tracking and the employment of complicated models such as Diffusion Basis Spectrum Imaging (DBSI) and Neurite Orientation Dispersion and Density Imaging (NODDI). These models include information about microstructural changes like fiber fraction, extracellular diffusion (hindered), and intracellular diffusion (limited).
- **Cross-Modal Integration:** Ex-vivo UHF MRI enables the co-registration of MRI data with optically-clear histology, allowing for a biological interpretation of MRI findings through direct comparison to Luxol Fast Blue (myelin) and iron stains (10–12).

V. CLINICAL APPLICATIONS IN NEUROLOGICAL AND NEUROVASCULAR DISORDERS

The therapeutic application of Ultra-High Field (UHF) MRI at 7 Tesla (7T) gives considerable diagnostic and predictive benefits in the management of neurological and neurovascular illnesses by identifying microstructural anomalies and tiny lesions that are typically unseen on conventional scanners.

1. Major Depressive Disorder (MDD)

In MDD, 7T MRI is utilized to explore microstructural pathomechanisms and predict disease occurrence.

- **Intracortical Myeloarchitecture:** According to UHF quantitative MRI, MDD is related with reduced intracortical myelin (higher T1 values) in the lateral orbitofrontal cortex (lOFC), which is important for processing negative affect. This decrease in myelin is also associated with the intensity of depression symptoms.
- **Predictive Diagnostics:** Machine learning models trained on gyrification data from the Default Mode Network (DMN) obtained at 7T may indicate the existence of MDD with an accuracy of 0.76. Whereas gray matter volume (GMV) is not a reliable predictor of diagnosis, GMV in the left parahippocampal gyrus is linked to symptom severity.
- **Cellular Insights:** These methods enable depth-dependent examinations of several cortical layers, generating "normative" baselines that may be compared to patient data to uncover cellular-level biomarkers for therapeutic targets.

2. Drug-Resistant Focal Epilepsy

For individuals with drug-resistant focal epilepsy who’s standard 3T MRI scans are "negative," 7T MRI provides an important diagnostic advantage:

- **Lesion Detection:** 7T structural analysis has resulted in a diagnostic gain of roughly 15%, uncovering previously undiagnosed epileptogenic lesions like focal cortical dysplasia (FCD), hippocampal atrophy, and amygdala lesions.
- **Surgical Planning:** The most important predictors of success in resective epilepsy surgery are accurate detection and delineation of these abnormalities.

- **Conspicuity:** When discovered at 7T, more than half (56%) of these lesions may be recognized retrospectively on 3T scans, while they are significantly less visible at lower field strengths.

3. Parkinson's Disease (PD)

7T MRI improves both surgical management and diagnostic characterisation of PD.

- **DBS Surgical Planning:** 7T MRI can clearly differentiate anatomical substructures, allowing for patient-specific anatomical modeling. This leads in more accurate Deep-Brain Stimulation (DBS) lead placement and fewer side effects.
- **Radiological Assessment:** The enhanced resolution at 7T allows for a distinct display of nigrosomes 1-5, which improves the identification of "swallow-tail" sign loss, a critical indication for Parkinson's disease diagnosis.
- **Quantitative Biomarkers:** 7T enhances the measurement of the neuromelanin-iron complex, allowing researchers to trace iron accumulation and volume loss in the substantia nigra more precisely than 3T.

4. Broader Neurological and Neurovascular Applications

7T MRI's enhanced image quality, contrast, and signal-to-noise ratio have led to greater detection of pathogenic alterations in a number of different domains.

- **Neurovascular/Ischemia:** 7T MRI is used to more accurately characterize brain abnormalities in ischemic stroke and chronic inflammatory diseases.
- **Neurodegenerative Disorders:** It has showed the ability to detect early indicators and pathological alterations in Alzheimer's disease and dementia.
- **Multiple Sclerosis (MS):** UHF imaging is utilized to map brain pathological gradients and track clinical uses in MS patients (13–16).

VI. CHALLENGES, SAFETY CONSIDERATIONS, AND MITIGATION STRATEGIES

Implementing clinical 7 Tesla (7T) MRI requires overcoming considerable technological, physical, and operational challenges, however recent advances have brought practical solutions to these concerns.

1. Challenges

- **Technical and Physics Obstacles:** Magnetic field (B0) and radiofrequency (RF/B1) inhomogeneity pose the most significant technical barrier. At 7T, the RF wavelength is smaller (about 12 cm), comparable to the size of a human head, resulting in constructive and destructive interference that causes signal dropouts and black patches, notably in the temporal lobes and cerebellum. Furthermore, higher magnetic susceptibility produces distortions and signal loss at air-bone contacts like the paranasal sinuses and skull base.
- **Operational and Infrastructure Limitations:** 7T magnets are huge, weighing more than 20,000 kg, need specialized helium-cooled superconducting conditions and strong magnetic shielding. Their installation frequently demands major infrastructure changes, and they are significantly more expensive to buy and maintain than 3T systems. Additionally, current clinical approval is primarily limited to the brain and knee, with spinal and body coils still in development.

- **Clinical Practicalities:** The conventional 60 cm bore size is narrower and longer (up to 297 cm) than many modern 3T systems, potentially increasing patient claustrophobia and limiting the size of individuals who can be scanned. There is also an absence of proven safety testing for several popular implants at 7T, which limits its usage in patients having devices that may be safe at lower field strengths.

2. **Safety Considerations**
   - **Heightened Magnetic Forces:** In comparison to a 3T field, a 7T field exerts at least 2.3 times the translational force and 5.4 times the rotational force (torque) on ferromagnetic materials. This necessitates rigorous screening of metal objects and implants.
   - **RF Heating and SAR:** Radiofrequency heating is a big concern since the shorter 7T wavelengths are more readily absorbed by tissue. Specific Absorption Rate (SAR) restrictions are typically a bottleneck, necessitating longer scan periods or sequence modifications to prevent excessive tissue heating.
   - **Biological and Physiologic Effects:** Patients frequently report temporary sensory effects like vertigo, dizziness, nausea, nystagmus (involuntary eye movement), or a metallic taste, particularly while moving through high-gradient fringe fields.
   - **Lenz Forces:** If a conducting material (even a non-ferromagnetic one) passes through the 7T field, electrical currents are created, resulting in "Lenz forces" that resist the object's movement. Patients who have orthopedic implants may experience this.

3. **Mitigation Strategies**
   - **Parallel Transmission (pTx):** This is one of 7T's most significant inventions, as it uses numerous independent RF channels to "shape" radio waves. It significantly increases B1 homogeneity, minimizes signal dropouts in locations such as the temporal lobes, and can assist reduce SAR.
   - **Advanced Shimming and AI:** Active shimming (using hardware combined with gradient coils) aids in homogenizing the B0 field for specific patients. Furthermore, deep learning-based reconstruction and AI algorithms are increasingly being employed to decrease artifacts, correct intensities, and shorten scan times, resulting in improved patient satisfaction and throughput.
   - **Dielectric Pads:** Using high-permittivity dielectric pads around the patient's head can assist focus the RF field and reduce B1 inhomogeneities, especially near the skull base and temporal areas.
   - **Modified Operational Protocols:** To reduce vertigo and Lenz forces, the scanner table is progressively advanced within the bore. Patients are also taught to keep their eyes closed or their heads steady as the table moves and to sit up carefully following the scan.
   - **Stringent Screening:** To reduce heating hazards, institutions frequently mandate that implants be placed a minimum of 30 cm away from the head coil. Clinical teams also use interdisciplinary safety officers to do patient-specific risk assessments for implants that have not yet been formally labeled for 7T (3,5,17–19).

VII. FUTURE DIRECTIONS AND EMERGING TECHNOLOGIES IN 7T MRI

Future trends and developing technologies in 7T MRI will focus on moving from macroscopic brain mapping to mesoscopic and microscopic neuroscience, allowing for the observation of human brain circuits at the cortical layer and fine white matter pathways.

These breakthroughs are fueled by cutting-edge hardware, personalized "precision" neuroimaging, and AI-powered picture interpretation.

1. Next-Generation Hardware (NexGen 7T)

Significant hardware advancements constantly challenge the physical limits of ultra-high-field (UHF) imaging to span spatial scales ranging from centimeters to microns.

- **High-Performance Gradient Coils:** The "Impulse" head-only asymmetric gradient coil is a key component of next-generation 7T systems, enabling mesoscopic functional MRI (fMRI). Its three-layer winding architecture (double-primary, intermediate, and shield layers) provides additional degrees of freedom for optimal Peripheral Nerve Stimulation (PNS) balancing. Bending magnetic fields can improve PNS thresholds by up to 41%, resulting in greater usable gradient performance.
- **High-Channel Receiver Arrays:** Emerging systems, like as 72-channel in vivo head arrays, use high-density receive coils to push sensitivity boundaries and achieve ultra-high-resolution acquisitions. These arrays enhance signal-to-noise ratio (SNR) in cortical regions by up to 1.5 times while providing faster acceleration than typical 32-channel coils.
- **Parallel Transmission (pTx):** Modern 7T protocols typically use pTx mode (for example, 8-transmit channels) with "Universal Pulses" to increase B1+ uniformity and address the radiofrequency (RF) inhomogeneity issues inherent in 7T.

2. Precision Neuroimaging and Connectomics (PNI)

The field is moving toward individualized mapping of individual human brains using intensive temporal sampling.

- **Multimodal Integration:** Future 7T research focuses on large datasets that combine T1 relaxometry, magnetization transfer (MT), T2*-weighted imaging, diffusion MRI (dMRI), and multi-state fMRI. Integrating these allows for a more specific definition of cortical network topology based on microstructure, connectivity, and function.
- **Naturalistic Paradigms:** Researchers are experimenting with movie-watching paradigms to increase participant compliance and pleasure while also identifying individual differences. These closely resemble real-world experiences and provide an environmentally friendly alternative to traditional resting-state or task-based fMRI.
- **Cortical Gradients:** Advanced investigations have now identified spatial "gradients" in brain organization. These gradients use a variety of neurobiological features, including structural and functional connectivity, to identify cortical hierarchy axes, such as the transition from sensorimotor to transmodal networks.

3. AI and Cross-Modality Image Translation

Artificial intelligence has been utilized to close the gap between readily available 3T data and advanced 7T imaging.

- **CycleGAN Architectures:** Deep learning models, particularly unpaired CycleGANs, can now produce 7T-like images from existing 3T datasets. This "style transfer" preserves anatomical information from 3T images while not converting qualities such as resolution and contrast-to-noise ratio (CNR) to meet 7T standards.
- **Longitudinal Harmonization:** This AI-driven synthesis enables researchers to transfer longitudinal patient studies to 7T systems while retaining the value of historical 3T data.

- **Future Architectural Enhancements:** Future research is expected to incorporate Vision Transformers (ViTs) into these AI models to capture long-range relationships in complex brain morphological systems, potentially improving segmentation and translational accuracy.

4. Resolving Microstructure and Fine Pathways

Ultra-strong gradients at 7T (together with high-performance 3T devices) allow for the evaluation of cellular-scale properties that were previously only quantifiable in animal investigations.

- **Inference of Cellular Size:** Biophysical modeling (e.g., SANDI or AxCaliber-SMT models) enables non-invasive measurement of axonal diameter and soma radius. Next-generation systems can identify axons as small as a single micron, increasing sensitivity to the small-diameter axons that comprise the majority of human white matter.
- **Deep Brain Circuitry:** Enhanced SNR enables the distinction of tiny diencephalic fibre tracts (such as the mammillo-tegmental tract) less than 2mm in size, that used to be hard to resolve reliably. This has immediate consequences for detecting imaging biomarkers for neurodegeneration and mental disorders (7,20,21).

VIII. CONCLUSION

The clinical application of 7-Tesla (7T) MRI marks a watershed moment in medical imaging, elevating it from a specialized research tool to a potent diagnostic method for neurological and musculoskeletal problems. Its principal advantage is the huge increase in signal-to-noise ratio (SNR), which allows for submillimeter isotropic spatial resolution (0.35-0.45 mm). This enables doctors to see human brain circuits at the cortical layer level and resolve tiny structures, like hippocampus subfields, that would otherwise be invisible at low field strengths.

In clinical practice, 7T MRI improves surgical precision for Deep-Brain Stimulation in Parkinson's illness by 15% and identifies lesions in drug-resistant epilepsy. It also has high sensitivity to identify iron deposits and metabolic abnormalities in diseases such as Multiple Sclerosis, Alzheimer's, and Major Depressive Disorder.

Although physical challenges like field inhomogeneities, high Specific Absorption Rates (SAR), and transient sensory effects such as vertigo persist, that they are effectively addressed by innovations such as parallel transmission (pTx), high-performance "Impulse" gradient systems, and AI-driven Deep Learning Reconstruction.

The next phase of 7T MRI focuses on "precision neuroimaging," which aims to bridge the gap between macroscopic mapping and mesoscopic neuroscience. AI-powered image interpretation and enhanced biophysical modeling are paving the way for non-invasive assessment of cellular-scale properties such as axonal diameter, which has the potential to change the diagnosis and treatment of neurodegenerative and mental disorders.

REFERENCES

[1] Feinberg DA, Beckett AJS, Vu AT, Stockmann J, Huber L, Ma S, et al. Next-generation MRI scanner designed for ultra-high-resolution human brain imaging at 7 Tesla. Nat Methods. 2023 Dec;20(12):2048–57. doi:10.1038/s41592-023-02068-7

[2] Nie L, Li S, Wu B, Xiong Y, McGovern J, Wang Y, et al. Advancements in 7T magnetic resonance diffusion imaging: Technological innovations and applications in neuroimaging. iRADIOLOGY. 2024 Aug;2(4):377–86. doi:10.1002/ird3.92

[3] De Vries E, Hagbohm C, Ouellette R, Granberg T. Clinical 7 Tesla magnetic resonance imaging: Impact and patient value in neurological disorders. J Intern Med. 2025 Mar;297(3):244–61. doi:10.1111/joim.20059

[4] Platt T, Ladd ME, Paech D. 7 Tesla and Beyond: Advanced Methods and Clinical Applications in Magnetic Resonance Imaging. Invest Radiol. 2021 Nov;56(11):705–25. doi:10.1097/RLI.0000000000000820

[5] Özütemiz C, White M, Elvendahl W, Eryaman Y, Marjańska M, Metzger GJ, et al. Use of a Commercial 7-T MRI Scanner for Clinical Brain Imaging: Indications, Protocols, Challenges, and Solutions—A Single-Center Experience. Am J Roentgenol. 2023 Dec;221(6):788–804. doi:10.2214/AJR.23.29342

[6] Klohs J, Chen WC, Araki R. Advanced preclinical functional magnetic resonance imaging of the brain. Npj Imaging. 2025 Jun 18;3(1):27. doi:10.1038/s44303-025-00085-z

[7] Ramos-Llordén G, Lee HH, Davids M, Dietz P, Krug A, Kirsch JE, et al. Ultra-high gradient connectomics and microstructure MRI scanner for imaging of human brain circuits across scales. Nat Biomed Eng. 2025 Jul 16;10(2):309–24. doi:10.1038/s41551-025-01457-x

[8] Liu H, Chen Z, Law LH, Liu Y, Wang Z, Wang J, et al. Accelerating CEST MRI through complementary undersampling and multi-offset transformer reconstruction. Commun Eng. 2026 Jan 10;5(1):24. doi:10.1038/s44172-025-00580-6

[9] Gulban OF, Stirnberg R, Tse DHY, Pizzuti A, Koiso K, Archila-Melendez ME, et al. Whole-brain meso-vein imaging in living humans using fast 7-T MRI. Sci Adv. 2026.

[10] Jubeir J, Jacob Y. Hippocampal subfield-specific imaging in depression: the translational power of ultra-high field MRI. Transl Psychiatry. 2026 Feb 10;16(1):78. doi:10.1038/s41398-026-03870-5

[11] Chu C, Santini T, Liou J, Cohen AD, Maki PM, Marsland AL, et al. Brain Morphometrics Correlations With Age Among 350 Participants Imaged With Both 3T and 7T MRI: 7T Improves Statistical Power and Reduces Required Sample Size. Hum Brain Mapp. 2025 Mar;46(4):e70195. doi:10.1002/hbm.70195

[12] Zhu Q, Li S, Cao Z, Shen Y, Xu H, Xu G, et al. 7 Tesla multimodal MRI dataset of ex-vivo human brain. Sci Data. 2025 May 22;12(1):845. doi:10.1038/s41597-025-04932-x

[13] Heij J, Van Der Zwaag W, Knapen T, Caan MWA, Forstman B, Veltman DJ, et al. Quantitative MRI at 7-Tesla reveals novel frontocortical myeloarchitecture anomalies in major depressive disorder. Transl Psychiatry. 2024 Jun 20;14(1):262. doi:10.1038/s41398-024-02976-y

[14] Schnellbächer GJ, Rajkumar R, Veselinović T, Ramkiran S, Hagen J, Collee M, et al. Structural alterations as a predictor of depression – a 7-Tesla MRI-based multidimensional approach. Mol Psychiatry. 2025 Jun;30(6):2517–24. doi:10.1038/s41380-024-02854-5

[15] Welton T, Hartono S, Shih YC, Schwarz ST, Xing Y, Tan EK, et al. Ultra-high-field 7T MRI in Parkinson's disease: ready for clinical use?—a narrative review. Quant Imaging Med Surg. 2023 Nov;13(11):7607–20. doi:10.21037/qims-23-509

[16] Van Lanen RHGJ, Uher D, Hoeberigs CMC, Hofman PAM, Santegoeds R, Wiggins C, et al. Value of ultra-high-field MRI in patients with drug-resistant focal epilepsy and negative 3T MRI (EPIULTRASTUDY): Diagnostic gain of 7T structural analysis. Epilepsia. 2025 Oct 17;epi.18682. doi:10.1111/epi.18682

[17] Cramer J, Ikuta I, Zhou Y. How to Implement Clinical 7T MRI—Practical Considerations and Experience with Ultra-High-Field MRI. Bioengineering. 2024 Dec 5;11(12):1228. doi:10.3390/bioengineering11121228

[18] Klodowski K, Zhang M, Jen JP, Scoffings DJ, Morris R, Lupson V, et al. Parallel transmit 7 T MRI for adult epilepsy pre-surgical evaluation. Epilepsia. 2025 Jul;66(7):2315–27. doi:10.1111/epi.18353

[19] Voelker MN, Kraff O, Goerke S, Laun FB, Hanspach J, Pine KJ, et al. The traveling heads 2.0: Multicenter reproducibility of quantitative imaging methods at 7 Tesla. NeuroImage. 2021 May;232:117910. doi:10.1016/j.neuroimage.2021.117910

[20] Diniz E, Santini T, Helmet K, Aizenstein HJ, Ibrahim TS. Cross-modality image translation of 3 Tesla Magnetic Resonance Imaging to 7 Tesla using Generative Adversarial Networks [Internet]. Radiology and Imaging; 2024 [cited 2026 Mar 3]. Available from: http://medrxiv.org/lookup/doi/10.1101/2024.10.16.24315609 doi:10.1101/2024.10.16.24315609

[21] Cabalo DG, Leppert IR, Thevakumaran R, DeKraker J, Hwang Y, Royer J, et al. Multimodal precision MRI of the individual human brain at ultra-high fields. Sci Data. 2025 Mar 29;12(1):526. doi:10.1038/s41597-025-04863-7

8
Chapter

Magnetic Resonance Fingerprinting (MRF) : A Paradigm Shift from Qualitative to Quantitative MRI

[1]Mohd. Harish Saifi
M.Sc. Research Scholar
Department of Radiological Imaging Techniques
College of Paramedical Sciences
Teerthanker Mahaveer University
Moradabad

[2]Rashmi Pandey
Assistant Professor
Department of Radiological Imaging Techniques
College of Paramedical Sciences
Teerthanker Mahaveer University
Moradabad

[3]Srishti Gaur
M.Sc. Research Scholar
Department of Radiological Imaging Techniques
College of Paramedical Sciences
Teerthanker Mahaveer University
Moradabad

[4]Mitali Monalisha
Assistant Professor,
Department of Paramedical Sciences, Ranchi

Abstract

Magnetic Resonance Fingerprinting (MRF) is a cutting-edge quantitative magnetic resonance imaging (MRI) technology that allows for the simultaneous determination of several tissue parameters, including T1 and T2 relaxation durations, in a single, time-efficient scan. This approach is a substantial improvement over traditional MRI, which usually evaluates only one tissue property at a time. MRF operates by purposely altering acquisition parameters to generate distinct signal evolutions, or 'fingerprints,' for various tissues. These recorded signals are then compared with precalculated fingerprints from a dictionary using pattern recognition algorithms to create quantitative maps of tissue parameters.

The essential principles of MRF include data gathering with varying sequence parameters, dictionary generation using signal simulation (typically utilizing Bloch equations), using pattern recognition to match obtained data to dictionary entries. The approach has various benefits, including efficiency, adaptability, thorough tissue characterization, and resistance to aberrations and noise. MRF has a wide range of clinical applications in neuroimaging, abdomen, breast, musculoskeletal, and cardiac imaging, assisting in the diagnosis of illnesses ranging from brain tumors to myocarditis. Despite its advantages, problems include the computational and memory requirements for large dictionaries, sensitivity to

inhomogeneities, and the necessity for optimum acquisition parameters. Future directions include advanced sequence optimization, deep learning integration for dictionary creation and reconstruction, and novel acquisition strategies to improve efficiency and accuracy.

Keywords: Magnetic Resonance Fingerprinting (MRF), Quantitative MRI, Dictionary Matching, Tissue Parameters (T1, T2 Relaxation), Deep Learning.

I. INTRODUCTION

Magnetic Resonance Fingerprinting (MRF) is a revolutionary quantitative magnetic resonance imaging (MRI) approach that allows for the simultaneous evaluation of many tissue parameters in a single, time-saving collection. This method is a substantial improvement over traditional MRI approaches, which typically assess only one tissue property at a time and can be time-consuming (1).

Magnetic Resonance Fingerprinting (MRF) is a fast-imaging technique that maps numerous tissue parameters, such as T1 and T2 relaxation durations. This method uses changeable acquisition settings, such as radiofrequency excitations and delays, to generate distinct magnetic resonance (MR) signal evolutions. Various tissues are frequently referred to as "fingerprints." Using pattern matching to compare the collected signal evolution with precalculated fingerprints from a dictionary, quantitative maps of tissue properties can be generated. This strategy enables the simultaneous acquisition of numerous tissue parameter maps, considerably lowering the total scan duration compared to standard, single-parameter quantitative MR imaging techniques (2).

II. FUNDAMENTAL PRINCIPLES AND PHYSICS OF MRF

1. Core Principle of MRF

MRF's fundamental principle involves quantifying multiple MR-sensitive tissue properties in a single acquisition, contrasting with traditional quantitative MRI which typically maps one tissue property at a time over a long acquisition period. Unlike conventional methods that rely on exponential models for signal recovery or decay, MRF utilizes more complex signal models to achieve higher-quality mapping (3).

2. Core Components of MRF

- **Data Acquisition:** This entails changing many sequence parameters during the acquisition to make the signal sensitive to different tissue qualities. The method creates distinct 'fingerprint-like' signal evolutions for various tissue features. The design of the acquisition sequence is critical since it impacts efficiency, estimability, and reliability.
- **Dictionary Generation:** A dictionary is produced by simulating signal time courses for expected combinations of tissue attributes with a suitable signal model. The dictionary includes a discretized subset of all tissue signals. The precision of the signal model is crucial for MRF accuracy; hence the dictionary should include all physiologically important tissue properties.
- **Pattern Recognition:** Following data capture, a pattern recognition algorithm compares each voxel's acquired fingerprint to the generated fingerprints in the database. To build property maps, the best matched entry from the dictionary is allocated to a voxel based on its related tissue qualities.This matching approach is

strong enough to identify tissue attributes even in the presence of undersampling artifacts, allowing for large acceleration factors.

3. Physics Underlying MRF

- **Signal Evolution:** Unlike typical quantitative methods that keep the signal steady to avoid errors caused by unwanted variations, MRF purposely alters acquisition settings (such flip angle and repetition duration) to establish individual signal evolutions, or 'fingerprints,' for different tissues. This enables the simultaneous quantification of many parameters, including T1, T2, and proton density
- **Bloch Equations and Extended Phase Graphs:** Bloch equations are frequently used during the dictionary generation process to simulate the effects of radiofrequency (RF) pulses and sequence timing on a single isochromat. In dephasing gradient sequences, each voxel's value is an average of many isochromats. Extended phase graph formalism effectively simulates spin system evolution with imbalanced gradients.
- **Spin History:** The balanced SSFP (bSSFP) sequence, often employed in early MRF implementations, is extremely appropriate because to its qualities of maintaining spin history, high SNR, high scan efficiency, and sensitivity to T1, T2, and off-resonance frequencies.
- **Spatial Incoherence of Undersampling:** MRF frequently uses variable density spiral trajectories for k-space sampling, allowing undersampling artifacts to be spatiotemporally incoherent. This incoherence, together with the fingerprint time course, prevents interference from many sites from mimicking a tissue fingerprint, allowing for reliable tissue property detection even at high acceleration (4).

III. SEQUENCE DESIGN, ACQUISITION STRATEGIES, AND OPTIMIZATION

Magnetic Resonance Fingerprinting (MRF) derives quantifiable tissue features such as T1 and T2 relaxation rates from arbitrary pulse sequences. These sequences require significant optimization due to a large number of adjustable factors and the need for precise in vivo performance prediction. This procedure seeks to maximize precision while minimizing scan time.

1. Sequence Design Challenges

- **Complex Cost Function:** It is challenging to create an effectively computed cost function that precisely forecasts the in vivo performance of MRF pulse sequences. Traditional techniques based on simple statistical noise models or crude heuristics are frequently unsuitable in clinical contexts where undersampling is prevalent.
- **High-Dimensional and Nonconvex Optimization:** The optimization problem is computationally difficult because the space of feasible pulse sequences is high-dimensional and nonconvex, rendering conventional approaches such as exhaustive search or gradient descent useless. For a sequence of 'n' pulses, the search space is 2n-dimensional, which can be in the thousands for 2D scans and considerably larger for 3D scans.
- **Physics-Inspired Optimization:** The authors conduct de novo automated design of MRF pulse sequences using physics-inspired algorithms. This approach utilizes an explicit first-principles simulation of systematic mistakes caused by Fourier undersampling and phase fluctuation, which tend to dominate random errors in MRF scans under medically relevant conditions of significant undersampling.

2. **Acquisition Strategies**
   - **Fast Imaging with Steady-State Precession (FISP):** The specific type of MRF pulse sequences considered are FISP sequences, which are used to generate 2D T1, T2, and proton density maps of the brain.
   - **Spiral Trajectories in k-space:** The'single-shot' setting samples a spiral trajectory around k-space after each pulse. The study used a variable-density spiral trajectory with 48 interleaves to traverse k-space. The readout duration is 5.9 ms, with a 300 × 300 mm^2 field of view and 256 × 256 matrix size.
   - **Temporal Variation in Sampling:** The spiral sampling is adjusted temporally from one TR to the next to keep aliasing artifacts from producing consistent signal bias. The Nonuniform Fast Fourier Transform (NUFFT) is then used to reconstruct pictures from MRF scans.
   - **Short Scan Times:** TR duration is limited to 10-100 ms, resulting in scan times of a few seconds for 2D MRF scans and several minutes for 3D MRF scans.
   - **Undersampling :** MRF scans typically sample. Fourier space is used sparingly to achieve short scan periods, with acceleration factors ranging from 48 to 400 reported in 2D and 3D in vivo scans.

3. **Optimization Algorithms and Cost Function**
   - **Cost Function Components:** There are three basic components to the optimization problem: a cost function, a search space for pulse sequences, and an optimization algorithm.
   - **Systematic Error Modeling:** The cost function is derived from precise first-principles simulations of systematic errors caused by Fourier undersampling and phase fluctuation. This involves accounting for spatially dependent phase variation and random error, that are substantial sources of inaccuracy in MRF brain imaging scans.
   - **Weighted Combination of Errors and Scan Time:** The cost function seeks to reduce T1 errors, T2 errors, and scan times. It utilizes a weighted mixture of expected values for these quantities. It combines RMSE values for systematic error with anticipated standard deviations for random error.
   - **Optimization Algorithms:** The study employs optimization algorithms such as simulated annealing and substochastic Monte Carlo, which are effective at avoiding local minima in the severely nonconvex search space. These algorithms begin with randomly generated pulse sequences and iteratively propose improved sequences based on feedback from the cost function.
   - **Spiked TR Durations:** Optimized sequences frequently exhibit qualitatively unique characteristics, such as "spiked" TR durations, in which most TRs are at their lowest allowable value, while some briefly surge to substantially longer lengths. This is viewed as "rest periods" that allow T1 relaxation and recharge magnetization levels, which aids in effective tissue differentiation (5).

IV. RECONSTRUCTION, POST-PROCESSING, AND QUANTITATIVE MAPPING

Magnetic resonance fingerprinting (MRF) uses advanced reconstruction, post-processing, and quantitative mapping approaches to extract various MR-sensitive tissue features from a single dataset. These techniques are critical for overcoming issues like as undersampling artifacts, dictionary size, and partial volume effects.

1. Reconstruction techniques

Reconstruction in MRF is largely concerned with converting extremely undersampled k-space information into the picture domain or directly into quantitative tissue property maps. Initial techniques used non-uniform rapid Fourier transformations followed by pattern matching, which frequently resulted in artifacts due to undersampling.

- **Iterative Algorithms**
  - These techniques seek to decrease aliasing artifacts and the number of timepoints necessary for a sequence, hence decreasing scan time. They work by iterating between k-space, which ensures data consistency, and the picture domain, which projects reconstructed signals onto the MRF dictionary.
  - Iterative approaches solve the general form as $\min_x \| y - Fx \| + AT(x)$, where x represents the reconstructed image series, y represents the acquired k-space data, F represents the encoding function, T represents a penalty functional, and A represents a regularization parameter. Constraints are frequently used to guarantee signal evolutions fit the dictionary subspace.

- **Low-Rank Reconstructions**
  - Several algorithms use the dictionary's low-rank property to shrink it with minimal information loss. This can include using Singular Value Decomposition (SVD) to minimize the temporal dimension of the dictionary, allowing for faster pattern matching.
  - **Low-rank and Subspace Modeling:** Apply a low-rank restriction to the reconstructed time series, and solve the issue using linear least squares and conjugate gradient techniques. This greatly lowers aliasing artifacts and the amount of timepoints required.
  - **Sparsity and Locally Low Rank Regularization:** SVD compression was used in the time domain, and a spatial low-rank assumption was established in the image domain, implying that small patches of pixels in reconstructed singular images had a low rank. Sparse regularization using wavelet transforms is also utilized.
  - **Matrix Completion:** To recover missing k-space data, we exploited the low-rank property of acquired data in the k-t domain, as well as SVD on a short, fully sampled calibration dataset. This approach just iterates in k-space, which makes it computationally efficient.

- **Other Reconstruction Improvements**
  - **Off-resonance Correction:** Multifrequency interpolation can remove blurring artifacts induced by B0 inhomogeneity in MRF.
  - **View Sharing:** View sharing, soft-weighted key-hole MRF (MRF SOHO), and sliding window reconstruction are methods for accelerating acquisition by lowering the number of timepoints or recreating fully sampled pictures from substantially undersampled frames.

2. Post-Processing and Quantitative Mapping

Quantitative mapping in MRF entails comparing obtained signal evolutions to a precomputed vocabulary of tissue attributes. The initial method employed an inner product of acquired signals and dictionary entries.

- **Dictionary Size and Matching Time:** The dictionary size may be a considerable barrier, increasing exponentially with a variety of tissue attributes. Strategies for addressing this include:
  - **SVD Compression:** reduces the temporal dimension of the dictionary, allowing for faster inner product matching.
  - **Randomized SVD:** Approximates singular vectors without saving the entire dictionary, which is handy when the vocabulary is too big for memory.
  - **Group Matching:** Pattern matching is accelerated by combining dictionary entries with comparable relaxation qualities, which reduces both the search space and matching time.
  - **Coarse Dictionary and Interpolation:** Applying a coarse dictionary with polynomial or linear interpolations to calculate more accurate T1 and T2 values, avoiding the discrete nature of tissue attributes.

- **Partial Volume Analysis:** This is an important post-processing step, particularly when voxel sizes exceed tissue structures, resulting in blurring and damaged boundaries.
  - **Linear Model Decomposition:** A linear model is utilized to partition MRF pixel signals into weights that correspond to pre-defined dictionary signal evolutions (including white matter, gray matter, and CSF). The weights are calculated using linear least squares.
  - **Partial Volume Dictionary:** An enhanced model employs a partial volume dictionary created using linear combinations, with only positive, real-valued weights for each of the established tissue type. This dictionary is used for pattern matching to determine quantity.
  - **Subject-Specific Dictionaries:** K-means is used on single-component MRF relaxometry maps to estimate acceptable tissue parameters for a subject-specific partial volume dictionary while allowing for natural variability in brain relaxation characteristics.
  - **Advanced Models:** Methods such as the Bayesian paradigm and reweighted l1 regularization eliminate the fixed tissue model assumption, resulting in more flexible tissue models when relaxation values are uncertain, which is especially relevant for sick tissues.

3. Machine and Deep Learning Applications

Machine and deep learning are now being used more frequently to handle MRF difficulties such as picture reconstruction and pattern matching.

- **Accelerated Dictionary Generation:** Unsupervised learning algorithms like neural networks can construct MRF dictionaries far faster than Bloch simulation, and they can even produce patient-specific dictionaries.
- **Dictionary-Free Parameter Estimation:** Deep learning can understand the relationship between tissue property values and the lexicon, minimizing the requirement for exhaustive pattern matching. Neural networks can generate synthetic qualitative images without going through the dictionary matching process.
- **Deep Reconstruction Networks:** Deep learning utilized for MRF signal evolutions after picture reconstruction may determine T1 and T2 values without requiring direct dictionary matching, which provides significant speed advantages over standard dictionary matching.

- **Spatially-Constrained Quantification:** This technique uses neural networks to determine T1 and T2 values directly from MRF signal evolutions. It decreases the temporal dimension of signal evolution for feature extraction before using a convolutional neural network to quantify T1 and T2 at each pixel while taking into account spatial properties of nearby pixels. This methodology drastically decreases the MRF acquisition time (3).

V. CLINICAL APPLICATIONS IN RADIOLOGICAL IMAGING

Magnetic Resonance Fingerprinting (MRF) has numerous clinical uses in radiology, including fast, simultaneous assessments of different tissue characteristics. Key areas involve:

1. Neuroimaging

- MRF is widely utilized in neuroimaging to assess healthy brain tissue, neurological malignancies, epilepsy, newborn imaging, and neuro-aging. T1 and T2 relaxation times can be used to distinguish between low-grade gliomas, high-grade gliomas, and metastases.
- It has been useful in detecting epileptogenic brain lesions, including those that are undetected on standard MRI, as well as assessing pediatric brain myelination and neurodevelopment abnormalities.

2. Prostate Imaging

Prostate MRF gives reproducible quantitative data for distinguishing between benign and malignant prostate disorders. It aids in differentiating prostate cancer from normal tissue and prostatitis throughout both the peripheral zone (PZ) and transition zone (TZ).

3. Abdominal Imaging

- MRF is useful for quick quantitative abdominal imaging, notably for detecting and distinguishing hepatic metastatic lesions from hepatic parenchyma.
- It may test multiple liver characteristics (T1, T2, T2*, FF, and T1rho) at the same time, allowing it to better define common liver diseases such inflammation, fibrosis, siderosis, and steatosis.
- Initial applications involve quantitative renal imaging for identifying corticomedullary distinction and pancreatic imaging to discriminate pancreatic lesions.

4. Breast Imaging

- Breast MRF is a promising tool for quantitative breast imaging and distinguishing between breast cancer and benign cysts from normal fibroglandular tissue using T1 and T2 relaxation times.

5. Musculoskeletal Applications

- Early research demonstrates the viability of MRF for muscle characterisation, measuring T1, T2, and fat fraction simultaneously in fat-infiltrated muscles, and describing several musculoskeletal tissues, including cortical bone.
- It is being tested for measuring age-related changes in cartilage and imaging hip cartilage (6).

6. Cardiac Applications

Because cardiac magnetic resonance fingerprinting (MRF) can concurrently obtain several co-registered tissue property maps, it presents a number of intriguing clinical applications in radiology imaging. Among these applications are:

- **Myocarditis Diagnosis**
  - MRF can help and perhaps automate the detection of myocarditis by giving co-registered T1 and T2 maps, which are critical diagnostic parameters.
- **Myocardial Infiltration and Amyloidosis**
  - MRF can identify myocardial infiltration, like cardiac amyloidosis, by identifying higher native T1 and ECV values. T2* mapping can also be used to discriminate among cardiomyopathies and monitor iron overload.
- **Myocardial Infarction and Ischemic Cardiomyopathy**
  - Cardiac MRF is a unified platform for detecting and defining myocardial infarctions. Postcontrast MRF maps can yield synthetic multicontrast Late Gadolinium Enhancement (LGE) pictures, that have been demonstrated to detect infarction zones with high accuracy.
- **Non-Ischemic Cardiomyopathy (NICM)**
  - MRF's multiparametric maps, possibly paired with fingerprint analysis, might improve phenotyping and diagnosis of certain NICM subtypes (7).

VI. ADVANTAGES, LIMITATIONS, CHALLENGES, AND ARTIFACTS

Magnetic Resonance Fingerprinting (MRF) provides a solid foundation for quantitative biomedical imaging, with several notable benefits over typical MRI methods. However, there are unique limits, problems, and artifacts that need continued study and development.

1. Advantages of MRF

- **Efficiency and Versatility**
  - MRF enables effective and adaptable acquisition and quantification of numerous tissue parameters from a single rapid MRI scan.
  - Unlike classic quantitative imaging approaches, it adds a joint architecture capable of rapidly obtaining and rebuilding numerous parametric maps while maintaining perfect alignment.

- **Comprehensive Tissue Characterization**
  - The approach allows for simultaneous sensitivity to various MR parameters, providing a more complete and quantitative assessment of scanned tissues.
  - Beyond T1 and T2, it may calculate quantitative characteristics that include 3D flow velocity, off-resonance effects, and water-molecule diffusion.

- **Robustness to Artifacts and Noise**
  - MRF dictionary matching is resilient to undersampling and motion artifacts.
  - Bayesian learning algorithms in MRF are resilient to high levels of noise, especially in vascular imaging.

- **Higher Resolution and Faster Acquisition**
  - MRF enables for greater resolution collection, particularly in cardiac imaging.

- The ultra-high-field MRF's high signal-to-noise ratio (SNR) allows for faster collection and greater resolution.

- **Clinical Utility**
  - MRF-enabled quantitative imaging delivers objective, precise, and standardized measures of tissue attributes that are repeatable among scanners and suited for automated diagnostics and disease progression tracking.
  - It has demonstrated viability in clinical applications such as heart, brain, musculoskeletal, and abdominal imaging, as well as radiation and cancer characterisation.

2. Limitations and Challenges of MRF

- **Computational and Memory Demands**
  - Large dictionaries are memory-intensive and computationally inefficient.
  - Dictionary matching is not ideal for online reconstruction since it is computational and memory intensive.

- **Specificity and Scan Time**
  - Single quantitative parametric maps are frequently susceptible to many pathologies, reducing specificity. Acquiring several parameters sequentially in classic quantitative MRI takes time, increases scan expenses, and may cause patient pain.

- **Susceptibility to Inhomogeneities**
  - Signal evolution mismatches can result from B0 field inhomogeneities in the first Inversion Recovery (IR) balanced Steady-State Free Precession (bSSFP) sequence.
  - MRF acquisition is similarly prone to B1+ heterogeneity.
  - Field inhomogeneities have a significant impact on ultra-high-field MRF.

- **Optimization of Acquisition Parameters**
  - Random selection of acquisition parameters (e.g., Flip Angles and Repetition Times) is not desirable since it might result in ambiguity and incorrect pattern matching owing to undersampling artifacts, noise, and phase inhomogeneity.
  - Optimizing acquisition settings is critical for efficiently recording tissue attributes despite preserving discrete signal evolutions and good SNR. This optimization is computationally intensive.

- **Motion Sensitivity**
  - Cardiac MRF (cMRF) is prone to motion irregularities caused by cardiac rhythms, and it is particularly susceptible to artifacts in persons with increased heart rates.
  - The abdomen area presents difficulties because of respiratory and cardiac motion abnormalities.

3. Artifacts in MRF

- **Undersampling Artifacts**
  - Undersampling artifacts are a common concern in MRF reconstruction, tainting signal evolution.

- These artifacts can be reduced by adjusting acquisition parameters and using techniques such as deep learning reconstructions and compressed sensing (CS).

- **Noise**
  - Noise affects the measurements of signal evolution, creating uncertainty in pattern matching.
  - An equation is suggested to model and mitigate the impacts of noise on MRF reconstruction.

- **Aliasing**
  - MRF reconstruction introduces aliasing effects into signals.
  - Model optimization can help to minimize the impact of aliasing on parametric maps.

- **Phase Inhomogeneity**
  - Phase inhomogeneity might distort the observed signal development.
  - B0 field inhomogeneities can cause inhomogeneity broadening and discrepancies between predicted and actual signal development.
  - MRF acquisition is similarly impacted by B1+ heterogeneities (8).

VII. FUTURE DIRECTIONS AND EMERGING TRENDS

Magnetic Resonance Fingerprinting (MRF) is evolving fast, with substantial advances and current research aimed at improving the tool's effectiveness, accuracy, and clinical application. Improved pulse sequences, sequence optimization, dictionary creation, reconstruction approaches, and a wide range of applications across many body areas are among the key rising trends and future prospects.

1. **Emerging Trends in MRF Pulse Sequences**
   - **Addressing Inhomogeneities and Quantitative Parameters Beyond T1/T2:** Inversion Recovery (IR) balanced Steady-State Free Precession (bSSFP) sequences were employed in the first MRF demonstrations; these sequences were sensitive to T1 and T2 but vulnerable to B0 field inhomogeneities.
   - More recent methods, including spoiled gradient echo (GRE) sequences (like FISP and FLASH), lessen the impacts of B0 inhomogeneity but may lower the signal-to-noise ratio (SNR). By embedding B1+ heterogeneities in the MRF vocabulary, future improvements seek to address them. Other quantitative factors such as 3D flow velocity, off-resonance effects, and water molecule diffusion are being estimated using MRF in addition to T1 and T2.
   - **Novel Acquisition Techniques:** Innovations such as Quick Echo Splitting (QUEST) for MRF collection are being investigated because they may be utilized with ultra-high-field scanners and need less RF energy, resulting in a reduced specific absorption rate (SAR).

2. **Emerging Trends in MRF Sequence Optimization**
   - **Advanced Optimization Algorithms:** Even though early MRF systems allowed for random selection of pulse sequence parameters, it was quickly understood that randomization might lead to artifacts and improper pattern matching. Optimization of acquisition parameters is critical for achieving high SNR, retaining discrete signal evolutions, and improving tissue feature encoding. This includes choosing algorithms

for optimization and establishing criteria to assess encoding capabilities; interior point techniques are a suitable fit.

- **Deep Learning Integration:** Deep learning approaches are increasingly being used to optimize acquisition settings and make MRF more sensitive to magnetization transfer (MT) effects. Surrogate networks are being developed to increase accuracy and efficiency by mapping acquisition parameters to reconstruction loss and minimizing the loss using deep learning algorithms.

3. **Emerging Trends in MRF Dictionary Generation**
   - **Improved Simulation Models:** MRF acquisitions are maintained in a dictionary for matching with obtained data after being simulated for different tissue qualities. While deterioration in GRE sequences is difficult to mimic, Bloch equations can simulate bSSFP-MRF sequences. It is possible to describe systems involving magnetization transfer using the Extended Phase Graph (EPG) framework, which has been suggested to mimic magnetization spoilage. Anisotropic diffusion imaging and modeling slice profile distortions are two more developments.

4. **Emerging Trends in MRF Reconstruction**
   - **Deep Learning-Based Reconstruction:** Due to their superior computational and memory efficiency over conventional dictionary matching, deep learning techniques are becoming more and more popular for MRF reconstruction. By directly mapping k-spaces or signal evolutions to parametric maps, these models can speed up computation and allow for online reconstruction. For mapping signal development to tissue attributes, feedforward neural networks, Multi-Layer Perceptrons (MLP), and Recursive Neural Networks (RNN) are a few examples. Additionally, k-spaces may be directly mapped to parametric maps using unrolled deep learning networks.
   - **Addressing Ancillary Limitations:** In order to specifically address problems such as motion artifacts, off-resonance artifacts, B1 inhomogeneities, and partial volume effects, MRF reconstruction is being improved. Using joint sparsity constraints and Bayesian techniques, partial volume effects are modeled as a weighted composite of sub-voxel signal evolutions. Additionally, deep learning is used to estimate T1 and T2 mapping in cardiac MRF while taking noise and periodic motion into consideration.

5. **Emerging Trends in MRF Applications**
   - **Cardiac Imaging:** MRF is being created for accurate cardiac tissue characterisation, addressing issues such as motion artifacts from heartbeats. Methods involve 3D cardiac MRF with respiratory motion correction and simultaneous multi-slice MRF for better coverage.
   - **Brain Imaging:** MRF is utilized to visualize brain architecture and function in detail, while simultaneously calculating parameters such as perfusion, diffusion, T1, and T2. Arterial Spin Labeling (ASL) is used to characterize brain tumors, diagnose Parkinson's disease, and measure blood flow, among other applications. Interleaved spiral MRF acquisitions enable high-resolution whole-brain coverage.
   - **Musculoskeletal Imaging:** MRF measures tissue characteristics (T1, T2, T1ρ, and fat fraction) in the musculoskeletal system, helping assess knee cartilage health and diagnose osteoarthritis.
   - **Abdomen Imaging:** To minimize motion sensitivity in abdominal imaging, approaches such as pilot tone navigators and oversampling at the k-space center are used. MRF's feasibility in liver and renal imaging is being established.

- **Radiotherapy and Cancer:** MRF is utilized to track tissue changes, identify malignant cells, and categorize tumors, providing quantitative tissue property assessments for brain tumors, ovarian tumors, and prostate cancer.
- **Fat-Water Separation:** To distinguish fat and water components, which are essential for musculoskeletal, breast, and abdominal imaging, approaches such as Dictionary-Based Fat–Water separation (DBFW) and three-point Dixon MRF methods are being developed (8).

6. Integration with Other Modalities

- **Glymphatic system research:** The ability of physiological MRF to explore the glymphatic system, which includes brain-wide water transport, is an interesting prospect. Integrating MRF with improved ASL contrasts, such as multi-echo or ultra-long TE ASL, can offer more information on brain fluid dynamics.
- **Simultaneous PET/MR:** Future simultaneous PET/MR and physiological MRF integration will enable simultaneously, co-registered capture of gold-standard metabolic data (such as oxygen or glucose metabolism) with MRF's high-resolution quantitative maps of tissue characteristics and hemodynamics. This will make it possible to directly examine neurovascular coupling and tissue viability at the voxel level (9).

VIII. CONCLUSION

Magnetic Resonance Fingerprinting (MRF) is an important boost in quantitative magnetic resonance imaging, allowing for the concurrent assessment of many tissue parameters in a single, time-efficient collection. This approach uses varied acquisition settings to produce distinct signal evolutions or 'fingerprints' for various tissues, which are then compared to a pre-calculated lexicon to provide quantitative maps of tissue parameters. MRF has many benefits, including efficiency, adaptability, thorough tissue characterization, resistance to artifacts and noise, and greater resolution with quicker capture.

Unfortunately, it confronts obstacles like as computational and memory demands caused by large dictionaries, sensitivity to inhomogeneities, and the complexity of tuning acquisition settings. Future directions include expanding its clinical applications across different body parts, such as neuroimaging, cardiac, musculoskeletal, and abdominal imaging, as well as addressing these limitations through sophisticated optimization algorithms and deep learning integration for dictionary generation and reconstruction.

REFERENCES

[1] Panda A, Mehta BB, Coppo S, Jiang Y, Ma D, Seiberlich N, et al. Magnetic resonance fingerprinting – An overview. Curr Opin Biomed Eng. 2017 Sep;3:56–66. doi:10.1016/j.cobme.2017.11.001

[2] Li+ H, Eck† BL, Yang M, Kim J, Liu R, Huang P, et al. SuperMRF: deep robust reconstruction for highly accelerated magnetic resonance fingerprinting. Quant Imaging Med Surg. 2025 Apr;15(4):3480–500. doi:10.21037/qims-23-1819

[3] McGivney DF, Boyacıoğlu R, Jiang Y, Poorman ME, Seiberlich N, Gulani V, et al. Magnetic resonance fingerprinting review part 2: Technique and directions. J Magn Reson Imaging. 2020 Apr;51(4):993–1007. doi:10.1002/jmri.26877

[4] Bipin Mehta B, Coppo S, Frances McGivney D, Ian Hamilton J, Chen Y, Jiang Y, et al. Magnetic resonance fingerprinting: a technical review. Magn Reson Med. 2019 Jan;81(1):25–46. doi:10.1002/mrm.27403

[5] Jordan SP, Hu S, Rozada I, McGivney DF, Boyacioğlu R, Jacob DC, et al. Automated design of pulse sequences for magnetic resonance fingerprinting using physics-inspired optimization. Proc Natl Acad Sci. 2021 Oct 5;118(40):e2020516118. doi:10.1073/pnas.2020516118
[6] Gaur S, Panda A, Fajardo JE, Hamilton J, Jiang Y, Gulani V. Magnetic Resonance Fingerprinting: A Review of Clinical Applications. Invest Radiol. 2023 Aug;58(8):561–77. doi:10.1097/RLI.0000000000000975
[7] Rashid I, Cruz G, Seiberlich N, Hamilton JI. Cardiac MR Fingerprinting: Overview, Technical Developments, and Applications. J Magn Reson Imaging. 2023 Dec 28;jmri.29206. doi:10.1002/jmri.29206
[8] Monga A, Singh D, De Moura HL, Zhang X, Zibetti MVW, Regatte RR. Emerging Trends in Magnetic Resonance Fingerprinting for Quantitative Biomedical Imaging Applications: A Review. Bioengineering. 2024 Feb 28;11(3):236. doi:10.3390/bioengineering11030236
[9] Lin C, Lu H, Fan AP. Technical Review of Magnetic Resonance Fingerprinting Applications in Cerebral Physiology. Magn Reson Med. 2025 Dec 7;mrm.70216. doi:10.1002/mrm.70216

9
Chapter

Liver Imaging Biomarkers: Fat Quantification and Fibrosis Assessment

[1]Aakash Kaushal
M.Sc. Research fellow
Department of Radiological
Imaging Techniques
College of paramedical Sciences
Teerthanker Mahaveer University
Moradabad

Abstract

Non-alcoholic fatty liver disease (NAFLD) and hepatic fibrosis represent major global health burdens, with histological liver biopsy long considered the reference standard for tissue characterisation but limited by sampling error, procedural risk, and poor patient acceptability. Advances in quantitative imaging have established a growing portfolio of non-invasive liver imaging biomarkers capable of detecting, staging, and longitudinally monitoring hepatic steatosis and fibrosis with clinically meaningful accuracy. This chapter provides a comprehensive review of the imaging techniques and quantitative metrics employed in liver fat quantification and fibrosis assessment across ultrasound, magnetic resonance imaging (MRI), computed tomography (CT), and nuclear medicine platforms.

Ultrasound-based hepatic steatosis indices, controlled attenuation parameter (CAP), and acoustic radiation force impulse (ARFI) elastography are examined alongside MRI proton density fat fraction (MRI-PDFF), magnetic resonance spectroscopy (MRS), MR elastography (MRE), and CT-based fat estimation. The physicochemical basis of each technique, acquisition protocols, validated threshold values, confounding factors, and comparative diagnostic performance are discussed with reference to current evidence and clinical guidelines. Emerging artificial intelligence-assisted quantification tools and multi-parametric liver assessment frameworks are also addressed. A thorough understanding of these biomarkers is essential for radiographers, radiologists, hepatologists, and researchers engaged in non-invasive liver disease assessment.

Keywords: Hepatic steatosis; liver fat quantification; fibrosis; MRI-PDFF; MR elastography; controlled attenuation parameter; liver stiffness measurement; NAFLD; quantitative imaging biomarkers; non-invasive assessment

I. INTRODUCTION

Chronic liver disease affects an estimated 1.5 billion individuals worldwide and is a leading cause of liver-related morbidity and mortality. Non-alcoholic fatty liver disease, encompassing simple hepatic steatosis through non-alcoholic steatohepatitis (NASH) to advanced fibrosis and cirrhosis, now constitutes the most prevalent chronic liver condition globally, driven by rising rates of obesity, type 2 diabetes mellitus, and metabolic syndrome.[1,2]

Accurate characterisation of the two cardinal pathological processes—hepatic fat accumulation and progressive fibrosis—is essential for risk stratification, treatment planning, and monitoring of therapeutic response. Liver biopsy, while capable of providing simultaneous histological grading of steatosis, inflammation, ballooning, and fibrosis stage, carries a complication rate of approximately 1–3% and is subject to significant sampling variability given that a standard needle core samples less than 1/50,000 of total liver volume.[3,4]

Quantitative imaging biomarkers have emerged as clinically validated, reproducible, and patient-acceptable alternatives. The past two decades have witnessed the transition from qualitative visual assessment to rigorous quantitative metrics—such as MRI-derived proton density fat fraction (MRI-PDFF) for steatosis and liver stiffness measurement (LSM) by MR elastography or ultrasound elastography for fibrosis—that meet regulatory and scientific standards for clinical trial endpoints and diagnostic decision-making.[5,6]

This chapter systematically reviews the imaging basis, quantitative methodology, diagnostic performance, and clinical application of the principal liver imaging biomarkers for fat quantification and fibrosis assessment, with the aim of providing a rigorous and practically oriented reference for academic and clinical practitioners.

II. HEPATIC STEATOSIS: PATHOPHYSIOLOGY AND GRADING

Hepatic steatosis is defined histologically as intracellular fat accumulation in more than 5% of hepatocytes. It is graded semiquantitatively by pathologists using the NAFLD Activity Score (NAS) system: S0 (<5% steatosis), S1 (5–33%), S2 (33–66%), and S3 (>66%). The predominant lipid species is triglyceride, though phospholipids and cholesterol esters also contribute. Fat accumulates primarily in the cytoplasm as macrovesicular droplets, altering hepatocyte density, acoustic properties, and magnetic resonance signal characteristics in ways exploitable by imaging.[7]

The clinical significance of hepatic steatosis extends beyond a surrogate marker of metabolic dysfunction. Steatosis potentiates hepatic insulin resistance, promotes oxidative stress, and creates conditions for the development of NASH, which is associated with a substantially elevated risk of progression to fibrosis, cirrhosis, and hepatocellular carcinoma. Quantitative imaging enables early detection of steatosis at thresholds below those reliably detected by standard B-mode ultrasound, facilitating timely intervention in high-risk individuals.[8]

III. ULTRASOUND-BASED FAT QUANTIFICATION

1. Conventional B-mode Ultrasound

Conventional B-mode ultrasound has historically served as the first-line imaging tool for hepatic steatosis assessment owing to its wide availability, absence of ionising radiation, and low cost. Fat-laden hepatocytes exhibit increased acoustic impedance mismatch relative to adjacent tissues, producing characteristic features including diffuse hepatic hyperechogenicity, increased liver-to-kidney echo ratio, posterior beam attenuation, and obscuration of intrahepatic vessels and diaphragm.[9]

Despite these recognisable qualitative features, conventional ultrasound demonstrates significant limitations as a quantitative tool. Its reported sensitivity for detecting steatosis grades S1 and above ranges from 60–94% with specificity of 66–95% across published meta-analyses, but performance deteriorates substantially for grade S1 steatosis (<33% hepatocytes affected), yielding sensitivities as low as 55–65%.[10]

Observer-dependent scoring systems (grade 0–3) further limit inter-reader reproducibility. Advanced quantitative ultrasound parameters—including the hepato-renal index (HRI), attenuation coefficient, and backscatter coefficient—have been proposed to improve objectivity, but none has achieved the standardisation required for broad multicentre deployment.

2. Controlled Attenuation Parameter (CAP)

Controlled attenuation parameter (CAP) is a proprietary quantitative ultrasound biomarker integrated into the FibroScan platform (Echosens, Paris). CAP measures ultrasonic attenuation of the shear wave pulse used for vibration-controlled transient elastography (VCTE), expressed in dB/m and acquired simultaneously with liver stiffness measurement (LSM).[11]

CAP exploits the positive correlation between hepatic fat content and ultrasound attenuation. Measured attenuation is quantified as:

$$CAP\ (dB/m) = attenuation\ coefficient \times frequency \times path\ length$$

Published threshold values for CAP differ modestly across studies owing to probe type (M-probe vs. XL-probe for obese patients), operator experience, and histological comparator methodology. Pooled meta-analytic thresholds are approximately: ≥238 dB/m for S≥1, ≥259 dB/m for S≥2, and ≥292 dB/m for S3, with AUROCs of 0.82–0.88 across steatosis grades.[12,13]

CAP is significantly influenced by body mass index (BMI), probe selection, interquartile range to median ratio (IQR/M > 0.30 indicating unreliable measurement), fasting status, and hepatic inflammation. The XL probe, mandatory for patients with BMI > 30 kg/m² or skin-to-liver capsule distance > 25 mm, yields systematically lower CAP values than the M probe, necessitating probe-specific cut-offs.[14]

3. Quantitative Ultrasound Attenuation Imaging

Beyond CAP, several real-time quantitative attenuation coefficient (QAC) systems have been developed by major ultrasound manufacturers, including attenuation imaging (ATI, Canon), tissue attenuation imaging (TAI, Siemens), and hepatic attenuation rate (HAR, Philips). These platforms measure the frequency-dependent attenuation slope (dB/cm/MHz) across a user-defined region of interest in liver parenchyma, providing a vendor-specific quantitative attenuation index.[15]

While initial validation studies are promising—with pooled AUROC values of 0.85–0.90 for S≥1 detection—cross-vendor comparability remains a critical limitation due to differences in pulse sequences, frequency ranges, and processing algorithms. International standardisation initiatives, including those led by the Quantitative Imaging Biomarkers Alliance (QIBA), are addressing these challenges through phantom-based calibration frameworks.[16]

IV. MRI-BASED LIVER FAT QUANTIFICATION

1. Principles of Fat-Water MRI

MRI offers the most accurate and reproducible non-invasive fat quantification available in clinical practice. The fundamental basis is the chemical shift between the resonant frequencies of protons in fat (lipid methylene groups) and water molecules. At 1.5T, fat and water protons resonate approximately 220 Hz apart (3.5 ppm), producing in-phase (IP) and out-of-phase (OOP) signal oscillations as a function of echo time (TE) in gradient-echo sequences.[17]

In the simple two-point Dixon method:

$$Fat\ fraction = (SI\_IP - SI\_OOP) / (2 \times SI\_IP)$$

However, this approach is confounded by T1 bias (differential saturation of fat and water due to their different T1 relaxation times), T2* decay (signal loss from iron-induced field inhomogeneity), the multi-peak spectral complexity of fat (triglyceride contains multiple chemically distinct proton groups), and noise bias. These confounders can cause substantial overestimation or underestimation of true fat fraction if not corrected.[18]

2. MRI Proton Density Fat Fraction (MRI-PDFF)

MRI-PDFF represents the current reference standard for non-invasive hepatic fat quantification, defined as the ratio of the MR signal from mobile protons in fat to the total mobile proton signal from fat and water in hepatic tissue. Unlike simple fat fraction estimates, MRI-PDFF is corrected for all major confounders: T1 bias (using low flip angle acquisitions), T2* decay (incorporated into the signal model), spectral complexity of fat (using a six-peak fat spectral model), and noise bias.[19]
The signal model is expressed as:

$$S(TE) = (\rho W + \rho F \cdot \Sigma[an \cdot exp(i2\pi \Delta fn \cdot TE)]) \cdot exp(-R2^* \cdot TE) \cdot exp(i2\pi \Delta B0 \cdot TE)$$

where ρW and ρF are water and fat signal amplitudes, an and Δfn represent the relative amplitude and frequency shift of the nth fat spectral peak, R2* is the effective transverse relaxation rate, and ΔB0 is the local field inhomogeneity. PDFF is then defined as: PDFF = ρF / (ρW + ρF).[20]

MRI-PDFF demonstrates excellent correlation with histological steatosis grade (r = 0.76–0.91 across multiple cohort studies) and can detect steatosis at PDFF thresholds of approximately ≥5.2% for S≥1, ≥11.3% for S≥2, and ≥17.1% for S≥3, with AUROCs of 0.90–0.97.[21,22]

MRI-PDFF is highly reproducible across scanners, field strengths (1.5T and 3T), and vendors when acquired using confounder-corrected multi-echo gradient-echo sequences (e.g., IDEAL-IQ, mDIXON Quant, LiverLab). Coefficient of variation for repeated measurements within a session is typically below 5%, supporting its use as a sensitive endpoint for therapeutic trials targeting hepatic fat reduction.[23]

3. Magnetic Resonance Spectroscopy (MRS)

MR spectroscopy, specifically single-voxel ^{1}H-MRS, has served as the original non-invasive reference standard for hepatic fat quantification against which MRI-PDFF was validated. MRS acquires the full proton frequency spectrum from a user-defined voxel (typically 3×3×3 cm) placed in the right hepatic lobe, enabling direct visualisation of the water peak (~4.7 ppm) and the dominant methylene lipid peak (~1.3 ppm), as well as minor fat peaks.[24]
Fat fraction from MRS is calculated as:

$$MRSFF = Fat\ signal\ area\ /\ (Fat\ signal\ area + Water\ signal\ area) \times 100\%$$

While MRS provides high sensitivity and direct spectral separation of fat and water signals, its clinical deployment is limited by long acquisition times (5–15 minutes per voxel), susceptibility to motion artefact, requirement for post-processing expertise, and sampling of only a small liver volume. Multi-voxel chemical shift imaging (CSI) overcomes volume limitation but further increases acquisition complexity. For clinical and large-scale research applications, MRI-PDFF has substantially superseded MRS as the preferred fat quantification method.[25]

4. CT-Based Liver Fat Estimation

Unenhanced CT provides an indirect estimate of hepatic steatosis through attenuation measurement. Normal liver parenchyma attenuates at 50–70 HU on unenhanced CT; fat deposition reduces attenuation proportionally, with each 1% increase in fat fraction reducing liver attenuation by approximately 1.6 HU. Diagnostic thresholds commonly applied include: absolute liver attenuation < 40 HU or liver-to-spleen attenuation ratio (L/S ratio) < 0.8 for moderate-to-severe steatosis.[26]

CT sensitivity for detecting mild steatosis (grade S1, < 33% fat) is limited—approximately 50–75%—partly because the relationship between HU and fat fraction is non-linear at low fat concentrations and is confounded by hepatic iron deposition, glycogen content, and concurrent fibrosis. CT is therefore not recommended as a primary tool for fat quantification in clinical or research settings where MRI-PDFF is accessible. However, CT-derived fat estimates from opportunistic screening of existing scans—using deep learning models trained on HU and liver morphology features—represent an emerging application for population-level metabolic liver disease screening.[27]

V. HEPATIC FIBROSIS: PATHOPHYSIOLOGY AND STAGING

Hepatic fibrosis results from the chronic wound-healing response to sustained hepatocyte injury, characterised by activation of hepatic stellate cells (HSCs) and their transdifferentiation into myofibroblasts that deposit excess extracellular matrix—principally collagen types I and III—in the space of Disse and periportal regions. Progressive fibrous deposition distorts the hepatic lobular architecture, increasing mechanical stiffness, impairing sinusoidal blood flow, and ultimately leading to cirrhosis and portal hypertension.[28]

Fibrosis is staged histologically using validated scoring systems, of which the METAVIR score is most widely employed in clinical research: F0 (no fibrosis), F1 (portal fibrosis without septa), F2 (portal fibrosis with few septa), F3 (numerous septa without cirrhosis), and F4 (cirrhosis). The Ishak and Knodell systems provide finer gradation for research applications. Clinically, the most critical thresholds are F≥2 (significant fibrosis, warranting antifibrotic treatment consideration) and F≥4 (cirrhosis, requiring hepatocellular carcinoma surveillance and portal hypertension management).[29]

VI. ULTRASOUND ELASTOGRAPHY FOR FIBROSIS ASSESSMENT

1. Vibration-Controlled Transient Elastography (VCTE)

Vibration-controlled transient elastography (VCTE), commercially implemented as FibroScan (Echosens), is the most extensively validated ultrasound-based fibrosis assessment tool in clinical practice. VCTE generates a low-frequency (50 Hz) mechanical vibration at the skin surface using a dedicated probe, propagating a shear wave into the liver. The velocity of shear wave propagation, measured by pulse-echo ultrasound tracking over a cylindrical measurement volume 1 cm wide and 4 cm long positioned 25–65 mm beneath the skin surface, is converted to liver stiffness measurement (LSM) through the relationship:[30]

$$E\ (kPa) = 3\rho Vs^2$$

where E is Young's modulus (liver stiffness, kPa), ρ is tissue density (assumed constant at 1,000 kg/m³), and Vs is shear wave velocity (m/s). LSM values are reported as the median of ≥10 valid measurements, with a success rate ≥60% and IQR/M ≤0.30 considered acceptable quality criteria.[31]

Published VCTE thresholds for METAVIR fibrosis staging vary across aetiologies, but widely adopted consensus values for NAFLD/NASH patients are: F≥1: ≥7.0 kPa, F≥2: ≥8.0 kPa, F≥3: ≥9.7 kPa, and F4 (cirrhosis): ≥13.0 kPa. AUROCs for significant fibrosis (F≥2) range from 0.79 to 0.87 and for cirrhosis (F4) from 0.89 to 0.95.[32,33]

VCTE is subject to several confounders that must be recognised in clinical and research contexts. LSM is significantly elevated by acute hepatic inflammation (elevated ALT, acute hepatitis flares), food intake (recommended fasting ≥2 hours prior to examination), hepatic congestion in right heart failure, and extrahepatic cholestasis. Failure rates are higher in patients with BMI > 30 kg/m² or intercostal space dimensions insufficient for probe placement, necessitating the XL probe and documented reporting of probe type.[34]

2. Point Shear Wave Elastography (pSWE) and ARFI

Point shear wave elastography, including acoustic radiation force impulse (ARFI) elastography, generates shear waves using focused acoustic radiation force pulses from a conventional ultrasound probe, enabling integrated B-mode imaging and elasticity measurement without dedicated hardware. Results are expressed in metres per second (m/s) and can be converted to kPa by the same relationship as VCTE.[35]

pSWE offers the practical advantages of simultaneous B-mode guidance for measurement site selection, avoidance of large vessels and focal lesions, and integration into routine ultrasound examinations. Meta-analytic performance for cirrhosis detection yields AUROCs of 0.87–0.93, broadly comparable to VCTE, though fewer large-scale multicentre validation studies exist relative to VCTE. The Siemens Virtual Touch IQ, GE ElastoQ, and Philips ElastPQ implementations are the most extensively evaluated.[36]

3. Two-Dimensional Shear Wave Elastography (2D-SWE)

Two-dimensional shear wave elastography (2D-SWE) extends pSWE to provide real-time colour-coded maps of tissue stiffness across a user-defined region of the liver, offering spatial information on stiffness heterogeneity that is unavailable from single-point measurements. Both Supersonic Shear Imaging technology (Aixplorer, SuperSonic Imagine) and conventional platform 2D-SWE implementations generate quantitative stiffness maps with good intra-session reproducibility.[37]

Aggregate evidence from systematic reviews indicates that 2D-SWE demonstrates AUROC values of 0.85–0.90 for significant fibrosis and 0.91–0.96 for cirrhosis detection, with performance broadly comparable to MRE in some cohorts. Measurement reliability is best when at least 10 acquisitions are averaged over a 1–3 cm² ROI placed in right lobe parenchyma free of large vessels, capsule, and motion artefact.[38]

VII. MR ELASTOGRAPHY

1. Principles and Acquisition

MR elastography (MRE) is currently the most accurate non-invasive method for hepatic fibrosis staging, combining the high tissue penetration and quantitative precision of MRI with mechanical wave propagation physics to generate quantitative stiffness maps of the entire liver. MRE involves three components: (i) an active driver—a pneumatic or electromechanical actuator placed over the right lower chest wall—generating continuous sinusoidal mechanical waves (typically 60 Hz); (ii) a modified phase-contrast MRI sequence with motion-encoding gradients (MEGs) synchronised to the mechanical oscillation to encode the resulting shear wave displacement pattern; and (iii) an inversion algorithm that converts the wave displacement maps into quantitative stiffness maps (elastograms).[39,40]

The stiffness value reported is the magnitude of the complex shear modulus G*, which for a viscoelastic medium is:

$$|G^*| = \rho \cdot \omega^2 \cdot \lambda^2 / (4\pi^2)$$

where ρ is tissue density, ω is angular frequency, and λ is the measured shear wavelength. Liver stiffness is expressed in kilopascals (kPa) and sampled across a whole-liver ROI, providing mean and pixel-wise stiffness values.[41]

Standard clinical MRE is performed on 1.5T or 3T MRI systems using 2D gradient-recalled echo (GRE) or spin-echo echo-planar imaging (SE-EPI) sequences, with GRE providing higher spatial resolution and SE-EPI offering greater robustness to B0 inhomogeneity and iron-related signal loss. Acquisition time is approximately 15–20 seconds per breath-hold per slice, with 4 axial slices typically acquired.[42]

2. Diagnostic Performance and Thresholds

MRE demonstrates consistently superior diagnostic performance for fibrosis staging compared to all ultrasound-based elastography modalities, particularly for intermediate fibrosis stages (F2 and F3) where clinical decision-making is most uncertain. A landmark meta-analysis by Singh et al. (2015) reported pooled AUROCs of 0.84 for F≥1, 0.88 for F≥2, 0.93 for F≥3, and 0.92 for F4, with mean stiffness thresholds of 2.61, 2.97, 3.62, and 4.71 kPa respectively for these METAVIR stages in NAFLD.[43]

Subsequent large prospective cohort studies have refined these thresholds, with the most widely cited clinical decision points for NAFLD being: F≥2 at ≥2.88–3.0 kPa, and cirrhosis at ≥4.67–5.0 kPa. MRE is less affected by BMI, ascites, and operator variability than ultrasound elastography methods, and its whole-liver sampling reduces the sampling error inherent in single-point measurements.[44,45]

Failure or unreliable MRE results (confidence map coverage < 95% of the liver ROI) occur in approximately 5–8% of examinations, primarily due to severe hepatic iron overload causing T2* signal loss that precludes adequate wave detection, severe obesity, and cardiac arrhythmia affecting breath-hold consistency. In patients with elevated liver iron, SE-EPI MRE sequences offer substantially reduced failure rates compared to GRE-MRE.[46]

3. Combined MRE and MRI-PDFF Assessment

The simultaneous acquisition of MRE and MRI-PDFF within a single imaging session—now achievable in a scan time of 20–30 minutes on current MRI platforms—provides complementary quantitative assessment of both the inflammatory-steatotic and fibrotic components of NAFLD, enabling comprehensive disease staging in a single examination. Multi-parametric liver MRI protocols incorporating T1 mapping (cT1, LiverMultiScan), MRE, MRI-PDFF, and T2* for iron quantification are being validated in multicentre studies as surrogates for histological NASH activity score and fibrosis stage in therapeutic trials.[47,48]

VIII. INTEGRATION OF IMAGING BIOMARKERS WITH SERUM MARKERS AND CLINICAL ALGORITHMS

Imaging biomarkers do not operate in isolation; clinical practice increasingly incorporates integrated algorithms that combine imaging metrics with serum markers and clinical variables to improve diagnostic precision and avoid unnecessary biopsy. For fibrosis assessment, the VCTE-based FibroScan-AST (FAST) score combines LSM, CAP, and serum AST to identify patients with NASH with significant fibrosis (F≥2) at risk for disease progression, with an AUROC of 0.80–0.85 reported in validation cohorts.[49]

The Agile 3+ and Agile 4 scores incorporate VCTE LSM with age, sex, diabetes status, platelet count, and ALT/AST ratio to stage advanced fibrosis (F≥3) and cirrhosis

respectively, demonstrating superior performance to LSM alone or serum-only markers such as FIB-4 and APRI.[50]

For fat quantification, MRI-PDFF combined with serum cytokeratin-18 (CK-18) fragments—a marker of hepatocyte apoptosis—improves NASH diagnosis beyond PDFF alone, as PDFF reflects fat content but not inflammatory activity. Multi-parametric scoring systems incorporating imaging and serum data are anticipated to form the backbone of non-invasive NASH diagnostic algorithms pending regulatory approval of NASH therapies requiring non-invasive staging endpoints.[51]

IX. NUCLEAR MEDICINE APPROACHES TO LIVER STEATOSIS ASSESSMENT

While nuclear medicine does not currently represent a primary clinical modality for liver fat quantification, several PET and SPECT-based approaches are under investigation. ^{11}C-acetate PET has been used in research settings to quantify hepatic de novo lipogenesis by measuring acetate incorporation into fatty acids in the liver, providing a functional readout of the metabolic activity driving steatosis rather than a static fat content measurement.[52]

^{18}F-FDG PET demonstrates reduced hepatic SUV in the presence of significant steatosis, reflecting competitive inhibition of FDG uptake by elevated intracellular fatty acid metabolism, though this inverse relationship is insufficiently specific for quantitative fat staging. ^{99}mTc-sulphur colloid scintigraphy and hepatobiliary iminodiacetic acid (HIDA) scanning indirectly reflect Kupffer cell function and hepatocyte secretory capacity impaired by progressive fibrosis, providing functional correlates of disease severity but without the quantitative precision of MRI or elastography.[53]

At present, nuclear medicine liver biomarkers serve primarily as adjunctive tools in complex cases or research protocols rather than as first-line staging instruments. Continued development of targeted radiolabelled probes—including tracers for collagen binding, HSC activation, and lipid metabolism—may expand the nuclear medicine role in precision liver assessment in future clinical practice.[54]

X. ARTIFICIAL INTELLIGENCE IN LIVER FAT AND FIBROSIS QUANTIFICATION

Artificial intelligence approaches—particularly deep convolutional neural networks and radiomics—are increasingly applied to automate and enhance quantitative liver imaging biomarker extraction. Deep learning models trained on large CT datasets have demonstrated the ability to predict MRI-PDFF and histological steatosis grade from unenhanced CT attenuation alone, enabling opportunistic steatosis screening from CT examinations performed for other indications without additional imaging.[55]

For fibrosis assessment, radiomic texture feature extraction from multiphasic CT and MRI—including first-order statistics, grey-level co-occurrence matrix (GLCM), grey-level run-length matrix (GLRLM), and wavelet-transformed features—has shown AUROC values of 0.75–0.86 for advanced fibrosis detection in retrospective studies. Automated liver segmentation using convolutional neural networks enables whole-liver radiomic analysis unconstrained by the sampling limitations of small ROIs.[56]

In ultrasound, AI-driven quantitative attenuation coefficient and backscatter coefficient analysis algorithms are being developed to standardise operator-dependent acquisition variability and improve cross-vendor comparability of attenuation-based fat quantification. Deep learning-assisted 2D-SWE interpretation, applying automated outlier rejection and spatial averaging, has demonstrated improved measurement reproducibility compared to manual ROI placement in preliminary studies.[57]

Challenges limiting AI translation include the need for large annotated multicentre datasets with paired histology, domain shift between training and deployment environments (scanner models, field strengths, and acquisition parameters), and the absence of prospective outcome validation. Explainability and regulatory approval frameworks for AI-derived imaging biomarkers are active areas of development.[58]

XI. STANDARDISATION, QUALITY ASSURANCE, AND REGULATORY CONSIDERATIONS

The clinical and research utility of liver imaging biomarkers depends critically on standardisation and quality assurance at every stage of the measurement chain. For MRI-PDFF, the QIBA Fat/Water MRI Technical Committee has established a standardisation framework that includes phantom-based scanner calibration using tissue-mimicking phantoms with known fat fraction values, acquisition parameter specifications, and limits for acceptable intra- and inter-scanner coefficient of variation.[59]

For VCTE and ultrasound elastography, the Liver Reporting and Data System (LI-RADS) Fibrosis supplement and EFSUMB guidelines specify minimum quality criteria for valid measurements, including probe selection rules, fasting requirements, operator certification standards, and IQR/M thresholds. Reporting templates for elastography examinations that document these quality parameters are recommended for all clinical reports to facilitate downstream clinical interpretation.[60]

The US Food and Drug Administration (FDA) Drug Development Tool (DDT) qualification process for liver imaging biomarkers has resulted in the regulatory qualification of MRI-PDFF as an enrichment biomarker for clinical trials of NAFLD/NASH treatments, enabling sponsor use of PDFF as an entry criterion and secondary endpoint without requiring independent FDA review. MRE-derived liver stiffness has been submitted for DDT qualification as a fibrosis staging endpoint, with qualification decision pending.[61]

Multisite reproducibility studies—fundamental to regulatory qualification—have demonstrated mean MRI-PDFF coefficients of variation of 2–7% across different scanner platforms and institutions when confounder-corrected sequences are used, meeting the requirements for a sensitive treatment endpoint. Similar studies for MRE report mean stiffness variability of 5–10% across sites, acceptable for staging purposes but requiring further optimisation for use as a sensitive continuous endpoint.[62]

XII. CLINICAL DECISION FRAMEWORKS AND FUTURE DIRECTIONS

Current clinical practice guidelines—including those from the European Association for the Study of the Liver (EASL), American Association for the Study of Liver Diseases (AASLD), and Asia Pacific Association for the Study of the Liver (APASL)—now incorporate non-invasive liver imaging biomarkers into diagnostic algorithms for NAFLD/NASH staging. The

EASL Clinical Practice Guidelines on NAFLD (2023) recommend non-invasive tests (NITs) including LSM by VCTE and MRI-PDFF as first-line tools for risk stratification in patients with suspected NAFLD, reserving biopsy for cases where NITs are discordant or indeterminate.[63]

The Baveno VII consensus on portal hypertension further recommends VCTE LSM thresholds for ruling in clinically significant portal hypertension (CSPH) and stratifying need for endoscopic variceal surveillance, extending the clinical application of liver stiffness beyond fibrosis staging to haemodynamic risk assessment.[64]

Future developments anticipated in this field include: (i) wider clinical adoption of multi-parametric liver MRI protocols (LiverMultiScan, LMS) combining cT1, PDFF, and T2* within a single 15-minute examination; (ii) regulatory approval of pharmacological NASH treatments conditional on non-invasive biomarker-based staging endpoints; (iii) integration of imaging biomarkers with polygenic risk scores and multi-omics data in precision hepatology frameworks; and (iv) development of novel MRI contrast agents and targeted PET tracers for molecular-level fibrosis and steatohepatitis characterisation.[65,66]

XIII. CONCLUSION

Quantitative liver imaging biomarkers for fat quantification and fibrosis assessment have transformed the non-invasive evaluation of chronic liver disease. MRI-PDFF has established itself as the reference-standard method for hepatic steatosis quantification, offering precision, reproducibility, and regulatory-grade performance across clinical and research settings. MR elastography provides the most accurate non-invasive fibrosis staging, particularly for intermediate fibrosis grades where biopsy-based staging uncertainty is highest. Ultrasound-based tools—including VCTE, CAP, pSWE, and 2D-SWE—offer widely accessible alternatives with strong validation bases, appropriate for population screening and resource-limited settings.

The integration of multiple imaging biomarkers within a single examination—paired MRI-PDFF and MRE, or VCTE with CAP—enables comprehensive, efficient disease characterisation that increasingly rivals biopsy for clinical staging purposes. Emerging AI-assisted analysis, standardisation frameworks, and regulatory qualification pathways are accelerating the adoption of these biomarkers into mainstream clinical practice and therapeutic trial design.

For radiological professionals and researchers, mastery of the physical principles, acquisition requirements, quantitative metrics, diagnostic thresholds, and confounding factors governing liver imaging biomarkers is now a core competency of advanced practice—one that positions imaging at the centre of precision medicine for the globally prevalent and clinically significant spectrum of chronic liver disease.

REFERENCES

[1] Asrani SK, Devarbhavi H, Eaton J, et al. Burden of liver diseases in the world. J Hepatol. 2019;70(1):151–171. doi:10.1016/j.jhep.2018.09.014

[2] Younossi ZM, Koenig AB, Abdelatif D, et al. Global epidemiology of nonalcoholic fatty liver disease—meta-analytic assessment of prevalence, incidence, and outcomes. Hepatology. 2016;64(1):73–84. doi:10.1002/hep.28431

[3] Ratziu V, Charlotte F, Heurtier A, et al. Sampling variability of liver biopsy in nonalcoholic fatty liver disease. Gastroenterology. 2005;128(7):1898–1906. doi:10.1053/j.gastro.2005.03.084
[4] Rockey DC, Caldwell SH, Goodman ZD, et al. Liver biopsy. Hepatology. 2009;49(3):1017–1044. doi:10.1002/hep.22742
[5] Reeder SB, Hu HH, Sirlin CB. Proton density fat-fraction: a standardized, fully-quantitative, MRI-based biomarker of tissue fat concentration. Magn Reson Med. 2012;68(6):1849–1859. doi:10.1002/mrm.24611
[6] Loomba R, Wolfson T, Ang B, et al. Magnetic resonance elastography predicts advanced fibrosis in patients with nonalcoholic fatty liver disease: a prospective study. Hepatology. 2014;60(6):1920–1928. doi:10.1002/hep.27362
[7] Kleiner DE, Brunt EM, Van Natta M, et al. Design and validation of a histological scoring system for nonalcoholic fatty liver disease. Hepatology. 2005;41(6):1313–1321. doi:10.1002/hep.20701
[8] Angulo P. Nonalcoholic fatty liver disease. N Engl J Med. 2002;346(16):1221–1231. doi:10.1056/NEJMra011775
[9] Saverymuttu SH, Joseph AE, Maxwell JD. Ultrasound scanning in the detection of hepatic fibrosis and steatosis. Br Med J (Clin Res Ed). 1986;292(6512):13–15. doi:10.1136/bmj.292.6512.13
[10] Hernaez R, Lazo M, Bonekamp S, et al. Diagnostic accuracy and reliability of ultrasonography for the detection of fatty liver: a meta-analysis. Hepatology. 2011;54(3):1082–1090. doi:10.1002/hep.24452
[11] Sasso M, Tengher-Barna I, Ziol M, et al. Novel controlled attenuation parameter for noninvasive assessment of steatosis using Fibroscan: validation in chronic hepatitis C. J Viral Hepat. 2012;19(4):244–253. doi:10.1111/j.1365-2893.2011.01534.x
[12] Karlas T, Petroff D, Sasso M, et al. Individual patient data meta-analysis of controlled attenuation parameter (CAP) technology for assessing steatosis. J Hepatol. 2017;66(5):1022–1030. doi:10.1016/j.jhep.2016.12.022
[13] de Lédinghen V, Vergniol J, Capdepont M, et al. Controlled attenuation parameter (CAP) for the diagnosis of steatosis: a prospective study of 5323 examinations. J Hepatol. 2014;60(5):1026–1031. doi:10.1016/j.jhep.2013.12.018
[14] Eddowes PJ, Sasso M, Allison M, et al. Accuracy of FibroScan controlled attenuation parameter and liver stiffness measurement in assessing steatosis and fibrosis in patients with nonalcoholic fatty liver disease. Gastroenterology. 2019;156(6):1717–1730. doi:10.1053/j.gastro.2019.01.042
[15] Park CC, Nguyen P, Hernandez C, et al. Magnetic resonance elastography vs transient elastography in detection of fibrosis and noninvasive measurement of steatosis in patients with biopsy-proven nonalcoholic fatty liver disease. Gastroenterology. 2017;152(3):598–607. doi:10.1053/j.gastro.2016.10.026
[16] Ozturk A, Grajo JR, Dhyani M, et al. Principles of ultrasound elastography. Abdom Radiol (NY). 2018;43(4):773–785. doi:10.1007/s00261-018-1475-6
[17] Reeder SB, Cruite I, Hamilton G, et al. Quantitative assessment of liver fat with magnetic resonance imaging and spectroscopy. J Magn Reson Imaging. 2011;34(4):729–749. doi:10.1002/jmri.22580
[18] Bydder M, Yokoo T, Hamilton G, et al. Relaxation effects in the quantification of fat using gradient echo imaging. Magn Reson Imaging. 2008;26(3):347–359. doi:10.1016/j.mri.2007.08.012
[19] Yokoo T, Serai SD, Pirasteh A, et al. Linearity, bias, and precision of hepatic proton density fat fraction measurements by using MR imaging: a meta-analysis. Radiology. 2018;286(2):486–498. doi:10.1148/radiol.2017170550
[20] Yu H, Shimakawa A, McKenzie CA, et al. Multiecho water-fat separation and simultaneous R2* estimation with multifrequency fat spectrum modeling. Magn Reson Med. 2008;60(5):1122–1134. doi:10.1002/mrm.21737
[21] Tang A, Tan J, Sun M, et al. Nonalcoholic fatty liver disease: MR imaging of liver proton density fat fraction to assess hepatic steatosis. Radiology. 2013;267(2):422–431. doi:10.1148/radiol.12120896
[22] Idilman IS, Aniktar H, Idilman R, et al. Hepatic steatosis: quantification by proton density fat fraction with MR imaging versus liver biopsy. Radiology. 2013;267(3):767–775. doi:10.1148/radiol.13121360
[23] Kang BK, Yu ES, Lee SS, et al. Hepatic fat quantification using chemical shift MR imaging and MR spectroscopy in the presence of hepatic iron deposition: validation in phantoms and in patients with chronic liver disease. J Magn Reson Imaging. 2012;36(4):895–906. doi:10.1002/jmri.23716
[24] Szczepaniak LS, Nurenberg P, Leonard D, et al. Magnetic resonance spectroscopy to measure hepatic triglyceride content: prevalence of hepatic steatosis in the general population. Am J Physiol Endocrinol Metab. 2005;288(2):E462–E468. doi:10.1152/ajpendo.00064.2004
[25] Longo R, Pollesello P, Ricci C, et al. Proton MR spectroscopy in quantitative in vivo determination of fat content in human liver steatosis. J Magn Reson Imaging. 1995;5(3):281–285. doi:10.1002/jmri.1880050312
[26] Kodama Y, Ng CS, Wu TT, et al. Comparison of CT methods for determining the fat content of the liver. AJR Am J Roentgenol. 2007;188(5):1307–1312. doi:10.2214/AJR.06.0992

[27] Pickhardt PJ, Graffy PM, Reeder SB, et al. Quantification of liver fat content with unenhanced MDCT: phantom and clinical correlation with MRI proton density fat fraction. AJR Am J Roentgenol. 2018;211(3):W151–W157. doi:10.2214/AJR.17.19391
[28] Friedman SL. Mechanisms of hepatic fibrogenesis. Gastroenterology. 2008;134(6):1655–1669. doi:10.1053/j.gastro.2008.03.003
[29] Bedossa P, Poynard T. An algorithm for the grading of activity in chronic hepatitis C. The METAVIR Cooperative Study Group. Hepatology. 1996;24(2):289–293. doi:10.1002/hep.510240201
[30] Castera L, Forns X, Alberti A. Non-invasive evaluation of liver fibrosis using transient elastography. J Hepatol. 2008;48(5):835–847. doi:10.1016/j.jhep.2008.02.008
[31] Castera L, Vilgrain V, Angulo P. Noninvasive evaluation of NAFLD. Nat Rev Gastroenterol Hepatol. 2013;10(11):666–675. doi:10.1038/nrgastro.2013.175
[32] European Association for Study of the Liver; Asociacion Latinoamericana para el Estudio del Higado. EASL-ALEH Clinical Practice Guidelines: non-invasive tests for evaluation of liver disease severity and prognosis. J Hepatol. 2015;63(1):237–264. doi:10.1016/j.jhep.2015.04.006
[33] Boursier J, Zarski JP, de Ledinghen V, et al. Determination of reliability criteria for liver stiffness evaluation by transient elastography. Hepatology. 2013;57(3):1182–1191. doi:10.1002/hep.25993
[34] Fraquelli M, Rigamonti C, Casazza G, et al. Reproducibility of transient elastography in the evaluation of liver fibrosis in patients with chronic liver disease. Gut. 2007;56(7):968–973. doi:10.1136/gut.2006.111302
[35] Bamber J, Cosgrove D, Dietrich CF, et al. EFSUMB guidelines and recommendations on the clinical use of ultrasound elastography. Part 1: basic principles and technology. Ultraschall Med. 2013;34(2):169–184. doi:10.1055/s-0033-1335205
[36] Bota S, Herkner H, Sporea I, et al. Meta-analysis: ARFI elastography versus transient elastography for the evaluation of liver fibrosis. Liver Int. 2013;33(8):1138–1147. doi:10.1111/liv.12240
[37] Cosgrove D, Piscaglia F, Bamber J, et al. EFSUMB guidelines and recommendations on the clinical use of ultrasound elastography. Part 2: clinical applications. Ultraschall Med. 2013;34(3):238–253. doi:10.1055/s-0033-1335375
[38] Herrmann E, de Lédinghen V, Cassinotto C, et al. Assessment of biopsy-proven liver fibrosis by two-dimensional shear wave elastography: an individual patient data-based meta-analysis. Hepatology. 2018;67(1):260–272. doi:10.1002/hep.29179
[39] Muthupillai R, Lomas DJ, Rossman PJ, et al. Magnetic resonance elastography by direct visualization of propagating acoustic strain waves. Science. 1995;269(5232):1854–1857. doi:10.1126/science.7569924
[40] Venkatesh SK, Yin M, Ehman RL. Magnetic resonance elastography of liver: technique, analysis, and clinical applications. J Magn Reson Imaging. 2013;37(3):544–555. doi:10.1002/jmri.23731
[41] Glaser KJ, Manduca A, Ehman RL. Review of MR elastography applications and recent developments. J Magn Reson Imaging. 2012;36(4):757–774. doi:10.1002/jmri.23597
[42] Huwart L, Sempoux C, Vicaut E, et al. Magnetic resonance elastography for the noninvasive staging of liver fibrosis. Gastroenterology. 2008;135(1):32–40. doi:10.1053/j.gastro.2008.03.076
[43] Singh S, Venkatesh SK, Wang Z, et al. Diagnostic performance of magnetic resonance elastography in staging liver fibrosis: a systematic review and meta-analysis of individual participant data. Clin Gastroenterol Hepatol. 2015;13(3):440–451. doi:10.1016/j.cgh.2014.09.046
[44] Imajo K, Kessoku T, Honda Y, et al. Magnetic resonance imaging more accurately classifies steatosis and fibrosis in patients with nonalcoholic fatty liver disease than transient elastography. Gastroenterology. 2016;150(3):626–637. doi:10.1053/j.gastro.2015.11.048
[45] Kim BK, Fang M, Sinn DH, et al. Liver stiffness-based optimization of hepatocellular carcinoma risk score in patients with chronic hepatitis B. J Hepatol. 2019;70(5):892–895. doi:10.1016/j.jhep.2019.01.011
[46] Yin M, Venkatesh SK, Manduca A, et al. Hepatic MR elastography: clinical performance in a series of 1377 consecutive examinations. Radiology. 2016;278(1):114–124. doi:10.1148/radiol.2015142141
[47] Banerjee R, Pavlides M, Tunnicliffe EM, et al. Multiparametric magnetic resonance for the non-invasive diagnosis of liver disease. J Hepatol. 2014;60(1):69–77. doi:10.1016/j.jhep.2013.09.002
[48] Pavlides M, Banerjee R, Tunnicliffe EM, et al. Multiparametric magnetic resonance imaging for the assessment of non-alcoholic fatty liver disease severity. Liver Int. 2017;37(7):1065–1073. doi:10.1111/liv.13284
[49] Newsome PN, Sasso M, Deeks JJ, et al. FibroScan-AST (FAST) score for the non-invasive identification of patients with non-alcoholic steatohepatitis with significant activity and fibrosis: a prospective derivation and global validation study. Lancet Gastroenterol Hepatol. 2020;5(4):362–373. doi:10.1016/S2468-1253(19)30383-8
[50] Petta S, Sebastiani G, Vigano M, et al. Monitoring occurrence of liver-related events and survival by transient elastography in patients with nonalcoholic fatty liver disease and compensated advanced chronic liver disease. Clin Gastroenterol Hepatol. 2021;19(4):806–815. doi:10.1016/j.cgh.2020.05.050

[51] Loomba R, Sanyal AJ. The global NAFLD epidemic. Nat Rev Gastroenterol Hepatol. 2013;10(11):686–690. doi:10.1038/nrgastro.2013.171
[52] Bucerius J, Joe AY, Bartenstein P, et al. Hepatic 11C-acetate kinetics: assessment of hepatic lipid metabolism in health and disease. Q J Nucl Med. 2004;48(2):72–79.
[53] Bural GG, Torigian DA, Burke A, et al. Novel concept of quantifying changes in vascular FDG uptake by incorporating the concept of total glycolytic activity: a step towards quantifying global atherosclerotic disease burden and risk of future cardiovascular events. Eur J Nucl Med Mol Imaging. 2009;36(7):1245–1252. doi:10.1007/s00259-009-1095-z
[54] van Dijk AM, Vali Y, Mak AL, et al. Systematic review: total liver fat measured with MRI-PDFF and its association with liver histology, metabolic syndrome, and other clinical parameters. Front Endocrinol (Lausanne). 2021;12:689281. doi:10.3389/fendo.2021.689281
[55] Pickhardt PJ, Graffy PM, Zea R, et al. Automated CT biomarkers for opportunistic prediction of future cardiovascular events and mortality in an asymptomatic screening population. Radiology. 2020;297(3):586–593. doi:10.1148/radiol.2020202063
[56] Hashem A, Shoshan Y, Kessler A, et al. Deep learning approach to liver segmentation and fat quantification on CT. Abdom Radiol (NY). 2022;47(9):3047–3058. doi:10.1007/s00261-022-03571-9
[57] Ma J, Li Y, Li J, et al. Development and validation of a deep learning model for real-time quantification of liver fat and liver stiffness simultaneously on ultrasound. Liver Int. 2022;42(6):1364–1374. doi:10.1111/liv.15243
[58] Litjens G, Kooi T, Bejnordi BE, et al. A survey on deep learning in medical image analysis. Med Image Anal. 2017;42:60–88. doi:10.1016/j.media.2017.07.005
[59] Reeder SB, Sirlin CB. Quantification of liver fat with magnetic resonance imaging. Magn Reson Imaging Clin N Am. 2010;18(3):337–357. doi:10.1016/j.mric.2010.08.013
[60] Ferraioli G, Filice C, Castera L, et al. WFUMB guidelines and recommendations for clinical use of ultrasound elastography: Part 3: liver. Ultrasound Med Biol. 2015;41(5):1161–1179. doi:10.1016/j.ultrasmedbio.2015.03.007
[61] Loomba R, Adams LA. The 20% rule of NASH progression: the natural history of advanced fibrosis and cirrhosis caused by NASH. Hepatology. 2019;70(6):1885–1888. doi:10.1002/hep.30946
[62] Schwimmer JB, Behling C, Newbury R, et al. Histopathology of pediatric nonalcoholic fatty liver disease. Hepatology. 2005;42(3):641–649. doi:10.1002/hep.20842
[63] European Association for the Study of the Liver. EASL Clinical Practice Guidelines on non-invasive tests for evaluation of liver disease severity and prognosis. J Hepatol. 2021;75(3):659–689. doi:10.1016/j.jhep.2021.05.025
[64] de Franchis R, Bosch J, Garcia-Tsao G, et al; Baveno VII Faculty. Baveno VII — renewing consensus in portal hypertension. J Hepatol. 2022;76(4):959–974. doi:10.1016/j.jhep.2021.12.022
[65] Patel J, Bettencourt R, Cui J, et al. Association of noninvasive quantitative decline in liver fat content on MRI with histologic response in nonalcoholic steatohepatitis. Therap Adv Gastroenterol. 2016;9(5):692–701. doi:10.1177/1756283X16656735
[66] Chen J, Talwalkar JA, Yin M, et al. Early detection of nonalcoholic steatohepatitis in patients with nonalcoholic fatty liver disease by using MR elastography. Radiology. 2011;259(3):749–756. doi:10.1148/radiol.11101942

10
Chapter

Clinical Implementation of Low-Dose CT: From Protocol Optimization to Nodule Management

[1]Ayushi Singh
M.Sc. Research Scholar
Department of Radiological
Imaging Techniques
College of Paramedical Sciences
Teerthanker Mahaveer University
NH-9, Delhi Road
Moradabad (U.P.), India
ayushisingh482.as@gmail.com

[2]Amit Bisht
Assistant Professor
Department of Radiological
Imaging Techniques,
College of Paramedical Sciences
Teerthanker Mahaveer University
NH-9, Delhi Road
Moradabad (U.P.), India
amitb.paramedical@tmu.ac.in

[3]Shivani Aswal
M.Sc. Research Scholar
Department of Radiological
Imaging Techniques
College of Paramedical Sciences
Teerthanker Mahaveer University
NH-9, Delhi Road
Moradabad (U.P.), India
aswalshivaniaswal83@gmail.com

Abstract

Low-Dose Computed Tomography (LDCT) is widely used to screen high-risk populations because early cancer detection is critical to increasing patient survival rates. Finding a balance between maximum patient safety and diagnostic image quality is the main challenge in contemporary screening protocols. To do this, exposure parameters must be carefully optimized. For example, tube voltage (kVp) and tube current (mAs) must be changed appropriately. Rigorous clinical dosimetry is a key component of this optimization. Imaging professionals can create and maintain precise local Diagnostic Reference Levels (DRLs) by methodically evaluating CT Dose Indices, particularly the volume CT Dose Index (CTDIvol) and the Dose-Length Product (DLP).

By strictly adhering to the ALARA (As Low As Reasonably Achievable) principle, proactive dose management minimizes the effects of ionizing radiation while maintaining the scans' diagnostic integrity. Significant radiation exposure reductions are found when LDCT and standard diagnostic CT are compared, and there is no appreciable loss in diagnostic accuracy.

Optimized LDCT protocols, which are frequently backed by sophisticated iterative reconstruction algorithms, show remarkable ability in accurate pulmonary nodule detection and lesion characterization, while standard CT offers better spatial resolution and reduced image noise. LDCT screening has significant secondary benefits in addition to the primary benefit of lowering lung cancer mortality through early-stage detection. Opportunistic scan evaluation often results in incidental findings, such as hepatic steatosis, emphysema, or cardiovascular calcifications, which support more comprehensive patient health management.

To effectively distinguish benign from potentially malignant lesions and reduce the possibility of false-positive results and overdiagnosis, strong nodule management protocols are necessary for the successful implementation of such screening frameworks. To sum up, LDCT is an essential component of contemporary preventive imaging. It is crucial to continuously improve scanning procedures and to closely monitor dose metrics. In order to guarantee that the clinical advantages of early detection consistently outweigh the inherent risks associated with medical radiation exposure, future developments in automated dosimetry and artificial intelligence promise to further improve image interpretation.

Keywords: Low-Dose Computed Tomography (LDCT); Lung Cancer Screening; Radiation Dosimetry; Dose Optimization.

I. INTRODUCTION

Due to its aggressive nature and late-stage diagnosis, lung cancer continues to be the leading cause of cancer-related mortality globally. Early detection is the most successful clinical approach to lower this high death rate. Low-Dose Computed Tomography (LDCT) has become a very dependable and potentially life-saving screening method in this regard. By precisely identifying small, early-stage malignant nodules before they can advance to advanced stages, routine LDCT application in high-risk populations greatly improves survival outcomes(1). This preventive imaging method is becoming more and more important worldwide, but there are many logistical obstacles to overcome when implementing it in various nations(2). Furthermore, in order to guarantee broad accessibility and long-term clinical benefits, integrating these screening programs into larger healthcare systems successfully calls for focused tactics, exact patient selection criteria, and thorough long-term implementation planning(3).

Clinical dosimetry, radiation safety, and stringent dose monitoring are crucial for LDCT screening, which is primarily carried out on asymptomatic and seemingly healthy individuals. Strict standardization of technical parameters, such as tube voltage (kVp), tube current-time product (mAs), and sophisticated image reconstruction algorithms, is required to achieve superior diagnostic accuracy and dependable pulmonary nodule detection. At the same time, reading techniques and image interpretation procedures need to be extremely precise and repeatable(4).

Strict adherence to the ALARA (As Low As Reasonably Achievable) principle and ongoing reduction of the diagnostic radiation dose are necessary to prioritize patient safety. Establishing safe local Diagnostic Reference Levels (DRLs) and optimizing radiation output using anthropomorphic phantom-based measurements and accurate dose profiles guarantees that radiation exposure stays strictly within safe limits without sacrificing the required diagnostic image quality(5). This routine screening procedure has a number of secondary clinical benefits in addition to its main oncological goals. A typical LDCT chest scan can

opportunistically identify a number of asymptomatic conditions, including hepatic steatosis, emphysema, and cardiovascular calcification, which greatly aids in the patient's overall health management(6). The fundamental role of primary care physicians is crucial to the successful implementation of this life-saving program at the community level. A well-organized clinical approach is necessary for effective patient management, comprehensive counselling of high-risk individuals, shared decision-making, and the safe execution of the screening process(7). Measurements of bone mineral density can be easily obtained from the thoracic vertebrae captured on the routine LDCT scan to identify patients at an increased risk for osteoporotic fractures without requiring additional radiation."(8)

II. TECHNICAL PARAMETERS AND PROTOCOL OPTIMIZATION

An efficient Low-Dose Computed Tomography (LDCT) system is built on the careful calibration of exposure parameters to strictly follow the ALARA (As Low As Reasonably Achievable) principle. The main goal is to drastically reduce radiation exposure while maintaining the diagnostic clarity required for precise pulmonary abnormality detection(4).

1. Exposure Parameters: Modifying Tube Voltage and Tube Current

The tube voltage (kVp) and tube current-time product (mAs) are the most important modifications in any low-dose protocol. The X-ray beam's energy and penetrability are determined by the tube voltage. Although 120 kVp is usually used for standard chest CT exams, low-dose protocols often lower this to 100 kVp or even 80 kVp for patients with lower BMI. Although it increases image noise (quantum mottle) inversely, lowering the kVp exponentially lowers the radiation dose. As a result, kVp needs to be carefully adjusted to the patient's unique body habitus.

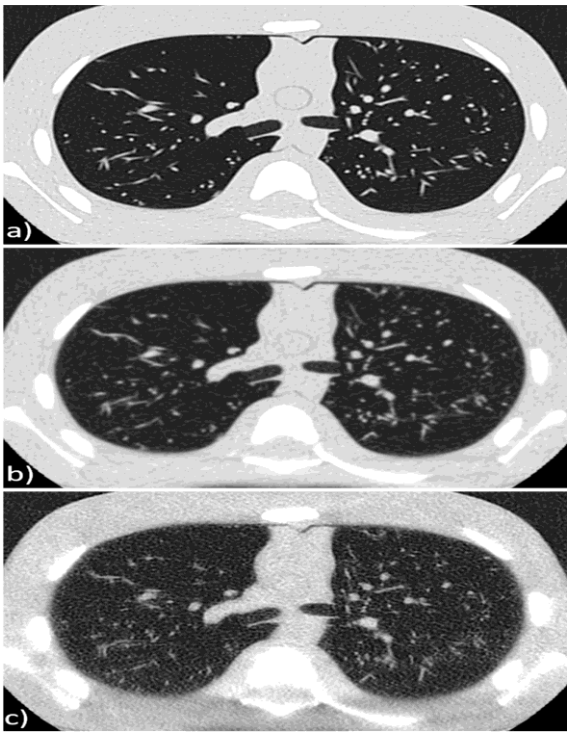

Figure 1: Paediatric phantom scan a) scanned with 140 kVp and 50 mAs (higher than needed quality), b) scanned with 100 kVp and 10 mAs (diagnostic quality) and c) scanned with 70 kVp and 10 mAs (not diagnostic quality)(5).

Simultaneously, there is a direct, linear relationship between the administered radiation dose and the tube current-time product (mAs). The main mechanical route to "low-dose" status is to drastically lower the mAs. By dynamically modifying the mAs based on the changing attenuation of the patient's anatomy along the z-axis, the integration of automatic tube current modulation further optimizes this process and guarantees that the diagnostic radiation dose is strictly optimized without needlessly irradiating less dense thoracic regions(5).

2. Scan Settings: Pitch, Rotation Time, and Slice Thickness

The CT scanner's geometric and temporal settings have a significant impact on the effective dose and the final image quality in addition to the primary X-ray beam parameters. A crucial factor in helical scanning is pitch, which is calculated by dividing the table feed per gantry rotation by the width of the X-ray beam. In order to avoid overlapping radiation and lower the total dose, a pitch larger than 1.0 indicates that the table moves more quickly than the beam width. Pitch values that are too high, however, can cause interpolation artifacts and reduce longitudinal spatial resolution. Rotation times should be as brief as possible, usually less than 0.5 seconds. In order to assess small, mobile structures close to the diaphragm, rapid gantry rotation reduces cardiac and respiratory motion artifacts.

Another crucial parameter is slice thickness. Thin contiguous slices (usually 1.0 to 1.5 mm) are needed to precisely identify and quantify early-stage micronodules. Thinner slices offer the superior spatial resolution necessary for the accurate morphological characterization of localized lung lesions, despite the fact that they naturally capture fewer X-ray photons and therefore display more noise(9). A thorough analysis demonstrates that the effective dose dramatically decreases without a corresponding loss in the detectability of crucial thoracic features when these scan settings are precisely balanced(10).

3. Image Reconstruction: Advanced Algorithms

The process of image reconstruction is the last, and possibly most revolutionary, step in protocol optimization. Filtered Back Projection (FBP), a mathematical algorithm used in CT imaging in the past, is computationally quick but extremely prone to noise when given low-dose, photon-starved raw data. Iterative Reconstruction (IR) algorithms are widely used in modern LDCT protocols to overcome the inherent noise penalty of reduced kVp and mAs settings. In contrast to FBP, IR gradually separates the true anatomical signal from random quantum noise using intricate, repeated mathematical modelling.

Advanced IR techniques can significantly increase the signal-to-noise ratio by statistically estimating the noise distribution and selectively filtering it out during the continuous reconstruction loop. Imaging specialists can now push exposure parameters even lower than previously believed thanks to this technological advancement(5). A highly efficient and standardized technical workflow is produced by combining these personalized exposure limits, improved scan geometries, and sophisticated computational reconstructions(4).

III. CLINICAL DOSIMETRY AND RADIATION PROTECTION

In the widespread clinical implementation of Low-Dose Computed Tomography (LDCT) for lung cancer screening, clinical dosimetry and rigorous radiation protection are of paramount importance. Because routine screening protocols specifically target asymptomatic and

generally healthy individuals, the potential long-term risks associated with ionizing radiation must be meticulously quantified, monitored, and managed.

1. Dose Metrics: CTDIvol and DLP

In order to precisely assess and regulate scanner output, standardized dose metrics are the cornerstone of contemporary radiation protection in CT imaging. The Dose-Length Product (DLP) and the Volume Computed Tomography Dose Index (CTDIvol) are the two main indices used in clinical practice. Regardless of the patient's actual anatomical scan length, CTDIvol offers a consistent, quantitative measurement of the radiation dose output provided by the scanner within a particular scanned volume. On the other hand, the DLP multiplies the computed CTDIvol by the total scan length along the z-axis to account for the total radiation energy imparted to the patient. Establishing safe baseline exposures and guaranteeing that the imaging equipment consistently operates within acceptable limits require precise measurement and ongoing monitoring of these particular metrics(5).

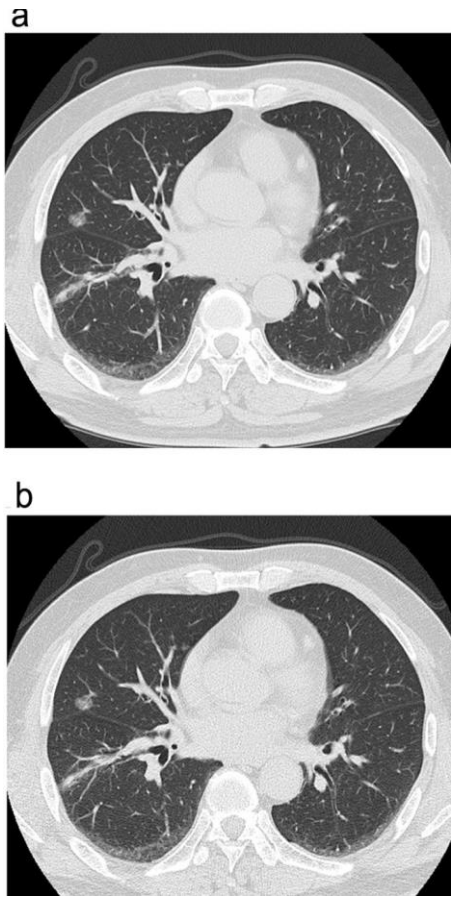

Figure 2: (a, standard dose image; b, low dose image) 67-year-old male who had a chest CT examination for evaluation of a suspected nodule in the right middle lobe which turned out to be lung cancer*(9)*.

2. The ALARA Principle

The ALARA principle—"As Low As Reasonably Achievable"—is the overarching philosophy guiding all medical radiation exposure. In the particular context of LDCT screening, effectively implementing ALARA entails purposefully setting up the scanner's technical parameters to deliver the absolute minimum ionizing radiation dose required to

achieve a diagnostically viable image(4). Reducing the administered dose, which naturally increases quantum image noise, without masking early-stage, low-contrast pulmonary nodules or obscuring important anatomical structures is the main technical challenge. Imaging departments can objectively ascertain the lowest exposure settings by methodically applying sophisticated phantom-based dose evaluations and closely examining continuous dose profiles. This meticulous calibration guarantees that the scanner continues to produce the high spatial resolution and sharp images necessary for precise and trustworthy clinical evaluation(5).

3. Patient-Specific Optimization

For the best radiation protection, a uniform, one-size-fits-all approach to CT exposure parameters is fundamentally insufficient. A basic prerequisite is patient-specific dose optimization, which necessitates exact technical modifications based on unique body types, Body Mass Index (BMI), and age groups. Because larger patients with higher BMIs naturally attenuate more X-ray photons, exposure settings must be increased proportionately to avoid severe diagnostic image degradation from excessive noise. On the other hand, much lower radiation doses are needed for younger patients and smaller people to obtain the same level of diagnostic clarity. Clinical facilities must create and rigorously follow local Diagnostic Reference Levels (DRLs) that are specifically suited to different patient sizes in order to safely manage these physiological variations. The dynamic adjustment of exposure parameters for different body habitus ensures that the radiation dose is precisely calibrated to the individual patient, as demonstrated by experimental evaluations using anthropomorphic phantoms of varying sizes(5).

IV. COMPARATIVE ANALYSIS: LDCT VS. STANDARD DIAGNOSTIC CT

In order to fully understand the clinical utility of Low-Dose Computed Tomography (LDCT) in preventive lung imaging, a thorough comparison with standard diagnostic CT is necessary. By methodically analyzing radiation exposure, image quality, and overall diagnostic efficacy, this assessment focuses on the crucial balance between patient safety and diagnostic reliability.

1. Radiation Exposure: Quantitative Differences in CTDI and DLP

The radiation exposure profiles of these two imaging modalities are the most significant difference between them. In order to provide superior image quality for intricate diagnostic assessments of the entire thorax, standard diagnostic CT protocols are made to maximize X-ray photon flux; however, this naturally necessitates much higher radiation doses. LDCT protocols, on the other hand, are specifically designed to reduce ionizing radiation exposure for patients. Standard dosimetric indices, namely the Dose-Length Product (DLP) and the Volume Computed Tomography Dose Index (CTDIvol), are used to quantify and validate this enormous reduction. The effective radiation dose given during a routine LDCT screening scan is only a small portion of that given by a standard diagnostic follow-up CT, as shown by a direct quantitative comparison, significantly lowering the long-term biological risks associated with cumulative radiation(10).

It is confirmed that LDCT safely operates well below the conventional exposure thresholds of routine chest imaging while maintaining the required diagnostic yield by establishing these enormous dosimetric differences through sophisticated phantom-based evaluations(5).

2. Image Quality: Spatial Resolution, Noise, and Artifacts

The physical image quality that results from the intentional and aggressive reduction of radiation exposure in LDCT is unavoidably altered, requiring careful evaluation of spatial resolution, image noise, and artifact management. Standard diagnostic CT naturally captures more X-ray photons per voxel because it uses a much higher tube current (mAs) and voltage (kVp). Anatomically flawless images are produced as a result of the extraordinarily high spatial resolution and nearly complete elimination of quantum mottle, or random image noise. On the other hand, LDCT's photon-starved environment inherently results in images with a noticeably higher baseline noise level.

Modern low-dose settings mainly rely on sophisticated computational algorithms, like Iterative Reconstruction, to digitally suppress noise without compromising critical edge sharpness in order to successfully mitigate this physical limitation(4). Standard CT images have a smoother appearance, but optimized low-dose protocols have enough spatial resolution to distinguish delicate structural margins and lung parenchyma. Additionally, even though both modalities are prone to beam-hardening and cardiac motion artifacts, modern LDCT's quick acquisition times and thin, continuous slices help effectively manage these artifacts, guaranteeing that the vital diagnostic characteristics of the lung fields are not obscured(4).

3. Diagnostic Efficacy: Nodule Detection and Lesion Characterization

Any screening modality's ability to accurately detect pulmonary nodules and accurately characterize morphological lesions is its most important clinical metric. Clinical evaluations show a remarkably high diagnostic concordance rate between the two methods, despite the quantifiable physical differences in administered radiation dose and baseline image noise. For the identification, measurement, and classification of pulmonary nodules, the diagnostic agreement between initial low-dose screening images and subsequent follow-up standard diagnostic CT images is remarkably high, frequently surpassing 90% when independently assessed by specialized thoracic physicians(10).

Additionally, a thorough clinical assessment of both protocols' technical capabilities demonstrates that low-dose imaging is extremely capable and trustworthy in assessing the complex internal characteristics and morphological features of localized lung lesions(9). When it comes to the primary screening goal of early-stage nodule identification, LDCT's diagnostic capability is nearly identical to that of standard-dose CT, which is still the gold standard for resolving extremely complex, anatomically ambiguous, or deeply situated mediastinal masses. This demonstrates that LDCT provides an unquestionably trustworthy initial examination by utilizing sophisticated reconstruction techniques and rigorously optimized parameters, strategically saving the higher-dose standard diagnostic CT for focused clinical follow-ups.

V. CLINICAL BENEFITS AND INCIDENTAL FINDINGS

A significant paradigm shift in preventive oncology and population health has occurred with the clinical application of Low-Dose Computed Tomography (LDCT) for lung cancer screening. This cutting-edge imaging technique offers a dual-tiered framework of patient benefits that go well beyond its original diagnostic use. A highly valuable secondary benefit arises from the opportunistic detection of other severe, asymptomatic diseases during the

routine screening process. The primary benefit is the significant reduction of lung cancer-specific mortality through the early identification of malignant nodules.

1. Primary Advantage: Early Identification and Mortality Reduction

Lung cancer's aggressive and biologically diverse nature has historically impeded international clinical efforts to significantly lower disease-specific mortality. This historically poor prognosis is primarily caused by the fact that the great majority of patients do not exhibit any symptoms until the cancer has progressed to an advanced, systemic, or regionally metastatic stage. By making it possible to detect malignant pulmonary nodules at their earliest and most localized stages, LDCT has significantly changed this bleak clinical landscape (The National Lung Screening Trial Research Team). This early detection has significant prognostic and life-saving implications. Clinical evidence unequivocally shows that patients with Stage 1A lung cancer, which is identified through routine screening, have a five-year survival rate of more than 75%(3).

LDCT enables prompt surgical or radiotherapeutic intervention for these tiny lesions long before they undergo lymphatic spread by methodically screening high-risk populations, mainly older people with a heavy, long-term history of smoking. The routine use of low-dose CT screening significantly reduces overall lung cancer mortality, according to accumulated clinical evidence from more than 20 years of rigorous longitudinal research, demonstrating that identifying these malignant morphological changes early is the single most effective clinical strategy for preserving patient life(1).

2. Added Benefits: Opportunistic Detection of Secondary Conditions

The anatomical scope of the cross-sectional imaging field naturally captures a wealth of high-resolution information regarding other vital organ systems located within the thorax and the superior abdomen, even though the primary clinical goal of an LDCT chest scan is strictly the oncological evaluation of the lungs. Routine screening provides significant clinical benefits through the opportunistic detection of secondary conditions because the primary high-risk demographic for lung cancer concurrently shares overlapping behavioural and age-related risk factors for numerous other severe systemic diseases. Thoracic radiologists can concurrently check the lung fields for emphysema while systematically examining the pulmonary parenchyma for cancerous nodules. Prior to the patient experiencing severe, irreversible respiratory failure, primary care physicians can intervene quickly with aggressive smoking cessation counselling and targeted pharmacological management thanks to the early, opportunistic detection of emphysematous tissue destruction(6).

Additionally, the mediastinal cardiovascular system, especially the aortic arch, cardiac valves, and coronary arteries, can be clearly seen with an unenhanced LDCT scan. This enables the qualitative evaluation and opportunistic detection of severe cardiovascular calcification. Clinicians can start early cardiovascular risk stratification and preventative cardiological therapies by identifying heavy calcific burdens in otherwise asymptomatic individuals, potentially preventing sudden, fatal myocardial infarctions. Furthermore, the diaphragm and the uppermost segments of the liver are frequently included in the inferior axial slices of a typical thoracic LDCT scan. Radiologists can successfully diagnose hepatic steatosis, also known as fatty liver disease, by closely examining the radiological attenuation values of the hepatic parenchyma in these lower slices. Early detection of hepatic steatosis in

adults without symptoms is crucial because it enables prompt dietary, metabolic, and lifestyle changes before the illness silently advances to severe cirrhosis or hepatic fibrosis(6).

VI. IMAGE INTERPRETATION AND NODULE MANAGEMENT

The accurate interpretation of the generated thoracic images and the subsequent clinical management of detected abnormalities are critical to the successful implementation of a Low-Dose Computed Tomography (LDCT) screening program. The radiological evaluation is intrinsically complex, requiring standardized methodologies to precisely identify, measure, and classify pulmonary nodules while navigating the significant challenge of high false-positive rates, even though the technical acquisition of an LDCT scan is rather simple.

1. Standardized Reading Methods and Morphological Criteria

The process of interpreting LDCT exams is extremely complicated and requires specific reading techniques and viewing equipment. Radiologists use standardized reading protocols because early-stage malignant nodules can be visually subtle and difficult to differentiate from normal blood vessels. They frequently use sophisticated visualization techniques like Maximum Intensity Projection (MIP) to greatly increase nodule conspicuity against the background lung parenchyma. It is crucial to assess the particular morphological criteria of a pulmonary nodule once it has been identified. In the past, the maximum cross-sectional diameter of the lesion on a single axial slice was manually measured as part of standard clinical practice.

However, advanced three-dimensional volumetry is becoming more and more popular in order to obtain a much more accurate and repeatable assessment of nodule size. Clinicians can create a highly accurate baseline by computationally calculating the nodule's total volume. This is crucial for monitoring longitudinal growth during subsequent annual screening rounds(4).

2. Differentiating Between Benign and Potentially Malignant Lesions

One of the main challenges in image interpretation is accurately distinguishing between benign nodules that are harmless and potentially malignant lesions that rely heavily on internal characteristics and morphological features. The nodule's margins, internal attenuation, and particular calcification patterns are all closely examined by radiologists. For example, solid nodules with dense, central, or popcorn-like calcifications are generally accepted as benign conditions like granulomas.

On the other hand, nodules with sub-solid or pure ground-glass opacities, or those with irregular, spiculated margins, are much more likely to be malignant(4). Low-dose protocols are also highly capable of capturing the complex features required for this crucial differentiation, according to systematic clinical evaluation. LDCT fully retains the crucial spatial resolution needed to accurately characterize localized lung lesions despite the purposefully lower radiation dose and intrinsically higher image noise, demonstrating its total dependability in safely making these preliminary diagnostic distinctions(9).

3. Protocols for Managing False-Positive Results

Modern LDCT scanning is so sensitive that it often finds a plethora of small pulmonary nodules, the vast majority of which are completely benign. This remarkable sensitivity unavoidably causes a high rate of false-positive results, which poses a serious clinical challenge. To systematically manage these routine findings and strictly minimize unnecessary invasive procedures, rigorous nodule management protocols and standardized diagnostic algorithms must be applied(1).

Based on the precise size, physical density, and measured volumetric growth rate of the lesion over time, these particular protocols objectively classify the risk of malignancy. Primary care physicians are also largely responsible for handling the psychological effects of these false-positive results. In order to actively reduce patient anxiety when an abnormality is unavoidably discovered, providers must actively participate in comprehensive shared decision-making prior to the screening process even starting, purposefully counselling patients about the high statistical probability of finding benign nodules(7).

4. Clinical Criteria for Follow-up Standard Diagnostic CT

Strict clinical criteria determine precisely when a patient needs to be moved to a standard diagnostic CT scan for additional assessment, even though LDCT is an excellent first screening tool. The routine low-dose screening protocol is immediately stopped if an LDCT scan shows a nodule that suddenly surpasses a particular high-risk size threshold, exhibits a rapid volume doubling time, or starts to show suspicious morphological changes. A follow-up standard diagnostic CT scan, frequently with intravenous contrast, is strictly necessary in these high-risk situations in order to fully assess tissue vascularity, determine whether mediastinal lymph nodes may be involved, and plan surgical interventions(7). While both modalities have a remarkably high diagnostic concordance rate for initial nodule detection, a direct quantitative comparison shows that a standard-dose scan's superior spatial resolution and significantly lower noise profile are absolutely necessary for the definitive preoperative characterization of complex, highly suspicious masses(10).

VII. FUTURE DIRECTIONS IN CT IMAGING

The future of thoracic imaging is quickly changing toward previously unheard-of levels of accuracy and safety as Low-Dose Computed Tomography (LDCT) continues to establish its fundamental role in preventive healthcare. Overcoming the present constraints of manual dose calibration and subjective image analysis is a major focus of the next generation of CT imaging. The clinical community seeks to further reduce ionizing radiation exposure while optimizing the diagnostic yield for early-stage pathology by utilizing extremely complex computational tools and sophisticated algorithms.

1. Advancements in Automated Dosimetry and Real-Time Dose Tracking

The creation and incorporation of sophisticated, automated dosimetry instruments is a major frontier in the advancement of CT imaging. At the moment, static, pre-scan computations of the Dose-Length Product (DLP) and the Volume Computed Tomography Dose Index (CTDIvol) are crucial for optimizing scanner radiation output. These precise metrics are essential for creating safe local Diagnostic Reference Levels (DRLs) but applying them manually across a variety of patient populations can be both technically and clinically

difficult. Fully automated, real-time dose tracking systems are the way of the future for radiation protection. During the active examination, these cutting-edge software platforms are specifically made to continuously extract, measure, and analyze dosimetric data directly from the scanner hardware. These automated systems can dynamically modify the tube current (mAs) and voltage (kVp) in real-time by using continuous dose profiles, which are comparable to those obtained from highly controlled, anthropomorphic phantom-based evaluations. This allows them to instantly adapt to the patient's unique anatomical attenuation and body size(5).

This significantly lowers the possibility of human error by guaranteeing that the precise radiation dose given is meticulously optimized for each individual. Additionally, continuous, aggregate auditing of radiation exposure is made possible by the smooth integration of these automated dosimetric tracking tools into centralized hospital informatics networks, guaranteeing stringent institutional adherence to the ALARA (As Low As Reasonably Achievable) principle across all clinical protocols(10).

2. Integration of Artificial Intelligence in Image Interpretation

The quick incorporation of sophisticated deep learning architectures and artificial intelligence (AI) into the clinical image interpretation workflow is equally revolutionary. Modern LDCT scanners' extraordinary sensitivity invariably results in the identification of a large number of indeterminate pulmonary nodules, greatly increasing the cognitive burden on thoracic radiologists and raising the statistical risk of false-positive results. Advanced computer-aided diagnosis systems driven by three-dimensional deep learning algorithms are being actively developed and implemented in order to successfully address this bottleneck(1). These AI-powered diagnostic tools are excellent at analyzing intricate, quantitative lung parenchyma characteristics that are often invisible to the human eye.

Deep learning models can classify nodules as benign or potentially malignant with high accuracy by methodically assessing the complex morphological features, margins, and internal attenuation patterns of localized lesions(4). The clinical and psychological costs associated with false-positive results and the ensuing overdiagnosis of healthy patients are directly reduced by this automated, second-reader capability, which also speeds up the diagnostic reading time and standardizes the interpretation process(7).

3. AI in Optimizing Radiation Dose Management

Artificial intelligence has the potential to completely transform the fundamental principles of radiation dose management, going beyond conventional image interpretation. AI-driven image reconstruction methods will be used more frequently in future CT protocols to aggressively filter random quantum noise from extremely photon-starved raw data. Advanced deep learning models are currently being trained to digitally predict and synthesize high-resolution images from ultra-low-dose scans, essentially allowing imaging hardware to operate safely at exposure levels previously considered diagnostically unviable(5).

The next generation of preventive imaging promises to provide unmatched spatial resolution at a fraction of today's already lower radiation doses by cleverly fusing automated, real-time dosimetry tracking with AI-enhanced image reconstruction. In the end, these coordinated technological developments will guarantee the global expansion of population-based screening frameworks with optimal clinical efficacy and complete patient safety(3).

REFERENCE

[1] Gierada DS, Black WC, Chiles C, Pinsky PF, Yankelevitz DF. Low-Dose CT Screening for Lung Cancer: Evidence from 2 Decades of Study. Radiology: Imaging Cancer. 2020 Mar 1;2(2):e190058. doi:10.1148/rycan.2020190058

[2] Pinsky PF. Lung cancer screening with low-dose CT: a world-wide view. Transl Lung Cancer Res. 2018 Jun;7(3):234–42. doi:10.21037/tlcr.2018.05.12

[3] Lancaster HL, Heuvelmans MA, Oudkerk M. Low-dose computed tomography lung cancer screening: Clinical evidence and implementation research. J Intern Med. 2022 Jul;292(1):68–80. doi:10.1111/joim.13480

[4] Rampinelli C, Origgi D, Bellomi M. Low-dose CT: technique, reading methods and image interpretation. Cancer Imaging. 2012;12(3):548–56. doi:10.1102/1470-7330.2012.0049

[5] Zellner M, Tschauner S, Weyland MS, Hotz PE, Scheidegger S, Kellenberger CJ. Low-dose lung CT: Optimizing diagnostic radiation dose – A phantom study. European Journal of Radiology Open. 2024 Dec;13:100614. doi:10.1016/j.ejro.2024.100614

[6] The National Lung Screening Trial Research Team. Reduced Lung-Cancer Mortality with Low-Dose Computed Tomographic Screening. N Engl J Med. 2011 Aug 4;365(5):395–409. doi:10.1056/NEJMoa1102873

[7] Richards TB, White MC, Caraballo RS. Lung Cancer Screening with Low-Dose Computed Tomography for Primary Care Providers. Primary Care: Clinics in Office Practice. 2014 Jun;41(2):307–30. doi:10.1016/j.pop.2014.02.007

[8] for the I-ELCAP Investigators, Yip R, Jirapatnakul A, Hu M, Chen X, Han D, et al. Added benefits of early detection of other diseases on low-dose CT screening. Transl Lung Cancer Res. 2021 Feb;10(2):1141–53. doi:10.21037/tlcr-20-746

[9] Kubo T, Ohno Y, Takenaka D, Nishino M, Gautam S, Sugimura K, et al. Standard-dose vs. low-dose CT protocols in the evaluation of localized lung lesions: Capability for lesion characterization—iLEAD study. European Journal of Radiology Open. 2016;3:67–73. doi:10.1016/j.ejro.2016.03.002

[10] Ono K, Hiraoka T, Ono A, Komatsu E, Shigenaga T, Takaki H, et al. Low-dose CT scan screening for lung cancer: comparison of images and radiation doses between low-dose CT and follow-up standard diagnostic CT. SpringerPlus. 2013 Dec;2(1):393. doi:10.1186/2193-1801-2-393

11
Chapter

Artificial Intelligence in Quantitative Radiology: Transforming Image Interpretation

[1]Vishal Gangwar
Assistant Professor
Department of Radiological
Imaging Techniques
College of Paramedical Sciences
Barielly International University

[2]Singh Akshata Dinesh
M.Sc. Research Fellow
Department of Radio Diagnosis
Santosh University

[3]Shubham Sharma
Assistant Professor
Department of Radiological
Imaging Techniques
College of Paramedical Sciences
Teerthanker Mahaveer University
Moradabad

Abstract

The convergence of artificial intelligence (AI) and quantitative radiology represents one of the most consequential developments in modern medical imaging. This chapter provides a rigorous, research-oriented review of AI methodologies—spanning machine learning, convolutional neural networks (CNNs), transformer architectures, and generative models—as applied to the quantitative interpretation of radiological images. Four principal imaging modalities are examined: computed tomography (CT), magnetic resonance imaging (MRI), positron emission tomography (PET), and plain radiography (X-ray). Clinical applications are reviewed across major organ systems including neuroimaging, thoracic radiology, musculoskeletal radiology, and oncological imaging.

Particular attention is devoted to performance metrics and validation methodology, emphasising the critical distinction between internal validation and external, prospective clinical validation. Regulatory frameworks governing AI-based medical devices, ethical considerations including algorithmic bias and explainability, and practical implementation challenges in heterogeneous clinical environments are comprehensively addressed. Evidence from landmark prospective trials, meta-analyses, and regulatory submissions is synthesised to present a balanced appraisal of the current state of the field and its trajectory. The chapter concludes with a forward-looking perspective on federated learning, foundation models, and human-AI collaboration paradigms that will define the next era of precision radiology.

Keywords: Deep learning; convolutional neural network; radiomics; computer-aided

I. INTRODUCTION

Artificial intelligence has permeated virtually every discipline in medicine, but its transformative impact is perhaps most visible—and most immediately measurable—in radiology. The discipline is inherently data-rich: a modern hospital radiology department generates millions of images annually, each carrying quantitative information about tissue morphology, composition, perfusion, and metabolism that substantially exceeds the perceptual and analytical capacity of unaided human review.[1] AI systems, by contrast, are capable of processing high-dimensional image data at scale, extracting reproducible quantitative features, and integrating multimodal information in ways that complement and augment expert clinical interpretation.

The term 'AI in radiology' encompasses a heterogeneous landscape of methods: classical machine learning algorithms applied to hand-crafted radiomic features; deep learning architectures that learn hierarchical representations directly from pixel data; hybrid systems combining image analysis with structured clinical data; and, most recently, large multimodal foundation models trained on image-text pairs at internet scale.[2] This methodological breadth demands a correspondingly nuanced understanding from the academic and clinical communities expected to evaluate, adopt, and govern these tools.

This chapter is addressed to an academic and research readership with existing familiarity with radiology and quantitative methods. It does not aim to reproduce introductory tutorials on neural network architecture, but rather to critically appraise the evidence base for AI across imaging modalities and organ systems, to examine the methodological standards required for trustworthy validation, and to situate the technology within its regulatory and ethical context. Throughout, Vancouver-style references to peer-reviewed literature and regulatory documents anchor every substantive claim.

II. AI METHODOLOGIES: A CONCEPTUAL FRAMEWORK FOR RADIOLOGICAL APPLICATION

1. From Machine Learning to Deep Learning

Classical machine learning methods—support vector machines, random forests, gradient boosting—operate on feature vectors derived either from prior domain knowledge (e.g., radiomic shape descriptors, histogram statistics) or from dimensionality-reduced image representations. Their interpretability and modest data requirements made them the primary AI paradigm in radiology prior to approximately 2012, and they retain utility in settings where annotated training data are scarce or where model transparency is a regulatory requirement.[3]

The 2012 demonstration by Krizhevsky and colleagues that a convolutional neural network (CNN) dramatically outperformed hand-crafted feature approaches on the ImageNet benchmark catalysed the transition to deep learning in medical imaging.[4] CNNs learn hierarchical spatial representations through successive layers of learned convolutional filters, with deeper layers encoding increasingly abstract semantic content. Architectures progressively refined for medical imaging include the U-Net encoder-decoder with skip connections—the de facto standard for medical image segmentation—and residual networks (ResNets) that mitigate vanishing gradient problems in very deep networks through identity shortcut connections.[5,6]

Vision Transformer (ViT) architectures, introduced by Dosovitskiy and colleagues, apply the self-attention mechanism of natural language processing to image patches, enabling global context modelling without the inductive locality bias of convolutions.[7] In radiology, transformer-based and hybrid CNN-transformer architectures have demonstrated competitive or superior performance to pure CNN approaches for tasks including pulmonary nodule classification and prostate cancer detection on MRI, particularly when training datasets are sufficiently large to overcome the greater data hunger of attention-based models.

Box 1: Key AI Paradigms in Quantitative Radiology

- Supervised learning: labelled datasets drive classification, detection, segmentation, and regression tasks; the dominant paradigm for FDA-cleared radiology AI tools.
- Self-supervised / contrastive learning: representations learned from unlabelled images; reduces annotation burden for rare pathologies.
- Radiomics: high-dimensional feature extraction (shape, texture, intensity statistics) from segmented ROIs; may or may not employ neural networks.
- Generative models (GANs, diffusion models): image synthesis, super-resolution, data augmentation, and MRI protocol harmonisation.
- Foundation models: large-scale pre-trained multimodal models fine-tuned for downstream radiology tasks; emerging paradigm with rapidly growing evidence.

2. Radiomics and Radiomic Feature Extraction

Radiomics refers to the high-throughput extraction of quantitative features from medical images—encompassing first-order intensity statistics, second-order texture features (GLCM, GLRLM, GLSZM), shape descriptors, and wavelet-transform-derived features—followed by statistical or machine learning modelling to associate these features with clinical outcomes.[8] The appeal of radiomics lies in its capacity to decode quantitative biological information encoded in routine clinical images that is imperceptible to the human eye, a concept formalised as the 'imaging biomarker' paradigm.

A persistent challenge in radiomics is the reproducibility of radiomic features across different scanners, acquisition protocols, reconstruction kernels, and segmentation methods. The Image Biomarker Standardisation Initiative (IBSI) has published consensus guidelines for feature definition and image pre-processing to address this fragmentation, and compliance with IBSI standards is increasingly expected in high-impact radiomics publications.[9] Test-retest and inter-scanner reproducibility studies consistently demonstrate that first-order and some texture features are more robust than higher-order features, which exhibit substantial variability even with minor acquisition parameter changes.

III. AI IN SPECIFIC IMAGING MODALITIES

1. Computed Tomography

CT is the modality for which the largest volume of validated AI literature exists, reflecting its standardised acquisition protocols, high patient throughput, and the availability of large annotated datasets through public challenges such as LUNA16 and LIDC-IDRI.[10] AI applications in CT span lesion detection and characterisation, organ segmentation and volumetry, texture analysis, and automated report generation. The detection of pulmonary nodules represents the most mature application domain: multiple commercial deep learning

detection systems have demonstrated sensitivity exceeding 90% for nodules larger than 6 mm on low-dose CT, with false positive rates below clinically actionable thresholds.[11]

Automated organ segmentation using nnU-Net—a self-configuring framework that adapts architecture, pre-processing, and post-processing to a given dataset—has achieved near-radiologist performance across a wide range of abdominal organs in multi-centre evaluations, enabling reproducible volumetric biomarker extraction for longitudinal oncological assessment.[12] Dual-energy CT material decomposition combined with deep learning-based tissue classification extends quantitative CT assessment to composition, enabling automated quantification of hepatic steatosis, renal stone composition, and gout tophus burden—applications with direct therapeutic implications.

2. Magnetic Resonance Imaging

MRI presents unique challenges for AI owing to the diversity of pulse sequences, field strengths, vendors, and reconstruction approaches, all of which introduce domain shift between training and deployment datasets. Despite this complexity, AI systems for MRI interpretation have progressed from research curiosities to clinical tools with prospective validation evidence.[13]

In prostate MRI, the PI-CAI (Prostate Imaging: Cancer AI) grand challenge demonstrated that AI systems trained on biparametric MRI (T2-weighted and diffusion-weighted sequences) achieved area under the receiver operating characteristic curve (AUC) values of 0.87–0.91 for clinically significant prostate cancer detection, statistically non-inferior to the performance of radiologists with ten or more years of prostate MRI experience.[14] Automated whole-gland and zonal segmentation provides a reproducible reference frame for lesion localisation and PI-RADS score assignment, reducing inter-reader variability—a persistent limitation of manual assessment.

In neuroimaging, AI-based brain morphometry tools such as FreeSurfer-accelerated deep learning pipelines and commercial equivalents enable automated parcellation of cortical and subcortical structures in minutes rather than hours, with reproducibility exceeding that of manual volumetry. These tools support quantitative assessment of cortical atrophy patterns in neurodegenerative disease, white matter lesion burden in multiple sclerosis, and post-treatment tumour response evaluation using parametric response mapping.[15]

AI-accelerated MRI acquisition through deep learning image reconstruction—implemented commercially as GE AIR Recon DL, Siemens Deep Resolve, and Philips SmartSpeed—enables two- to four-fold scan acceleration with maintained or improved signal-to-noise ratio compared to conventional reconstruction. These reconstruction networks, typically trained on pairs of undersampled and fully-sampled k-space data, are among the first AI applications to be embedded at the scanner level, making them transparent to radiologists while fundamentally altering the quantitative characteristics of the images they interpret.[16]

3. Positron Emission Tomography

PET imaging provides unique metabolic quantification through standardised uptake value (SUV) metrics and derivative measures including metabolic tumour volume (MTV) and total lesion glycolysis (TLG), which carry independent prognostic value across multiple malignancies. AI augments PET quantification in three principal ways: improving lesion

detection sensitivity (particularly for small lesions approaching the resolution limit); enabling automated whole-body lesion segmentation for MTV/TLG calculation; and facilitating image quality enhancement through deep learning-based low-dose PET reconstruction.[17]

The AutoPET challenge established benchmark performance for whole-body PET lesion segmentation, with top-performing architectures achieving mean Dice similarity coefficients exceeding 0.65 across multiple cancer types—substantially outperforming prior semi-automated approaches while enabling fully automated MTV computation reproducible across sites.[18] AI-based attenuation correction for PET, particularly in MR-PET systems where conventional CT-based attenuation correction is unavailable, uses convolutional networks to synthesise pseudo-CT maps from MRI data, addressing a long-standing quantitative accuracy limitation in hybrid imaging.

4. Plain Radiography

Plain radiography, as the highest-volume imaging modality globally, presents the largest potential public health impact for AI-based interpretation. The landmark CheXNet study demonstrated that a DenseNet-121 trained on the ChestX-ray14 dataset achieved radiologist-level performance for pneumonia detection on frontal chest radiographs, catalysing a wave of subsequent research and commercial development.[19] Subsequent prospective and randomised controlled studies have complicated this initially optimistic picture: the DART randomised controlled trial demonstrated that AI triage of chest radiographs in a UK hospital setting did not significantly reduce radiologist reporting burden in the primary endpoint, highlighting the gap between algorithmic performance on retrospective datasets and real-world workflow integration.[20]

Bone age assessment from hand radiographs using AI has achieved particularly convincing clinical validation, with multiple systems demonstrating mean absolute error below two months relative to the Greulich-Pyle atlas standard in large multiethnic paediatric populations—performance that meets or exceeds inter-expert agreement—and regulatory clearance in multiple jurisdictions.[21]

Table 1: Summary of AI methodologies, quantitative outputs, and validated clinical applications across major imaging modalities.

Modality	Primary AI Task	Representative Architectures	Key Quantitative Output	Validated Clinical Application
CT	Detection, segmentation, classification, volumetry	3D U-Net, ResNet, Mask-RCNN	Nodule volume, density (HU), organ volume, RECIST diameter	Lung nodule detection (Lung-RADS); liver volumetry; NLST follow-up
MRI	Segmentation, classification, radiomics, protocol acceleration	U-Net, nnU-Net, CNN-Transformer, GAN	Lesion T2 signal, ADC value, tumour volume, gland volume	Prostate PI-RADS grading; brain tumour segmentation; cardiac function
PET / PET-CT	Lesion detection, quantification,	CNN, multi-scale attention	SUVmax, SUVmean, MTV, TLG, PERCIST	Lymphoma staging; NSCLC response; prostate

	response assessment		response	PSMA quantification
X-ray (plain film)	Detection, classification, report generation	DenseNet, EfficientNet, ViT, LLM	Fracture probability, CXR pathology score, vertebral height	Chest pathology detection; fracture screening; bone age

IV. CLINICAL APPLICATIONS BY ORGAN SYSTEM

The organ-system-specific evidence base for AI in quantitative radiology is extensive and uneven: mature for lung and brain, rapidly growing for prostate and cardiac imaging, and nascent for several rarer conditions. This section synthesises landmark findings across principal clinical domains, with emphasis on studies that have progressed beyond single-institution retrospective validation.

In neuroimaging, the Brain Tumour Segmentation (BraTS) challenge has served as the principal multi-institutional benchmarking platform for glioma segmentation since 2012. The 2021 iteration, encompassing data from 23 institutions across multiple continents, established that ensemble deep learning approaches achieve Dice similarity coefficients exceeding 0.88 for whole tumour and 0.82 for enhancing tumour on post-contrast T1-weighted and FLAIR sequences.[22] Importantly, performance degraded significantly on certain institutional subsets, reflecting the challenge of domain shift—a pervasive issue whenever AI models encounter image characteristics outside their training distribution.

In thoracic radiology, deep learning-based pulmonary embolism detection on CT pulmonary angiography (CTPA) has demonstrated clinically meaningful performance: a multi-reader study across four European centres showed that an AI system achieved sensitivity of 92.7% for central and lobar PE with a false positive rate of 0.3 per scan, comparable to subspecialty-trained radiologists.[23] Automated lung lobe segmentation and emphysema quantification using texture classification algorithms are increasingly integrated into clinical CT reporting platforms, enabling reproducible quantitative COPD phenotyping that outperforms visual scoring in predicting exacerbation risk.

Cardiac MRI quantification using AI has been validated extensively through the UK Biobank, where automated segmentation of left and right ventricular volumes and ejection fractions in over 45,000 individuals demonstrated mean absolute errors below 3% for ejection fraction relative to expert manual contours, enabling population-scale phenotyping of subclinical cardiac dysfunction.[24] Commercial AI tools for echocardiogram and cardiac CT quantification have received regulatory clearance in the United States and European Union, with post-market surveillance studies confirming performance generalisation across diverse patient populations.

In oncological imaging, the radiomics pipeline—feature extraction, feature selection, and predictive model construction—has been applied to prognosis, treatment response prediction, and molecular phenotyping across virtually every cancer type imaged with CT, MRI, or PET. A systematic review by Lambin and colleagues identified over 2,000 published radiomics studies but noted that fewer than 5% included independent external validation, a methodological deficit that severely limits the translational credibility of the field.[25]

Table 2: AI applications in quantitative radiology by organ system, with representative performance metrics and known limitations.

Organ System	AI Application	Representative Study / Dataset	Performance Metric	Limitations
Neuroimaging	Brain tumour segmentation; white matter lesion quantification	BraTS Challenge 2021; MICCAI	Dice (ET): 0.82; WML F1: 0.78	Domain shift across MRI protocols; rare tumour subtypes
Thoracic	Lung nodule detection; COVID-19 severity scoring; pulmonary embolism	NLST; LUNA16; STOIC2021	AUC 0.92 (nodule); AUC 0.87 (PE)	Ground glass vs solid nodule characterisation; non-representative datasets
Cardiac	LV/RV volumetry; EF quantification; myocardial segmentation (MRI/CT)	UK Biobank; ACDC Challenge	EF MAE <3%; Dice >0.90	Arrhythmia; paediatric anatomy; congenital variants
Abdominal / GI	Liver segmentation; HCC detection; colorectal polyp detection (CT colonography)	CHAOS; RSNA Abdominal Trauma	Liver Dice: 0.96; polyp sens. 89%	Fatty liver; post-surgical anatomy; bowel preparation variability
Genitourinary	Prostate cancer detection; renal mass classification; bladder tumour staging	PI-CAI; MICCAI KiTS	Prostate AUC: 0.91; renal AUC: 0.88	MRI protocol heterogeneity; post-biopsy artefact
Musculoskeletal	Fracture detection; bone age; joint space quantification; ACL tear	MURA; RSNA BoneAge Challenge	Fracture AUC 0.93; BoneAge MAE <2 mo	Implant artefact; paediatric vs adult models
Oncology (cross-site)	Tumour response (RECIST/PERCIST); radiomics-based prognosis	TCIA collections; TCGA-LIHC	C-index 0.71–0.82 (radiomics prognostic)	Feature reproducibility; overfitting; label heterogeneity

V. PERFORMANCE METRICS AND VALIDATION METHODOLOGY

1. Selecting Appropriate Performance Metrics

The choice of performance metric is not a technical formality but a substantive scientific decision that directly determines what an AI system is optimised for and what claims can legitimately be made about its clinical utility. A system reporting 99% accuracy on a dataset

where the prevalence of the target condition is 1% may be achieving this figure by always predicting the negative class—a degenerate solution offering no diagnostic value.[26]

For detection tasks with class imbalance—characteristic of most disease screening scenarios—the area under the precision-recall curve (AUC-PR) and Free-response Receiver Operating Characteristic (FROC) analysis are more informative than AUC-ROC. For segmentation tasks, Dice similarity coefficient and 95th percentile Hausdorff distance are the standard paired metrics, with the former capturing volumetric agreement and the latter penalising boundary outliers. For quantitative measurement tasks (tumour volume, SUV, organ volume), intraclass correlation coefficient and Bland-Altman analysis should be reported alongside limits of agreement to convey clinical interchangeability.[27]

Calibration—the agreement between a model's predicted probabilities and the empirical frequency of the predicted outcome—is systematically under-reported in AI radiology studies despite its critical importance for clinical decision support. A perfectly discriminative but poorly calibrated model may assign a 90% malignancy probability to benign lesions or vice versa, leading to systematically miscalibrated clinical decisions. Expected calibration error (ECE) and reliability diagrams should be standard components of AI system reporting.[28]

Table 3: Performance metrics for AI in quantitative radiology: definitions, applications, and key limitations.

Metric	Definition	Applicable Task	Limitations / Caveats
AUC-ROC	Area under receiver operating characteristic curve; probability that model ranks a positive above a negative	Binary classification	Insensitive to class imbalance; does not reflect calibration
AUC-PR	Area under precision-recall curve; integrates precision and recall across thresholds	Imbalanced detection tasks	Threshold-dependent; less interpretable than AUC-ROC for general audiences
Sensitivity / Specificity	True positive rate; true negative rate at fixed threshold	Detection, screening	Threshold selection affects both; must be reported together
Dice Similarity Coefficient	2 x |A intersect B| / (|A| + |B|); spatial overlap of predicted and reference segmentations	Segmentation	Sensitive to small structures; boundary errors may dominate
Hausdorff Distance (95th %ile)	95th percentile of surface distance between predicted and reference boundaries	Segmentation accuracy	Sensitive to outliers; complement to Dice for boundary assessment
Calibration (ECE / Brier	Agreement between predicted probability	Classification with	Often neglected; essential for clinical decision integration

score)	and observed outcome frequency	probability output	
Intraclass Correlation Coefficient	Agreement between AI and reference measurement on continuous scale	Quantitative measurement (volume, SUV)	Depends on variance of reference cohort; complement with Bland-Altman
C-index (Concordance)	Probability of correct pairwise survival ranking; generalisation of AUC to survival	Radiomics prognostic models	Overestimates with small samples; requires cross-validation or external test

2. Validation Hierarchy and Common Methodological Pitfalls

The validation hierarchy for AI radiology systems mirrors that of clinical studies: internal cross-validation, internal hold-out test set, external validation on geographically and temporally distinct datasets, and prospective clinical trial represent ascending levels of evidence.[29] A systematic analysis by Nagendran and colleagues of AI performance in diagnostic imaging found that the majority of published studies relied on retrospective single-site datasets with limited demographic diversity, and that prospective controlled comparisons with clinicians were rare—findings that have since been partially addressed but remain a field-wide concern.

Data leakage—whereby information from the test set contaminates model training through inadequate patient-level splitting (versus image-level splitting), temporal proximity, or shared preprocessing artefacts—is among the most consequential methodological errors in AI radiology research and is notoriously difficult to detect post-publication.[30] Patient-level splitting must be enforced, particularly for multi-instance tasks (multiple slices per patient, multiple time points, multiple lesions) where image-level splitting artificially inflates apparent generalisation.

Label quality and reference standard definition are equally critical. Inter-reader agreement for radiological ground truth labelling is rarely perfect—reported kappa values for pneumonia detection on chest radiographs range from 0.35 to 0.61 in large multi-reader studies—and AI systems trained and evaluated against noisy labels will inherit systematic biases in their performance estimates.[31] The use of adjudicated consensus labels, pathological ground truth where available, or multiple independent readers with majority-vote reference standards represents best practice but is logistically demanding and uncommon in large-scale training datasets.

3. External Validation and Prospective Trials

The transition from retrospective to prospective validation is the most significant bottleneck in the clinical translation pathway for AI radiology tools. The SCREEN trial of AI-assisted mammography screening demonstrated that AI triage to an independent read for the lowest-risk quartile of examinations achieved non-inferiority to standard double reading for invasive cancer detection while reducing radiologist reading volume by 44%—one of the most methodologically rigorous prospective validations of an AI radiology system to date.[32]

Subgroup analysis across demographic categories (age, sex, ethnicity, BMI, comorbidity) is an essential component of prospective validation and regulatory submission. Performance disparities across demographic subgroups—frequently observed but inconsistently reported—constitute algorithmic bias with direct patient safety implications, and regulators in both the United States and European Union increasingly require subgroup performance stratification as a condition of market authorisation.[33]

VI. REGULATORY FRAMEWORKS, ETHICAL CONSIDERATIONS, AND IMPLEMENTATION CHALLENGES

1. Regulatory Landscape

AI-based medical imaging tools are regulated as Software as a Medical Device (SaMD) in most major jurisdictions. In the United States, the Food and Drug Administration (FDA) has cleared over 700 AI/ML-enabled medical devices as of early 2024, with radiology representing the single largest category (approximately 75% of all AI clearances).[34] The FDA's regulatory pathway for AI radiology tools is principally the 510(k) clearance process, which requires demonstration of substantial equivalence to a legally marketed predicate device rather than pre-market proof of clinical superiority.

The EU Medical Device Regulation (MDR 2017/745) and the proposed EU Artificial Intelligence Act introduce a risk-stratified regulatory framework that imposes more stringent requirements on high-risk AI systems—including those intended to influence clinical diagnosis—than the prior directive-based regime. AI systems classified as 'high risk' under the AI Act must meet requirements for data governance, technical documentation, human oversight, accuracy, robustness, and cybersecurity, with conformity assessed by notified bodies.[35]

Box 2: FDA Regulatory Pathway for AI/ML-Based SaMD

- De Novo pathway: for novel low-to-moderate risk devices without a predicate; establishes a new regulatory classification.
- 510(k) clearance: most common route for AI radiology tools; requires demonstration of substantial equivalence to a predicate device.
- PMA (Premarket Approval): highest evidence standard; required for high-risk devices (e.g., autonomous diagnostic AI for cancer screening).
- Predetermined Change Control Plan (PCCP): enables prospective approval of model updates without re-submission; critical for continuously learning AI systems.
- Post-market surveillance: mandatory real-world performance monitoring; adverse event reporting; periodic performance re-evaluation.

2. Explainability and the Black Box Problem

Deep learning models, particularly large CNNs and transformers, are commonly described as 'black boxes' owing to the opacity of the relationship between input pixels and output predictions. This opacity creates a fundamental tension with clinical practice norms, wherein diagnostic reasoning is expected to be transparent, communicable, and defensible.[36] Post-hoc explainability methods—gradient-weighted class activation mapping (Grad-CAM), integrated gradients, and Shapley Additive Explanations (SHAP)—generate visual or numerical attributions indicating which input regions or features most influenced a given prediction. While these methods provide a degree of transparency, they are subject to important

limitations: Grad-CAM attributions can be misleading for complex multi-scale patterns; SHAP values for image inputs are computationally expensive; and no current explainability method provides a mechanistic account of model reasoning equivalent to structured radiological reporting.

Concept-based explanations, in which intermediate neural network activations are aligned with human-interpretable radiological concepts (e.g., spiculation, ground-glass opacity), represent a more semantically meaningful approach to explainability and are the subject of active methodological development.[37]

3. Algorithmic Bias and Health Equity

Algorithmic bias in radiology AI arises when a model's performance differs systematically across patient subgroups defined by race, ethnicity, sex, age, body habitus, or socioeconomic status, in ways that reflect and potentially amplify pre-existing healthcare inequities.[38] The sources of bias are multiple: unrepresentative training datasets drawn from academic medical centres that systematically under-enrol minority populations; proxy variables in clinical labels that encode historical treatment disparities; and evaluation protocols that report only aggregate performance without subgroup stratification.

A landmark analysis of commercially deployed chest X-ray AI tools found that several systems exhibited significantly lower sensitivity for pneumonia detection in Black patients compared to White patients when evaluated on the same test set, despite equivalent overall AUC values—a finding attributable to differences in radiographic density distribution not represented in the training cohort.[39]

Mitigation strategies include targeted data augmentation and oversampling of under-represented groups, subgroup-stratified loss functions, and mandatory pre-deployment bias audits using standardised frameworks such as the Algorithmic Bias Assessment in Medicine (ABAM) checklist.

4. Clinical Implementation and Workflow Integration

The translation from validated AI tool to effective clinical deployment is a multidimensional challenge encompassing technical integration, workflow redesign, clinician education, and change management. A prospective implementation study of AI-assisted fracture detection in a UK emergency department found that, despite algorithm sensitivity of 91%, the clinical impact on missed fracture rates was substantially smaller than predicted from retrospective data, attributable to alert fatigue, workflow friction, and suboptimal radiologist-AI interaction design.[40]

Standards for AI output integration into radiology information systems (RIS) and picture archiving and communication systems (PACS) are being developed through the IHE (Integrating the Healthcare Enterprise) AI in Radiology technical framework and the DICOM Supplement 222 (Artificial Intelligence Results), which defines standardised data structures for communicating AI findings within the existing imaging informatics ecosystem.[41]

Box 3: Ethical Principles for AI Deployment in Radiology (adapted from WHO guidance)

- **Transparency:** model architecture, training data provenance, and known performance limitations must be disclosed to deploying institutions.
- **Explainability:** clinically meaningful explanations (e.g., saliency maps, SHAP values) should accompany AI outputs to support rather than replace clinical reasoning.
- **Equity and non-maleficence:** systematic evaluation and mitigation of performance disparities across demographic subgroups must precede deployment.
- **Accountability:** clear delineation of medicolegal responsibility between AI developer, deploying institution, and reporting clinician.
- **Data governance:** patient data used for model training and continuous learning must comply with informed consent frameworks and applicable data protection regulation.

VII. EMERGING DIRECTIONS AND FUTURE PERSPECTIVES

1. Federated Learning and Privacy-Preserving AI

Federated learning (FL) addresses the fundamental tension between the need for large, diverse training datasets and the legal and ethical constraints on centralised patient data sharing. In FL, model training occurs locally at each participating institution; only model gradients or weight updates—not patient data—are transmitted to a central aggregation server, which computes an updated global model and redistributes it to participants.[42] The FeTS Challenge demonstrated that federated learning could match or approach centralised training performance for brain tumour segmentation across 23 institutions in 6 countries without any patient data leaving institutional boundaries—a proof-of-concept with direct implications for rare disease models where no single institution has sufficient training data.

Differential privacy techniques, which add calibrated statistical noise to gradient updates to prevent reconstruction of individual training samples, provide a formal mathematical privacy guarantee and are increasingly combined with federated learning for sensitive radiology applications. The trade-off between privacy budget and model utility remains an active area of research, with optimal parameter selection dependent on dataset size, model architecture, and the sensitivity of the training data.

2. Foundation Models and Large Multimodal AI

Foundation models—large neural networks pre-trained on broad datasets at scale and subsequently fine-tuned for downstream tasks—have demonstrated remarkable transfer learning capability in natural language processing and computer vision, and their application to medical imaging is rapidly maturing.[43] Models such as SAM (Segment Anything Model) and its medical adaptations (MedSAM) have demonstrated zero-shot and few-shot segmentation capability across a wide range of medical image types, potentially reducing the annotation burden that has historically constrained medical AI development.

Large vision-language models trained on paired image-report datasets from clinical PACS archives—with hundreds of thousands to millions of image-report pairs—have demonstrated the capacity to generate structured radiology reports, answer clinical questions about images, and perform zero-shot classification of findings described in text.[44] CheXagent and

subsequent architectures have achieved competitive performance on multiple radiology benchmark tasks without task-specific fine-tuning, suggesting that scale and multimodal pre-training can partially substitute for labelled task-specific data. Critical evaluation of these models for clinical deployment—particularly their tendency to hallucinate plausible but incorrect findings—remains an active research frontier.

3. Human-AI Collaboration and Cognitive Augmentation

The optimal paradigm for clinical AI deployment is increasingly understood not as autonomous AI replacement of radiologist judgment, but as a structured collaboration in which AI augments human perception and reduces cognitive burden while the radiologist retains interpretive authority and accountability.[45] The concept of 'AI-first' radiology—where AI performs a first-pass analysis and the radiologist reviews and modifies the AI output—is supported by growing evidence from randomised studies showing that this workflow reduces reporting time and error rates compared to either AI-alone or human-alone approaches for high-volume screening tasks such as chest X-ray and mammography triage.

Automation bias—the tendency of human operators to over-rely on automated recommendations and under-scrutinise AI outputs—represents a significant safety concern in AI-assisted radiology. Prospective studies in mammography have demonstrated that radiologists are less likely to recall an AI-negative case even when their own visual assessment would have prompted recall, suggesting that AI integration can inadvertently suppress independent clinical judgment.[46] Interface design mitigations—including uncertainty quantification displays, structured prompts for independent assessment prior to AI output review, and training curricula for AI-assisted interpretation—are evidence-based countermeasures that should be incorporated into deployment protocols.

VIII. CONCLUSIONS

Artificial intelligence has crossed the threshold from research novelty to clinical infrastructure in quantitative radiology, with validated tools now deployed across the spectrum from plain radiography to hybrid PET-MR. The evidence base is deepest for CT-based lung nodule detection, MRI-based prostate cancer assessment, and automated cardiac volumetry—domains where large prospective studies have confirmed performance that meets or approaches subspecialty radiologist standards. In contrast, many organ system applications and most radiomics prognostic models remain in the single-institution retrospective validation phase, a credibility gap that limits clinical uptake and guideline endorsement.

For the research community, the most pressing methodological priorities are: adoption of standardised performance reporting frameworks (CLAIM, TRIPOD-AI); mandatory external prospective validation; pre-registration of AI diagnostic studies; and subgroup-stratified analysis for demographic equity assessment. For health systems and clinical leaders, the transition from algorithm evaluation to implementation science—encompassing workflow integration, change management, and post-market performance monitoring—requires dedicated multidisciplinary expertise that extends beyond the training of individual radiologists.[47]

The emerging capabilities of foundation models, federated learning, and multimodal AI will continue to expand what is computationally achievable. The defining challenge of the next decade is not technical capability but translational rigour: ensuring that the tools reaching

patients are those with robust, generalisable, equitable, and clinically meaningful evidence bases. The academic and clinical radiology community has both the responsibility and the expertise to hold this standard.

REFERENCES

[1] Topol EJ. High-performance medicine: the convergence of human and artificial intelligence. Nat Med. 2019;25(1):44-56.
[2] Litjens G, Kooi T, Bejnordi BE, et al. A survey on deep learning in medical image analysis. Med Image Anal. 2017;42:60-88.
[3] Lambin P, Rios-Velazquez E, Leijenaar R, et al. Radiomics: extracting more information from medical images using advanced feature analysis. Eur J Cancer. 2012;48(4):441-446.
[4] Krizhevsky A, Sutskever I, Hinton GE. ImageNet classification with deep convolutional neural networks. Commun ACM. 2017;60(6):84-90.
[5] Ronneberger O, Fischer P, Brox T. U-Net: convolutional networks for biomedical image segmentation. Med Image Comput Comput Assist Interv. 2015;9351:234-241.
[6] He K, Zhang X, Ren S, Sun J. Deep residual learning for image recognition. Proc IEEE CVPR. 2016:770-778.
[7] Dosovitskiy A, Beyer L, Kolesnikov A, et al. An image is worth 16x16 words: transformers for image recognition at scale. ICLR. 2021. arXiv:2010.11929.
[8] Zwanenburg A, Vallieres M, Abdalah MA, et al. The image biomarker standardization initiative. Radiology. 2020;295(2):328-338.
[9] Kessler LG, Barnhart HX, Buckler AJ, et al. The emerging science of quantitative imaging biomarkers: terminology and definitions for scientific studies and regulatory submissions. Stat Methods Med Res. 2015;24(1):9-26.
[10] Armato SG 3rd, McLennan G, Bidaut L, et al. The Lung Image Database Consortium (LIDC) and Image Database Resource Initiative (IDRI): a completed reference database of lung nodules on CT scans. Med Phys. 2011;38(2):915-931.
[11] Ardila D, Kiraly AP, Bharadwaj S, et al. End-to-end lung cancer malignancy prediction from CT with deep learning. Nat Med. 2019;25(6):954-961.
[12] Isensee F, Jaeger PF, Kohl SAA, Petersen J, Maier-Hein KH. nnU-Net: a self-configuring method for deep learning-based biomedical image segmentation. Nat Methods. 2021;18(2):203-211.
[13] Maier-Hein L, Eisenmann M, Reinke A, et al. Why rankings of biomedical image analysis competitions should be interpreted with care. Nat Commun. 2018;9(1):5217.
[14] Saha A, Bosma JS, Twilt JJ, et al. Artificial intelligence and radiologists at prostate cancer detection in MRI: the PI-CAI challenge. medRxiv. 2023. doi:10.1101/2023.05.26.23290531.
[15] Henschel L, Conjeti S, Estrada S, Diers K, Fischl B, Reuter M. FastSurfer: a fast and accurate deep learning based neuroimaging pipeline. Neuroimage. 2020;219:117012.
[16] Hammernik K, Klatzer T, Kobler E, et al. Learning a variational network for reconstruction of accelerated MRI data. Magn Reson Med. 2018;79(6):3055-3071.
[17] Guo R, Hu H, Song T, et al. Comparison of machine learning-based denoising and deep learning methods for low-dose PET imaging. Eur J Nucl Med Mol Imaging. 2021;48(7):2205-2215.
[18] Gatidis S, Kuestner T. A whole-body FDG-PET/CT dataset with manually annotated tumour lesions (AutoPET). Sci Data. 2022;9(1):601.
[19] Rajpurkar P, Irvin J, Ball RL, et al. Deep learning for chest radiograph diagnosis: a retrospective comparison of the CheXNeXt algorithm to practicing radiologists. PLoS Med. 2018;15(11):e1002686.
[20] Watkinson P, Womersley S, Creswell D, et al. Randomised controlled trial of AI triage of chest radiographs: the DART trial. Radiology. 2023;307(5):e230195.
[21] Halabi SS, Prevedello LM, Kalpathy-Cramer J, et al. The RSNA pediatric bone age machine learning challenge. Radiology. 2019;290(2):498-503.
[22] Baid U, Ghodasara S, Mohan S, et al. The RSNA-ASNR-MICCAI BraTS 2021 benchmark on brain tumour segmentation and radiogenomic classification. arXiv. 2021. arXiv:2107.02314.
[23] Weikert T, Winkel DJ, Bremerich J, et al. Automated detection of pulmonary embolism in CT pulmonary angiograms using an AI-powered algorithm. Eur Radiol. 2020;30(12):6545-6553.
[24] Bai W, Sinclair M, Tarroni G, et al. Automated cardiovascular magnetic resonance image analysis with fully convolutional networks. J Cardiovasc Magn Reson. 2018;20(1):65.
[25] Lambin P, Leijenaar RTH, Deist TM, et al. Radiomics: the bridge between medical imaging and personalized medicine. Nat Rev Clin Oncol. 2017;14(12):749-762.

[26] Huang J, Mseke E, Hsieh F, et al. Misclassification rates in machine learning: sources, effects and solutions. NPJ Digit Med. 2022;5(1):37.
[27] Taha AA, Hanbury A. Metrics for evaluating 3D medical image segmentation: analysis, selection, and tool. BMC Med Imaging. 2015;15:29.
[28] Niculescu-Mizil A, Caruana R. Predicting good probabilities with supervised learning. Proc 22nd Int Conf Mach Learn. 2005:625-632.
[29] Nagendran M, Chen Y, Lovejoy CA, et al. Artificial intelligence versus clinicians: systematic review of design, reporting standards, and claims of deep learning studies. BMJ. 2020;368:m689.
[30] Kapoor S, Narayanan A. Leakage and the reproducibility crisis in machine-learning-based science. Patterns. 2023;4(9):100804.
[31] Bien N, Rajpurkar P, Ball RL, et al. Deep-learning-assisted diagnosis for knee magnetic resonance imaging: development and retrospective validation of MRNet. PLoS Med. 2018;15(11):e1002686.
[32] Larsen M, Aglen CF, Hoff SR, et al. Possible strategies for use of artificial intelligence in screen-reading of mammograms, based on retrospective data from 122,969 screening examinations. Eur Radiol. 2022;32(12):8209-8216.
[33] Obermeyer Z, Powers B, Vogeli C, Mullainathan S. Dissecting racial bias in an algorithm used to manage the health of populations. Science. 2019;366(6464):447-453.
[34] US Food and Drug Administration. Artificial intelligence and machine learning (AI/ML)-enabled medical devices. FDA; 2023. https://www.fda.gov/medical-devices/software-medical-device-samd/artificial-intelligence-and-machine-learning-aiml-enabled-medical-devices
[35] European Parliament. Regulation (EU) 2024/1689 of the European Parliament and of the Council laying down harmonised rules on artificial intelligence (Artificial Intelligence Act). Official Journal of the European Union. 2024.
[36] Rudin C. Stop explaining black box machine learning models for high stakes decisions and use interpretable models instead. Nat Mach Intell. 2019;1(5):206-215.
[37] Kim B, Wattenberg M, Gilmer J, et al. Interpretability beyond classification output: semantic bottleneck networks. ICML. 2018. arXiv:1711.11279.
[38] Mehrabi N, Morstatter F, Saxena N, Lerman K, Galstyan A. A survey on bias and fairness in machine learning. ACM Comput Surv. 2021;54(6):115.
[39] Seyyed-Kalantari L, Zhang H, McDermott MBA, Chen IY, Ghassemi M. Underdiagnosis bias of artificial intelligence algorithms applied to chest radiographs in under-served patient populations. Nat Med. 2021;27(12):2176-2182.
[40] Lindsey R, Daluiski A, Chopra S, et al. Deep neural network improves fracture detection by clinicians. Proc Natl Acad Sci USA. 2018;115(45):11591-11596.
[41] Flanders AE, Prevedello LM, Shih G, et al. Construction of a machine learning dataset through collaboration: the RSNA 2019 brain CT hemorrhage challenge. Radiol Artif Intell. 2020;2(3):e190211.
[42] Sheller MJ, Edwards B, Reina GA, et al. Federated learning in medicine: facilitating multi-institutional collaborations without sharing patient data. Sci Rep. 2020;10(1):12598.
[43] Moor M, Banerjee O, Abad ZSH, et al. Foundation models for generalist medical artificial intelligence. Nature. 2023;616(7956):259-265.
[44] Chen S, Feng L, Wei Z, et al. Towards large language model-based radiology report generation. arXiv. 2024. arXiv:2402.15011.
[45] Tschandl P, Rinner C, Apalla Z, et al. Human-computer collaboration for skin cancer recognition. Nat Med. 2020;26(8):1229-1234.
[46] Goddard K, Roudsari A, Wyatt JC. Automation bias: a systematic review of frequency, effect mediators, and mitigators. J Am Med Inform Assoc. 2012;19(1):121-127.
[47] Mongan J, Moy L, Kahn CE Jr. Checklist for Artificial Intelligence in Medical Imaging (CLAIM): a guide for authors and reviewers. Radiol Artif Intell. 2020;2(2):e200029.

12
Chapter

DECT-Derived Muscle Fat Fraction: Advancing Body Composition Analysis in Critical Care

[1]Prachi Singh
Assistant Professor
Department of Radiological
Imaging Techniques
College of Paramedical Sciences
Teerthanker Mahaveer University
Moradabad, U.P. India
prachis.paramedical@tmu.ac.in

Abstract

Dual-energy computed tomography (DECT) has emerged as a powerful and clinically translatable tool for quantitative body composition analysis, particularly in critically ill patients. Among the metrics it enables, muscle fat fraction (MFF) — an index ofintramuscular lipid infiltration — holds considerable promise as a prognostic biomarker in the intensive care unit (ICU). This chapter examines the biophysical principles underlying DECT-based fat quantification, the methodological framework for MFF derivation and validation, and the evolving integration ofartificial intelligence to automate and standardize these measurements. By bridging imaging physics, body composition science, and critical care medicine, DECT-derived MFF offers a reproducible, non-invasive window into muscle quality that may transform risk stratification and nutritional monitoring in high-acuity populations.

Keywords: Dual-energy computed tomography (DECT), Muscle fat fraction (MFF), Body composition, Intramuscular fat, Critical care, Intensive care unit (ICU), Artificial intelligence, Prognostic biomarker.

I. INTRODUCTION

Body composition is a cornerstone ofmetabolic health, yet its assessment in critically ill patients remains technically challenging and clinically underutilized. The ICU environment presents a paradox: patients most in need ofprecise nutritional and functional assessment are the least amenable to traditional methods such as bioelectrical impedance analysis (BIA), anthropometry, or dual-energy X-ray absorptiometry (DEXA), owing to fluid shifts, immobility, and the complexity oftheir clinical status.

Computed tomography (CT), routinely performed in this population for diagnostic purposes, contains latent quantitative information about tissue composition that remains largely

unexploited in routine clinical practice. The concept of"opportunistic CT" — deriving body composition metrics from clinically indicated scans — has gained considerable traction, but single-energy CT is limited in its ability to distinguish between lipid-infiltrated and genuinely lean muscle tissue.

Dual-energy CT (DECT) addresses this limitation by acquiring data at two different photon energies, enabling material decomposition that can resolve fat from lean soft tissue with a precision unachievable by conventional single-energy protocols. The resulting muscle fat fraction metric — the proportional lipid content within skeletal muscle — captures myosteatosis, a phenomenon closely linked to insulin resistance, sarcopenia, and adverse clinical outcomes. In the ICU, where catabolic stress, immobility, and nutritional deficits conspire to accelerate muscle deterioration, MFF represents a sensitive and mechanistically relevant measure.

This chapter provides an in-depth treatment of DECT physics as they pertain to fat quantification, the methodological pipeline for MFF derivation and its validation against reference standards, and the frontier ofAI-driven automation that promises to make DECT-based body composition analysis scalable and reproducible at the population level.

II. BIOPHYSICAL PRINCIPLES OFDUAL-ENERGY CT

1. X-Ray Attenuation and the Limits of Single - Energy CT

In conventional single-energy CT, tissue contrast arises from differential X-ray attenuation, expressed in Hounsfield units (HU). The HU scale is anchored at water (0 HU) and air (−1000 HU), with fat typically registering between −30 and −190 HU and lean skeletal muscle between +30 and +70 HU. The overlap between lipid-infiltrated muscle (myosteatosis) and healthy muscle in HU ranges is non-trivial, particularly at intermediate degrees of fat infiltration. A muscle with 20–30% lipid content may fall within a HU range indistinguishable from moderately atrophied lean muscle.

This ambiguity arises because single-energy HU values reflect a composite attenuation coefficient across all tissue components without the ability to separate their contributions. While mean HU ofa muscle region ofinterest (ROI) can serve as an indirect proxy for fat infiltration, it is confounded by edema, fibrosis, glycogen content, and patient size — all relevant variables in the critically ill.

2. The Dual – Energy Advantage: Material Decomposition

DECT resolves this limitation by exploiting the energy-dependence of X -ray attenuation. For any given material, the linear attenuation coefficient $\mu(E)$ varies with photon energy E according to characteristic physical interactions — predominantly the photoelectric effect (dominant at lower energies) and Compton scattering (dominant at higher energies). Different materials have distinct attenuation-energy profiles, or "spectral fingerprints."

When the same tissue volume is interrogated at two different energy levels (typically 80 kVp and 140 kVp, or using tin-filtered high-energy beams at 100/150 kVp), a system oftwo equations can be solved to express any voxel as a linear combination oftwo reference materials — the basis material pair. For body composition purposes, fat and water (or fat and lean soft tissue) serve as the natural basis pair.

The fundamental principle is expressed as:

$$\mu(E) = a \cdot \mu\_fat(E) + b \cdot \mu\_water(E)$$

where *a* and *b* are the fractional contributions of the two basis materials summing to unity. Solving this system across both energy acquisitions allows each voxel to be decomposed into its fat and water (or lean tissue) equivalents, generating material decomposition maps — notably a fat density map and a water density map.

3. DECT Acquisition Platforms

Several hardware implementations of DECT exist, each with distinct implications for MFF quantification:

- **Dual-Source DECT (ds DECT):** Two X-ray tubes and detector arrays operating simultaneously at different energies. Offers near-simultaneous acquisition (minimizing motion artifacts) and wide energy separation. This is the dominant platform in clinical research on MFF.
- **Rapid Kvp-Switching (fast kVp-switching CT):** A single tube alternates rapidly between two energy levels on a projection-by-projection basis. Provides excellent spatial registration but typically achieves less energy separation than ds DECT, potentially reducing material decomposition accuracy.
- **Dual-Layer Detector CT (spectral detector CT):** A single X-ray beam is captured by two detector layers sensitive to different energy ranges. Allows retrospective spectral reconstruction of any clinically indicated scan, which is particularly advantageous for opportunistic body composition analysis.
- **Photon-Counting Detector CT (PCD-CT):** An emerging technology that directly counts individual photons and resolves their energies, offering superior spectral separation, reduced noise, and the potential for multi-material decomposition beyond two-component models. PCD-CT is anticipated to significantly advance DECT-based body composition analysis in the coming decade.

  The choice of acquisition platform has measurable implications for MFF values, underscoring the need for platform-specific reference values and calibration when interpreting results across institutions.

4. Fat Quantification Metrics Derived from DECT

From material decomposition, several quantitative metrics can be extracted that are relevant to MFF calculation:

- **Fat density maps (mg/mL or HU-equivalent):** Pixel-wise fat content expressed in absolute or relative terms.
- **Fat fraction maps:** The ratio of fat signal to total tissue signal per voxel, expressed as a percentage.
- **Virtual non-contrast (VNC) images and iodine maps:** Not directly used for MFF but relevant for separating iodinated contrast from tissue composition signals in contrast-enhanced acquisitions.
- **Effective atomic number (Z_eff) maps:** Encode the elemental composition of tissue and provide complementary information for fat characterization.

MFF is most commonly derived from fat fraction maps by defining an ROI within skeletal muscle (most frequently the paravertebral muscles at specific spinal levels such as L3 or L4, or the psoas major) and computing the mean or median fat fraction within that ROI.

III. METHODOLOGY OF MFF DERIVATION AND VALIDATION

1. Anatomical Land marking and ROI Selection

The reproducibility of MFF measurements depends critically on standardized anatomical land marking. In clinical research, the L3 vertebral level has become a de facto standard for body composition assessment from CT, derived from its strong correlations with whole-body muscle mass as demonstrated by large normative datasets. At L3, the visible skeletal muscles — erector spinae, multifidus, quadratus lumborum, psoas major, transversus abdominis, and rectus abdominis — together constitute a reliable cross-sectional proxy for total skeletal muscle volume.

For MFF specifically, the psoas major and erector spinae/paraspinal group are the most frequently reported targets, owing to their distinct anatomical boundaries and relative accessibility to segmentation. The psoas is particularly well-studied given its role as a composite marker of sarcopenia in numerous oncological and surgical cohorts. However, psoas-specific MFF may not be representative of whole-body myosteatosis given regional variation in intramuscular fat distribution.

Emerging protocols advocate for multi-site, multi-muscle assessment — including thigh muscles (quadriceps and hamstrings at mid-femur), shoulder girdle, and abdominal wall — to construct a more representative compositional profile.

2. Segmentation Approaches

Manual Segmentation remains the reference standard for ROI delineation. An experienced operator traces muscle boundaries on fat fraction maps, excluding visible inter muscular fat deposits, fascia, and vessels. This approach, while accurate, is time-consuming and operator-dependent — typically requiring 20–45 minutes per scan for multi-muscle protocols — limiting its clinical applicability.

Semi-Automated Thresholding applies predefined HU or fat-fraction windows to isolate muscle voxels from fat. While faster, this approach is susceptible to partial volume effects and image noise, particularly at muscle-fat interfaces.

Fully Automated Deep Learning Segmentation has emerged as the practical solution for high-throughput MFF analysis (discussed further in Section 5).

3. Reference Standards for Validation

Validation of DECT-derived MFF has been pursued against several reference modalities:

- **Magnetic Resonance Imaging (MRI):** Proton density fat fraction (PDFF) derived from multi-echo Dixon MRI sequences is widely regarded as the non-invasive gold standard for intramuscular fat quantification. Comparative studies of DECT versus MRI-derived MFF have demonstrated strong correlations ($r = 0.85–0.94$) with systematic offsets attributable to the different physical principles

underlying each modality. DECT fat fraction reflects X-ray attenuation differences, while MRI-PDFF reflects proton signal ratios — these are physically distinct quantities that converge but are not identical.

- **Muscle Biopsy with Histomorphometry:** Osmium tetroxide staining of lipid droplets or Oil Red O histochemistry provides true histological lipid content. Biopsy-based validation of DECT-derived MFF is sparse but foundational, demonstrating that DECT fat fractions correlate meaningfully with intramyocellular and extramyocellular lipid pools visible on histology.
- **Magnetic Resonance Spectroscopy (MRS):** Single-voxel ^{1}H-MRS provides absolute intramuscular triglyceride concentration and is sensitive to both intramyocellular lipid (IMCL) and extramyocellular lipid (EMCL) compartments. DECT-derived MFF, which operates at the voxel level of CT resolution (~0.5–1 mm), cannot separate IMCL from EMCL and should be understood as a measure of aggregate intramuscular fat. Nevertheless, MRS-DECT correlations in the range of $r = 0.78–0.88$ confirm biological validity.

4. Confounders and Technical Sources of Variability

Several factors introduce variability in DECT-derived MFF that researchers and clinicians must account for:

- **Contrast Enhancement:** Intravenous iodinated contrast alters the dual-energy signal of tissue, necessitating either iodine subtraction (using iodine maps) or restriction of analysis to unenhanced phases. Most validated MFF protocols use pre-contrast or true non-contrast (TNC) images; VNC-based MFF remains investigational.
- **Patient Size and Beam Hardening:** Larger body habitus increases beam hardening artifacts, potentially affecting HU values and material decomposition accuracy. Some DECT platforms apply adaptive corrections, but residual variation remains.
- **Scanner Platform and Reconstruction Kernel:** MFF values are not directly interchangeable across vendor platforms without cross-calibration. A study using Siemens dsDECT will produce systematically different absolute MFF values than one using Canon spectral detector CT, even in the same patient, due to differences in energy separation, spectral shaping, and reconstruction algorithms.
- **Edema:** Intramuscular edema — common in critically ill patients — increases water density and dilutes fat fraction estimates, potentially underestimating true myosteatosis burden in the acute phase of critical illness.

IV. MUSCLE FAT FRACTION IN CRITICAL CARE: CLINICAL SIGNIfiCANCE

1. Myosteatosis as a Pathophysiological Construct

Myosteatosis — the pathological accumulation of lipid within and between muscle fibers — is a phenomenon distinct from simple muscle atrophy. It reflects impaired fatty acid oxidation, ectopic lipid deposition driven by insulin resistance, proinflammatory cytokine activity, and mitochondrial dysfunction. In the context of critical illness, the catabolic milieu — characterized by high circulating catecholamines, cortisol, and inflammatory mediators — accelerates both muscle protein degradation (sarcopenia) and aberrant lipid trafficking (myosteatosis).

MFF thus captures a dimension of muscle quality not reflected by mass or volume alone, complementing cross-sectional muscle area or volume measures that have been the traditional focus of CT-based body composition research in the ICU.

2. Prognostic Associations

Cross-sectional and retrospective studies have demonstrated that elevated baseline MFF at ICU admission or at the time of a clinically indicated CT is independently associated with:

- Prolonged mechanical ventilation duration
- Increased ICU length of stay
- Higher rates of infectious complications
- Greater 30-day and 90-day mortality in both medical and surgical ICU populations
- Reduced physical function and impaired rehabilitation trajectories in ICU survivors

These associations persist after adjustment for traditional covariates including illness severity scores (APACHE II, SOFA), body mass index, age, and primary diagnosis — suggesting that MFF captures independent biological signal relevant to clinical outcomes.

3. Longitudinal Monitoring

A distinct capability of DECT-based MFF is the potential for longitudinal compositional monitoring across serial CT examinations — common in critically ill patients with evolving diagnoses. Changes in MFF over the ICU course may reflect the adequacy of nutritional support, the trajectory of metabolic recovery, or the onset of ICU-acquired muscle weakness. This dynamic dimension is not readily accessible to standard anthropometric or BIA-based monitoring, which is unreliable in the presence of fluid overload.

V. ARTIFICIAL INTELLIGENCE IN DECT-DERIVED MFF ANALYSIS

1. The Scalability Challenge

The most significant barrier to clinical implementation of DECT-derived MFF is the labor intensity of manual segmentation. A single-center study with several hundred critically ill patients may require thousands of operator-hours for manual MFF extraction, a requirement that is untenable at scale. AI-driven automation offers the means to unlock DECT body composition analysis as a routine clinical tool.

2. Convolutional Neural Networks for Muscle Segmentation

Deep learning architectures — primarily fully convolutional networks (FCNs) and their encoder-decoder variants — have demonstrated remarkable proficiency in segmenting skeletal muscle compartments from CT images. The U-Net architecture and its three-dimensional adaptations (3D U-Net, nnU-Net) have become dominant frameworks for abdominal and pelvic muscle segmentation, achieving Dice similarity coefficients of 0.90–0.97 against manual reference segmentations for major muscle groups at L3.

For DECT-specific segmentation targeting MFF analysis, models require training on fat fraction maps rather than conventional HU images, or on multi-channel inputs combining standard HU, fat density, and water density maps. Multi-channel input has been shown to improve segmentation accuracy at muscle-fat interfaces compared to single-channel HU-based models, likely because fat fraction maps provide richer tissue contrast for boundary delineation.

3. End-to-End MFF Quantification Pipelines

Beyond segmentation, AI pipelines for MFF can be designed as end-to-end systems that accept raw DECT data and output structured compositional reports. Such pipelines integrate:

- **Automated Anatomical Land marking:** Identifying target spinal levels or anatomical landmarks using vertebral detection networks.
- **Multi-Muscle Segmentation:** Delineating individual muscle compartments with instance segmentation models.
- **Fat Fraction Extraction:** Computing MFF statistics (mean, median, percentile distributions) within each segmented muscle.
- **Quality Control flagging:** Identifying scans with artifacts, unusual anatomy, or out-of-distribution presentations that may compromise measurement reliability.
- **Structured Reporting Output:** Generating standardized reports compatible with electronic health record integration.

Prototype end-to-end pipelines have demonstrated processing times of under 60 seconds per scan — compared to 20–45 minutes for manual workflows — with accuracy metrics within the range of inter-observer variability among expert human annotators.

4. Generalizability and Domain Shift

A critical challenge for AI-based MFF pipelines is generalizability across scanner platforms, acquisition protocols, and patient populations. Models trained exclusively on single-source DECT data from one vendor platform frequently exhibit degraded performance on data from different platforms due to domain shift — systematic differences in image appearance arising from hardware and reconstruction differences.

Strategies to address domain shift include:

- **Multi-site, Multi-Vendor Training Datasets** that expose models to the full spectrum of expected input variability.
- **Domain Adaptation Techniques** Including adversarial training, style transfer, and contrastive learning — that enable models trained on one domain to generalize to another.
- **Federated Learning Frameworks** that allow model training across multiple institutions without centralizing sensitive patient data, enabling large-scale diverse training while preserving privacy.
- **Test-Time Augmentation and Uncertainty Quantification** methods that provide confidence estimates alongside predictions, allowing downstream users to identify cases where model reliability may be reduced.

5. AI-Enabled Longitudinal and Predictive Modeling

Beyond segmentation and measurement automation, AI methods open new dimensions of body composition science. Longitudinal deep learning models trained on serial CT examinations can model the trajectory of MFF change over the ICU course, potentially identifying patients at risk for accelerated myosteatosis or predicting nutritional response. Multi-modal models that integrate DECT-derived MFF with clinical variables, laboratory biomarkers, and physiological monitoring streams could substantially improve prognostic accuracy compared to either modality alone.

Transformer-based architectures and large vision-language models (VLMs) trained on multimodal clinical data represent a longer-term frontier — systems capable of ontextualizing quantitative body composition metrics within the full clinical narrative to generate actionable insights for critical care clinicians.

VI. FUTURE DIRECTIONS

1. Standardization and Reference Intervals

A priority for the field is the establishment ofvalidated, platform-specific normative reference intervals for DECT-derived MFF across age, sex, and body habitus strata. The absence ofsuch reference data currently limits the clinical interpretability ofMFF values — a measured MFF of, for example, 12% has different implications depending on the platform, level ofanalysis, and reference population. Multi-center studies with harmonized acquisition protocols and cross-calibration procedures are needed to construct actionable reference ranges.

2. Photon-Counting Detector CT

The clinical introduction ofphoton-counting detector CT (PCD-CT) represents a technological inflection point for body composition science. PCD-CT achieves superior spectral separation, reduced electronic noise, and the ability to simultaneously decompose voxels into more than two basis materials — enabling, in principle, a three-component model of muscle, fat, and water that more faithfully represents the true histological complexity ofsoft tissue. Early validation studies using PCD-CT for intramuscular fat quantification demonstrate improved accuracy at low fat fractions and reduced susceptibility to artifacts — precisely the scenarios most relevant to ICU patients with early-stage or mild myosteatosis.

3. Integration with Nutritional and Therapeutic Interventions

DECT-derived MFF has potential as a surrogate endpoint in clinical trials evaluating nutritional interventions, anabolic agents, and rehabilitation strategies in the ICU. The sensitivity of MFF to compositional change — potentially detecting lipid mobilization or accumulation before changes in muscle mass become apparent — could reduce sample sizes and shorten trial durations compared to traditional endpoints such as functional recovery or lean mass preservation.

4. Toward Precision Body Composition Medicine

The convergence of DECT-based quantitative imaging, AI-driven analysis, and multi-omic characterization of muscle biology points toward a vision ofprecision body composition medicine — where compositional phenotyping informs individualized nutritional prescriptions, guides rehabilitation intensity, and stratifies patients for pharmacological or interventional strategies targeting myosteatosis. In the ICU, where the consequences ofmuscle deterioration are both acute and enduring, realizing this vision holds substantial promise for improving patient outcomes.

VII. CONCLUSION

DECT-derived muscle fat fraction represents a methodologically rigorous and clinically relevant advance in the body composition toolkit available to critical care researchers and clinicians.

Grounded in well-established X-ray physics, validated against multiple reference standards, and increasingly amenable to AI-driven automation at scale, MFF offers a window into muscle quality that complements volume-based measures and captures pathophysiologically meaningful variation relevant to ICU outcomes. The transition from research tool to clinical standard will require further standardization ofacquisition protocols, establishment of normative reference data, and prospective validation ofMFF-guided interventional strategies.

With the advent ofphoton-counting CT and increasingly capable AI pipelines, the technical barriers to this transition are progressively diminishing — positioning DECT-derived MFF as a potentially transformative biomarker in the evolving landscape ofcritical care medicine.

REFERENCES

[1] Parra-Rodenas L, et al. Dual-energyCTforbodycomposition analysis: asystematicreview ofacquisition andquantification methodology. European Radiology. 2023.
[2] Boutin RD, et al. Myosteatosis in the criticallyill: mechanisms, measurement, andclinical significance. Critical Care Medicine. 2022.
[3] AlbrechtMH, et al. Dual-energyCTfortheassessmentofbodycompositioninoncological patients. European Journal of Radiology. 2021.
[4] Derstine BA, et al. Skeletal muscle cutoffvalues forsarcopenia diagnosis usingT10 toL5 measurements in a healthyUS population. Scientific Reports. 2018.
[5] Wassertheurer T, et al. Deep learning-basedautomatedbody composition analysis from dual-energyCT: a multi-center feasibilitystudy. Insights into Imaging. 2024.
[6] Kullberg J, et al. Whole-body adipose tissue and lean tissue volumes derived from dual-energy CT: comparison with MRI-basedmethods. JournalofMagnetic Resonance Imaging. 2020.
[7] ArdaK, et al. Photon-countingdetectorCTforbodycompositionassessment:earlyclinical validation. Radiology. 2024.
[8] Isensee F, et al. nnU-Net: aself-configuringmethodfordeeplearning-basedbiomedical imagesegmentation. Nature Methods. 2021.
[9] Coen PM, et al. Skeletal muscle lipid content and insulin resistance: evidence for a role of fattyacidmetabolism. Cell Metabolism. 2010.
[10] Weiss J, et al. Dual-energy CTfor opportunistic osteoporosis and body composition screeningin the ICU. Intensive Care Medicine. 2023.

About The Authors

Amit Bisht is an Assistant Professor and Head of the Department of Radiological Imaging Techniques, College of Allied & Healthcare Sciences, Teerthanker Mahaveer University, where he has been shaping the next generation of radiological professionals for over seven years. With a deep-rooted expertise in advanced imaging technologies, quantitative analysis, and multimodal diagnostic techniques, he brings both academic rigor and clinical insight to his teaching and research. He is the author of more than ten publications in the field of radiological sciences, reflecting his sustained commitment to advancing evidence-based practice in medical imaging. Through this book, Mr. Bisht extends his passion for precision radiology beyond the classroom, offering students and practitioners a comprehensive resource grounded in both theory and real-world application.

Ankita Kumari is an accomplished radiology professional and academician with over three years of clinical experience in diagnostic imaging. She has expertise in X-ray, CT, and MRI, with a focus on emergency radiology and abdominal imaging. She serves as an Assistant Professor at TS Mishra University, contributing to teaching, practical training, and academic mentorship. Her research interests lie in advancing evidence-based radiology and improving diagnostic accuracy in emergency settings. She actively participates in academic research and scholarly activities aimed at enhancing imaging practices and patient outcomes. She is committed to continuous learning and integrating clinical insight with radiological excellence.

Prof. (Dr.) Navneet Kumar is the Principal of the College of Allied & Healthcare Sciences, Teerthanker Mahaveer University, bringing over nineteen years of distinguished academic and administrative experience to the field of allied health education. A prolific researcher and thought leader, he has contributed more than thirty publications to the scientific literature, underscoring his unwavering dedication to advancing knowledge in health sciences. His visionary leadership and scholarly contributions have played a pivotal role in shaping curriculum, research culture, and academic excellence at the institutional level. Through this book, Prof. Kumar lends his vast experience and expertise to provide readers with a rigorous yet accessible exploration of advanced quantitative and multimodal imaging techniques in clinical practice.

Prof. (Dr.) Ruchi Kant is a distinguished academician and Member of the Uttar Pradesh State Allied & Healthcare Council (NCAHP), and a senior faculty member at the College of Allied & Healthcare Sciences, Teerthanker Mahaveer University, with over eighteen years of extensive experience in allied health education and research. A prolific contributor to the scientific community, she has authored more than thirty-three publications, demonstrating her enduring commitment to advancing evidence-based practice and academic discourse in health sciences. Her dual role as a policymaker and educator reflects a rare blend of regulatory insight and pedagogical excellence, giving her a unique perspective on the evolving landscape of allied healthcare. Through this book, Prof. Kant brings her wealth of knowledge and institutional expertise to bear, offering readers a thoughtful and authoritative guide to precision radiology and advanced imaging techniques in clinical practice.

Selfypage Developers Pvt Ltd

ISBN: 978-93-7020-458-4

MRP: Rs.490/-